

Geometrically Frustrated Quantum Magnets

by

Predrag Nikolić

Submitted to the Department of Physics
in partial fulfillment of the requirements for the degree of

Doctor of Philosophy

at the

MASSACHUSETTS INSTITUTE OF TECHNOLOGY

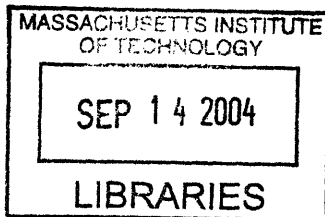
September 2004

© Massachusetts Institute of Technology 2004. All rights reserved.

Author
..... Department of Physics
..... July 28, 2004

Certified by
.....
Senthil Todadri
Assistant Professor
Thesis Supervisor

Accepted by
.....
Thomas J. Greytak
Professor, Associate Department Head for Education



ARCHIVES



Geometrically Frustrated Quantum Magnets

by

Predrag Nikolić

Submitted to the Department of Physics
on July 28, 2004, in partial fulfillment of the
requirements for the degree of
Doctor of Philosophy

Abstract

In this thesis we attempt to reach a physical understanding and theoretical description of some of the greatest challenges in the field of frustrated quantum magnetism, mainly the Kagome lattice antiferromagnets. After an introductory review of concepts, we closely examine the Kagome lattice quantum Heisenberg and Ising models. We apply several new techniques based on lattice gauge theories, duality mappings and field theory in order to explore phase diagrams of these models.

Our approach provides a microscopic picture of the mysterious phenomena observed numerically and experimentally in the Kagome Heisenberg antiferromagnets. Namely, we argue that the spinless excitations, thought to be gapless in absence of any symmetry breaking in this system, are in fact gapped, but at an extremely small emergent energy scale. This scenario is realized in an unconventional valence-bond ordered phase, with a very large unit-cell and complex structure. We also discuss properties of a spin liquid that could be realized in the Kagome antiferromagnet, and argue that its elementary excitations are clearly gapped and extremely massive or even localized.

We demonstrate that the Kagome lattice quantum Ising models are an excellent platform for learning about effects of quantum fluctuations on classically degenerate ground-states. We consider several ways in which spins can acquire quantum dynamics, including transverse field, XXZ exchange and ring-exchange perturbations. Using two different setups of compact $U(1)$ gauge theory we find circumstances in which many characteristic quantum phases occur: disordered phase, topologically ordered spin liquid, valence-bond crystal, and a phase with coexistence of magnetic and valence-bond order. From this variety of results we attempt to learn more general lessons on frustrated quantum magnetism.

At the end, we demonstrate some new mathematical tools on two other frustrated two-dimensional systems, and summarize our conclusions, with an outlook to remaining open problems.

Thesis Supervisor: Senthil Todadri
Title: Assistant Professor

Acknowledgments

Looking back at these six long years that I have spent at MIT, I repeatedly find myself amazed with amount of sheer luck that fell upon me.

The greatest of all of my academic fortunes began with arrival of my advisor, Professor Senthil Todadri to MIT. Oddly enough, his arrival coincided with my last chance to embark on theoretical research in a late stage of my graduate studies, and now when I am leaving, he is leaving too, to a distant place in his home country India. If the world were spinning around me, I could say that he came to help me graduate and fulfill my scientific dream. In three years of working under his wise guidance I have learned a tremendous deal of things, which not so long ago I couldn't believe I would ever know. It is my impression that completion of this thesis research and three papers in a timely manner is largely founded on his talent to find many challenging, important and yet solvable problems (which is famous among everybody who have academically interacted with him). In fact, he miraculously guessed what kind of physics interested me the most, even before I knew it myself. During our numerous discussions, often a couple of hours long, he shared with me his amazing intuition, with deep and simple understanding of difficult concepts. And he always had a plenty of patience to help me out with basics, and listen to my stray ideas. I am also very grateful to him for preparing and sending me to the big world: I received a lot of encouragement to attend schools and conferences, and precious insider's advice on how to interact with other physicists and present my results. And above all, his young spirit, unconditional and contagious good mood, cheerfulness and friendliness will never be forgotten. I must say that I have been extremely lucky to have the best of all advisors.

Being at MIT made me privileged to interact with many great experts and hear their thoughts in various occasions. I wish to thank Professor Xiao-Gang Wen for several insightful discussions, and his interest in my work. I feel that a significant portion of advanced level knowledge that I use in my everyday research comes from his beautiful course, called 8.513. His willingness to help me and guide me through

a hobby theoretical research in my “experimental days” is greatly appreciated. I also wish to thank Professor Young Lee for sharing with me an experimentalist point of view related to my research, and reminding me that there are many natural and tough questions that a theorist must always try to answer. I am sincerely grateful to Professor Patrick Lee for advice and support in delicate times of my transition from experimental to theoretical physics. He has also been a great teacher, the first one to challenge me with problems of strongly correlated electrons in his masterful course 8.514, and definitely turn my heart to theoretical physics. Acceptance of Professors Young Lee and Patrick Lee to be a part of my theses committee makes me feel very privileged. I would also like to thank Professor Leonid Levitov for considering my “application” for research with him, lending me his books, and challenging me to read the unforgettable book by Abrikosov, Gorkov and Dzyaloshinski (for a long time I felt I didn’t need to read anything else). Professor Mehran Kardar had a very important role in my academic life as well, both due to his perfect courses on Statistical Mechanics, and to his suggestion to get in touch with my present advisor, Senthil Todadri.

Of many people whose friendliness has made my days in the CMT corridor much more enjoyable let me mention Olexei Motrunich (Lasik), Ashvin Vishwanath, Carsten Honerkamp, Hoiland Sit, Jung-Tsung Shen (or JT), Dinesh Raut, Dima Novikov, Roman Barankov, Kevin Beach, Alex Seidel, Adam Durst, Tiago Ribeiro and Dan Greenbaum. Lasik has been appointed my deputy advisor, and in several occasions he patiently went through my messy calculations. All of my knowledge of Monte Carlo I owe to him. Ashvin, as my deputy co-advisor, has also helped juggle my mind in several discussions. The happiest of times were during a year when JT and I shared the office. He has been a real friend and always cheerful and enthusiastic companion. He is among very rare people whose never-ending frequent interruptions of my work wouldn’t bother me. In fact, his intelligence, kind heart and resourcefulness made a big impression on me. I also enjoyed talking about physics and various other nonsense with my friends Dima, Roman and Dan. Dan also has my special gratitude as an organizer of a party where I met my fiance, Meital.

A half of my graduate studies I spent doing experiments in the group of Professor Ray Ashoori. It almost amazes me how charming and unique those first three years of my MIT experience now seem, when back then they looked as pure hardship to a spoiled kid who never before had to get his hands dirty. Due to my lack of talent for experimental work and manual labor that follows it, I had to leave otherwise very interesting and challenging projects for paper-and-pencil adventures. But, I wish to thank Professor Ashoori for giving me the first chance to become a physicist in America, and for providing me with plenty of challenges. I sincerely apologize to him for not turning out to be a good investment. I am grateful to senior students Ho-Bun Chan and Misha Brodsky who taught me the art of chemical sample processing, playing with golden wires under microscope and operating very cool cryostat and dilution refrigerator. Warmest thanks to Dmitri Pouchine, my comrade and officemate who helped lift together the heavy burden of difficult life. His presence brought into the labs that greatly missed spirit of bonding from undergraduate school. I spent numerous great moments with other members of the group, Pavlos Glicofridis, Gleb Finkelstein, Kazumasa Nomoto, as well as with our floormate Jessica Thomas who has been a very good friend. Thanks also go to Gary Steele, and to Oliver Dial who let me use his skillfully build bridge.

Darius Torchinsky is another comrade from my “experimental days”, and a roommate for three years. I will remember him for his human side and numerous hours spent discussing everything, from physics and politics, to people and meaning of life. He has inspired my amateurish musical aspirations many times by inviting me to hear him play Cello in public performances. Many of my Serbian friends have been a valuable part of my life in Boston, among which I would especially like to mention Milka Kostić, Darko Marinov, Milica and Zoran Radišić, Nataša Miladinović, Vlada Božin, Gojko Lalić, Bosiljka Tasić, Aleksandar and Nikola Kojić, Neda and Rada Vukmirović, Mirko and Nataša Ristivojević, and Jelena Madić. Coincidentally, a good friend of mine from high school in Belgrade, Zoran Hadžibabić, came to MIT to study physics a year before me, and his help during my early days in this country will never be forgotten.

Finally, none of my academic adventures would have made sense if I didn't have people who loved me to share them with. My parents have always been a great support and a source of strength from far away. Their unconditional belief in me is deeply rooted in every success of mine. And perhaps all of my creativity and overall happiness in the past three years I owe to my angel and the greatest love of my life, Meital Orr. She has been the most wonderful inspiration ever.

Za mamu i tatu

Contents

1	Introduction	21
1.1	Magnetism of Mott Insulators	23
1.2	Conventional and Unconventional Phases of Quantum Magnets	27
1.3	Resonant-Valence-Bond State and Spin Liquid	32
1.4	Intriguing New Materials	36
1.5	Geometric Frustration	41
1.6	Overview of the Thesis	45
2	Kagome Quantum Heisenberg Antiferromagnet	47
2.1	The Kagome Puzzle	48
2.1.1	Experiments	48
2.1.2	Numerical Studies	50
2.1.3	Questions and Some Attempts to Find Answers	53
2.2	Effective Theory at Low Energies	55
2.2.1	Promising Approaches to Paramagnetic Phases	55
2.2.2	Effective \mathbb{Z}_2 Gauge Theory for the Singlet States	56
2.2.3	Effective Theory of the Kagome Heisenberg Model	59
2.2.4	The Limit of Short-Range Singlet Bonds	60
2.2.5	The Limit of Strong Singlet Fluctuations	69
2.2.6	Magnetic Excitations and Confinement	73
2.2.7	Finite Lattices	75
2.3	Qualitative Physical Picture From Comparison With Numerics	76
2.4	Weak Dispersion of Excitations and Some Other Issues	78

2.4.1	Monte-Carlo Studies	79
2.4.2	A Large- N Limit	82
3	Kagome Lattice Quantum Ising Model in Transverse Field	87
3.1	How the Quantum Fluctuations Lift Classical Degeneracy?	88
3.1.1	Order-by-Disorder	88
3.1.2	Disorder-by-Disorder on the Kagome Lattice?	89
3.2	Lattice-Field Theory of Fluctuating Spins	90
3.2.1	Effective Compact $U(1)$ Gauge Theory	91
3.2.2	Duality Transformation	95
3.2.3	Field Theory	103
3.2.4	Phase Diagram	106
3.2.5	Phase With Broken Translational Symmetry	108
3.3	Discussion	110
4	Bridging Between Ising and Heisenberg Magnets on the Kagome Lattice	113
4.1	Models and Overview	114
4.2	Transverse Field Ising Model	116
4.2.1	Compact $U(1)$ Gauge Theory of the Frustrated Bonds	116
4.2.2	Duality Transformation	125
4.2.3	Degeneracy and Fluctuations	129
4.2.4	Disorder-by-Disorder	138
4.2.5	Variational Wavefunctions for the Ground and Excited States	141
4.3	XXZ Model and Heisenberg Model With Easy-Axis Anisotropy	142
4.3.1	$U(1)$ Gauge Theory and Duality Transformation	143
4.3.2	“Sign-Problem” Can Be Avoided	146
4.3.3	Degeneracy and Fluctuations	149
4.3.4	Revealing the Long-Range Order	151
4.3.5	Stability of the Ordered Phase	155
4.3.6	Valence-Bond Picture of the Ordered Phase	159

4.3.7	Spin Liquid Phase	164
4.4	A Big Picture	166
4.4.1	Phase Diagram of the Kagome Quantum Ising Models	166
4.4.2	Roles of Geometry and Quantum Dynamics	167
5	Quantum Ising Models on Other Frustrated Lattices	169
5.1	Fully Frustrated Square Lattice	170
5.2	Triangular Lattice XXZ Model	179
6	Conclusions	191
6.1	Phases of the Kagome Lattice Antiferromagnets	192
6.2	New Methods for Frustrated Quantum Magnets	195
6.3	Open Problems	197
A	Ground-State Average of the Gauge Field	201
B	Estimates of the Couplings in the \mathbb{Z}_2 Gauge Theory	205
C	Degenerate Perturbation Theory	209
D	Properties of the TFIM Lattice Theory	211

List of Figures

1-1	Magnetically ordered states on the square lattice	28
1-2	Long and short range valence-bond states	30
1-3	Characteristic types of short-ranged valence-bond crystals (on the square lattice)	32
1-4	Topological quantum numbers of dimer coverings in cylindrical space geometry	34
1-5	Conservation of topological quantum numbers	35
1-6	Phase diagram of Cs_2CuCl_4	38
1-7	Spin-wave dispersion and lineshape in the ordered phase of Cs_2CuCl_4	38
1-8	Comparison between the neutron scattering lineshapes in ordered and disordered phases of Cs_2CuCl_4	39
1-9	Schematic phase diagram of the BEDT-TTF organic superconductors	40
1-10	Frustration of spins on a triangular plaquette	42
1-11	Neel order on the triangular lattice	42
1-12	Corner-sharing lattices	43
1-13	Chirality vectors on the Kagome lattice	43
2-1	Traditional Japanese Kagome basket	48
2-2	Kagome lattice	48
2-3	Heisenberg model exact spectra on $N=36$ samples	52
2-4	Dice lattice: duality to Kagome and full frustration	59
2-5	Flippable loops and dimer moves	62
2-6	Neighboring perfect hexagons	63

2-7	Maximum number of perfect hexagons	64
2-8	Restrictions imposed by the dense perfect hexagons	65
2-9	Examples of the dice lattice paths between two sites	72
2-10	Path cancellation on the dice lattice	73
2-11	Regimes of the (2+1)D classical Ising model on the fully frustrated dice lattice	80
2-12	Vison-vison correlations in the disordered phase	81
2-13	Unit-cell of the fully frustrated dice lattice	83
3-1	Relationship between the honeycomb and Kagome lattices	92
3-2	Background charge on the honeycomb lattice	94
3-3	Duality between the honeycomb and triangular lattices	97
3-4	Convenient definition of the fixed dual background gauge field	100
3-5	Fractional offsets of the dual gauge and matter fields	100
3-6	Staggered flux and staggered external XY field	104
3-7	Direct triangular and its reciprocal lattice	105
3-8	Schematic phase diagram of the effective XY model	108
3-9	Long-range ordered phase	109
4-1	Frustrated bonds on the Kagome lattice	117
4-2	Duality between the Kagome and dice lattices	117
4-3	Frustrated bonds represented by dimers on the dice lattice	118
4-4	Reference bond orientations of the Kagome and dice lattices	120
4-5	Elementary processes on a dice plaquette that preserve the minimum frustration	122
4-6	Special bond signs on the Kagome and dice lattices	123
4-7	Bond orientations of the triangular lattice formed by the Kagome hexagon centers	124
4-8	One characteristic and periodic configuration of background field . . .	129
4-9	Unphysical fluctuations in the lattice field theory	132
4-10	Examples of preferred states	138

4-11	Maximally flippable states	139
4-12	Flipping a pair of aligned spins creates extra frustration	143
4-13	Four possible processes that keep frustration at the minimum	144
4-14	Explanation for the derivation of equations (4.51)	147
4-15	Preferred saddle-point configuration with zero magnetization, entropically selected by the XXZ fluctuations	154
4-16	Effective band structure of the sine-Gordon theory for the entropically selected state	158
4-17	Covering the lattice with flippable pairs of spins	160
4-18	Unfrustrating the defect triangles	162
4-19	Perfect hexagons minimize XXZ exchange energy	162
4-20	Characteristic variational ground-states	163
4-21	Overlap between the preferred configuration of frustrated bonds and the variational states	164
5-1	Fully frustrated square lattice	170
5-2	Square lattice staggered flux and dual background charge	172
5-3	Free energy spectral weight of the square lattice transverse field Ising model	177
5-4	Valence-bond crystal in the square lattice transverse field Ising model	177
5-5	A background field configuration on the triangular lattice	182
5-6	Triangular lattice staggered flux and dual background charge	183
5-7	Kagome lattice representation of triangular lattice bonds	184
5-8	Triangular lattice XXZ model represented on the Kagome lattice . . .	186
5-9	Free energy spectral weight of the triangular lattice XXZ model . . .	189
5-10	Columnar order of dimers on the honeycomb lattice	190
5-11	An entropically favored state in the triangular lattice XXZ model . .	190
D-1	Local neighborhood of a Kagome site	212

List of Tables

2.1	Elementary flippable loops on the Kagome lattice	62
4.1	Notation for the Kagome and dual dice lattices	119
4.2	Site classification	138
4.3	Kinetic energy operators in the XXZ U(1) gauge theory	144
4.4	Action of the spatial (potential) part of the coupling matrix on the field vectors	149
4.5	Components of the XXZ saddle-point vectors	149
4.6	Bond characterization	153
4.7	Triangle characterization	153
4.8	Quantum phases of the Kagome lattice Ising antiferromagnets with different kinds of spin dynamics	166

Chapter 1

Introduction

Recent years have been characterized by many experimental discoveries and theoretical explorations of unconventional condensed matter physics. This quest for unconventional phenomena was initially motivated by the discovery of high-temperature cuprate superconductors in 1986 [1]. After almost twenty years of a tremendous effort to understand the cuprates, and a considerable theoretical progress especially in the field-theoretical descriptions of strongly correlated electrons, there is still no real consensus on the cuprate physics. Meanwhile, several new kinds of challenging materials caught attention of condensed matter physicists, such as heavy fermion systems and geometrically frustrated magnets. All of their puzzling properties seem to be shaped by strong interactions and quantum fluctuations.

Some of these incompletely understood materials can be viewed in certain limits as Mott insulators, whose insulating properties are shaped by repulsive interactions between electrons instead of the band structure. If the valence electron band of a Mott insulator is half filled (one valence electron per atom), then every electron remains localized on one atom, since in order to move in any direction it would have to overcome a large Coulomb barrier of the surrounding electrons. In such circumstances electron spins can be viewed as the only degrees of freedom at low energies, and the material can be treated as a magnetic system where a localized magnetic moment (spin) sits on every atom. The residual interaction between these localized moments is spin-exchange, and it usually gives rise to magnetically ordered phases at not too

high temperatures.

This description applies well to the cuprates before they are doped. However, by doping one can remove a number of valence-band electrons and make room for the remaining electrons to move around. If the doping level is sufficiently high, magnetism of the “parent” Mott insulator can be destroyed, and interesting unconventional phases may result. In the cuprates, one obtains a pseudo-gap phase, which is still not well understood (at even higher dopings the cuprates become superconducting). If one decided to pay close attention only to the electron spins, then one would notice that motion of doped holes causes spins to fluctuate more, until eventually the magnetic order is destroyed with sufficient doping. It would appear that by doping one cranks up amount of *quantum* fluctuations for the spins (this happens even at zero temperature). In a very broad sense, similar point of view can be taken in certain other materials, such as the heavy-fermion systems. There, the local magnetic moments coexist with conduction-band electrons, and through an interaction between them the electron motion causes quantum fluctuations for the local moments, yielding unconventional phases in some regimes (a non Fermi liquid metal).

Geometrically frustrated quantum magnets are Mott insulators, but with special properties that make them extremely sensitive to quantum fluctuations, even at half filling. They are very interesting since various unconventional phases can be expected to occur in them more easily than in other systems. In this introduction we will start by reviewing magnetism of the Mott insulators. We will survey quantum phases that can be realized in magnetic systems, and circumstances in which such phases could be found. Then, we will turn to the unconventional phases, and explain what makes the frustrated magnets promising for finding them. The introduction will be finished with an overview of this thesis.

1.1 Magnetism of Mott Insulators

We will first review how magnetism arises in Mott insulators. The simplest theoretical model that captures essential physics of Mott insulators is Hubbard model given by the Hamiltonian:

$$H = -t \sum_{\langle ij \rangle} \left(c_{i\alpha}^\dagger c_{j\alpha} + c_{j\alpha}^\dagger c_{i\alpha} \right) + U \sum_i n_{i\uparrow} n_{i\downarrow} , \quad (1.1)$$

where $c_{i\alpha}^\dagger$ and $c_{i\alpha}$ are local electron creation and annihilation operators respectively, and $n_{i\alpha}$ is local electron number operator:

$$n_{i\uparrow} = c_{i\uparrow}^\dagger c_{i\uparrow} \quad , \quad n_{i\downarrow} = c_{i\downarrow}^\dagger c_{i\downarrow} . \quad (1.2)$$

In these expressions i and j label sites (atoms) of the material's crystal lattice, and $\alpha \in \{\uparrow, \downarrow\}$ is a spin-index, summed over if repeated. Hubbard model describes electrons that are always localized on single atoms, but they may tunnel between nearest-neighbor atoms $\langle ij \rangle$ as captured by the t term (kinetic energy). In this regard, Hubbard model is similar to a tight-binding approximation. However, Coulomb repulsion between electrons is also taken into account through the U term: due to Pauli exclusion principle there can be at most two electrons at one site, but this costs large Coulomb energy U . It is possible to represent long-range electron interactions more realistically (extended Hubbard model), but even simplifying them as short-ranged (that is, as present only when two electrons are exactly on the same atom) often allows capturing essential physics. This will be demonstrated in the following, where we will recover antiferromagnetism from this simple picture.

Hubbard model admits different phases. In the limit $U \ll t$ kinetic energy wins over electron interactions, and a metallic phase is obtained with delocalized electron wavefunctions. On the other hand, $U \gg t$ can give rise to Mott insulator physics: electrons are not free to move if there are surrounding electrons that repel them. In this limit we can treat t as a small perturbation to the pure Coulomb part U . Consider a half-filled band, with one electron per lattice site. Such a situation describes the

cuprates before doping, and frustrated magnets in general. Then, a ground-state of the pure Coulomb part U is any state without double-occupied sites. Such states are numerous and degenerate, since electron spins are free to point in any direction as long as every electron sits alone on one lattice site. The perturbation t mixes these unperturbed ground-states and lifts their degeneracy. As a result, one obtains a low energy effective theory whose degrees of freedom are only the localized spin variables, which we now derive.

Let us denote the pure Coulomb part (U -term) of (1.1) by H_0 and the kinetic perturbation (t -term) by H' . Let $|\Psi\rangle$ be the true ground-state of the Hubbard Hamiltonian $H = H_0 + H'$ with energy E . We can express the ground-state $|\Psi\rangle$ as a superposition of all unperturbed eigenstates $|\psi\rangle$:

$$|\Psi\rangle = \sum_{\psi} a_{\psi} |\psi\rangle \quad , \quad H_0 |\psi\rangle = E_{\psi} |\psi\rangle . \quad (1.3)$$

We substitute this in the Schrödinger equation $H|\Psi\rangle = E|\Psi\rangle$ in order to solve it perturbatively, and after multiplying by $\langle\psi'|\psi\rangle$ we find:

$$E_{\psi'} a_{\psi'} + \sum_{\psi} \langle\psi'|H'|\psi\rangle a_{\psi} = E a_{\psi'} . \quad (1.4)$$

This is a system of equations for the unknown probability amplitudes a_{ψ} . Clearly, if $U \gg t$ the largest amplitudes (by modulus) will correspond to the ground-states of the pure Coulomb part, that is to the states with no double-occupied sites. Let us label such states by $|\psi_G\rangle$ in the following, they are degenerate with the unperturbed ground-state energy E_0 : $H_0|\psi_G\rangle = E_0|\psi_G\rangle$. All excited states of the pure Coulomb part will be labeled by $|\psi_E\rangle$, and their amplitudes a_{ψ_E} can be eliminated from the system (1.4) using perturbation theory. First we express the ground-state amplitudes as a separated sum over unperturbed ground and excited states in (1.4):

$$a_{\psi'_G} = \frac{1}{E - E_0} \left(\sum_{\psi_G} \langle\psi'_G|H'|\psi_G\rangle a_{\psi_G} + \sum_{\psi_E} \langle\psi'_G|H'|\psi_E\rangle a_{\psi_E} \right) . \quad (1.5)$$

Then we substitute excited-state amplitudes a_{ψ_E} from (1.4):

$$\begin{aligned}
a_{\psi'_G} &= \frac{1}{E - E_0} \sum_{\psi_G} \langle \psi'_G | H' | \psi_G \rangle a_{\psi_G} \\
&+ \frac{1}{E - E_0} \sum_{\psi_E} \sum_{\psi} \langle \psi'_G | H' | \psi_E \rangle \frac{1}{E - E_{\psi_E}} \langle \psi_E | H' | \psi \rangle a_{\psi} ,
\end{aligned} \tag{1.6}$$

and again separate summation over unperturbed ground and excited states in the second part of the last expression. This cycle can be repeated many times to yield higher order corrections. At the second order of perturbation theory we have the following system of equations that contains only the ground-state amplitudes a_{ψ_G} :

$$\begin{aligned}
a_{\psi'_G} &= \frac{1}{E - E_0} \sum_{\psi_G} \langle \psi'_G | H' | \psi_G \rangle a_{\psi_G} \\
&+ \frac{1}{E - E_0} \sum_{\psi_E} \sum_{\psi_G} \langle \psi'_G | H' | \psi_E \rangle \frac{1}{E - E_{\psi_E}} \langle \psi_E | H' | \psi_G \rangle a_{\psi_G} \\
&+ \mathcal{O}\left(\frac{t^3}{U^2}\right) .
\end{aligned} \tag{1.7}$$

We now proceed by calculating the matrix elements in this perturbative expansion. At the first order of perturbation theory, the matrix element $\langle \psi'_G | H' | \psi_G \rangle$ evaluates to zero. The perturbation H' moves an electron, and when it acts on the state $|\psi_G\rangle$, which has exactly one electron on every site, it yields an excited state with a double-occupied site. Such an excited state has energy $E_{\psi_E} = E_0 + U$. The matrix elements at the second order of perturbation theory are non-zero. Since in our particular case H' always creates an excited state with a fixed energy when it acts on any ground-state, we can simplify (1.7):

$$a_{\psi'_G} = \frac{1}{E} \frac{1}{E - U} \sum_{\psi_G} \langle \psi'_G | H'^2 | \psi_G \rangle a_{\psi_G} + \mathcal{O}\left(\frac{t^3}{U^2}\right) , \tag{1.8}$$

where we have also set $E_0 = 0$. Taking square of the electron hopping perturbation H' generates various operators among which we need to consider only those that convert one unperturbed ground-state into another. Since no double-occupied sites may be

created, we are looking for the operators that have one $c_{i\alpha}^\dagger$ and $c_{i\alpha}$ on every involved site. We find:

$$\langle \psi'_G | H'^2 | \psi_G \rangle = 2t^2 \sum_{\langle ij \rangle} \langle \psi'_G | c_{i\alpha}^\dagger c_{j\alpha} c_{j\beta}^\dagger c_{i\beta} | \psi_G \rangle . \quad (1.9)$$

Using electron anti-commutation relations $\{c_{i\alpha}^\dagger, c_{j\beta}\} = \delta_{ij}\delta_{\alpha\beta}$ we obtain:

$$\begin{aligned} \langle \psi'_G | H'^2 | \psi_G \rangle &= -2t^2 \sum_{\langle ij \rangle} \langle \psi'_G | c_{i\alpha}^\dagger c_{i\beta} c_{j\beta}^\dagger c_{j\alpha} - c_{i\alpha}^\dagger c_{i\alpha} | \psi_G \rangle \\ &= -2t^2 \sum_{\langle ij \rangle} \langle \psi'_G | c_{i\alpha}^\dagger c_{i\beta} c_{j\alpha}^\dagger c_{j\beta} \delta_{\alpha\beta'} \delta_{\alpha'\beta} + \text{const.} | \psi_G \rangle , \end{aligned} \quad (1.10)$$

where the bilinear term evaluates to a constant since there is one electron on every site in all unperturbed ground-states. If we define electron spin operators as:

$$\mathbf{S}_i = \frac{1}{2} c_{i\alpha}^\dagger \boldsymbol{\sigma}_{\alpha\beta} c_{i\beta} , \quad (1.11)$$

where $\boldsymbol{\sigma}_{\alpha\beta}$ is vector of Pauli matrices, then we can substitute in (1.10) the following identity:

$$\boldsymbol{\sigma}_{\alpha\beta} \boldsymbol{\sigma}_{\alpha'\beta'} = 2\delta_{\alpha\beta'} \delta_{\alpha'\beta} - \delta_{\alpha\beta} \delta_{\alpha'\beta'} , \quad (1.12)$$

and obtain:

$$\langle \psi'_G | H'^2 | \psi_G \rangle = -4t^2 \sum_{\langle ij \rangle} \langle \psi'_G | \mathbf{S}_i \mathbf{S}_j + \text{const.} | \psi_G \rangle . \quad (1.13)$$

The second order perturbative expansion (1.8) can finally be written as:

$$E a_{\psi'_G} = \frac{4t^2}{U} \sum_{\psi_G} \sum_{\langle ij \rangle} \langle \psi'_G | \mathbf{S}_i \mathbf{S}_j + \text{const.} | \psi_G \rangle a_{\psi_G} + \mathcal{O}\left(\frac{t^3}{U^2}\right) , \quad (1.14)$$

where E was treated as small in comparison to U . This system of equations can be interpreted as an operator equation if we reverse the procedure that led to (1.4). Let H_{eff} be an operator that acts in the Hilbert space spanned only by the unperturbed ground-states $|\psi_G\rangle$, but whose spectrum at low energies coincides with spectrum of

the full Hubbard Hamiltonian. Then:

$$H_{\text{eff}} = \frac{4t^2}{U} \sum_{\langle ij \rangle} \mathbf{S}_i \mathbf{S}_j + \text{const.} + \mathcal{O}\left(\frac{t^3}{U^2}\right). \quad (1.15)$$

This is a low energy effective theory of the Hubbard model in the large- U limit, called Heisenberg model. Its degrees of freedom are localized electron spins \mathbf{S}_i which interact antiferromagnetically. Strength of the *exchange* interaction between spins is $J = \frac{4t^2}{U}$. This is how antiferromagnetism arises in Mott insulators.

If higher order perturbative corrections are included, then the effective spin model acquires more complicated operators. They include exchange interactions between next nearest neighbor spins, and spins that are further apart from each other. Also, operators with more than two \mathbf{S}_i factors appear, and they are called multiple spin exchange. All terms, however, are $SU(2)$ symmetric, that is invariant under global spin rotation. If the electron band were not half-filled to begin with, then additional degrees of freedom would have to be present in the effective theory, since motion of charge through the lattice could be possible. A popular way to describe such circumstances close to half-filling is a so called $t - J$ model.

1.2 Conventional and Unconventional Phases of Quantum Magnets

Here we will consider materials whose only degrees of freedom are magnetic moments localized on sites of some lattice. This idealization is a good description of Mott insulators when electrons are strongly localized on individual atoms due to a dominant Coulomb repulsion. Low temperature properties of such materials can be generally captured by an $SU(2)$ symmetric Hamiltonian:

$$H = \sum_{i,j} J_{ij} \mathbf{S}_i \mathbf{S}_j + \sum_{i,j,k,l} J_{ijkl} (\mathbf{S}_i \mathbf{S}_j) (\mathbf{S}_k \mathbf{S}_l) \cdots, \quad (1.16)$$

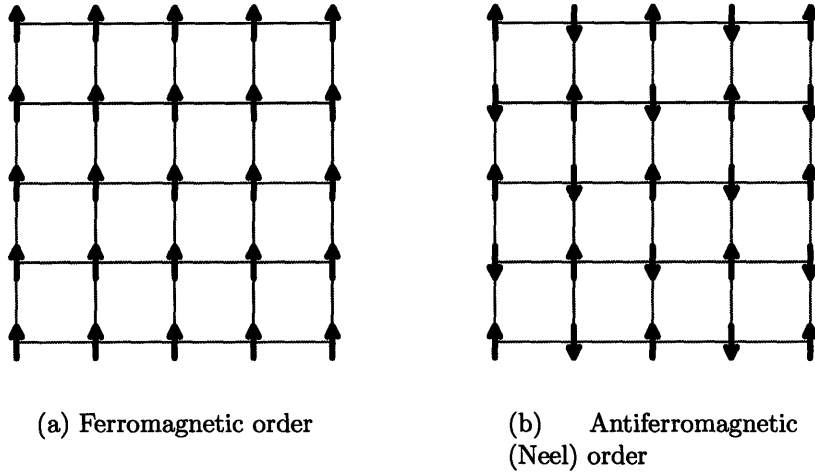


Figure 1-1: Magnetically ordered states on the square lattice

where \mathbf{S}_i is a vector spin operator at the lattice site i . The spin S of the localized magnetic moments is equal to the total spin of unpaired valence electrons at each site. Quantum fluctuations at low temperatures can be important when S is small. The coupling constants J_{ij} correspond to the simplest spin exchange between two sites, and normally decay as separation between the sites i and j increases. It is often permissible to neglect all couplings except J_{ij} between the nearest-neighbor sites, in which case one obtains a simple Heisenberg model:

$$H = J \sum_{\langle ij \rangle} \mathbf{S}_i \mathbf{S}_j . \quad (1.17)$$

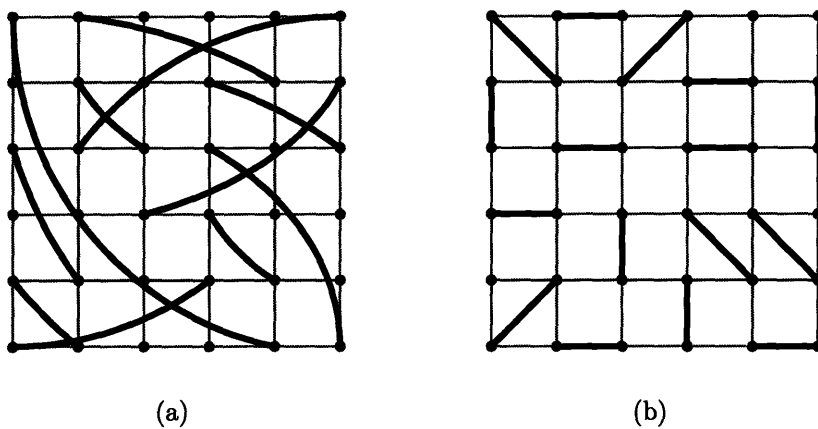
However, when Coulomb repulsion between electrons is not strong enough compared to their kinetic energy, further-neighbor exchange has to be included in the model, as well as multiple-spin exchange described by the coupling constants J_{ijkl} , etc. Sometimes, single-ion anisotropies and other perturbations that occur in realistic materials, or have some specific theoretical importance, require that the $SU(2)$ symmetry be abandoned in the model (1.16). Besides Heisenberg models, we will consider models with Ising symmetry in this thesis.

The models (1.16) and (1.17) are very general and in principle admit many different phases. The most conventional phases possess magnetic order, which is nor-

mally stabilized by the dominant nearest-neighbor exchange. Thus, the Heisenberg model is sufficient to account for their properties, at least qualitatively. If realized in a particular system, type of magnetic ordering is ferromagnetic for $J < 0$, and antiferromagnetic for $J > 0$ (Figure 1-1). These phases are conventional in the sense that quantitative theories for them are available, such as the spin-wave theory which provides tools for calculating quantities that can be measured in experiments (response functions and mode dispersion). Appropriate Landau-Ginsburg theories can be derived from microscopic models, and the magnetic order parameter is easy to describe. Elementary excitations are Goldstone modes, that is gapless bosonic spin-waves (magnons).

However, interesting things can happen if magnetic order is not favorable in the ground-state. Magnetic order is generally a feature of classical magnets at zero temperature, and quantum fluctuations may destabilize it if they are strong enough. General circumstances in which quantum fluctuations are stronger and more important are the following: small spin magnitude S , low lattice dimensionality, small coordination number (number of nearest-neighboring sites), geometric frustration, etc. Fundamentally, a small spin magnitude is source of quantum fluctuations according to the Heisenberg uncertainty principle. On a lattice, exchange interactions typically work against this mechanism since they tend to correlate spins at short distances and group them into larger “rigid” objects that are less prone to quantum fluctuations (clustering of spins can actually happen in disordered systems). But, such an effect is reduced when the lattice is poorly connected, either due to low coordination number or low dimensionality. And geometric frustration is the most efficient and direct way to prevent building up of spin correlations, as will be explained later in this introduction.

Quantum paramagnetic states are invariant under global spin rotation ($\langle \mathbf{S}_i \rangle = 0$), and they are usually envisioned and referred to as “spin singlets”, even though this terminology is somewhat inadequate (they are not unique in many-spin systems). In fact, the “singlet states” can be constructed from spin-pairs that form singlet



(a) Random valence-bond state. Every spin participates in a valence-bond with another spin; (b) Short-range valence-bond state.

Figure 1-2: Long and short range valence-bond states

valence-bonds on the lattice:

$$|\psi_{ij}\rangle = \frac{|\uparrow_i\downarrow_j\rangle - |\downarrow_i\uparrow_j\rangle}{\sqrt{2}}. \quad (1.18)$$

The simplest kind of “singlet states” are valence-bond (VB) states. They are direct products of non-overlapping valence-bonds that completely cover the lattice in an arbitrary way (Figure 1-2):

$$|\Psi_{vb}\rangle = |\psi_{12}\rangle \otimes |\psi_{34}\rangle \otimes |\psi_{56}\rangle \otimes \dots. \quad (1.19)$$

Other more complex “singlet states” can be always expressed as quantum superpositions of the VB states. As a matter of principle, the valence-bonds may be formed between any two sites on the lattice, no matter how far from each other they are, but in normal circumstances the short-ranged valence-bonds will provide more realistic platform for describing quantum paramagnetic phases (since the exchange interactions are short-ranged).

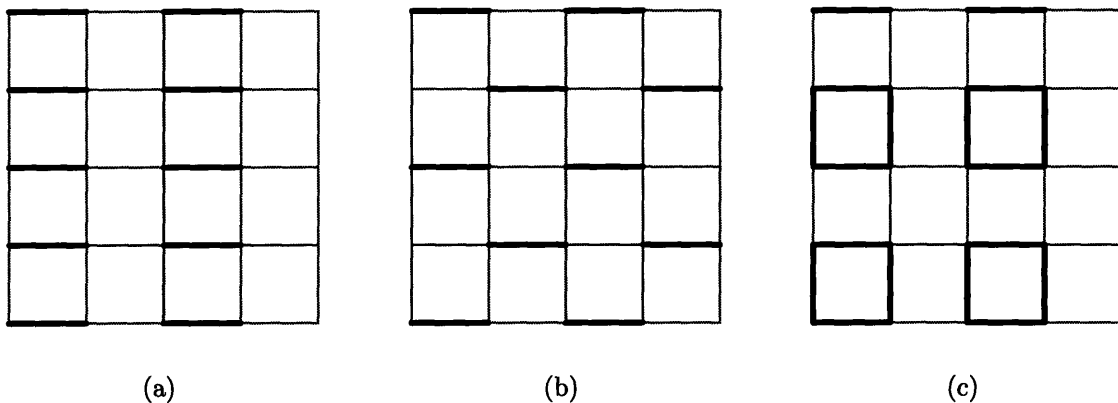
Assuming that quantum fluctuations destabilize magnetic order and give rise to a “singlet” ground-state, we can in principle find an effective low-energy Hamiltonian that lives in the Hilbert space spanned by the VB states. For simplicity, one usually

includes only the shortest-range valence-bonds in the effective theory; while this has a clear physical motivation, there are no known means to estimate what quantitative or even qualitative errors may be introduced. One arrives at a so called “dimer model”, where elementary degrees of freedom are hard-core dimers that live on the lattice bonds and represent the valence-bonds. Only the shortest-range dimer operators are usually considered in the effective dimer Hamiltonian, which on the square lattice takes form:

$$H = -t \sum_{\square} (|\square\rangle\langle\square| + |\square\rangle\langle\square|) + v \sum_{\square} (|\square\rangle\langle\square| + |\square\rangle\langle\square|) . \quad (1.20)$$

The first term (t) is a kinetic energy operator that flips a pair of dimers on a small loop (elementary plaquette), while the second term (v) is potential energy of short-range interactions between dimers. Such theories have been extensively analyzed on several lattices, mostly in two spatial dimensions [2, 3, 4, 5]. Frequently, the ground-state is found to spontaneously break translational symmetry and form a valence-bond crystal. Typical dimer ordering patterns are shown in Figure 1-3. If $|v| \gg t$, then depending on whether the dimer pairs on the same plaquette are favorable ($v < 0$) or not ($v > 0$) the columnar and staggered order obtains respectively. What happens in the region $|v| < t$ is difficult to analyze, but there are several options. On the square lattice there is numerical evidence [6] that a so called plaquette order develops (Figure 1-3(c)): the ground-state is a superposition of many dimer coverings. Similar is expected of other bipartite lattices (which can be decomposed into two sublattices, so that the sites of one sublattice are connected only to the sites of the other). In contrast, on the triangular lattice, which is not bipartite, there is numerical evidence for a disordered phase in the region $|v| < t$ [4, 5]. For $v = t$ a very interesting Rokhsar-Kivelson critical point is found.

The valence-bond crystals can be regarded as almost conventional phases. Even though quantitative theories are available only in some special cases (when translational symmetry is explicitly broken in the spin Hamiltonian [7]), it is qualitatively known that all elementary excited states are gapped. They include “singlet” states,



(a) Columnar order; (b) Staggered order; (c) Plaquette order (a pair of parallel dimers resonates between horizontal and vertical orientation on every emphasized plaquette). In all figures dimers indicate a high probability of finding a singlet valence-bond.

Figure 1-3: Characteristic types of short-ranged valence-bond crystals (on the square lattice)

and states with magnetic moment (gapped magnons, or triplons). Conventionally, the energy gap is set by the nearest-neighbor exchange coupling, and may become small only in the vicinity of a second order phase transition. However, unconventional situations can be sometimes found in geometrically frustrated magnets when the singlet states acquire a very low energy scale even away from phase transitions.

Fully disordered quantum paramagnetic phases can also be interesting. Conventional quantum phases that do not break any symmetries are analogous (and smoothly connected) to classical disordered phases at high temperatures, where the spins are essentially decoupled. However, the quantum fluctuations are coherent unlike the thermal ones, and even if they restore all symmetries of the Hamiltonian, they can yield non-trivial quantum effects and unconventional physics, which will be discussed in the next section.

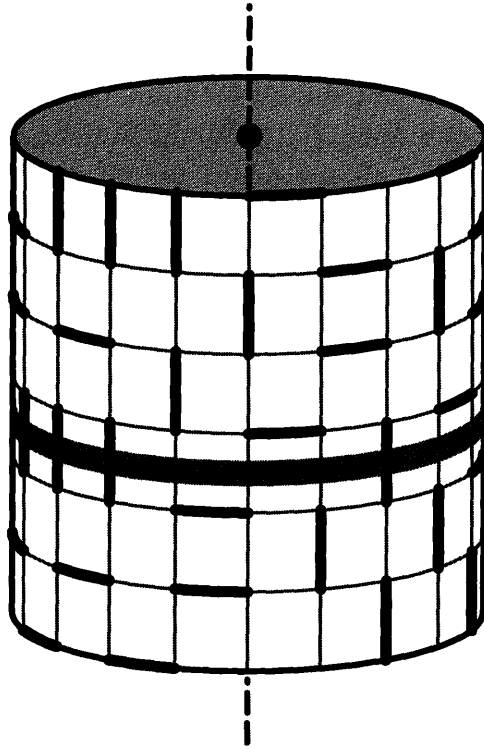
1.3 Resonant-Valence-Bond State and Spin Liquid

The resonant valence-bond (RVB) state is a completely disordered state of fluctuating valence-bonds, first envisioned by Anderson [8, 9]. It is symmetric under both spin rotations and translations, and realized as a ground-state in the so called *spin*

liquid quantum phase. It can be naively visualized as a roughly equal-amplitude superposition of all VB states.

If the valence-bonds are short-ranged (SR), the resulting SR-RVB state could be in principle obtained by quantum melting of the valence-bond crystal phases from Figure 1-3. The dimer model (1.20) on the square lattice has only ordered phases, and a SR-RVB ground-state obtains only at the Rokhsar-Kivelson critical point between two dimer orders ($v = t$). This ground-state is exactly known to be an equal-amplitude superposition of dimer states. In contrast, the triangular lattice dimer model seems to have a spin liquid phase, so that a SR-RVB ground-state can be found in a finite region of $\frac{v}{t}$.

The spin liquid phase is very special and unconventional. Even though there are no broken symmetries, this phase cannot be connected to the conventional disordered phase of completely decoupled spins without a phase transition. The spin liquid possesses a so called *topological order*, a concept first introduced by Wen in context of Quantum Hall Effect [10] and named “topological” because it relies on topology of the real space. In order to illustrate it, suppose that the dimer model (1.20) lives on an infinite cylinder instead on a flat infinite square lattice. Consider an arbitrary dimer covering on such wrapped lattice, and count the number of dimers crossed by a closed path that goes around the cylinder (see Figure 1-4). The parity of this number can be regarded as a “topological quantum number” of the considered dimer covering. If one looks carefully at the dimer Hamiltonian (1.20), one can see that this is a good quantum number, conserved by the dimer dynamics - this is illustrated in Figure 1-5. Thus, it makes sense to define topological sectors by grouping together all dimer states that have the same “topological quantum number” - the Hamiltonian cannot mix states from different topological sectors. In the spin liquid phase, the ground-state is roughly an equal amplitude superposition of all dimer states *from one topological sector*, and there is a twofold ground-state degeneracy on an infinite cylinder associated to the two possible values of the “topological quantum number”. It is said that the spin liquid possesses “topological order”. This remains true even if other perturbations are added to the dimer Hamiltonian. All local dimer-

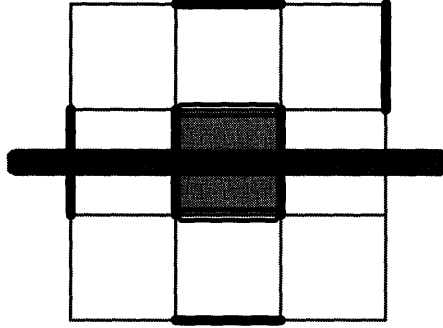


The square lattice is placed on an infinitely large cylinder and covered by dimers. A fictitious closed path (thick line) that goes around the cylinder crosses bonds of the lattice, and intersects a certain number of dimers. Parity of the number of intersected dimers defines a “topological quantum number”, as explained in the text. Alternatively, the parity can be associated to an object dual to the closed path, which is threaded through the opening of the cylinder (dashed). This duality can be expressed in language of a gauge theory, so that the closed path goes along the gauge field-lines, and the threaded object represents the gauge flux.

Figure 1-4: Topological quantum numbers of dimer coverings in cylindrical space geometry

flip operators conserve the “topological quantum number”, so that the spin liquid can exist as a stable phase. Also, these considerations can be generalized to arbitrary-ranged valence-bonds, and some models with less than $SU(2)$ symmetry, which will be discussed in Chapter 4. Ground-state degeneracy of the spin liquid is 2^g , where g the number of wrapped dimensions.

Topological order is a purely quantum phenomenon that distinguishes unconventional spin liquids from conventional disordered phases. However, the spin liquid has additional unconventional features. Most notably, excited particles can carry *fractional* quantum numbers [2, 9, 11, 12, 13, 14, 15, 16, 17]. They include *spinons*, which



The parity of the number of dimers intersected by a closed path cannot be changed by local dimer flips. Suppose that the kinetic t term of the dimer Hamiltonian (1.20) flips two dimers on the shaded plaquette into the configuration denoted by hollow dimers. The number of dimers that intersects the path (thick line) changes by two, which does not affect the parity.

Figure 1-5: Conservation of topological quantum numbers

are neutral particles with spin $S = \frac{1}{2}$ instead of conventional spin $S = 1$ of magnons and triplons. Also, if the system has additional charged degrees of freedom (introduced by doping for example), charge carriers can be spinless charged bosons, called *holons* or *chargons*. A bound state of a spinon and a chargon would make up an electron, so that it appears that electrons are *fractionalized* in the spin liquid phase. Similarly, bound states of two spinons would make up conventional magnetic excitations, such as the magnons and triplons. Since such bound states do not necessarily form in the spin liquid, this phase is also referred to as *deconfined* or *fractionalized*.

The simplest theoretical framework that reveals how the fractional particles can emerge in appropriate regimes of Mott insulators is provided by the \mathbb{Z}_2 gauge theory [16, 17]. This is a slave-fermion formulation of the Hubbard-like models in which a \mathbb{Z}_2 (Ising) gauge field mediates interactions between the slave particles (spinons and chargons). Basics of this approach will be reviewed in the Chapter 2, where it will be applied to a particular microscopic model. The actual mechanism of fractionalization will also be briefly discussed there. However, full details of the \mathbb{Z}_2 gauge theory are beyond the scope of this thesis, and can be found in the work of Senthil and Fisher [16, 17]. Here, it is only important to mention that another kind of excitations emerges in this theory: the \mathbb{Z}_2 gauge fields can form vortices. These vortices, called *visons*, are Ising-like objects that can be found in only two states (locally “present”

or “absent”). Since all particles carry \mathbb{Z}_2 “charge”, proliferation of visons normally prevents coherent motion of spinons and chargons, and forces them to bind into conventional quasiparticles. However, if visons are gapped, spinons and chargons are deconfined. Topological order is directly related to visons: for example, the two-valued “topological quantum number” of the RVB states in cylindrical space geometry is simply an indication of whether a vison is threaded through the axis of the cylinder (see Figure 1-4).

The RVB states and spin liquids have been initially considered in context of the cuprates, in hope that they can shed light on the puzzling pseudo-gap region of the cuprate phase diagram. One of the popular ideas for cuprate superconductivity looks at the superconducting phase as a doped spin liquid. Still, it proves very hard to pinpoint signatures of a spin liquid in actual experimental situations. Cleverly designed experiments to trap visons in superconducting cylinders [18] have not yet yielded conclusive or even encouraging results [19]. Nowadays, the spin liquid is searched for in various other materials, such as the frustrated magnets. As will be discussed in the next section, there are promising experimental indications that some materials are at least close to being true spin liquids. However, direct unambiguous measurements of topological order are hard to imagine, because there are no local probes that could be sensitive to it.

1.4 Intriguing New Materials

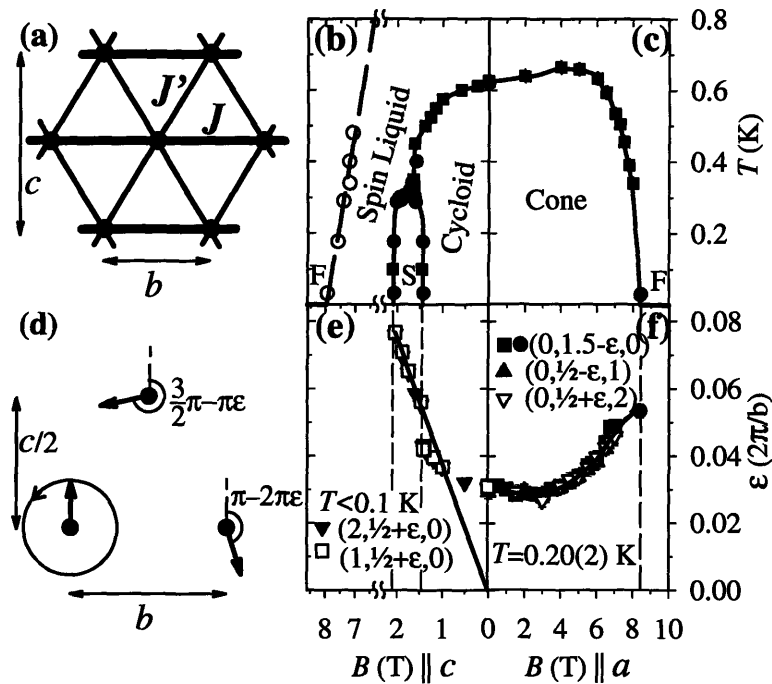
This section will briefly present recent experiments on two materials that possibly exhibit unconventional behavior, and illustrate an experimental perspective regarding unconventional phases. Both materials are Mott insulators with half-filled band, realized in frustrated geometry of the triangular lattice. Another class of promising materials will be discussed in Chapter 2.

Coldea et. al. have measured neutron scattering from large high-quality Cs_2CuCl_4 crystals [20]. The Cu^{2+} ions, which carry nearly isotropic $S = \frac{1}{2}$ Heisenberg spins, are arranged into a layered anisotropic triangular lattice whose interlayer coupling is

more than an order of magnitude below the exchange within layers (Figure 1-6(a)). An advantage of this material, from experimental point of view, is a relatively weak exchange scale that can be completely overcome by large magnetic fields. Thus, the spin Hamiltonian was determined in great detail and accuracy by studying spin-wave dispersion in externally ferromagnetized state. The phase diagram is shown in the Figures 1-6 (b) and (c). In zero magnetic field below $T = 0.62K$ spins assume a nearly coplanar incommensurate long-range order (“spiral” phase), with the common plane selected by explicit symmetry breaking. Magnetic field perpendicular to this “easy” plane smoothly cants the spins further (“cone” phase), while the parallel field stretches the spiral order until a phase transition is reached before ferromagnetic saturation. For not very large parallel fields ($B > 2.1T$) there appears to exist an unsaturated phase with no broken lattice symmetries, which is smoothly connected to the disordered phase above $T = 0.62K$ in zero field. Inelastic neutron scattering data provided reasons to speculate that this disordered phase could be a spin liquid.

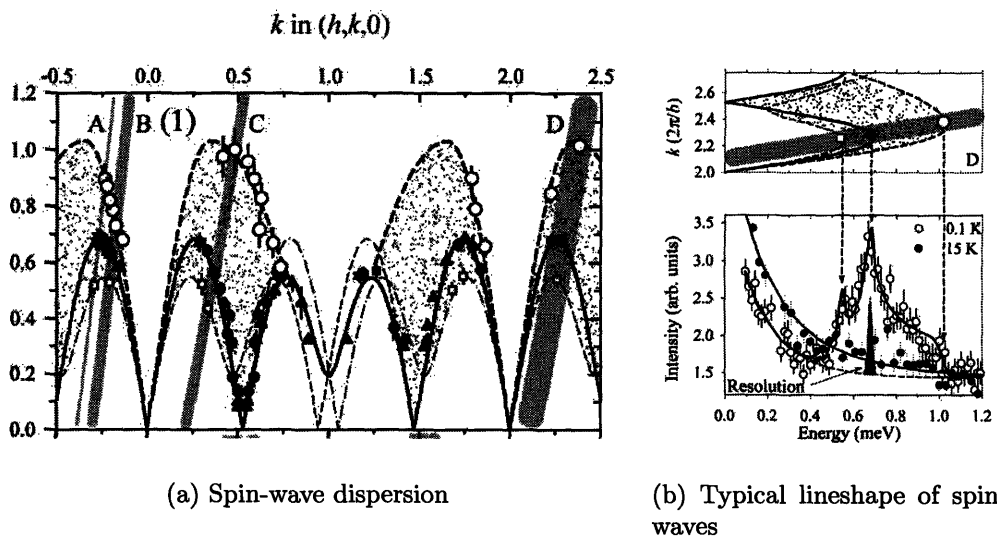
For the reference, Figure 1-7(a) shows dispersion of spin-waves in the spiral-ordered phase. There are three spin-wave modes, one polarized perpendicular to the easy plane (solid line and circles), and two polarized in-plane (thin dot-dashed lines). The top-most dashed line and open circles mark extent of scattering. This data was extracted from measured neutron scattering lineshapes, such as the one shown in Figure 1-7(b). It is important to observe that the line-shape is very asymmetric in this ordered phase, with a long high-energy tail of significant scattering. Features of such shape cannot not be explained by linear spin-wave theory, or by non-linear effects of two-magnon interactions. When magnetic order is destroyed, the spin-wave peaks disappear from the lineshapes, but not the high-energy tail. In fact, the Figure 1-8 shows that the tail is practically unaffected by the phase transition.

An intriguing possible interpretation of these observations is the following. The disordered phase could be a topologically ordered spin liquid. Its elementary excitations are spin $S = \frac{1}{2}$ spinons to which the spin $S = 1$ neutrons cannot couple directly. When a neutron scatters inelastically from a spin liquid, a pair of spinons is excited, but since the spinons are not confined such excitation quickly decays. As a conse-



(a) Anisotropic triangular lattice of Cs_2CuCl_4 ($J' \sim \frac{J}{3}$); (b), (c) Phase diagram in magnetic field, parallel (b) and perpendicular (c) to the easy plane. (d) Definition of incommensuration ε of the spiral (cycloid) order; (e), (f) Incommensuration of the spiral order as a function of magnetic field. Plots are taken from Coldea et. al., cond-mat/0007172 and cond-mat/0307025.

Figure 1-6: Phase diagram of Cs_2CuCl_4



(a) Spin-wave dispersion

(b) Typical lineshape of spin-waves

Figure 1-7: Spin-wave dispersion and lineshape in the ordered phase of Cs_2CuCl_4 .

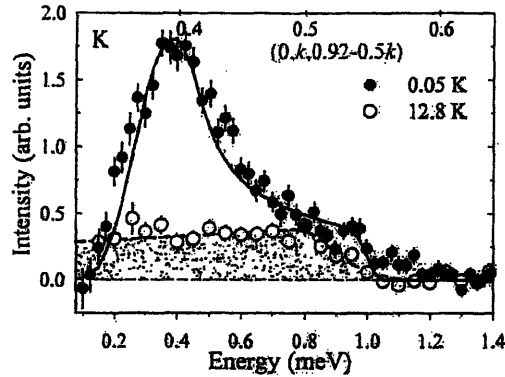
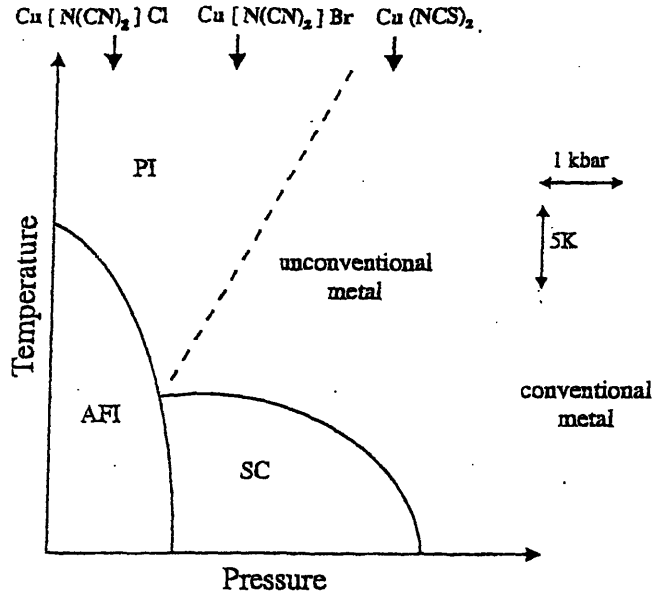


Figure 1-8: Comparison between the neutron scattering lineshapes in ordered and disordered phases of Cs_2CuCl_4

quence, scattering lineshapes are very broad. In the magnetically ordered phase, on the other hand, elementary excitations are spin-waves or bound spinon pairs. However, if the binding interactions are weak, the spinons are loosely bound and may appear free at intermediate and higher energies. This scenario can account for the robust high-energy tail. An indication that the spinons could indeed be only loosely bound in the ordered phase is the smallness of the magnetic field ($B = 2.1T$) needed to destroy the spiral order: long-range order is clearly stabilized by weak forces that can be easily overcome. Unfortunately, however, these experiments cannot unambiguously determine whether the disordered phase has topological order. Topological order cannot be directly probed and thermal fluctuations alone could yield similar effects and trivial disordered phases.

Another promising class of materials are organic superconductors $\kappa\text{-(BEDT-TTF)}_2\text{-X}$ [21]. κ stands for a particular structural phase, BEDT-TTF stands for bis-(ethylenedithia-tetrathiafulvalene) molecules, and X is one of many possible anions such as I_3 , $\text{Cu}[\text{N}(\text{CN})_2]\text{Br}$, $\text{Cu}[\text{N}(\text{CN})_2]\text{Cl}$, $\text{Cu}(\text{SCN})_2$, etc. These materials behave as layered Mott insulators at half filling on generally anisotropic triangular lattice. Their phase diagram, shown in the Figure 1-9, is very rich and quite analogous to that of the cuprates if doping is replaced by externally applied pressure. At the lowest pressures and temperatures a Neel ordered phase is found, at intermediate pressures there is a superconducting phase (most likely d-wave with critical temperature $T_c \sim$



Plot taken from McKenzie, cond-mat/9802198.

Figure 1-9: Schematic phase diagram of the BEDT-TTF organic superconductors.

10K), and for large enough pressures a Fermi liquid obtains. Like in the cuprates, there is a pseudo-gap phase in the vicinity of the Neel and superconducting regions, and it exhibits unconventional physics. A striking difference from the cuprates is a direct phase transition between the Neel and superconducting phases, and observed coexistence of Neel and superconducting order in some cases.

The frustrated geometry of these Mott insulators gives hope that the spin liquid could be found as a stable phase. In addition, Coulomb repulsion is not much stronger than electron hopping in these materials, so that additional quantum fluctuations are introduced into the effective spin model in the form of ring and multiple-spin exchange perturbations. Therefore, there is a chance that the BEDT-TTF compounds could provide platform for the physics initially envisioned in the cuprates better than the cuprates themselves: the superconductor can indeed be an RVB spin liquid frustrated by charge motion. In the cuprates charge motion happens upon doping, while in the BEDT-TTF compounds it is stimulated by applied pressure. When pressure is raised from the insulating regions, atoms become closer to each other and electron hopping amplitudes grow, until eventually the electrons become mobile and superconducting. This is reflected in the effective spin model by growing ring and multiple-spin exchange

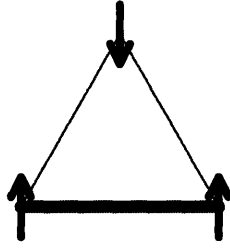
terms.

One of the BEDT-TTF compounds appears special [22]. The organic material κ -(BEDT-TTF)₂-Cu₂(CN)₃ is composed of stacked nearly isotropic triangular lattice layers, and has phases similar to those of the other compounds in its family. However, NMR, static susceptibility and $\mu - SR$ measurements have not detected any magnetic order in the regions where the Neel ordered phase is expected (at temperatures well below the exchange scale). In particular, the NMR spectra show no peak broadening or splitting as the temperature is decreased down to $32mK$, which is characteristic of antiferromagnetic ordering and observed in other BEDT-TTF compounds below their Neel temperature. If indeed a spin liquid replaces the usual Neel phase, then this material could be the first explicit and unobscured realization of a superconductor that is a doped spin liquid. At least until more direct measurements of magnetic order parameter are performed, this material remains one of the most promising candidates for the spin liquid.

1.5 Geometric Frustration

Geometrically frustrated quantum magnets (GFQM) are a class of magnetic materials, usually modeled by simple nearest-neighbor exchange Hamiltonians, in which the lattice geometry makes it impossible for spins to minimize exchange energy on every lattice bond. In other words, there are no collinear low-energy configurations of spins in GFQM (exchange energy of two spins is always minimized by a collinear arrangement). A classic example is given by the triangular lattice antiferromagnet. If one considers just one triangular plaquette and places two antialigned spins on one bond in order to minimize its exchange energy (see Figure 1-10), then no matter how the third spin is oriented it cannot be antialigned with both initially placed spins. That is, if one of the remaining bonds is chosen to have the minimum exchange energy, the other one will be maximally frustrated.

The combination of strong frustration and quantum effects makes GFQM excellent candidates for unconventional strongly correlated physics. However, geometric



If two bonds of a triangle are minimally frustrated, the third (emphasized) bond is maximally frustrated.

Figure 1-10: Frustration of spins on a triangular plaquette

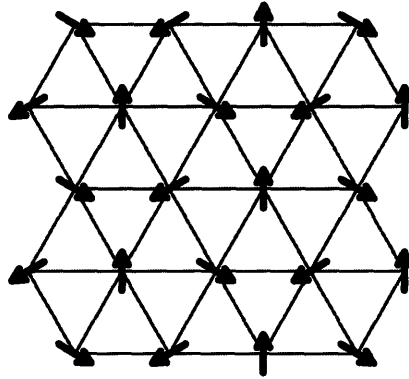


Figure 1-11: Neel order on the triangular lattice

frustration alone need not be enough to destabilize the Neel order. It is by now reasonably well established that the quantum Heisenberg model on triangular lattice has a Neel ordered ground state in which the spins lie in the same plane (Figure 1-11). This kind of order is established in a *classical* Heisenberg model on triangular lattice, and quantum fluctuations are simply not strong enough to destabilize it. The trick is to find lattices on which there is no Neel order even in the classical limit.

Most intensively studied lattices among those that do not support antiferromagnetic order in the classical limit are the so called *corner-sharing* lattices. Kagome, checkerboard and pyrochlore lattices from the Figure 1-12 are such lattices. They are composed of frustrated units, triangles and tetrahedra, which touch each other only at the corners. Such poorly connected structures create a huge degeneracy for the *classical* ground states. This can be easily illustrated on the Kagome lattice in the Figure 1-12(a). A triangular plaquette is minimally frustrated if its three spins lie in the same plane making 120° angles. The common plane can be specified by

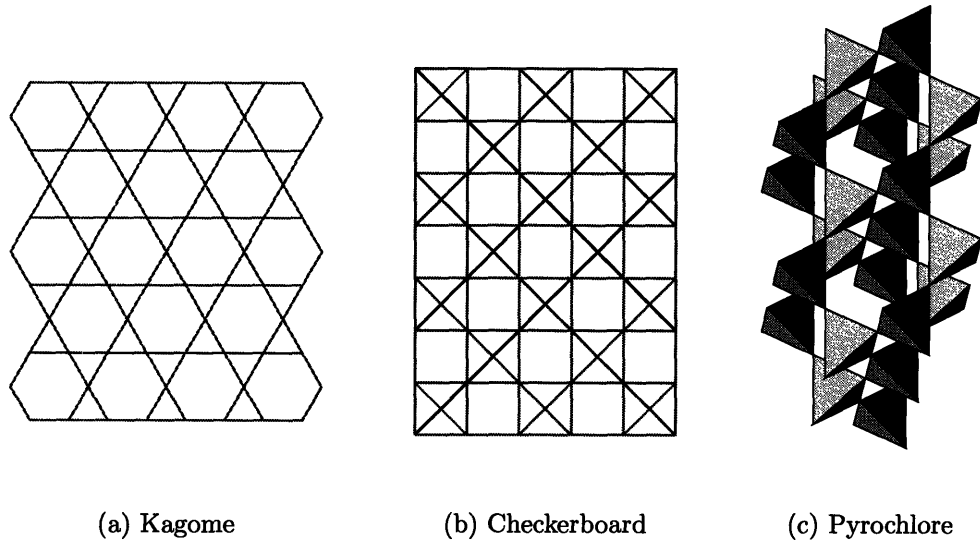
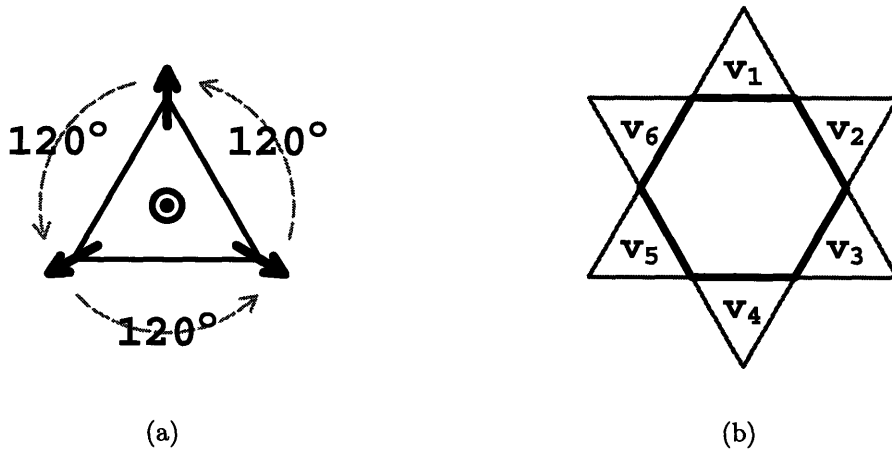


Figure 1-12: Corner-sharing lattices



(a) Chirality vector of a least frustrated state on a triangle is perpendicular to the common plane of the three spins, and oriented according to the “right hand rule” with respect to direction in which the spin orientation changes by $+120^\circ$. (b) Six chirality vectors $v_1 \dots v_6$ around a hexagonal plaquette are not independent. Starting from a site i on the hexagon, the spin S_{i+1} on the next site in clockwise direction is obtained by 120° rotation of S_i about the chirality vector v_i : $S_{i+1} = \mathcal{R}_{v_i} S_i$. Total spin transformation in going a full circle about the hexagon must be identity: $\mathcal{R}_{v_1} \circ \mathcal{R}_{v_2} \circ \mathcal{R}_{v_3} \circ \mathcal{R}_{v_4} \circ \mathcal{R}_{v_5} \circ \mathcal{R}_{v_6} = \mathcal{I}$.

Figure 1-13: Chirality vectors on the Kagome lattice

a “chirality” unit-vector perpendicular to it, whose direction (“in” or “out” of the plane) corresponds to chirality of the three spins on the triangle (see Figure 1-13(a)). Then, a minimally frustrated spin configuration on a triangle is fully specified by one spin and the chirality vector. Since two neighboring triangles share only one spin, their chiralities are independent: one triangle’s common plane can be rotated about the shared spin’s direction without energy cost. There is only one constraint per Kagome hexagon that chirality vectors of the six surrounding triangles must satisfy: these chirality vectors specify how the local spin orientation is transformed as one goes from site to site around the hexagon, and the total transformation must be identity when the whole hexagon is passed (see Figure 1-13(b)). The number of hexagons is twice smaller than the number of triangles on the Kagome lattice, so that a half of chirality vectors are ultimately independent. Consequently, there are local continuous transformations that transform one classical ground state to another, and the classical ground-state degeneracy is huge.

Quantum fluctuations generally mix the classical degenerate ground-states of frustrated systems and lift their degeneracy, no matter how weak they are. Frustrated systems are extremely sensitive even to the weakest perturbations because the potential energy (“classical” Hamiltonian) at a large energy scale essentially fails to distinguish states. Similar situation is found in Quantum Hall systems where interactions can yield exotic physics (Fractional Quantum Hall Effect) due to Landau degeneracy. The central question of frustrated quantum magnetism is what kinds of quantum phases result. What are the symmetries of the *quantum* ground-state, and what quantum numbers are carried by elementary excitations?

The possibility of finding unconventional quantum phases in frustrated magnets, such as the spin liquid, attracts more and more attention of condensed matter physicists. These systems are an excellent platform for exploring fundamental aspects of emergent low-energy physics, which can be completely different from the physics of frustrated exchange interactions at “high” energy scales. Another motivation to study them comes from efforts to engineer quantum computers: spin liquid phases (likely present in frustrated magnets) have topological order, which is a very robust

quantum number even in presence of decoherence sources [23, 24].

The field of frustrated magnetism is very young, with very few conclusive results. Experimentalists are mainly struggling to find or engineer materials that are clean enough to unambiguously exhibit unconventional behavior at attainable low temperatures. The difficulty comes from unavoidable small crystal imperfections or crystal-field effects that usually add bias to the frustrated forces and select conventionally ordered phases. Theory is also in its early stage, and most of research is conducted by numerical and ab-initio means.

1.6 Overview of the Thesis

In this thesis we will mainly consider the Kagome lattice antiferromagnets. They are perhaps the most puzzling two-dimensional frustrated magnets, and a large amount of effort is invested both by theorists and experimentalists to understand them. Chapter 2 (based on [25]) introduces the quantum Heisenberg antiferromagnetism on the Kagome lattice. It begins with a review of experimental work, ab-initio calculations and several theoretical ideas on these systems. The main goal is to present a new theory for this system, based on a \mathbb{Z}_2 gauge-theoretical approach to $SU(2)$ symmetric quantum paramagnets. It provides physical insight into the nature of its ground-state and allows one to qualitatively understand its mysterious excited “singlet” states. This theory reveals an unconventional valence-bond crystal phase in the Kagome magnet with an extremely small emergent energy scale, as well as a possible spin liquid phase. In Chapter 3 (based on [26]) we switch to quantum Ising models on the Kagome lattice. A $U(1)$ gauge theory that exploits corner-sharing structure of the Kagome lattice is applied together with duality transformations and field theory analysis. A disordered phase, unique among two-dimensional frustrated Ising magnets, is found to exist for small transverse fields, and suggested to be smoothly connected to the trivial phase for large transverse fields. In chapter 4 (based on [27]) we consider effects of total-spin conserving quantum dynamics on Kagome Ising models, and discover unconventional valence-bond ordered and spin liquid phases. A new method

is presented to seek order parameters caused by entropy of quantum fluctuations. Finally, in Chapter 5 we apply this new method to the square and triangular lattice quantum Ising models. Concluding remarks and open problems are given in Chapter 6.

Chapter 2

Kagome Quantum Heisenberg Antiferromagnet

The Kagome pattern may have entered the lives of people as an ornament a long time ago. It borrows its name from traditional Japanese bamboo-woven baskets such as the one in Figure 2-1. But in modern times, condensed matter physicists have found a way to promote this pretty and even useful design into a difficult mind-pondering problem. Through a survey of experimental and computational research we will summarize indications that the Kagome lattice quantum Heisenberg antiferromagnet (Figure 2-2) may be a spin liquid at low temperatures with strange non-magnetic excited states that seem gapless in absence of broken continuous symmetries. Then we will briefly describe several theoretical attempts to elucidate this unconventional quantum paramagnetism.

This chapter is devoted to a new qualitative theory of quantum Heisenberg antiferromagnets on the Kagome lattice. We will formulate an effective \mathbb{Z}_2 gauge theory of the puzzling non-magnetic states in this system and explore its phase diagram. Two phases will be clearly identified: a spin liquid and a valence-bond solid. We will argue that the latter agrees best with the experiments and numerics, and is most likely realized in the Kagome Heisenberg antiferromagnet. We will also discover that elementary excitations appear localized, or that they have an extremely large effective mass.

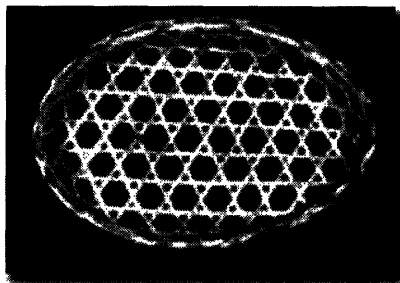


Figure 2-1: Traditional Japanese Kagome basket

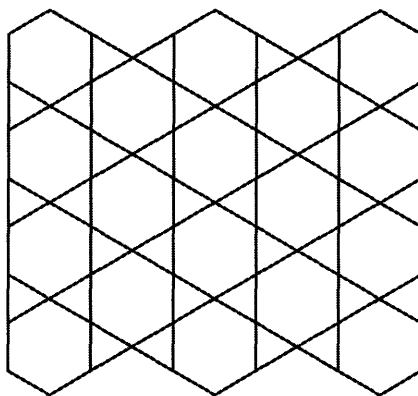


Figure 2-2: Kagome lattice

2.1 The Kagome Puzzle

2.1.1 Experiments

When it became possible to directly measure properties of cold Helium monolayer films absorbed on graphite surfaces [28], it was discovered that the ^3He atoms form a triangular lattice in the first layer, and that the second layer of atoms could also solidify, but at a smaller density than in the first layer. This second layer was found to have unusual properties. Its heat capacity C was sensitively measured as a function of temperature above $T_{\min} = 2\text{mK}$, and the entropy $S(T)$ was extracted from this data:

$$S(T) = \int_{T_{\min}}^T \frac{C(T)}{T} dT . \quad (2.1)$$

Most of entropy in the considered temperature range was coming from the spin degrees of freedom that reside on the ^3He atoms in the crystallized second layer. Surprisingly, at high temperatures when the spins decouple, about a half of the expected entropy

($k_B \log 2$ per spin) was missing [29]. This led to a speculation that some unknown but numerous spin degrees of freedom can be excited even below 2mK, or that the ground-state itself could have finite entropy. Elser proposed that this was a consequence of geometric frustration within the second layer [30]. In absence of unambiguous neutron diffraction data, he relied on the known second layer density and the triangular-lattice structure of the first layer, and suggested that the atoms nearest to each other form a Kagome lattice. The dominant exchange interactions between them defined a Heisenberg spin Hamiltonian. As magnetic order of the spins was experimentally ruled out, Elser argued that the missing entropy originated from the freedom that the spins had in forming various configurations of short-ranged singlet bonds.

Since then, the search for magnetic Kagome crystals has been steadily intensifying as part of a larger interest in frustrated systems. A crucial role in this quest has been played by chemistry and material engineering. Unfortunately, even nowadays there are no ideal Kagome materials. Most available materials have the $S \geq \frac{3}{2}$ magnetic moments, and therefore less pronounced quantum fluctuations at low temperatures than the ideal $S = \frac{1}{2}$ system. Also, it is very hard to make clean samples without missing sites (dilution), too strong inter-layer couplings, single-ion anisotropies and other small perturbations that usually obscure the interesting physics of frustration.

One of the most studied Kagome materials is the $\text{SrCr}_{9p}\text{Ga}_{12-9p}\text{O}_{19}$ compound (or SCGO); the parameter p determines amount of dilution, which cannot be completely avoided. This material is probably best modeled as a bilayer Kagome magnet where each Cr^{3+} ion carries a spin $S = \frac{3}{2}$. Neutron scattering experiments have revealed that this material does not magnetically order even at very low temperatures (down to 100mK) [31, 32]. Instead, a spin-glass behavior was typically observed below about 3 – 4K, and claimed to occur even in clean samples. However, dynamic spin fluctuations persisting well below the “freezing” temperature (at least down to 100mK) have been reported in muon relaxation measurements [33], contradicting the spin-glass picture. Absence of antiferromagnetic magnetization at temperatures that are orders of magnitude lower than the Curie-Weiss (515K) was immediately understood as a hallmark of geometric frustration. Most intriguing was the behavior of heat

capacity at the lowest accessible temperatures [34, 35]. Its power-law dependence on temperature (different than expected from a spin-glass) and the missing entropy effect indicated possible presence of gapless modes in the Kagome antiferromagnet. These modes could not be naively identified with the usual spin-wave Goldstone modes since there was no magnetic order. Furthermore, these unusual modes appeared to carry no magnetic moment: the heat-capacity was found to be virtually independent on magnetic field [35].

Even though SCGO is an exotic material worth understanding in its own right, its complex crystal structure, dilution and other imperfections prompt researchers to seek better materials. Among the promising materials with clean crystals are Jarosites, but they usually suffer from too prominent additions to the simple Heisenberg exchange, and typically have magnetically ordered low temperature phases [36, 37, 38]. A significant improvement has been achieved with the QS-ferrite $\text{Ba}_2\text{Sn}_2\text{ZnGa}_3\text{Cr}_7\text{O}_{22}$ that has essentially clean Kagome layers [39], and magnetic moments residing again on Cr^{3+} ions. This material has very similar properties to the SCGO, most notably in the puzzling low temperature behavior of heat capacity. However, the greatest challenge remains to engineer a material with $S = \frac{1}{2}$ moments. One attempt in that direction is Volborthite $\text{Cu}_3\text{V}_2\text{O}_7(\text{OH})_2 \cdot 2\text{H}_2\text{O}$ [40], which however has distorted and anisotropic Kagome structure (not planar).

2.1.2 Numerical Studies

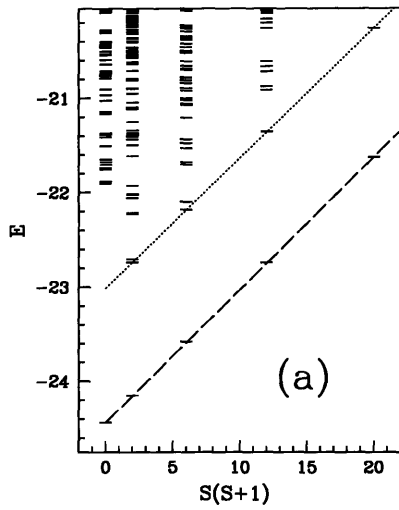
Since apparently, the interesting physics of Kagome antiferromagnets is shaped at very low energy scales, it is important to explore the nearly ideal systems. Ab-initio calculations proved to be very valuable in this respect. Several groups have studied numerically the ideal spin $S = \frac{1}{2}$ quantum Heisenberg model on finite Kagome clusters with up to 36 sites [41, 42]:

$$H = J \sum_{\langle ij \rangle} \mathbf{S}_i \cdot \mathbf{S}_j . \quad (2.2)$$

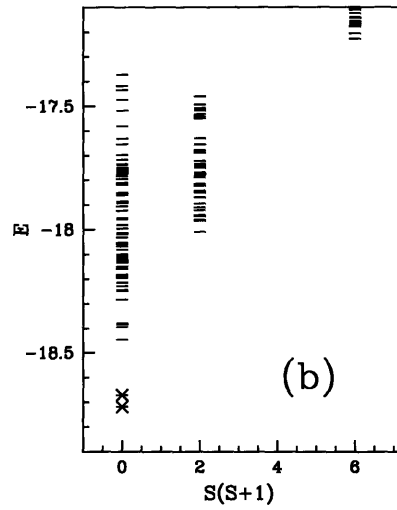
One of the first attempts was to focus on the “dimerized” states in which every spin participates in a singlet valence bond (dimer) with one of its nearest neighbors

[41]. The Heisenberg Hamiltonian was then projected to the Hilbert space spanned by such states. The obtained quantum dimer model was argued to adequately describe low-energy dynamics: other approaches already provided evidence that the correlations in the Kagome system were short-ranged, and that the spinful excitations lived at much higher energies. A perturbative analysis of this model seemed to favor broken translational symmetry in the ground-state, at least at low orders. However, it was problematic, since the “small” parameter (related to the overlap between dimer coverings) was only $\frac{1}{2}$. On the other hand, exact diagonalization of the projected Heisenberg Hamiltonian on a 36-site sample suggested that the higher-order resonances tend to restore the translational symmetry.

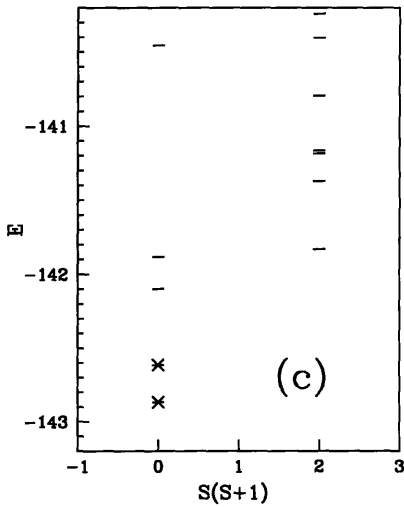
Recently, the Heisenberg models on several finite two-dimensional lattices have been exactly diagonalized and systematically studied [43, 44]. The Kagome antiferromagnet exhibited a surprisingly different behavior than practically all other systems (Figure 2-3). Calculations were done on a variety of samples with different shapes and sizes up to 36 sites [42]. This provided means to extrapolate data toward thermodynamic limit, and characterize boundary effects. Spatial correlation functions of several observables were directly obtained from the ground-state: spin \mathbf{S}_i , valence bond $\mathbf{S}_i\mathbf{S}_j$, plaquette chirality $\sum_{\langle ij \rangle} \mathbf{S}_i \times \mathbf{S}_j$, etc. They were all exponentially decaying, with correlation length smaller than the characteristic length of the sample. Therefore, the ground-state was declared a spin liquid. The spectrum supported this conclusion: an energy gap was found for the states with magnetic moment, and there were no indications of degenerate energy levels characteristic for broken translational symmetry. Using finite-size scaling the spin-gap was estimated to be about $\frac{1}{20}J$ in the thermodynamic limit. However, below the spin-gap a band of seemingly *gapless* singlet states was found. A typical separation between the singlet energy levels, including the energy of the first excited state, was three orders of magnitude smaller than the exchange coupling J . The total number of singlet states below the spin-gap was found to scale with the (even) sample size N as 1.15^N ; this exponential scaling ruled out a Goldstone mechanism for the lack of energy gap. For the sake of comparison, a spin $S = 1$ Heisenberg model was also diagonalized on the Kagome lattice, and



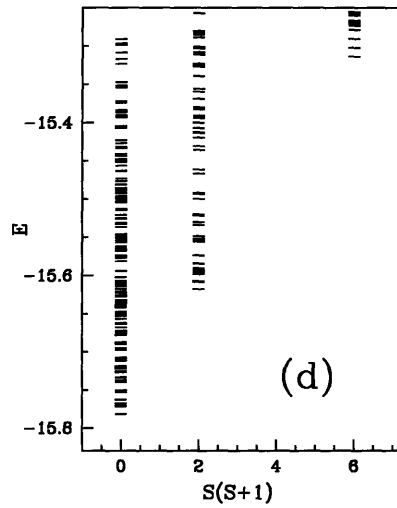
(a) Neel phase on the square lattice. Dashed lines denote Goldstone modes.



(b) Valence-bond order on the checker-board lattice. Crossed levels become degenerate in the thermodynamic limit due to broken translational symmetry.



(c) Spin liquid on the triangular lattice with ring exchange. Crossed levels become degenerate in thermodynamic limit due to topological order.



(d) Spin liquid on the Kagome lattice. Energy is measured in units of J .

Plots are taken from Lhuillier et. al., cond-mat/0110283.

Figure 2-3: Heisenberg model exact spectra on $N=36$ samples

its spectrum was clearly fully gapped. The difference between the $S = \frac{1}{2}$ and $S = 1$ cases somewhat resembles the situation found in Heisenberg chains, which further encouraged a belief that the $S = \frac{1}{2}$ Kagome antiferromagnet was indeed a spin liquid with spinon excitations. This hypothesis was tested by observing how the ground-state energy depends on the distance between two static holes deliberately placed in the sample [45]. No evidence of spinon confinement within the sample boundaries was found. Exact diagonalization was extended to finite temperatures as well, and behavior of the heat capacity essentially matched the one found in the experiments [46].

2.1.3 Questions and Some Attempts to Find Answers

The Kagome antiferromagnet is clearly not even a usual frustrated magnet. While paramagnetic behavior and absence of translational symmetry breaking are not strange in frustrated systems, abundance of *gapless* singlet states below the spin-gap is very hard to understand. Nature of these singlet states has been the central puzzle in the Kagome problem. One possibility is that the Kagome antiferromagnet is at a second-order quantum critical point, or very close to it. This in fact seems to be the case in the only other two-dimensional frustrated magnet that numerically looked as a gapless spin liquid: the Heisenberg model with ring exchange on the triangular lattice [47, 48]. However, proximity to a quantum critical point might not be a good explanation for the Kagome spectrum: all correlations in the Kagome system appear to be markedly short-ranged. If indeed there is no gap, then perhaps the strange gapless singlet states are Goldstone modes of some hidden continuous and non-magnetic long-range order. Or maybe they are some massless gauge bosons, or something completely new and undiscovered in the world around us.

Another possibility that will be explored in this thesis is that there actually is an energy gap in the singlet spectrum of the Kagome antiferromagnet. This gap would then have to be extremely small, at least about three orders of magnitude below the exchange coupling J according to the numerics. Such a scenario would not be very unusual for a very frustrated system such as the Kagome. This lattice is corner-

sharing, which makes it a barely connected network of sites. Consequently, there is substantial freedom to partially relieve frustration at “large” energy scales J , and yield new emergent physics at much lower energies. The gap is small at least due to frustration, and not (only) due to a nearby critical point. Microscopic aspects of this mechanism will be revealed in this chapter, and in the chapter 4.

Theoretical efforts so far have been mostly geared toward a “gapless spin liquid” picture. One of the most successful approaches was explored by Mila who considered a so called “trimerized” Kagome lattice [49]. If the bonds of all “up” triangles are assigned a much stronger exchange coupling than the bonds of all “down” triangles (see Figure 2-2), that perturbative methods can be used. This approach has recovered the scaling of the singlet states 1.15^N below the spin-gap. Mila argued that this number corresponds to different short-range singlet bond coverings of the Kagome lattice after the non-zero state-overlaps between such coverings are taken into account. Semiclassical large- N generalizations have also been attempted. Using the $Sp(N)$ symmetry group, which was very successfully applied to a variety of quantum magnets, Sachdev explored the phase diagram of the Kagome model [50]. This generalization of the $S = \frac{1}{2}$ problem retains the “spin-magnitude” as an independent parameter. For large spins a magnetic order appears in the ground-state. For small spins, however, the ground-state does not break any symmetries, and the elementary spin carrying excitations are unconfined spin-1/2 bosonic spinons. The $SU(N)$ symmetry group was explored by Marston and Zheng [51]: it opened up a possibility of a valence-bond order developing in the Kagome system by predicting that the singlet bonds dynamically prefer to create benzene-like resonances on the Kagome hexagonal plaquettes. Their approach was unable to verify stability of such an ordered state. The other theoretical efforts focused on phenomenological dimer models [52, 53], RVB description [54], chiral liquid description [55], hidden Goldstone mechanism [56], variational valence bond crystals [57, 58], etc.

2.2 Effective Theory at Low Energies

2.2.1 Promising Approaches to Paramagnetic Phases

It has been realized for some time now that essential properties of certain paramagnetic systems can be captured by much simpler models [59, 60, 16]. The simplification takes form of a fully frustrated quantum Ising model in transverse field (TFIM) on the lattice dual to that of the original spin system. There are several ways in which this connection can be made. The earliest approach involves a slave particle theory of quantum paramagnets on bipartite lattices. Fluctuations about the mean field state in this approach are described by a gauge theory, which in the case of frustrated magnets has a local \mathbb{Z}_2 symmetry [60]. This is then related by duality to TFIM, which is also fully frustrated due to the non-trivial Berry phase terms in the gauge theory. Another connection is through the quantum dimer description of paramagnetic phases. In appropriate limits, the quantum dimer model can be related to the fully frustrated TFIM [59]. The connection is made by noting that in zero transverse field, the ground states of the classical fully frustrated Ising model are (up to a global spin flip) in one-to-one correspondence with hard-core dimer coverings of the dual lattice. A small transverse field essentially introduces quantum resonances between dimer configurations.

In this thesis we will take a more general approach developed by Senthil and Fisher [16, 17]. It is possible to directly formulate the Heisenberg spin model on any lattice as a theory of fermionic spinons coupled to a \mathbb{Z}_2 gauge theory. In the spin-gapped quantum paramagnetic phases (such as the one found in the Kagome antiferromagnet), the spinon fields may formally be integrated out, leaving a pure \mathbb{Z}_2 gauge theory as a description of physics below the spin gap. As a matter of principle this approach can handle both the further-neighbor and ring exchange interactions. In cases of simple two-dimensional lattices the connection to the fully frustrated quantum Ising model can be established by duality transformation.

2.2.2 Effective \mathbb{Z}_2 Gauge Theory for the Singlet States

In this section we will consider general quantum Heisenberg models whose ground-states have no magnetic long-range order. We will assume that the gap to magnetic excitations (spin-gap) is large and essentially determined by the spin-exchange energy scale. Also, we will assume that there are singlet (non-magnetic) excited states well below the spin-gap, and we will derive an effective theory that describes them. Then, we will directly apply the effective theory to the Kagome problem in the next section. More detailed discussion can be found in the References [16, 17, 18].

The starting point is the Heisenberg model:

$$H = J \sum_{\langle ij \rangle} \mathbf{S}_i \cdot \mathbf{S}_j , \quad (2.3)$$

where the sum runs over the nearest-neighbor sites. The Heisenberg model can be viewed as a special limit of another model. Consider a theory of hopping spinons $f_{\alpha i}$ coupled to a \mathbb{Z}_2 gauge field σ_{ij}^z that lives on the lattice bonds:

$$H = -h_0 \sum_{\langle ij \rangle} \sigma_{ij}^x - \sum_{\langle ij \rangle} \sigma_{ij}^z \left[t_{ij} \sum_{\alpha=\uparrow\downarrow} (f_{\alpha i}^\dagger f_{\alpha j} + h.c.) + \Delta_{ij} (f_{\uparrow i}^\dagger f_{\downarrow j}^\dagger - f_{\downarrow i}^\dagger f_{\uparrow j}^\dagger + h.c.) \right] . \quad (2.4)$$

The spinon operators obey fermion anticommutation relations, and the gauge-field operators are Pauli matrices. This theory possesses a local \mathbb{Z}_2 gauge symmetry: if the signs of $f_{\alpha i}$ at a particular site i and $\sigma_{ii'}^z$ on all bonds emanating from that site are simultaneously changed, the Hamiltonian (2.4) remains invariant. Appearance of the local symmetry means that the Hilbert phase is larger than that of the Heisenberg model, and a constraint per site is needed to project back to the physical Hilbert space. This is achieved through a gauge requirement on the physical states:

$$G_i = \prod_{i' \in i} \sigma_{ii'}^x \times (-1)^{\sum_{\alpha=\uparrow\downarrow} f_{\alpha i}^\dagger f_{\alpha i}} = -1 . \quad (2.5)$$

The operators G_i are generators of the local gauge transformations at sites i , and the product runs over all bonds $\langle ii' \rangle$ emanating from the site i . In the $h_0 \gg t_{ij}, \Delta_{ij}$ limit

of (2.4), all gauge spins tend to align in the x-direction, so that the gauge requirement (2.5) fixes the number of spinons to be one-per-site. Then, the perturbation theory can be applied to (2.4), and at the second order a Heisenberg model is recovered with:

$$J \sim \frac{t_{ij}^2}{h_0}, \frac{\Delta_{ij}^2}{h_0} \quad , \quad \mathbf{S}_i = \frac{1}{2} f_{\alpha i}^\dagger \boldsymbol{\sigma}_{\alpha\beta} f_{\beta i} . \quad (2.6)$$

Physical meaning of the gauge field follows from the ground-state average of σ_{ij}^x that we derive at the second order of perturbation theory in Appendix A:

$$\langle 0 | \sigma_{ij}^x | 0 \rangle = C_1 + C_2 \langle \mathbf{S}_i \mathbf{S}_j \rangle \quad , \quad 1 \approx C_1 \gg C_2 > 0 . \quad (2.7)$$

The x-component of the gauge field is directly related to the valence-bond between two neighboring spins. Presence of fluctuations into states with $\sigma_{ij}^x = -1$ signifies a non-zero singlet amplitude on the bond $\langle ij \rangle$.

So far the \mathbb{Z}_2 gauge theory handles all Heisenberg models. In the following we assume that the spin-carrying excitations of the original Heisenberg model are gapped, and that there are many singlet states below the spin-gap. Then, an effective low-energy theory for the singlet states can be obtained by integrating out the high-energy spin degrees of freedom. There are no clear means within this approach to verify whether the spin-gap actually exists. However, in the case of the Kagome antiferromagnet, which is our primary interest, it is known from numerics that the spin-gap exists. Integrating-out the spinons yields:

$$H = -h \sum_{\langle ij \rangle} \sigma_{ij}^x - \sum_{\text{loops}} K_n \prod_{\langle ij \rangle \in \text{loop}} \sigma_{ij}^z . \quad (2.8)$$

The products involving σ^z operators are taken over all closed loops on the lattice, weighted by the loop shape and size dependent couplings K_n , and summed up. The lattice plaquettes appear at the lowest order(s), but in principle all connected clusters of bond-loops can appear at higher orders. This form of the effective Hamiltonian is required by the \mathbb{Z}_2 gauge symmetry: the sign change of $\sigma_{ii'}^z$ on all bonds emanating from any site i must leave the Hamiltonian invariant. The spin-gap results with a

local and perturbative nature of (2.8): the coupling constants K_n corresponding to the n -bond clusters are of the order of ϵx^n , where ϵ is some energy scale, and $x \ll 1$. The coupling constant h_0 has been renormalized into h , and we may expect that h should be large, although the opposite cannot be ruled out. The spinon “integration” also modifies the gauge requirement (2.5) to:

$$G_i = \prod_{i' \in i} \sigma_{ii'}^x = -1 . \quad (2.9)$$

At this stage it is not obvious why this new G_i should be -1 ; however, a more detailed path-integral approach reveals that this indeed is the case [16]. The expressions (2.8) and (2.9) define a pure *odd* \mathbb{Z}_2 gauge theory on the Kagome lattice.

If the lattice is two-dimensional and without intersecting bonds, we can easily express this theory in its dual form. Let $v_i^{x,y,z}$ be the Pauli operators defined on the sites of the dual lattice. Their relation to the \mathbb{Z}_2 gauge field of the original lattice is the following:

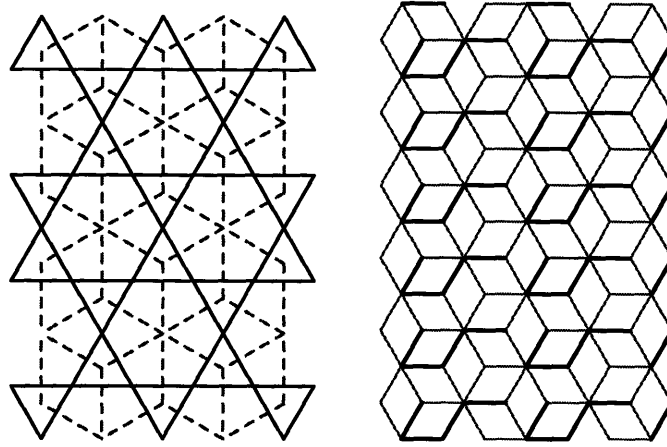
$$\sigma_{ij}^x = \epsilon_{lm} v_l^z v_m^z , \quad (2.10)$$

$$\prod_{\text{plaq.}} \sigma_{ij}^z = v_l^x . \quad (2.11)$$

In (2.10) the dual lattice bond $\langle lm \rangle$ intersects the original lattice bond $\langle ij \rangle$, while in (2.11) the dual lattice site l sits inside the elementary plaquette of the original lattice that appears in the product on the left-hand side. The numbers ϵ_{lm} are fixed to $+1$ and -1 in such a way that on every dual lattice elementary plaquette the condition of full frustration holds:

$$\prod_{\text{dual plaq.}} \epsilon_{lm} = -1 . \quad (2.12)$$

This is a consequence of the gauge requirement (2.9). In case of the Kagome lattice, one choice of sign-arrangement for ϵ_{lm} on its dual *dice* lattice is depicted in Figure 2-4. The pure \mathbb{Z}_2 gauge theory (2.8) can now be rewritten as the transverse field



(a) Kagome and its dual *dice* lattice (dashed).

(b) Full frustration on the dice lattice: bold links have $\epsilon_{lm} = -1$.

Figure 2-4: Dice lattice: duality to Kagome and full frustration

quantum Ising model on the fully frustrated dual lattice:

$$H = -h \sum_{\langle lm \rangle} \epsilon_{lm} v_l^z v_m^z - \sum_{\text{clusters}} K_n \prod_{l \in \text{cluster}} v_l^x . \quad (2.13)$$

The “kinetic energy” terms contain in general the products of v_l^x on various connected clusters of the dual lattice sites.

2.2.3 Effective Theory of the Kagome Heisenberg Model

Specializing to the Kagome lattice, we have the following pure \mathbb{Z}_2 gauge theory that describes the singlet sector below the spin-gap:

$$H = -h \sum_{\langle ij \rangle} \sigma_{ij}^x - K_3 \sum_{\Delta} \prod_{\Delta} \sigma_{ij}^z - K_6 \sum_{\square} \prod_{\square} \sigma_{ij}^z - K_{3+3} \sum_{\bowtie} \prod_{\bowtie} \sigma_{ij}^z - \dots . \quad (2.14)$$

Only the three smallest loop terms have been explicitly written: triangles (K_3), hexagons (K_6), and connected pairs of triangles that will be called bowties (K_{3+3}). The bowties are just as important as hexagons since they have the same size.

The dual theory on the dice lattice is (see Figure 2-4):

$$H = -h \sum_{\langle lm \rangle} \epsilon_{lm} v_l^z v_m^z - K_3 \sum_{l_3} v_{l_3}^x - K_6 \sum_{l_6} v_{l_6}^x - K_{3+3} \sum_{(l_3 m_3)} v_{l_3}^x v_{m_3}^x - \dots, \quad (2.15)$$

where l_3 and l_6 denote the 3 and 6-coordinated dice sites respectively (dual to the Kagome triangles and hexagons), and $(l_3 m_3)$ denotes pairs of next-nearest-neighbor 3-coordinated sites.

These theories were obtained solely by symmetry arguments, and values of the coupling constants are not available. Therefore, the consequent analysis has to cover all relevant limits. The section 2.2.4 deals with $h \gg K_3, K_6, \dots$ limit; as will become apparent, this limit describes physics of short-range singlet bonds. The section 2.2.5 deals with the opposite $h \ll K_3, K_6, \dots$ limit where the quantum fluctuations in the singlet sector are very strong. Some analytical arguments in favor of the former limit are provided in Appendix B.

2.2.4 The Limit of Short-Range Singlet Bonds

Here we begin analysis of the effective \mathbb{Z}_2 gauge theory (2.14) for the low-lying singlet states of the Kagome antiferromagnet. We are particularly interested in the $h \gg K_3, K_6, K_{3+3}, \dots$ limit. Using a degenerate perturbation theory in small $\frac{K_n}{h}$ we will construct a quantum dimer model that describes dynamics of the short-range singlet bonds (dimers), and explore its ground state and excitations.

When all couplings K_n are set to zero, any gauge field configuration of $\sigma_{ij}^x = \pm 1$ at every Kagome bond is an eigenstate of (2.14). Every $\sigma_{ij}^x = -1$ bond costs a large energy h and may be visualized by a dimer. The gauge constraint (2.9) then requires that an odd number of dimers emanate from every site. Therefore, the unperturbed ground-states will simply be the hard-core dimer coverings of the Kagome lattice. From (2.7) we see that this limit describes dynamics of short-range singlet bonds (dimers).

The non-zero couplings K_n introduce quantum fluctuations between different dimer coverings and lift the ground-state degeneracy. We build perturbatively the

low-energy effective theory by restricting the initial and final states of all processes to be the hard-core dimer coverings. The dimers are moved in such processes only along the *flippable* loops (see Figure 2-5 for explanation). The Kagome lattice has a remarkable property that regardless of the actual hard-core dimer covering, there is always one elementary flippable loop realized on each hexagon, enclosing that hexagon and an even number of surrounding triangles [41]. It is convenient to introduce the following terminology: if a plaquette carries no dimers on its bonds, we will call it a *defect* plaquette, and if it carries a flippable loop on its bonds, we will call it *perfect*. Apparently, a plaquette can be perfect only if it has an even number of bonds. Some examples of the elementary flippable loops and this terminology are shown in Table. 2.1.

Perturbative terms in the effective theory are obtained as outlined in the Appendix C. The lowest order terms are dimer flips on the single plaquettes. The K_3 and K_{3+3} terms cannot connect between two hard-core dimer coverings, so that to the lowest order the effective theory is:

$$H = -Nh - K_6 W_6 , \quad (2.16)$$

where N is the number of Kagome sites, and W_6 is the *kinetic energy* operator of the perfect hexagons:

$$W_6 = \sum_{\diamond} \left(\left| \begin{array}{c} \star \\ \star \\ \star \end{array} \right\rangle \left\langle \begin{array}{c} \star \\ \star \\ \star \end{array} \right| + \left| \begin{array}{c} \star \\ \star \\ \star \end{array} \right\rangle \left\langle \begin{array}{c} \star \\ \star \\ \star \end{array} \right| \right) . \quad (2.17)$$

The sum runs over all hexagonal plaquettes of the Kagome lattice. Quantum fluctuations created by this kinetic term yield the ground states in which the number of resonating perfect hexagons is maximized. This is an exact statement, since all perfect hexagon flips commute with one another: as illustrated in Figure 2-6, the perfect hexagons can never be nearest neighbors, and therefore cannot affect one another. In order to gain more insight about these states, we want to recall some observations from References [30] and [51]. The total number of dimers in a hard-core dimer covering on the Kagome lattice is $N_2 = N/2$, and the number of triangular plaquettes is $N_{\Delta} = 2N/3$, so that $N_2 = 3N_{\Delta}/4 = (1 - 1/4)N_{\Delta}$. Since a trian-

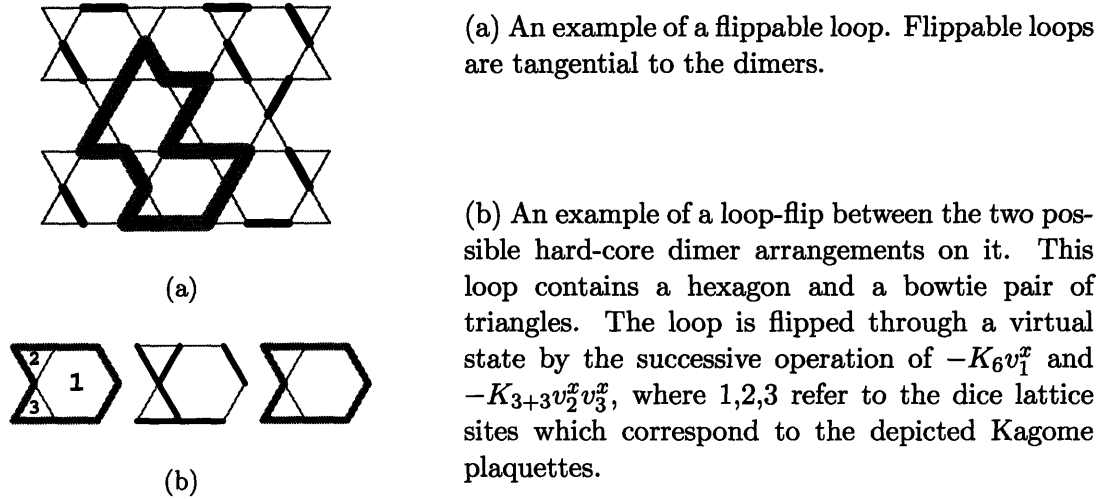
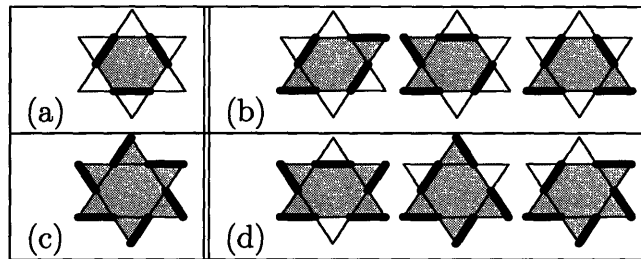
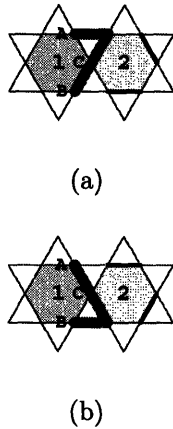


Figure 2-5: Flippable loops and dimer moves



(a) flippable hexagon, (b) flippable 8-bond loops (rhombus, arrow and trapeze, from left to right), (c) the star, (d) flippable 10-bond loops. The elementary flippable loops by definition enclose only one hexagon. For arbitrary dimer covering, a unique elementary flippable loop can be found on every hosting hexagonal plaquette: it goes through all the hexagon sites, and includes those surrounding triangles which hold a dimer on a bond that does not belong to the hexagon. The hexagon in (a) is *perfect*, while the hexagon in (c) is a *defect* hexagon. The length of the elementary loop is directly related to the number of dimers sitting on the hexagon, which is equal to the number of *defect* triangles around the hexagon: 3 in (a), 2 in (b), 1 in (d), and none in (c).

Table 2.1: Elementary flippable loops on the Kagome lattice

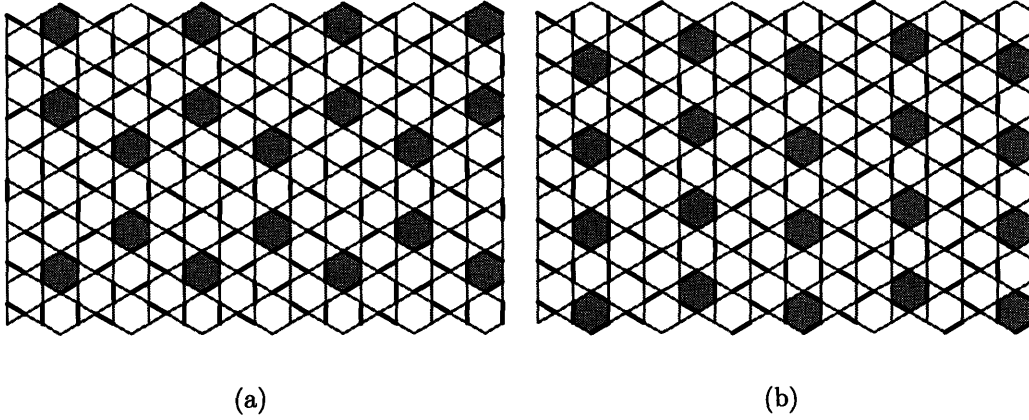


Two perfect hexagons cannot be nearest neighbors, and the perfect hexagon flip does not affect length of any other elementary flippable loop. Consider a perfect hexagon 2 being flipped from the configuration (a) to (b). The flippable loop on the hexagon 1 has to go through the sites A, B, and C, and therefore pass through the shaded bonds in order to be tangential to the dimers. As a consequence, it has to include at least one triangle, so that it cannot be a perfect hexagon, and also, its length is not affected by the flip on the hexagon 2.

Figure 2-6: Neighboring perfect hexagons

gle can carry at most one dimer, we see that one quarter of all triangles are the *defects* in any hard-core dimer covering: $N_{\Delta d} = N_{\Delta}/4$. Next, we note that every perfect hexagon has exactly three neighboring *defect* triangles, and since no two perfect hexagons can be neighbors, those defect triangles are not shared between them. It follows from this that the total number of perfect hexagons has an upper bound: $N_{\text{Op}} \leq N_{\Delta d}/3 = N_{\Delta}/12 = N_{\text{O}}/6$. The maximum possible density of perfect hexagons is one per six hexagonal plaquettes, and it can be achieved in a variety of ways. In Figure 2-7 we show two characteristic possibilities, (a) the *honeycomb*, and (b) the *stripe* state. In general, these states are constructed by placing the perfect hexagons as close as possible to each other. The closest they can be is the next nearest neighbors, provided that between them is another hexagonal plaquette, and not a bowtie pair of triangles (\bowtie), because in the latter case there would have been a site (the center of the bowtie) involved in no dimers. This rule allows one to arrange perfect hexagons in strings that may be straight, bent at an angle of 120° , or forked into two new strings at the 120° angles. The *stripe* state is an example of straight strings, while the *honeycomb* state has strings forking at each perfect hexagon.

Before we proceed with the next order of perturbation theory, we need to make some additional remarks. If we look at the elementary flippable loops realized on various hexagonal plaquettes in Figure 2-7, we observe that between every two closest perfect hexagons there is an 8-bond flippable loop, right on the sides of the strings



Two hard-core dimer patterns that maximize the number of perfect hexagons: (a) honeycomb pattern; (b) stripe pattern. The perfect hexagons are shaded to guide the eye. Note that the 8-bond flippable loops appear only as “connections” between the perfect hexagons, and the 10-bond flippable loops touch exactly one perfect hexagon. The honeycomb pattern has the 12-bond flippable loops, the stars: they sit inside the honeycomb cells.

Figure 2-7: Maximum number of perfect hexagons

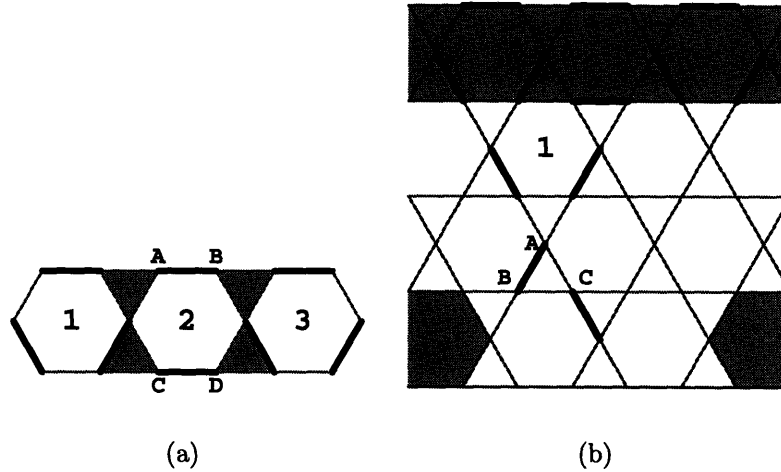
there are only 10-bond flippable loops, and in the case of the *honeycomb* state, there is a 12-bond *star*-shaped flippable loop sitting at the center of every honeycomb cell. Also, one never finds an *arrow*-shaped 8-bond flippable loop between two perfect hexagons. These are quite general features of the states with the maximum number of perfect hexagons, which we explain in more detail in the Fig. 2-8.

At the second order of perturbation theory, we need to include the combinations of two K_3 , K_6 , and K_{3+3} flips. One of them is the flip on the *arrow* shaped 8-bond flippable loop (a hexagon, and a bowtie: see Fig.2-5(b)):

$$\Delta H_{\text{ar}}^{(2)} = -\frac{K_6 K_{3+3}}{2h} W_8^{(\text{ar})} ; \quad (2.18)$$

$$W_8^{(\text{ar})} = \sum_{\square} \left(\left| \begin{array}{c} \star \\ \star \end{array} \right\rangle \left\langle \begin{array}{c} \star \\ \star \end{array} \right| + \left| \begin{array}{c} \star \\ \star \end{array} \right\rangle \left\langle \begin{array}{c} \star \\ \star \end{array} \right| + \text{rotations} \right) .$$

All other allowed combinations flip the same plaquette twice, leaving the dimer configuration unchanged. A hexagonal plaquette can be flipped twice if it is not a flippable loop: it has to be the part of an elementary flippable loop with 8, 10, or 12 bonds. As the potential energy associated with the flip is different in each case, we need to know the numbers U_n of the n -bond flippable loops in the dimer configuration in order to



(a) The hexagonal plaquette between a pair of perfect hexagons always hosts an 8-bond flippable loop. Once the perfect hexagons 1 and 3 are placed, the only way for all of the sites A,B,C, and D to be involved in dimers is to pair A,B and C,D. Then, the hexagonal plaquette 2 carries two dimers on its bonds, and therefore hosts an 8-bond flippable loop. However, it cannot be an *arrow*-shaped loop (see Table 2.1), because both shaded bowties must have one normal and one *defect* triangle due to the perfect hexagons, and an *arrow*-shaped loop must contain a bowtie with two normal triangles.

(b) Only 10-bond flippable loops surround the perfect hexagon strings. Consider a string, and a neighboring hexagon 1. One cannot put there a 6-bond flippable loop, because this would be a perfect hexagon next to another perfect hexagon from the string. A *star*-shaped 12-bond flippable loop is not an option either, because this hexagon always has one neighboring *defect* triangle from the string. There is only one way to place two dimers on the bonds of hexagon 1 in attempt to create an 8-bond flippable loop on it. However, this requires the site A to pair with either B or C, which in turn makes it impossible for another string of perfect hexagons to take its normal place. At least a spot is lost for a perfect hexagon, and this costs energy K_6 ! Similar is true for the corners of the outward bending strings, while this issue does not occur for the inward bending, as in the case of the *honeycomb* state, since 10-bond loops are the only choice there.

Relative positions of various kinds of elementary flippable loops can also be established by using the relation between their length and the number of *defect* triangles around them (Table 2.1). When the number of *perfect* hexagons is maximized, all *defects* are placed around them ($N_{\Delta d} = 3N_{\text{Op}}$), and the length of any flippable loop depends on the number of its perfect hexagon neighbors.

Figure 2-8: Restrictions imposed by the dense perfect hexagons

write the appropriate contribution in the effective theory:

$$\Delta H_{\square \times 2}^{(2)} = -\frac{K_6^2}{4h} U_8 - \frac{K_6^2}{8h} U_{10} - \frac{K_6^2}{12h} U_{12} . \quad (2.19)$$

The number operators (dimer potential energy) U_n are:

$$\begin{aligned} U_6 &= \sum_{\square} (|\star\rangle\langle\star| + |\star\rangle\langle\star|) \quad (2.20) \\ U_8 &= \sum_{\square} (|\star\rangle\langle\star| + |\star\rangle\langle\star| + |\star\rangle\langle\star| \\ &\quad + |\star\rangle\langle\star| + |\star\rangle\langle\star| + |\star\rangle\langle\star| + \text{rotations}) \\ U_{10} &= \sum_{\square} (|\star\rangle\langle\star| + |\star\rangle\langle\star| + |\star\rangle\langle\star| \\ &\quad + |\star\rangle\langle\star| + |\star\rangle\langle\star| + |\star\rangle\langle\star| + \text{rotations}) \\ U_{12} &= \sum_{\square} (|\star\rangle\langle\star| + |\star\rangle\langle\star|) \end{aligned}$$

We treat the triangular plaquette double flips similarly. Every triangle can be either a *defect*, or normal in any dimer covering. The *defects* contain no dimers, while the normal triangles contain one dimer. If their numbers are $N_{\Delta d}$ and N_{Δ} respectively, then the contribution of the triangle double flips is:

$$\Delta H_{\Delta \times 2}^{(2)} = -\frac{K_3^2}{6h} N_{\Delta d} - \frac{K_3^2}{2h} (N_{\Delta} - N_{\Delta d}) = -\frac{K_3^2}{h} \frac{5N}{18} . \quad (2.21)$$

We have used the identities $N_{\Delta d} = N_{\Delta}/4$, and $N_{\Delta} = 2N/3$, where N is the number of Kagome sites. Finally, it remains to consider the double flips of bowties (\bowtie). They can contain either one *defect* triangle or none. For every *defect* there are three bowties containing it, while the total number of bowties in the lattice is equal to the number of Kagome sites N . Therefore, the contribution of the bowties is:

$$\Delta H_{\bowtie \times 2}^{(2)} = -\frac{K_{3+3}^2}{8h} 3N_{\Delta d} - \frac{K_{3+3}^2}{4h} (N - 3N_{\Delta d}) = -\frac{K_{3+3}^2}{h} \frac{3N}{16} . \quad (2.22)$$

We see that the triangle and bowtie contributions reduce to mere constants for arbitrary dimer covering. Then, it pays to investigate closer the contribution of double hexagon flips. First, we want to express the number of defect triangles in terms of the U_n operators. This can be achieved by noting that every type of elementary flippable loop has a fixed number of both kinds of triangles (see Table 2.1): $N_{\Delta d} = (3U_6 + 2U_8 + U_{10})/3$, where the factor of $1/3$ corrects the over-counting of triangles shared between the elementary flippable loops. Using this, we can eliminate U_8 and U_{10} from (2.19):

$$\Delta H_{\square \times 2}^{(2)} = -\frac{K_6^2}{12h}U_{12} + \frac{3K_6^2}{8h}(U_6 - N_{\Delta d}) . \quad (2.23)$$

Now, we can add (2.18, 2.23, 2.21, 2.22), and write the effective theory to the second order:

$$H = -Nh - K_6 W_6 - \frac{K_6 K_{3+3}}{2h} W_8^{(\text{ar})} + \Delta H_{\Delta \times 2}^{(2)} + \Delta H_{\square \times 2}^{(2)} + \Delta H_{\bowtie \times 2}^{(2)} . \quad (2.24)$$

The ground-state of this Hamiltonian can be obtained by the *second level* perturbation theory in which the unperturbed Hamiltonian is given by (2.16). The $W_8^{(\text{ar})}$ term slightly spreads the ground-state wavefunction from the sharp *honeycomb*, *stripe*-like or similar state, but the correction to the ground-state energy due to this term appears only at the higher orders: none of the unperturbed ground-states with maximum number of perfect hexagons can contain the *arrow*-shaped 8-bond flippable loops, and even if they could, the flip would destroy the two neighboring perfect hexagons, so that $\langle 0 | W_8^{(\text{ar})} | 0 \rangle = 0$. Therefore, the energy shift is dominated by the *potential energy* part of (2.24) involving U_n operators. This part fully commutes with (2.16): the perfect hexagon flips W_6 cannot change the length of any elementary flippable loop (see Fig. 2-6), and the U operators simply count the number of flippable loops with the given length. Only the double hexagon flips (2.23) select the actual ground state: when the number of perfect hexagons is maximized, the U_6 operator behaves as a number, taking the value $N_{\square}/6 = N/18$, so that the potential energy is controlled by the number of the 12-bond *star*-shaped flippable loops. The *honeycomb* state

(Fig. 2-7(a)) maximizes their number, and therefore the quantum fluctuations select it as the ground-state. The degeneracy of this ground-states is exponentially large in the system size, at this order of perturbation theory. It comes from the freedom to flip any *star*-loop without energy cost.

Various new kinetic and potential terms appear in the effective dimer model at the higher orders. They further spread the ground-state wavefunction, but its main component remains the *honeycomb* structure. The ground-state degeneracy is finally lifted when the *star* kinetic terms appear (only the *star*-flips do not destroy the perfect hexagons):

$$W_{12} = \sum_{\circlearrowleft} (|\star\rangle\langle\star| + |\star\rangle\langle\star|) . \quad (2.25)$$

In terms of K_n/h , this first happens at the fourth order by combining the flips on one hexagon and three bowties:

$$\Delta H_{\text{star}}^{(4)} \propto -\frac{K_6 K_{3+3}^3}{h^3} W_{12} . \quad (2.26)$$

However, since in principle it might happen that $K_{3+3} \ll K_3^2/h$, the dominant *star* kinetic term may occur when a hexagon flip is combined with six triangle flips:

$$\Delta H_{\text{star}}^{(7)} \propto -\frac{K_6 K_3^6}{h^6} W_{12} . \quad (2.27)$$

In any case, the ground-state will be the *honeycomb* state with resonating perfect hexagons and stars, while the lowest lying excitations will be gapped. The gap is very small, of the order of $K_6 K_{3+3}^3/h^3$ or $K_6 K_3^6/h^6$, which is much smaller than the spin exchange J , since $K_n < J$ in the effective theory (2.14). The only remaining degeneracy is 12-fold, due to the broken translational symmetry (the honeycomb unit-cell has 12 hexagonal plaquettes).

It is also interesting to understand this ground-state in the dual Ising picture. A dimer on the Kagome lattice represents a frustrated bond of the dual Ising model on the dice lattice. Every Kagome dimer covering corresponds to two Ising spin configurations on the dice lattice, related to each other by the global spin-flip. If the

Kagome dimers are flipped along a flippable loop, the corresponding effect in the dual picture is the simultaneous flip of all dice Ising spins that sit “inside” the Kagome plaquettes enclosed by that flippable loop. Now we can translate the description of the ground-state. Every resonating perfect hexagon is a *flippable* spin on a 6-coordinated site of the dice lattice, in the state of equal superposition of “up” and “down“. Every resonating star-shaped flippable loop is a *flippable* cluster of seven Ising spins that coherently fluctuate between two states of defined spin orientation (one spin is on a 6-coordinated site, and the other six are on the surrounding 3-coordinated sites). However, certain dimers are static in the ground-state: two of them reside between every pair of neighboring perfect hexagons. In order to describe them in the dual language, it is sufficient to arrange the corresponding Ising spins on the dice lattice in some appropriate static configuration. Therefore, the ground-state breaks the global spin-flip symmetry of the dual Ising model, with 3/4 of all spins assuming a fixed orientation, and 1/4 of spins fluctuating. The translational symmetry is broken only by the arrangement of frustrated bonds, and locations of the fluctuating spins; there need not be actual long-range order in terms of the orientation of non-fluctuating spins, since this depends on a relatively arbitrary assignment of $\epsilon_{lm} = \pm 1$ in (2.15). In the dual language, this state is formed first by minimizing the number of frustrated bonds, and then by maximizing the number of flippable spins which gain the kinetic energy from the transverse field.

Finally, note that this phase is stable against the weak fluctuations of the large loops that have been ignored from the Hamiltonian (2.14). The stability has essentially been demonstrated in the perturbation theory.

2.2.5 The Limit of Strong Singlet Fluctuations

The limit $h \ll K_3, K_{3+3}, K_6 \dots$ is convenient to analyze directly in the frustrated Ising model on the dice lattice (2.15). If h vanishes, then all Ising spins in (2.15) are aligned with the transverse fields in the x -direction, making the ground-state completely disordered and uncorrelated in terms of v_i^z . An elementary excitation is created when one spin is flipped against the transverse field. These excitations

are \mathbb{Z}_2 vortices, or visons according to (2.11), and they are localized and gapped. For finite h , the visons can in principle hop between sites and lower their gap by acquiring kinetic energy. However, for small h the gap is guaranteed to persist, and the ground-state remains disordered, and unique.

In the following we will assume that K_3 and K_6 are positive, and we will ignore K_{3+3} and other terms for simplicity. One way to study the properties of the excited states is to consider perturbatively the effective theory for one vison. At the lowest order, this effective theory is simply the nearest neighbor hopping Hamiltonian:

$$H = -h \sum_{\langle lm \rangle} (|l\rangle \epsilon_{lm} \langle m| + h.c.) + 2K_3 \sum_{l_3} |l_3\rangle \langle l_3| + 2K_6 \sum_{l_6} |l_6\rangle \langle l_6| ,$$

where l_3 and l_6 are the 3 and 6-coordinated sites of the dice lattice, and $|l\rangle = v_l^z |0\rangle$. It can be easily diagonalized in the momentum space by working with the 6-site elementary cells of the tile in Fig. 2-4. It was shown in the reference [61] that for $K_3 = K_6$ the energy spectrum of this model is completely dispersionless and divided into three macroscopically degenerate levels. Remarkably, this remains true for arbitrary values of K_3 and K_6 (and K_{3+3}):

$$\begin{aligned} E_1 &= 2K_6 , \\ E_2 &= 2K_3 - \sqrt{6}h , \\ E_3 &= 2K_3 + \sqrt{6}h . \end{aligned} \tag{2.28}$$

Therefore, the visons are localized at the lowest order of perturbation theory, in the similar way to a single electron in magnetic field (this analogy does not hold for general lattices). A natural question to ask is whether this localization persists to higher, or maybe all orders of perturbation theory. We try to find an answer by considering the time-ordered Green's function in the interaction picture:

$$iG(l, m; t_l, t_m) = \frac{\langle 0|T v_l^z(t_l) v_m^z(t_m) S|0\rangle}{\langle 0|S|0\rangle} , \tag{2.29}$$

where T is the time-ordering operator, and:

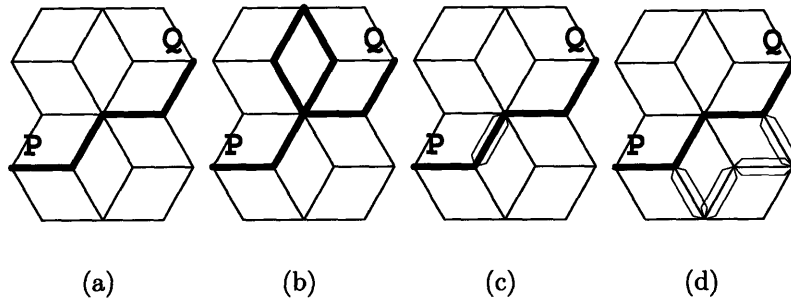
$$S = T \exp\left(-i \int_{-\infty}^{\infty} dt H'(t)\right),$$

$$v^z(t) = e^{iH_0 t} v^z(0) e^{-iH_0 t}. \quad (2.30)$$

The perturbation H' is the vison-hopping part of (2.15), while H_0 is the vison potential energy. The expansion of S in (2.29) generates many vacuum expectation values of the products of v^z operators, which are then integrated over the internal time variables. These vacuum expectations are easy to calculate for any given set of time moments: the $v^z(t)$ operators can be evolved to $t = 0$ when they simply flip a spin, while the evolution parts $e^{\pm iH_0 t}$ only introduce a phase factor, since they always act on a H_0 eigenstate. We immediately see that a vacuum expectation which appears in (2.29) can be non-zero only if the product of v^z is made from a path of bonds bridging between the sites l and m . We only need to turn our attention to the *connected* clusters of bonds.

Consider a particular pair of sites P and Q , and the n^{th} order term in the perturbative expansion of $iG(P, Q; t_P, t_Q)$. Its value, proportional to h^n , is contributed separately by all paths of the length n between P and Q . The two paths cancel out each other if they enclose an odd number of rhombic dice plaquettes: the total “flux” through the loop formed by them is π , that is, $\prod_{\text{loop}} \epsilon_{lm} = -1$. Let us distinguish the two types of paths: *simple* and *complex*. The *simple* paths never visit any site more than once, while the *complex* paths visit at least one site more than once. The *complex* paths can be obtained from the *simple* ones by adding the loop segments to them, where a loop may take some bonds an even number of times. We illustrate this in the Fig. 2-9.

For any given *simple* path between some two *distant* sites P and Q , we can construct a path that cancels it out. In demonstrating this, we also explore what the sufficient distance between the P and Q is. (a) Consider first the simple paths that contain only the three 6-coordinated sites depicted in the Fig. 2-10(a). If the path goes through the sites $A_1 - B_1 - A_2$, and never visits the site B_2 , then it can



(a) Simple path; (b) Complex path with a loop segment; (c) Complex path with a bond visited three times; (d) Complex path with a segment visited twice.

Figure 2-9: Examples of the dice lattice paths between two sites

be canceled by the path that goes through $A_1 - B_2 - A_2$, and continues beyond as the original one. The only way to avoid the path cancellation is to visit all the depicted B -sites, and this can be done only by choosing the path's end points among them (otherwise, more 6-coordinated sites would belong to the path). We see that in this case the path's end-points are the next-nearest-neighbors. (b) Next, consider the paths that contain the four 6-coordinated sites depicted in the Fig. 2-10(b). For the same reason as before, all the B -sites must be included in the path, otherwise there will be another path that cancels it out. But this time, in attempting to do so we would have to introduce another 6-coordinated site into the path (the remaining neighbors of the depicted B -sites - analyzed as the case c), since the path-ends can take only two out of three B -sites left "outside" of the straight segment of the path. We can already see that all simple paths with more than three 6-coordinated sites arranged in a chain cancel out. This chain may, of course, bend, but somewhat special situation occurs when a triplet of 6-coordinated sites (A_1, A_2, A_3) of the path sits on the three touching plaquettes, as shown in the Fig. 2-10(c). (c) Again, all the B -sites must be visited, or the path is canceled out, and one of them must be a path's end-point if no other 6-coordinated sites may belong to the path. Since all B -sites are now the next-nearest-neighbors, we may try to choose another 3-coordinated site further away as the path's end-point, and construct the path like the one plotted with the solid line in the Fig. 2-10(c). But, again there is a path that cancels it out, and it is plotted with the dashed line. By trying to add more 6-coordinated sites to the case

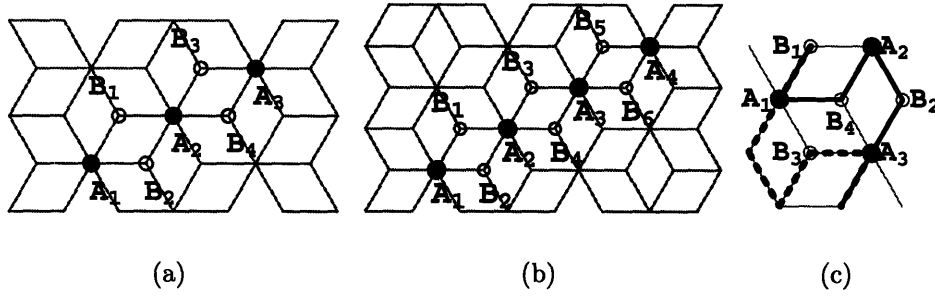


Figure 2-10: Path cancellation on the dice lattice

(c)) we would only have too many B -sites to cover as before. In conclusion, all the simple paths whose end-points are separated more than the next-nearest-neighbors must cancel out.

Many complex paths are also canceled - namely, whenever we can construct another path of the same topology, and between the same end-points that encloses an odd number of plaquettes with the original one. However, for some paths this construction is not possible, and a different approach is needed in order to see whether they are canceled out or not. The smallest such path appears at the 12th order of the perturbation theory, and it is shown in the Fig. 2-9(d). Below the 12th order of perturbation theory the Green's function between distant sites (and arbitrary times) strictly vanishes, and the visons appear strictly localized.

At present, we cannot tell whether the vison localization persists to all orders. If not, they would have an extremely large inertia in the small- \hbar limit, and this would be a novel mechanism for creation of the large quasi-particle effective mass.

2.2.6 Magnetic Excitations and Confinement

We have seen that the \mathbb{Z}_2 gauge theory on the Kagome lattice (or equivalently its dual frustrated Ising model on the dice lattice) supports at least two phases: one with long-range valence-bond order, and one disordered. The order parameter was defined in terms of the singlet states only. However, these two phases have radically different magnetic excitations as well.

The spin carrying excitations must be built from the spinon operators in the

spinon \mathbb{Z}_2 gauge theory (2.4). From the gauge symmetry of (2.4) we conclude that the spinons carry a \mathbb{Z}_2 charge. Therefore, by moving a spinon around a \mathbb{Z}_2 vortex, the spinon will pick a phase π , that is change sign. Physically, this is due to the fact that a \mathbb{Z}_2 antivortex and vortex are indistinguishable, so that moving a spinon around two visons, which picks twice the phase, should change nothing. In absence of visons, the spinons can coherently move through the lattice as free $S = \frac{1}{2}$ particles. However, if the visons proliferate, than they obstruct coherent motion of single spinons (pairs of different paths between the same end-points destructively interfere). In such circumstances, only a bound pair of spinons, an $S = 1$ particle without \mathbb{Z}_2 charge, can coherently propagate through the lattice: the spinons are said to be *confined*.

The disordered phase found in the section 2.2.5 is *deconfined*, or a *spin liquid*: the visons are gapped, so that fermionic spinons exist as free (gapped) quasiparticles. In contrast, the valence-bond ordered phase from the section 2.2.4 is *confined*, and its elementary magnetic excitations are bosonic gapped magnons (also called triplons). The latter can be naively guessed from the fact that the global Ising symmetry is broken in the dual vison theory on the dice lattice: this generally indicates proliferation of visons. However, a precise reason follows from consideration of energy it takes to pull two spinons apart.

First we note a consequence of (2.5): the gauge constraint (2.9) is locally modified at every site occupied by an additional spinon:

$$G_i = \prod_{i' \in i} \sigma_{ii'}^x = \begin{cases} -1 & , \text{ site } i \text{ unoccupied} \\ 1 & , \text{ site } i \text{ occupied} \end{cases}$$

Consider two spatially separate spinons in the valence-bond crystal phase. Their effect in the pure \mathbb{Z}_2 gauge theory is to constraint the number of dimers emanating from their two sites to be even. All other sites are involved with an odd number of dimers. To fulfill these requirements, one can start from a Kagome lattice dimer covering in absence of extra spinons, and then exchange dimers with vacancies (string-flip) on all bonds of a string that connects the two sites where the extra spinons sit. In the low-energy sector, we have a hard-core dimer covering modified by the string-flip.

When the couplings K_n are equal to zero, any string following a path tangential to the dimers will cost the minimal energy. On such a string the bond segments are successively occupied and unoccupied, and the string-flip can at most cost the energy of one dimer. Therefore, in absence of all loop terms in (2.8), the spinons will be unconfined. However, in the *honeycomb* ordered state (Figure 2-7(a)), these strings necessarily go through the perfect hexagons. The string-flips then destroy the perfect hexagons, and the total energy cost ($2K_6$ per destroyed hexagon) grows linearly with the string length. Therefore, the spinons are confined. It is interesting to notice that the *stripe* state (Figure 2-7(b)) would have supported unconfined spinons along the stripes (one dimension), between the rows of flippable hexagons, if it were realized as the ground-state.

2.2.7 Finite Lattices

Our goal is to compare results of our calculations with numerics. Therefore, it pays to consider changes that a finite lattice would introduce in the \mathbb{Z}_2 gauge theory of the Kagome singlet states (2.14). Clearly, there is no need to re-explore the spin liquid phase in the $h \ll K_3, K_6 \dots$ limit: this phase has a clear gap to all excitations, and very well localized excitations whose nature cannot be seriously affected even in very small samples. We focus only on the valence-bond crystal phase in the $h \gg K_3, K_6 \dots$ limit.

The *honeycomb* patterned ground-states, found in the thermodynamic limit, are 12-fold degenerate, and related to one another by translations. When the lattice becomes finite, this degeneracy is lifted, and no symmetry is spontaneously broken. Dimer flips on some large flippable loops that enclose a finite portion of the sample plaquettes can translate entire dimer configuration and mix the states that break translational symmetry. The coupling constants for such flips in the dimer effective theory define a “mixing” energy scale, which then depends on the sample size. The spectrum of a finite system will not accurately reflect the spectrum of the infinite system. Accuracy is set by the “mixing” energy scale, because it determines the fine splitting of energy levels that would be 12-fold degenerate in thermodynamic limit.

In order to make sure that the finite-size effect does not obscure signature of the long-range order in the spectrum, the “mixing” energy scale must be made much smaller than the singlet gap (which is the smallest energy scale in the thermodynamic limit). However, even for $N = 36$ sites the “mixing” scale could be comparable with the already small singlet gap, and the spectrum would look randomized. Another finite-size effect can be absence of spinon confinement: it is noticeable only at distances much larger than the size of the *honeycomb* pattern unit-cell.

On the other hand, the overall structure of the spectrum is not very sensitive to system size. Namely, presence of very small energy scales (deep below the exchange scale J) and abundance of singlet states below the spin-gap can be captured even in very small samples. For example, just by naively counting the excited singlet states in the *honeycomb* “phase” on a $N = 36$ site lattice one arrives at a number of states below the spin-gap quite close to that reported in the numerical studies (1.15^N).

2.3 Qualitative Physical Picture From Comparison With Numerics

The analysis in the preceding sections has established some properties of the pure \mathbb{Z}_2 gauge theory that describes the singlet states of the Kagome antiferromagnet. Specifically, we analyzed two characteristic limits, and described two distinct phases that obtain in those limits. The spin liquid phase ($h \ll K_n$) has a unique ground-state and a clear gap in its spectrum. On the other hand, the *honeycomb* valence-bond crystal phase ($h \gg K_n$) is long-range ordered. The latter phase has a number of interesting properties. It clearly describes a spin-Peierls order of the original Kagome magnet with a very large unit-cell of 36 sites. The spinful excitations are gapped spin-1 magnons. However, below the spin-gap this state has a large number of low-energy excitations, with a non-zero gap which is nevertheless much smaller than the spin exchange. This is in agreement with the numerical calculations [42] on the Kagome Heisenberg magnet. Based on this, we propose the *honeycomb* valence-bond

crystal phase as a description of low energy physics of the Kagome lattice quantum antiferromagnet. Also, in Appendix B we provide some analytical argument in favor of the $h \ll K_n$ limit in which the valence-bond crystal is realized.

However, when making comparison with the numerics, one has to keep in mind limitations of both approaches. This theory is not able to provide quantitative information about the energy levels relative to the spin exchange; it only reveals that the singlet gap is much smaller than the exchange scale. On the other hand, the numerical exact diagonalization can be performed only on very limited system sizes, which at best contain as many sites as the unit cell of the valence bond crystal that we propose. Due to this, some properties deduced by the finite-size scaling (extrapolation) may not be realized in the thermodynamic limit: the exact magnitude of the singlet-gap, the number of singlet states below the spin-gap, the structure of the singlet spectrum below the spin-gap (from which one learns about broken symmetries), confinement, etc. In other words, assuming that the *honeycomb* valence-bond crystal is realized in the Kagome antiferromagnet, the finite-size scaling should go well beyond 36 sites in order to yield more reliable results. However, some gross features of the low-lying spectrum are reliably obtained in both approaches, and this is where they agree: the presence of a large number of singlet excitations below the spin-gap, and the smallness of the singlet gap.

Quite generally, we expect that the \mathbb{Z}_2 gauge theoretical analysis is applicable to a variety of spin models in paramagnetic phases. These include the checkerboard lattice, and various other lattices frustrated by the next-nearest neighbor exchange. Then, if we were to generalize our hypothesis to other models with near neighbor exchange interactions, we would expect that the $h \gg K_n$ limit always describes the effective theory for singlet excitations. This theory is a quantum dimer model dominated by the kinetic energy. A naive guess for the ground-state is that the smallest resonating flippable loops assume the maximum possible density, typically leading to a *plaquette* long range order of valence-bonds. Indeed, such *plaquette* phases have been numerically observed in the Heisenberg model on the checkerboard lattice [62], and the phase diagrams of the quantum dimer models on the square [6],

and honeycomb [3] lattices, while a dimer RVB phase was found on the triangular lattice [4, 5]. We demonstrated analytically a plaquette phase in the Kagome lattice Heisenberg model, while a numerical work showed a similar bond-order in the one-dimensional Kagome strip [63].

Peculiarity of the Kagome lattice is that the maximum density of the smallest resonating flippable loops is not sufficient to lift the macroscopic degeneracy of the ground-states. In fact, the crystalline structure of the valence-bonds is established at much higher energy scales than the singlet gap. This is seen in the perturbation theory: the crystal is established at the second order, while the gap is not opened before the fourth order. On other lattices, the checkerboard for example, the degeneracy is fully lifted at the same time when the long-range order is established.

2.4 Weak Dispersion of Excitations and Some Other Issues

Another interesting feature that emerged from the calculations in preceding sections is a rather small (possibly zero) dispersion of elementary excitations in both phases of the pure \mathbb{Z}_2 gauge theory. The elementary singlet excitations of both the ordered and disordered phases appear dispersionless at least to the twelfth order of perturbation theory. Although at present we don't know whether this persists to all orders, we speculate that it might be the case, at least in the disordered phase. Here we demonstrate further this phenomenon in the spin liquid phase using a simple Monte Carlo calculation, and a simple Landau-Ginsburg large- N limit analysis.

In addition, the Monte Carlo will demonstrate that thermal fluctuations alone cannot entropically select an ordered state from the degenerate manifold of states in the pure \mathbb{Z}_2 gauge theory. This only reveals importance of quantum fluctuations in shaping the valence-bond crystal. The \mathbb{Z}_2 gauge theory of the singlet states was derived from an inherently quantum theory, and it does not represent a classical Heisenberg model on the Kagome lattice, which actually experiences order-by-disorder

due to thermal fluctuations.

Also, the Landau-Ginsburg analysis will expose one of the fundamental difficulties in the Kagome problem. The modes in this theory will be strictly dispersionless (see also [64]). As a consequence, various perturbations are relevant in the renormalization group sense, making a sharp contrast to usual circumstances in which the modes are dispersive. This means that this kind of analysis is less useful for exploring phase diagrams of the Kagome models. Interactions between the modes that are gradually introduced as $\frac{1}{N}$ corrections are very important, but unfortunately very difficult to handle.

2.4.1 Monte-Carlo Studies

The frustrated quantum Ising model on the dice lattice (2.15) translates into the 3-dimensional classical Ising model on the time-stacked dice-lattice layers. The corresponding Boltzmann weights are all positive and hence the model can be simulated by Monte Carlo without a sign problem. The classical action we consider is analogous to (2.15):

$$S = \sum_{\tau} \left[-\tilde{h} \sum_{lm} \epsilon_{lm} v_{l,\tau} v_{m,\tau} - \tilde{K}_3 \sum_{l_3} v_{l_3,\tau} v_{l_3,\tau+1} - \tilde{K}_6 \sum_{l_6} v_{l_6,\tau} v_{l_6,\tau+1} \right]. \quad (2.31)$$

We have to regard this problem as a classical one, because the quantum limit $\tilde{h} \rightarrow 0$, and $\tilde{K}_{3,6} \rightarrow \infty$ is not accessible. If $\tilde{K}_3 = \tilde{K}_6 = \tilde{K}$, two regimes emerge, depicted in the Fig. 2-11. In order to obtain this diagram, we scan along $\tilde{K} \propto \tilde{h}$ lines, and measure the heat-capacity, using \tilde{h} as the inverse “temperature” β ; then we record position of the heat-capacity peak, and join the peak positions (\tilde{h}, \tilde{K}) from different scans into a crossover line between the two regimes.

For small \tilde{h} and \tilde{K} a disordered regime occurs. It is characterized by seemingly vanishing spatial spin-spin correlations beyond the nearest-neighbor sites, as shown in Fig. 2-12, while the time correlations decay exponentially. This regime corresponds to the disordered phase and the small- h limit of (2.15). The numerical result for the spatial correlations is consistent with the statement made in the Section 2.2.5 that the

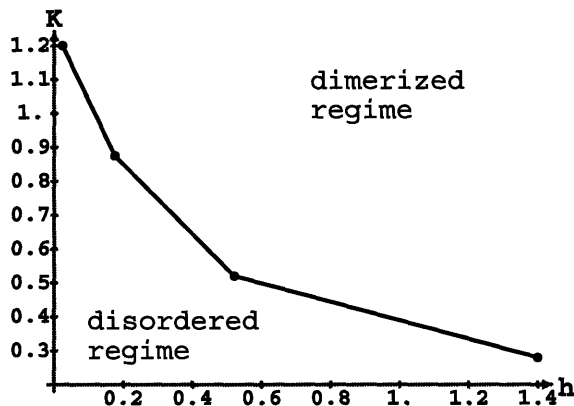
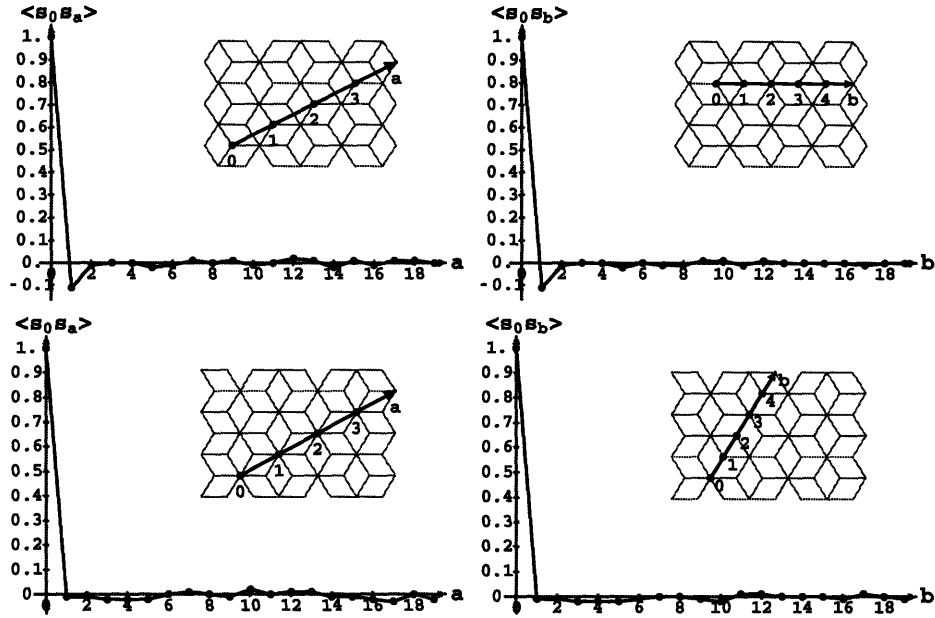


Figure 2-11: Regimes of the (2+1)D classical Ising model on the fully frustrated dice lattice

visons may be localized in the vicinity of the next-nearest-neighbor sites. We would like to contrast this with another case of a fractionalized spin-liquid on the Kagome lattice: in a particular easy-axis limit explored in Reference [65] the vison correlations are short-ranged, but they exhibit a clear exponential decay over a significant range of separations.

For large \tilde{h} and \tilde{K} , a “dimerized” regime occurs: if the frustrated dice bonds (with positive bond energy) are plotted as dimers on the Kagome lattice (wherever a Kagome bond intersects a frustrated dice bond), then a hard-core dimer covering is obtained. Our present method was not able to establish whether the crossover line between these two regimes is actually a phase transition line or not. However, based on our analytical study we expect that this is the phase transition. Since large coupling constants yield the dimerized regime in which all dimer coverings have the same action, the remaining phase properties can be decided only by entropy, which is a manifestation of quantum fluctuations. In the Ising language, once the action is fixed to its lowest value, the maximum entropy state has the largest number of *flippable* clusters of spins (free to fluctuate without changing the action). In the dimer language, the *honeycomb* pattern will be selected, in a mechanism essentially analogous to that obtained in the Section 2.2.4. Indeed, every perfect hexagon of dimers represents a *flippable* spin on the dice-lattice. Once their number is maximized by entropy, the only other elementary flippable loops which could possibly resonate



The sample size was $20 \times 18 \times 20$ unit-cells (each with 6 sites), with $\tilde{h} = 0.15$, and $\tilde{K}_3 = \tilde{K}_6 = 0.75$. The type of the site at the origin, and the spatial direction are shown in the legend.

Figure 2-12: Vison-vision correlations in the disordered phase

without action cost are the *stars*, and to maximize their number, the perfect hexagons must arrange in the *honeycomb* pattern. Unfortunately, our simulation could not reach equilibrium in this regime, at least due to very slow dynamics at large coupling constants.

Since the quantum fluctuations are capable of producing order-by-disorder, it is natural to ask whether the thermal fluctuations are capable too. If we set the transverse field couplings K_n in (2.15) to zero, we obtain the classical two-dimensional Ising model on the fully frustrated dice lattice. In this case, the Monte Carlo easily reveals that there are no phase transitions, measured through the “heat capacity”, and the model is always in its disordered phase. Therefore, the thermal fluctuations alone cannot introduce a long-range order, even when \tilde{h} becomes large and the “dimerized” regime occurs. The presence of the transverse fields is crucial for the entropical selection of a long-range ordered state in the Monte Carlo.

2.4.2 A Large- N Limit

A relatively simple way to gain some intuition for the quantum Ising model on the frustrated dice lattice (2.15) is to generalize it to a limit where the semiclassical approximations become exact. Consider the $O(N)$ generalization of spins in the large- N limit. We will demonstrate that this Gaussian theory has a dispersionless spectrum, and supports only a disordered phase for all values of the coupling constants.

We write the imaginary time path-integral and impose the spin-magnitude constraint using a field λ of Lagrange multipliers. The action obtained from (2.15) by keeping only the elementary transverse field terms is:

$$S_\lambda = \int d\tau \left\{ -h \sum_{\langle lm \rangle} \epsilon_{lm} \mathbf{S}_{l\tau} \cdot \mathbf{S}_{m\tau} - \frac{K_3}{2} \sum_{l_3} \mathbf{S}_{l_3\tau} \frac{\partial^2 \mathbf{S}_{l_3\tau}}{\partial \tau^2} - \frac{K_6}{2} \sum_{l_6} \mathbf{S}_{l_6\tau} \frac{\partial^2 \mathbf{S}_{l_6\tau}}{\partial \tau^2} - \sum_l i\lambda_{l\tau} (\mathbf{S}_{l\tau}^2 - 1) \right\}. \quad (2.32)$$

In the saddle-point approximation, the Lagrange multiplier field λ becomes “homogeneous”, with only two independent values λ_3 and λ_6 corresponding to the 3 and 6-coordinated dice lattice sites. This is a consequence of the \mathbb{Z}_2 gauge-invariance, namely arbitrariness of ϵ_{lm} , subject to the condition (2.12). If ϵ_{lm} are chosen to be negative on the thick bonds in the Fig. 2-4(b), then the action can be diagonalized on the six by six matrices in the frequency-momentum space, and the spin degrees of freedom can be easily integrated out:

$$S_\lambda = N \left[\frac{1}{2} \sum_{\omega} \sum_{q_x q_y} \log \det(H_{q_x q_y \omega} + i\Lambda) + \mathcal{N} \text{tr}(i\Lambda) \right].$$

Here we used the elementary cell in Figure 2-13, \mathcal{N} is the number of space-time sites,

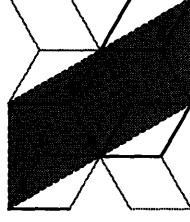


Figure 2-13: Unit-cell of the fully frustrated dice lattice

$\Lambda = \text{diag}(\lambda_6, \lambda_6, \lambda_3, \lambda_3, \lambda_3, \lambda_3)$. The matrix $H_{q_x q_y \omega}$ is:

$$\begin{pmatrix} -\frac{K_6}{2}\omega^2 & 0 & \frac{\hbar}{2}(1 + e^{-iq_y}) & -\frac{\hbar}{2}e^{-iq_y} & \frac{\hbar}{2}e^{-iq_x} & \frac{\hbar}{2}e^{-iq_x}(1 - e^{-iq_y}) \\ 0 & -\frac{K_6}{2}\omega^2 & \frac{\hbar}{2} & \frac{\hbar}{2}(1 + e^{-iq_y}) & \frac{\hbar}{2}(-1 + e^{-iq_y}) & -\frac{\hbar}{2}e^{-iq_y} \\ \frac{\hbar}{2}(1 + e^{iq_y}) & \frac{\hbar}{2} & -\frac{K_3}{2}\omega^2 & 0 & 0 & 0 \\ -\frac{\hbar}{2}e^{iq_y} & \frac{\hbar}{2}(1 + e^{iq_y}) & 0 & -\frac{K_3}{2}\omega^2 & 0 & 0 \\ \frac{\hbar}{2}e^{iq_x} & \frac{\hbar}{2}(-1 + e^{iq_y}) & 0 & 0 & -\frac{K_3}{2}\omega^2 & 0 \\ \frac{\hbar}{2}e^{iq_x}(1 - e^{iq_y}) & -\frac{\hbar}{2}e^{iq_y} & 0 & 0 & 0 & -\frac{K_3}{2}\omega^2 \end{pmatrix}$$

and its internal indices correspond to the site labeling in the Figure 2-13.

The matrix under the determinant in (2.33) has three two-fold degenerate eigenvalues that have no dependence on the momentum. If we relabel $i\lambda_3 = -m_3^2$ and $i\lambda_6 = -m_6^2$, they are:

$$v_3 = \frac{K_3}{2}\omega^2 + m_3^2, \\ v_{1,2} = \frac{1}{2} \left[\frac{K_3 + K_6}{2}\omega^2 + m_3^2 + m_6^2 \pm \sqrt{6h^2 + \left(\frac{K_3 - K_6}{2}\omega^2 + m_3^2 - m_6^2 \right)^2} \right].$$

The action then becomes:

$$S_\lambda = N\mathcal{N} \left[\int \frac{d\omega}{2\pi} \log(v_1 v_2 v_3) - (2m_6^2 + 4m_3^2) \right]. \quad (2.33)$$

In order for this action to correspond to a physical hermitian Hamiltonian, both m_3^2 and m_6^2 must be real numbers. In addition, the path-integral converges only when all eigenvalues v_i are real and positive for all frequencies. These requirements are satisfied if:

$$m_3^2 > 0 \quad , \quad m_6^2 > 0 \quad , \quad 4m_3^2 m_6^2 > 6h^2. \quad (2.34)$$

A failure to satisfy these conditions by the saddle-point values of m_3 and m_6 would signify an instability.

Now we vary m_3^2 and m_6^2 to find the minimal action, integrate out the frequency, and obtain the following saddle-point equations:

$$\begin{aligned} \frac{1}{\sqrt{2K_3m_3^2}} + K_3K_6 \frac{(K_3 + K_6) + \frac{2(m_3^2+m_6^2)}{\sqrt{\alpha_1\alpha_2}}}{\sqrt{\alpha_1} + \sqrt{\alpha_2}} &= 6, \\ \frac{1}{\sqrt{2K_3m_3^2}} - K_3K_6 \frac{(K_3 - K_6) + \frac{2(m_3^2-m_6^2)}{\sqrt{\alpha_1\alpha_2}}}{\sqrt{\alpha_1} + \sqrt{\alpha_2}} &= 2, \end{aligned} \quad (2.35)$$

where:

$$\alpha_{1,2} = \left(\frac{m_3^2}{K_3} + \frac{m_6^2}{K_6} \right) \pm \sqrt{\left(\frac{m_3^2}{K_3} - \frac{m_6^2}{K_6} \right)^2 + \frac{6h^2}{K_3K_6}}. \quad (2.36)$$

The conditions (2.34) directly translate to $\alpha_{1,2} > 0$. The saddle-point equations are too complicated to be solved exactly. If the solution that meets the conditions (2.34) exists for every finite non-zero K_3 , K_6 , and h , then the system is always in the paramagnetic phase. In order to prove that such solutions always exist, we can solve the inverse problem: assume that m_3^2 and m_6^2 are known, real and positive, fix arbitrary values for K_3 and K_6 , and find the value of h that satisfies the saddle-point equations.

A couple of straight-forward algebraic manipulations reduce the saddle-point equations (2.35) to:

$$\begin{aligned} \frac{K_6\alpha + 2m_6^2}{K_3\alpha + 2m_3^2} &= 2 - \frac{1}{2\sqrt{2K_3m_3^2}}, \\ \left(\alpha + \frac{2m_3^2}{K_3} \right)^2 &= 8K_6^2\alpha^2 \left(\frac{m_3^2}{K_3} + \frac{m_6^2}{K_6} + \alpha \right), \end{aligned} \quad (2.37)$$

and $\alpha = \sqrt{\alpha_1\alpha_2}$. It follows that:

$$\frac{m_3^2}{K_3} = \frac{x^2}{2}, \quad (2.38)$$

$$\frac{m_6^2}{K_6} = \frac{(\alpha + x^2)^2}{8K_6^2\alpha^2} - \frac{x^2}{2} - \alpha, \quad (2.39)$$

$$x^3 + \alpha[1 - 4K_6(2K_3 + K_6)\alpha]x + 2K_6\alpha^2 = 0. \quad (2.40)$$

Treating (2.40) as a quadratic equation for α , we find the real and positive solution:

$$\alpha = x \frac{1 + \sqrt{1 + 8K_6[2(2K_3 + K_6)x - 1]}x}{4K - 6[2(2K_3 + K_6)x - 1]},$$

for $x > \frac{1}{2(2K_3 + K_6)}$.

(2.41)

We can now study the dependence of $\beta = 6h^2/K_3K_6$ on x . From (2.36) we obtain:

$$\beta = 4 \frac{m_3^2 m_6^2}{K_3 K_6} - \alpha^2, \quad (2.42)$$

and using (2.38), (2.39), and (2.41) we express β as a function of x . One can easily check that $\beta = 0$ for $m_3^2 = \frac{1}{8}K_3$, $m_6^2 = \frac{1}{8}K_6$, and $\beta \rightarrow \infty$ for $m_3^2 = \frac{\sqrt{3}}{2}h$, $m_6^2 = \sqrt{3}h$. In between these limiting cases, $\beta(x)$ is a continuous, monotonously growing function in the region $x > \frac{1}{K_3}$, for all values of K_3 and K_6 . Due to a very complicated dependence of β on x , we verify this by numerical plotting for a variety of K_3 and K_6 values, including all important limits. The fact that $\beta(x)$ is a monotonous function means that for every value of h there is a unique solution for x , i. e. for the saddle-point equations. The “squared masses” m_3^2 and m_6^2 are real and positive for all h , K_3 , and K_6 , and vary continuously with the coupling constants. Therefore, this theory does not support a phase transition, and always remains in the paramagnetic phase.

This simple Gaussian Landau-Ginsburg analysis gives a dispersionless spectrum. Also, the model is always in the paramagnetic phase in this approximation. It is clear that both the Landau-Ginsburg approach and the large- N approximation have fundamental limitations in this problem. As we have argued, the correct phase diagram includes an ordered phase, albeit of a somewhat unconventional kind.

Chapter 3

Kagome Lattice Quantum Ising Model in Transverse Field

A simple theoretical context in which effects of quantum dynamics on classical geometrically frustrated magnets may be studied is provided by considering frustrated Ising models perturbed by a transverse magnetic field. On one hand, frustration is even stronger in the Ising than in the Heisenberg systems because spins have much less freedom to partially relax competing forces. On the other hand, discrete Ising degrees of freedom often prove to be tractable using standard analytical techniques that involve qualitative but well controlled approximations. In this chapter we will explore the transverse field quantum Ising model on the Kagome lattice. After a brief motivation of the problem, we will take a sequence of steps that transform a generalized Kagome Ising model into a field theory in the same universality class. We will make use of a compact $U(1)$ gauge theory and duality transformations. At the end, in the spirit of Reference [66], we will discover a quantum disordered phase, as well as a phase with spontaneous ferromagnetic magnetization. We will argue that the disordered phase is always realized in the plain Kagome quantum Ising model.

3.1 How the Quantum Fluctuations Lift Classical Degeneracy?

3.1.1 Order-by-Disorder

One of the defining characteristics of frustrated systems is their pronounced sensitivity to small perturbations. In absence of fluctuations (quantum or thermal) competing forces in these systems typically produce a vast number of *static* degenerate states at low energies. Even the number of such *classical* ground-states often scales as an exponential function of the system size. Since a frustrated system is quite undecided at energy scales of the competing forces, it will yield even to a slightest disbalance caused by quantum perturbations or finite temperatures. It is then said that quantum or thermal fluctuations lift the classical ground-state degeneracy. An interesting situation, called “order-by-disorder”, occurs when the phase shaped by fluctuations has broken symmetries. This is in some sense unusual phenomenon since the dominant forces appear not to prefer a long-range order, while fluctuations usually work against a long-range order. Our focus will be turned to frustrated two-dimensional quantum Ising models in *weak* transverse fields, which generally exhibit order-by-disorder (in strong transverse fields all such models are trivially disordered).

One of the best examples of order-by-disorder is found in the quantum Ising antiferromagnet on the triangular lattice. Since every elementary plaquette has an odd number of sites, at least one of its three bonds must be frustrated at any time by holding two aligned Ising spins. Static configurations of Ising spins that minimize exchange energy have exactly one frustrated bond on every triangle, and hence can be mapped to hard-core dimer coverings of the dual honeycomb lattice (up to a global spin-flip) where every honeycomb dimer intersects a frustrated triangular bond. A small transverse field than introduces quantum dynamics, which can be captured by a quantum dimer model on the honeycomb lattice. Systematic numerical calculations (as well as some theoretical approaches) have provided ample evidence that the honeycomb lattice quantum dimer model is always in an ordered phase, except at

certain quantum critical points. In terms of the original Ising spins, these ordered phases have no Ising magnetization, but break the lattice symmetries in terms of the frustrated bond arrangement.

Another example is a fully frustrated quantum Ising model on the square lattice. It can be mapped to a square lattice quantum dimer model, which again has only long-range ordered phases. In fact, every frustrated quantum Ising model in weak transverse field on a lattice whose dual lattice is bipartite will experience order-by-disorder. This is so because every two-dimensional quantum dimer model on a bipartite lattice can be represented as a discrete height (solid-on-solid) model in $2+1$ dimensions, which is known to always live in the “smooth” long-range ordered phase. However, even the other studied two-dimensional quantum Ising models that do not have a height representation seem to typically order. They include models on fully frustrated honeycomb lattice [4, 5] and “pentagonal” lattice [67].

3.1.2 Disorder-by-Disorder on the Kagome Lattice?

One of the main reasons for great interest in frustrated magnets is their promise for realizing quantum disordered and spin liquid phases. As discussed in the previous section, it turns out that at least among simple two-dimensional frustrated quantum Ising magnets in weak transverse fields order-by-disorder is most common. The question is then whether disordered ground-states can be supported at all by the quantum Ising systems in *weak* transverse fields. Finding at least one example where existence of such a disordered phase can be explicitly demonstrated proved to be a challenge.

The Kagome lattice Ising antiferromagnet in weak transverse fields is the only so far explored exception. Monte Carlo calculations performed by Moessner and Sondhi have not detected any phase transitions as the strength of transverse field was varied from large values to zero [67, 68]. Furthermore, no apparent long-range order was ever observed, and the spin-spin correlations turned out to be markedly short-ranged as if the fluctuations were strictly local. In order to emphasize the contrast to typical situations in other similar systems, Moessner and Sondhi called this behavior “disorder-by-disorder”.

Theory of the Kagome quantum Ising antiferromagnet in weak transverse fields was not available until now. The complicated Kagome lattice structure prohibited usual mappings, and standard Landau-Ginsburg analysis turned out to be problematic due to appearance of dispersionless soft modes. The work that will be presented in this chapter is the first theoretical proof that a disordered quantum phase indeed exists in the Kagome system, and it provides explanation of why the Kagome lattice is so special.

3.2 Lattice-Field Theory of Fluctuating Spins

The basic model that we want to study is the antiferromagnetic Ising model in transverse magnetic field on the Kagome lattice (TFIM):

$$H = J \sum_{\langle ij \rangle} S_i^z S_j^z - \Gamma \sum_i S_i^x . \quad (3.1)$$

Here i, j label the sites of the Kagome lattice, and \mathbf{S}_i is a spin $S = \frac{1}{2}$ moment at site i . J is the antiferromagnetic Ising interaction strength, and Γ is the strength of the transverse magnetic field. More generally, we will focus on the regime where the energy scale J , which fixes an easy axis, is much larger than all other energy scales ($J \gg \Gamma$), and consider various ways in which dynamics can be given to the spins, without conserving any quantities (clearly, the alternate limits of large Γ is trivial). The main goal is to study the structure of possible phases that can emerge when the frustrated Ising antiferromagnet is endowed with weak quantum dynamics (that preserves Ising, but no other spin symmetries).

Our strategy is as follows. We derive a low energy effective theory that is appropriate in the easy axis limit. This may be represented as a compact U(1) gauge theory on the honeycomb lattice that is coupled to a bosonic “matter” field (with gauge charge 1). There is in addition a non-zero static *background* charge at each site. The utility of a compact U(1) gauge theory (with appropriate background charges) to describing the low energy physics of frustrated easy-axis magnets has been pointed out several

times in the literature. However, in contrast to the Kagome lattice, on other lattices typically the gauge theory has no dynamical matter fields. In two spatial dimensions on these other lattices the gauge theory is in a confined phase, and the presence of background charges leads to broken translation symmetry. Presence of the additional dynamic matter field distinguishes the Kagome lattice from these other lattices. As we will see, it is now possible to have a phase that is also “confining” (more precisely a Higgs phase), which preserves translation symmetry even in the presence of the background charges. For the original Kagome TFIM this describes a translation invariant paramagnet. The general possibility of such translation invariant Higgs phases in such gauge theories has been discussed before [69].

We analyze the gauge theory appropriate for the Kagome TFIM using duality transformations. The dual theory will turn out to be equivalent to a certain XY model with a three-fold anisotropy. The disordered phase of this model is the Higgs phase discussed above. The ordered phase describes a situation where there is order-by-disorder in the original Kagome magnet.

3.2.1 Effective Compact U(1) Gauge Theory

The nearest neighbor Ising coupling on the Kagome lattice can be conveniently written as a sum of terms defined on the triangular plaquettes:

$$H_z = J \sum_{\langle ij \rangle} S_i^z S_j^z = \frac{J}{2} \sum_{\Delta} \left(\sum_{i \in \Delta} S_i^z \right)^2 + \text{const.} . \quad (3.2)$$

This allows us to easily describe the sector of low energy states: total spin on every triangle should be $\pm 1/2$. Spin configurations that satisfy this condition are *least frustrated*. Let us express these states using a set of variables defined on the *honeycomb* lattice, whose sites we will label by p and q . Figure 3-1 illustrates relationship between the Kagome and honeycomb lattices. The honeycomb bonds contain Kagome sites, and we can associate with them the Kagome spins: $S_i^z \equiv S_{(pq)}^z$. On the other hand, the honeycomb sites reside inside the Kagome triangular plaquettes. It is useful to keep track of the total spin (whether it is $+1/2$ or $-1/2$) on any triangular Kagome

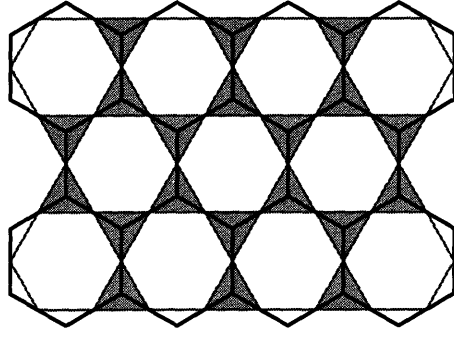


Figure 3-1: Relationship between the honeycomb and Kagome lattices

plaquette. We therefore introduce a variable s_p^z that measures the total plaquette spin:

$$(\forall p) \quad s_p^z = \sum_{q \in p} S_{\langle pq \rangle}^z . \quad (3.3)$$

We impose restriction to the low energy sector by requiring that s_p^z take only values $\pm \frac{1}{2}$. Note that when a Kagome spin is flipped (provided that flipping does not introduce more frustration), s_p^z on the triangles that contain it change sign in the same direction. With only the Ising interaction present there is a large number of classical ground states: every spin configuration that satisfies Equation (3.3) with $s_p^z = \pm 1/2$ is a classical ground state. Inclusion of the Γ or other terms in the Hamiltonian will split this huge degeneracy of the ground state manifold.

It is possible to perturbatively construct an effective theory that describes the low energy dynamics in the ground state manifold, and express it on the honeycomb lattice:

$$H_{\text{eff}} = -\frac{\Gamma}{2} \sum_{\langle pq \rangle} \left(s_p^+ S_{\langle pq \rangle}^+ s_q^+ + h.c. \right) - \dots \quad (3.4)$$

$$-t \sum_{\square} \left(S_{\langle 12 \rangle}^+ S_{\langle 23 \rangle}^- S_{\langle 34 \rangle}^+ S_{\langle 45 \rangle}^- S_{\langle 56 \rangle}^+ S_{\langle 61 \rangle}^- + h.c. \right) - \dots .$$

The Hilbert space of this theory is defined only by the least frustrated states. The lowest order dynamical term is a single Kagome spin flip S^\pm caused by the transverse field, and the operators s^\pm simply project-out the states that are not minimally frustrated. At higher orders of perturbation theory multiple spins are being flipped,

and the smallest “ring-exchange” term appears at the sixth order, so that $t \sim \frac{\Gamma^6}{J^5}$. Alternately, we could have imagined adding such a ring-exchange term to the original model (in addition to the transverse field term). We will examine the properties of this effective Hamiltonian in the low energy subspace for arbitrary Γ and t . The pure transverse field model then corresponds to the particular limit $\Gamma \gg t$. All fluctuations are constrained by (3.3). The effective theory will have this general form for all kinds of Kagome spin models with an easy axis, provided that dynamics preserves only the Ising symmetry.

The Hamiltonian (3.4) can be interpreted as a model of charged bosons moving in presence of a fluctuating electromagnetic field. In order to formulate this interpretation, we need to exploit the bipartite nature of the honeycomb lattice. Let us introduce a fixed field ε_p that takes values $+1$ and -1 on two different sublattices, as shown in Fig. 3-2. Then, define:

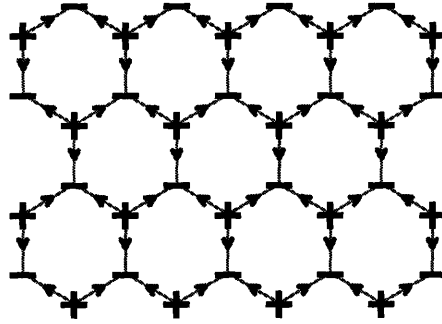
$$\begin{aligned} n_p &= \varepsilon_p \left(s_p^z + \frac{1}{2} \right) \\ E_{pq} &= \varepsilon_p \left(S_{\langle pq \rangle}^z + \frac{1}{2} \right). \end{aligned} \quad (3.5)$$

Note that $E_{pq} = -E_{qp}$, so that it can be viewed as a vector living on the bonds of the honeycomb lattice. This will be interpreted as an integer-valued “electric” field. The integer n_p will be interpreted as the gauge charge of a bosonic “matter” field that couples to the electric field. The constraint (3.3) becomes:

$$(\forall p) \quad \sum_{q \in p} E_{pq} = n_p + \varepsilon_p, \quad (3.6)$$

where the sum on the left-hand side is taken over three honeycomb sites neighboring to p . Natural interpretation of this equation is Gauss’ Law: divergence of the electric field E_{pq} is equal to the total local charge. Note that the boson occupation numbers n_p take values 0 and ε_p . There is an additional fixed background charge distribution ε_p .

At this level, the boson occupation number and electric field strength are con-



Fixed background charge $\varepsilon_p = \pm 1$ on the honeycomb sites, and the electric field $E_{pq}^{(0)}$ created by it (up to a multiplicative factor). On every honeycomb bond we define $E_{pq}^{(0)} = \varepsilon_p/2 = -E_{qp}^{(0)} = -\varepsilon_q/2$ ($\text{div}E^{(0)} = \frac{3}{2}\varepsilon_p$).

Figure 3-2: Background charge on the honeycomb lattice

strained to only two integer values by (3.5). It is useful to soften this “hard-core” by allowing n_p and E_{pq} to take arbitrary integer values, but penalizing fluctuations where either quantity assumes values different from that dictated by the hard-core condition. It will also be useful to introduce the corresponding conjugate operators, φ_p and \mathcal{A}_{pq} , which are angular variables in $[0, 2\pi)$. The boson creation and annihilation operators s_p^\pm simply become $\exp(\pm i\varepsilon_p\varphi_p)$, and similar holds for the electric field: $S_{\langle pq \rangle}^\pm \rightarrow \exp(\pm i\varepsilon_p\mathcal{A}_{pq})$. Now it is straight forward to rewrite the Hamiltonian (3.4) as a compact $U(1)$ gauge theory (up to a constant):

$$\begin{aligned}
 H = U_1 \sum_{\langle pq \rangle} \left(E_{pq} - E_{pq}^{(0)} \right)^2 + U_2 \sum_p \left(n_p - \frac{\varepsilon_p}{2} \right)^2 \quad (3.7) \\
 - \Gamma \sum_{\langle pq \rangle} \cos \left(\varphi_q - \varphi_p - \mathcal{A}_{pq} \right) - \dots - t \sum_{\square} \cos \left(\sum_{\langle pq \rangle} \mathcal{A}_{pq} \right) - \dots
 \end{aligned}$$

We have labeled by $E_{pq}^{(0)}$ a fixed background electric field that originates due to the background charge (see Fig.3-2). The terms proportional to U_1 and U_2 penalize fluctuations of the boson number and the electric field away from the preferred “hard-core” values.

We see that \mathcal{A}_{pq} plays role of a vector potential. The term at the lowest order of perturbation theory describes boson hopping on the honeycomb lattice, while

the term at the sixth order gives energy cost to the “magnetic flux” (away from $2\pi \times$ integer values). It is also easy to write down other terms consistent with the symmetries and the $U(1)$ gauge structure. Fluctuations are subject to the Gauss’ Law (3.6). Note that the charged bosons cannot screen out the background charge ($n_p \rightarrow \{0, \varepsilon_p\}$) without paying a large price (U_1, U_2). This is a consequence of magnetic frustration in the original Kagome spin model. In fact, there is a large number of degenerate boson configurations that accomplish the best possible screening, and they correspond to the least frustrated states. However, the very fact that there is a matter field in this compact $U(1)$ gauge theory distinguishes the Kagome lattice from other commonly studied lattices. It gives hope that a translation symmetric paramagnetic phase could exist on the Kagome lattice, in contrast to the situation for the triangular Ising antiferromagnet, or the fully frustrated square lattice Ising magnets (with weak transverse field dynamics).

3.2.2 Duality Transformation

In this section we perform a duality transformation on the compact $U(1)$ gauge theory derived above. This will enable us to analyze the structure of the possible phases. The duality transformation proceeds in a standard fashion. We first derive the path-integral form of the compact $U(1)$ gauge theory. All terms denoted by ellipses in (3.7) will be ignored. The action will contain a usual Berry’s phase (we will omit the time index):

$$S_B = -i \sum_{\tau} \left(\sum_{\langle pq \rangle} \mathcal{A}_{pq} \Delta_{\tau} E_{pq} + \sum_p \varphi_p \Delta_{\tau} n_p \right), \quad (3.8)$$

and a potential energy part:

$$S_P = \sum_{\tau} \delta\tau \left[U_1 \sum_{\langle pq \rangle} \left(E_{pq} - E_{pq}^{(0)} \right)^2 + U_2 \sum_p \left(n_p - \frac{\varepsilon_p}{2} \right)^2 \right]$$

where $\delta\tau$ is the imaginary time increment. The kinetic energy part will be obtained by applying Villain's approximation to the cosine terms in (3.7):

$$e^{t \cos \theta} \approx \sum_{m=-\infty}^{\infty} e^{-Km^2 - im\theta} \quad , \quad t = 2e^{-K} \rightarrow 0 . \quad (3.9)$$

Two new integer-valued Villain fields will appear: a particle current j_{pq} , and a magnetic field scalar B_r that lives inside plaquettes of the honeycomb lattice, or equivalently on the dual triangular lattice sites (see Fig. 3-3):

$$S_K = \sum_{\tau} \left[K_1 \sum_{\square_r} B_r^2 + K_2 \sum_{\langle pq \rangle} j_{pq}^2 \right. \\ \left. + i \sum_{\langle pq \rangle} j_{pq} (\varphi_q - \varphi_p - \mathcal{A}_{pq}) + i \sum_{\square_r} B_r \left(\sum_{\langle pq \rangle} \mathcal{A}_{pq} \right) \right] . \quad (3.10)$$

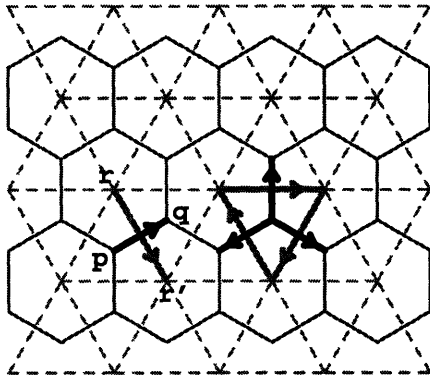
We will treat the constants K_1 and K_2 as free parameters (they are in principle determined in terms of the microscopic parameters that define the original Kagome Hamiltonian). Our interest is in exploring the general nature of the possible phases that are contained in this dual action. The angular variables φ_p and \mathcal{A}_{pq} can now be formally integrated out, yielding Kronecker-delta factors in the path-integral for all integer-valued expressions that they couple to. Such factors simply express familiar laws of electrodynamics. The integral over the boson phase angle will give rise to the current conservation law:

$$\int_0^{2\pi} d\varphi_p \quad \longrightarrow \quad \Delta_{\tau} n_p + \sum_{q \in p} j_{pq} = 0 , \quad (3.11)$$

while the integral over the vector potential will reproduce a two-dimensional Maxwell's equation:

$$\int_0^{2\pi} d\mathcal{A}_{pq} \quad \longrightarrow \quad \Delta_{\tau} E_{pq} + j_{pq} = B_r - B_{r'} . \quad (3.12)$$

The direction of the triangular lattice vector $B_r - B_{r'}$ in the last equation is related to the direction of E_{pq} by the right-hand rule (see Fig. 3-3).



The triangular lattice sites sit inside the honeycomb plaquettes, and vice versa. Duality between a honeycomb lattice vector $p \rightarrow q$ and a triangular lattice vector $r \rightarrow r'$ is shown in the lower-left portion of the graph: their directions are related by the right-hand rule. Divergence on the honeycomb lattice translates into negative lattice curl on the triangular lattice (we always take circulation in the counter-clockwise sense).

Figure 3-3: Duality between the honeycomb and triangular lattices

The equations (3.6), (3.11), and (3.12) can be solved on the dual triangular lattice, whose sites will be labeled by r and r' . As is standard, we first define spatial components of a dual gauge field $A_{rr'}$ on the dual triangular lattice, and a fixed background gauge field $A_{rr'}^{(0)}$, such that their circulations on a triangular plaquette are determined by the charge contained “inside” the plaquette:

$$(\forall p) \quad \sum_{\langle rr' \rangle}^{\triangleleft_p} A_{rr'} = n_p \quad , \quad \sum_{\langle rr' \rangle}^{\triangleleft_p} A_{rr'}^{(0)} = \varepsilon_p . \quad (3.13)$$

The background gauge field $A_{rr'}^{(0)}$ can be specified in many different ways, and we will discuss a convenient choice later. For now, we will only assume that it does not depend on imaginary time. If we substitute these definitions into the Gauss’ Law (3.6), and note that the honeycomb lattice divergence of the electric field translates into the negative triangular lattice curl, we can solve it by writing:

$$E_{pq} = \chi_r - \chi_{r'} - A_{rr'} - A_{rr'}^{(0)} . \quad (3.14)$$

Again, orientation of the vectors on the right-hand side is related to that of E_{pq} by the right-hand rule. The new field χ_r is an allowed degree of freedom, since lattice curl of a pure gradient vector field is zero. Care must be taken to ensure the integer-valued nature of E_{pq} . A convenient way to enforce this will be discussed below. Let us also

define temporal components of the dual gauge fields:

$$(\forall r) \quad A_{r,r+\hat{\tau}} = B_r - \Delta_\tau \chi_r \quad , \quad A_{r,r+\hat{\tau}}^{(0)} = 0 . \quad (3.15)$$

Substituting this and (3.14) into (3.12) gives us an expression for the particle current:

$$j_{pq} = A_{r,r+\hat{\tau}} - A_{r',r'+\hat{\tau}} + \Delta_\tau A_{rr'} = \hat{r}_{pq} \cdot \text{curl} A . \quad (3.16)$$

Therefore, the current becomes expressed as lattice curl of the dual vector potential, taken on the triangular lattice temporal plaquette that is pierced by the current vector $\mathbf{j} = j\hat{\mathbf{r}}$. Finally, we note that the current conservation (3.11) is not independent from the Gauss' Law (3.6) and the Maxwell's equation (3.12).

We can now obtain dual form of the following action that remained after integrating out the conjugate angles:

$$S = \sum_\tau \left[U_1 \delta\tau \sum_{\langle pq \rangle} \left(E_{pq} - E_{pq}^{(0)} \right)^2 + K_1 \sum_{\square_r} B_r^2 \right. \\ \left. + U_2 \delta\tau \sum_p \left(n_p - \frac{\varepsilon_p}{2} \right)^2 + K_2 \sum_{\langle pq \rangle} j_{pq}^2 \right] \quad (3.17)$$

We will eliminate E_{pq} , B_r , n_p , and j_{pq} using (3.14), (3.15), (3.13), and (3.16) respectively. The particle number and current terms together yield curls of the dual vector potential on spatial and temporal plaquettes of the triangular lattice. Though not necessary, for simplicity we set $U_2 \delta\tau = K_2 = g/2$, and $U_1 \delta\tau = K_1 = e^2/2$ and consider the phase diagram in the resulting section of coupling constant space. In order to complete the duality transformation, we must also translate the quantities $E_{pq}^{(0)}$, and ε_p into the dual language. A natural dual counterpart of the background electric field vector $E_{pq}^{(0)}$ is $A_{rr'}^{(0)}$, since both are determined by the background charge distribution ε_p . In the spirit of equation (3.14) this suggests the identification $E_{pq}^{(0)} = -\frac{3}{2}A_{rr'}^{(0)}$, shown in the Fig. 3-4. However, the values of $A_{rr'}^{(0)}$ are then not integers, and compensation is necessary in order to keep E_{pq} integer-valued in (3.14). A convenient solution is to require that χ_r fields take particular non-integer and site-dependent set

of values. Specifically, we demand that $\chi_r - \chi_r^{(0)}$ be integers, with the fixed fractional offsets $\chi_r^{(0)}$ as illustrated in the Fig. 3-5. Then, the dual action is:

$$S = \frac{e^2}{2} \sum_{\langle rr' \rangle} \left(\chi_r - \chi_{r'} - A_{rr'} + \frac{1}{2} A_{rr'}^{(0)} \right)^2 + \frac{g}{2} \sum_{\text{plaq.}} \left(\text{curl} \left(A - \frac{1}{2} A^{(0)} \right) \right)^2, \quad (3.18)$$

where the first summation extends over all space-time links, and the second over all spatial and temporal plaquettes. Let us also shift

$$A \rightarrow A - \frac{1}{2} A_0. \quad (3.19)$$

The action then reads:

$$S = \frac{e^2}{2} \sum_{\langle rr' \rangle} \left(\chi_r - \chi_{r'} - A_{rr'} \right)^2 + \frac{g}{2} \sum_{\text{plaq.}} (\text{curl} A)^2. \quad (3.20)$$

In this theory $\chi_r - \chi_r^{(0)}$, and $A_{rr'} + A_{rr'}^{(0)}/2$ take integer values. The fractional residua $\chi_r^{(0)}$ are given in the Fig. 3-5(d).

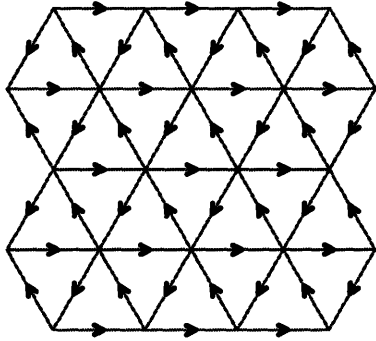
It will actually be convenient to impose these integer conditions on the χ_r and $A_{rr'}$ fields softly (in the same spirit as the usual sine-Gordon description of Coulomb gases). The result is a generalized sine-Gordon theory with the structure:

$$S = \frac{e^2}{2} \sum_{\langle rr' \rangle} \left(\chi_r - \chi_{r'} - A_{rr'} \right)^2 + \frac{g}{2} \sum_{\text{plaq.}} (\text{curl} A)^2 \quad (3.21)$$

$$- K \sum_{\langle rr' \rangle} \cos 2\pi \left(A_{rr'} + \frac{1}{2} A_{rr'}^{(0)} \right) - \dots - \gamma \sum_r \cos 2\pi (\chi_r - \chi_r^{(0)}) - \dots .$$

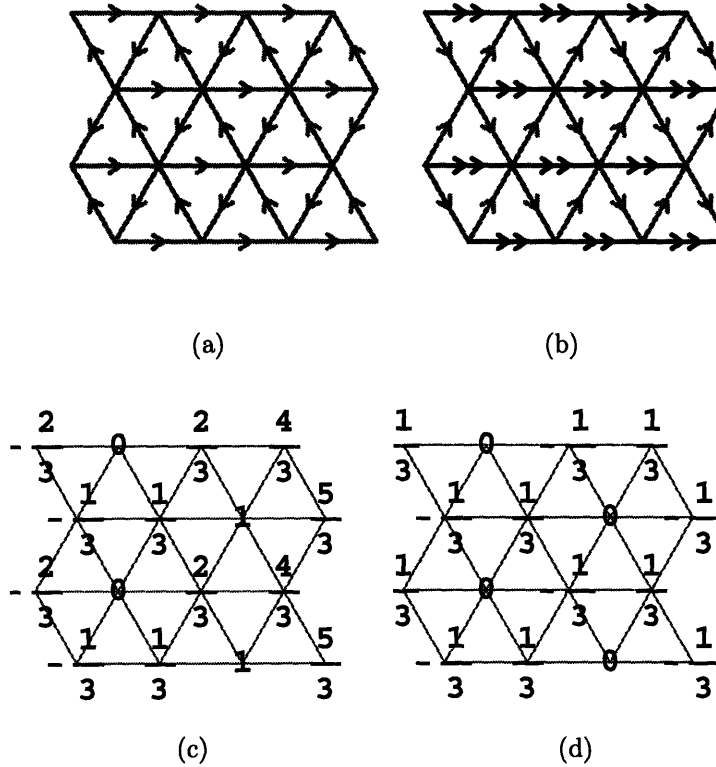
In principle, higher harmonics of the lowest order cosine terms shown above must also be included. The fields χ_r and $A_{rr'}$ now take real values. Let us absorb the field χ_r into $A_{rr'}$ by the shift:

$$A_{rr'} \rightarrow A_{rr'} + \chi_r - \chi_{r'} \quad (3.22)$$



On every bond $A_{rr'}^{(0)} = 1/3$ in the given direction $r \rightarrow r'$, so that its (counter-clockwise) circulations yield ε_p on every plaquette. This vector field is formally dual to that of $E_{pq}^{(0)}$ on the honeycomb lattice (up to a factor).

Figure 3-4: Convenient definition of the fixed dual background gauge field



(a) Fixed background gauge field $A_{rr'}^{(0)}$. (b) A curl-less vector field $A'_{rr'}$. Every arrow contributes $1/3$ in the given direction, so that the sum $A_{rr'}^{(0)} + A'_{rr'}$ is an integer-valued vector field. (c) A scalar field χ'_r whose gradient gives the curl-less vector field: $A'_{rr'} = \chi'_{r'} - \chi'_r$. (d) Fractional parts $\chi_r^{(0)}$ of the scalar field χ'_r . Requiring that the fields χ_r in (3.14) have fractional parts equal to $\chi_r^{(0)}$ compensates for fractional values of $A_{rr'}^{(0)}$, and makes E_{pq} an integer.

Figure 3-5: Fractional offsets of the dual gauge and matter fields

to get the action:

$$\begin{aligned}
S = & \frac{e^2}{2} \sum_{\langle rr' \rangle} A_{rr'}^2 + \frac{g}{2} \sum_{\text{plaq.}} (\text{curl}A)^2 \\
& - K \sum_{\langle rr' \rangle} \cos 2\pi \left(\chi_r - \chi_{r'} + A_{rr'} + \frac{1}{2} A_{rr'}^{(0)} \right) - \gamma \sum_r \cos 2\pi (\chi_r - \chi_r^{(0)}) .
\end{aligned} \tag{3.23}$$

Note that the term proportional to e^2 appears as a “mass” term for the gauge field $A_{rr'}$. We therefore integrate out $A_{rr'}$. This may be explicitly done in the following manner. We formally expand $\exp(-S)$ in powers of K , and decompose every cosine factor from the expansion using the Euler’s formula $2 \cos \theta = \exp(i\theta) + \exp(-i\theta)$. The expansion takes the following form:

$$\begin{aligned}
e^{-S} = & \exp \left\{ \gamma \sum_r \cos 2\pi (\chi_r - \chi_r^{(0)}) \right\} \times \\
& \times \sum_{\{m_{rr'}\}} C_{\{m_{rr'}\}} \exp \left\{ - \left[\frac{e^2}{2} \sum_{\langle rr' \rangle} A_{rr'}^2 + \frac{g}{2} \sum_{\text{plaq.}} (\text{curl}A)^2 \right. \right. \\
& \left. \left. + \sum_r 2\pi i m_{rr'} \left(\chi_r - \chi_{r'} + A_{rr'} + \frac{1}{2} A_{rr'}^{(0)} \right) \right] \right\} ,
\end{aligned} \tag{3.24}$$

where $m_{rr'}$ are integers, and $\{m_{rr'}\}$ denotes their distribution on the whole lattice. This is a Gaussian form, and $A_{rr'}$ can be easily integrated out. Clearly, this causes $\{m_{rr'}\}$ dependent renormalization of the $C_{\{m_{rr'}\}}$ factors, which in turn corresponds to renormalization of K . After re-summation over $m_{rr'}$, an XY model is obtained at the lowest order in (renormalized) K :

$$S = -K \sum_{\langle rr' \rangle} \cos 2\pi \left(\chi_r - \chi_{r'} + \frac{1}{2} A_{rr'}^{(0)} \right) - \gamma \sum_r \cos 2\pi (\chi_r - \chi_r^{(0)}) - \mathcal{O}(K^2, \gamma^2) . \tag{3.25}$$

The variables $2\pi\chi_r$ should be treated as angles. Adding integers to χ_r in the gauge theory (3.20) can always be compensated by a gauge transformation, so that the gauge inequivalent states in (3.25) correspond to different fractional parts of χ_r . This is why the obtained effective theory is an XY model. Physically, the dual field $2\pi\chi_r$ represents the phase of an operator that creates 2π units of vorticity in the

bosonic matter field of the original honeycomb lattice U(1) gauge theory (3.7), and thus must fundamentally be a phase, after the redundant gauge degrees of freedom have been removed. The structure of this theory is such that the XY field fluctuates in presence of a fixed staggered flux, and there is also an external field that apparently explicitly breaks the XY (and apparently also lattice) symmetries (see Fig. 3-6). The physical meaning of this explicit symmetry breaking term is as follows. In the original honeycomb lattice gauge theory 2π vortices of the bosonic matter field carry 2π units of the U(1) gauge flux. As the theory is *compact*, instanton events where this gauge flux changes by 2π are allowed - thus the vorticity is not strictly conserved. The explicit XY symmetry breaking term in the dual representation precisely describes these instanton events.

What is the actual symmetry of this action? As discussed above, when $\gamma = 0$ there is a global XY symmetry that is apparently broken when $\gamma \neq 0$. However, a discrete \mathbb{Z}_3 subgroup of the global XY symmetry survives when combined with translation by one lattice spacing. For instance, the action is invariant under translation along the horizontal x -axis by one unit:

$$\chi_r \rightarrow \chi_{r-\hat{x}} + \frac{2}{3}. \quad (3.26)$$

Similar transformation properties obtain under other translations (as well as the other lattice symmetries).

Let us finally note that manipulations similar to those presented in this chapter have been used in some analogous problems of quantum paramagnets [70, 71] (see also [72, 73] for more introductory reading). Also, theories similar to the one developed here emerge in the context of paramagnetic phases of frustrated Heisenberg magnets: they then describe instanton events which originate from the non-trivial Berry's phases in the Heisenberg model path-integral [74, 75].

3.2.3 Field Theory

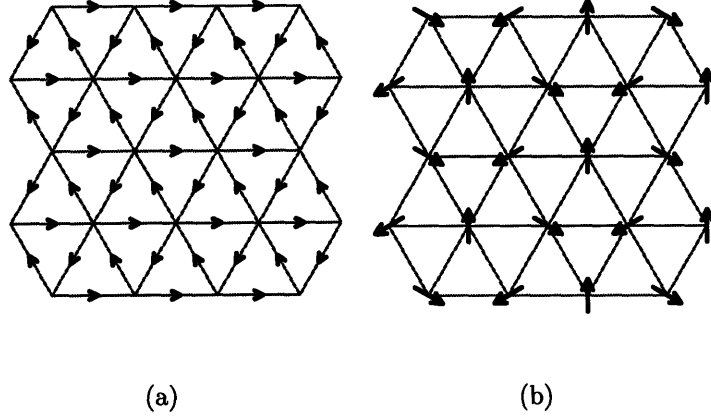
Armed with the dual formulation, we can now see qualitatively why a translation invariant phase is possible in this model. Consider the limit $\gamma = 0$. Then the resulting global XY model will (for K small enough) possess a disordered phase with short-ranged correlations for the χ_r field. Upon increasing K a transition to an ordered phase with some pattern of XY ordering will occur. Now consider turning on a small γ . Its effects will be innocuous in the small- K disordered phase. In particular, the discrete \mathbb{Z}_3 symmetry of $\frac{2}{3}$ shifts of the χ_r field, which realize lattice translations (3.26), will continue to stay unbroken. This is therefore a translation-invariant phase. It is readily seen that this phase is also invariant under all other lattice symmetries.

The existence of the disordered translation-invariant phase is our primary conclusion. How do we think about it in terms of the original gauge theory? From the physical discussion above, the field $e^{2i\pi\chi_r}$ creates 2π flux of the original gauge field, which in turn is bound to a 2π vortex in the phase of the bosonic matter field. Thus the disordered phase is to be thought of as a ‘‘Higgs’’ phase where the bosonic matter fields have condensed - which gaps out their vortices. Indeed, our gauge model is closely related to a similar one discussed in Ref. [69] (the ‘‘ $N = 1$ SJ model’’) where similar phenomena were shown to arise. Note that the Higgs phase is preferred by the boson hopping term in the gauge theory. Thus it is reasonable to expect that this phase is realized in the limit $\Gamma \gg t$. This expectation is indeed consistent with the numerical results of Ref. [67, 68].

We can formally back up this discussion by considering an alternate soft-spin version of the dual XY model. To that end we define:

$$\Phi_{\mathbf{r}} \sim e^{2\pi i\chi_{\mathbf{r}}} . \tag{3.27}$$

We have labelled the triangular lattice sites by their corresponding vectors \mathbf{r} . After substituting this into the XY model (3.25) and relaxing the ‘‘hard-spin’’ condition



(a) Field lines of the background gauge field $A_{rr'}^{(0)}/2$ that produces a staggered flux. (b) External XY field $2\pi\chi_r^{(0)}$ that breaks XY and translational symmetries (compare with Fig. 3-5(d)). This field is constant on any given sublattice of the triangular lattice.

Figure 3-6: Staggered flux and staggered external XY field

on $\Phi_{\mathbf{r}}$ we obtain a “soft-spin” lattice theory:

$$S = -\frac{K}{2} \sum_{\langle \mathbf{r}\mathbf{r}' \rangle} (\Phi_{\mathbf{r}}^* e^{-i\pi A_{rr'}^{(0)}} \Phi_{\mathbf{r}'} + h.c.) + r|\Phi_{\mathbf{r}}|^2 + u|\Phi_{\mathbf{r}}|^4 + \dots \quad (3.28)$$

$$-\gamma \sum_{\mathbf{r}} (e^{-i\mathbf{Q}\mathbf{r}} \Phi_{\mathbf{r}} + h.c.) - \dots .$$

The quadratic part of this action can be diagonalized to obtain:

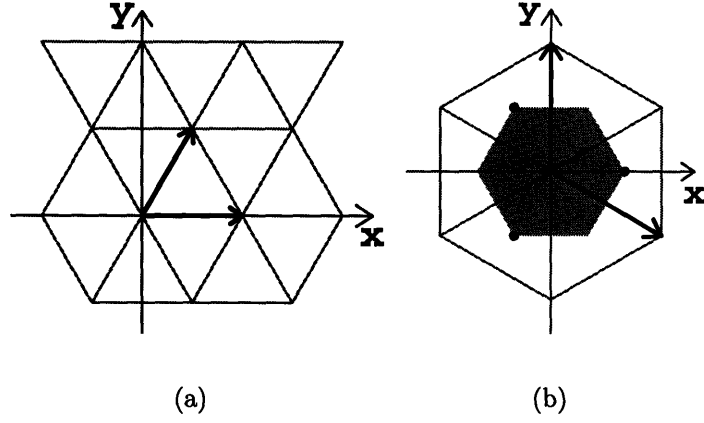
$$\sum_{\mathbf{q}} (-K\varepsilon_{\mathbf{q}} + r) |\Phi_{\mathbf{q}}|^2, \quad (3.29)$$

where

$$\varepsilon_{\mathbf{q}} = \cos\left(q_x - \frac{\pi}{3}\right) + \cos\left(\frac{-q_x + \sqrt{3}q_y}{2} - \frac{\pi}{3}\right) + \cos\left(\frac{-q_x - \sqrt{3}q_y}{2} - \frac{\pi}{3}\right). \quad (3.30)$$

It is straight-forward to show that $\varepsilon_{\mathbf{q}}$ is maximized at two different wavevectors: $\mathbf{q} = 0$, and $\mathbf{q} = -\mathbf{Q}$, where \mathbf{Q} is the wavevector that describes spatial variation of the external XY field:

$$\mathbf{Q} = \frac{4\pi}{3} \hat{\mathbf{x}}, \quad e^{2\pi i \chi_r^{(0)}} = e^{i\mathbf{Q}\mathbf{r}}. \quad (3.31)$$



(a) Direct triangular lattice, and a choice of primitive vectors: $\mathbf{a}_1 = \hat{x}$, $\mathbf{a}_2 = \frac{1}{2}\hat{x} + \frac{\sqrt{3}}{2}\hat{y}$. (b) Reciprocal lattice with primitive vectors $\mathbf{b}_1 = 2\pi(\hat{x} - \frac{1}{\sqrt{3}}\hat{y})$, $\mathbf{b}_2 = 2\pi \cdot \frac{2}{\sqrt{3}}\hat{y}$. Shaded region represents the first Brillouin zone. Emphasized corners of the Brillouin zone represent the wavevector $\mathbf{Q} = \frac{4\pi}{3}\hat{x}$ (three equivalent points).

Figure 3-7: Direct triangular and its reciprocal lattice

In order to aid understanding of this special wavevector, we plot its location on the reciprocal lattice in the Fig. 3-7.

In the following, we focus on the limit $K \gg \gamma$. The fluctuations at low energies will be dominated by the modes in vicinity of the two different wavevectors, $\mathbf{q} = 0$ and $\mathbf{q} = -\mathbf{Q}$. Such fluctuations can be expressed by:

$$\Phi_{\mathbf{r}} = \psi_{1,\mathbf{r}} + e^{-i\mathbf{Q}\cdot\mathbf{r}}\psi_{2,\mathbf{r}} , \quad (3.32)$$

where $\psi_{1,\mathbf{r}}$ and $\psi_{2,\mathbf{r}}$ are fields that vary slowly on the scale of the lattice spacing. It is then useful to go to a continuum limit which focuses on the long wavelength fluctuations of these two fields. This continuum theory must be expressed in terms of $\psi_{1,\mathbf{r}}$ and $\psi_{2,\mathbf{r}}$ only, and must be invariant under all symmetry transformations of the lattice theory (3.28). First, we note that the quadratic part (3.29) is invariant under global XY rotations $\Phi_{\mathbf{r}} \rightarrow e^{i\theta}\Phi_{\mathbf{r}}$, as well as all lattice symmetry transformations at small deviations \mathbf{k} from the wavevectors $\mathbf{q} \in \{0, -\mathbf{Q}\}$:

$$(\forall\alpha) \quad -K\varepsilon_{\mathbf{q}+\mathbf{k}} = \text{const.} + \kappa k^2 + \mathcal{O}(k^3) . \quad (3.33)$$

In addition, there is also a symmetry under exchanging the two kinds of slowly varying fields, $\psi_{1,\mathbf{r}} \leftrightarrow \psi_{2,\mathbf{r}}$. On the other hand, as discussed in the previous section, the γ term (and various similar higher order terms) break the XY symmetry explicitly, and reduce the symmetry group to a discrete set of transformations. It is easy to show that under a unit translation by $\hat{\mathbf{r}}$ the fields transform as:

$$\psi_{1,\mathbf{r}} \rightarrow e^{i\mathbf{Q}\hat{\mathbf{r}}}\psi_{1,\mathbf{r}-\hat{\mathbf{r}}} \quad , \quad \psi_{2,\mathbf{r}} \rightarrow e^{-i\mathbf{Q}\hat{\mathbf{r}}}\psi_{2,\mathbf{r}-\hat{\mathbf{r}}} . \quad (3.34)$$

Note that this rotates the phases of ψ_1 and ψ_2 by 120 degrees in opposite directions. Similarly, the symmetry transformation $\psi_{1,\mathbf{r}} \leftrightarrow \psi_{2,\mathbf{r}}$ of the quadratic part of the action must be accompanied by lattice inversion $\mathbf{r} \rightarrow -\mathbf{r}$ in order to keep the whole action (3.28) invariant:

$$\psi_{1,\mathbf{r}} \rightarrow \psi_{2,-\mathbf{r}} \quad , \quad \psi_{2,\mathbf{r}} \rightarrow \psi_{1,-\mathbf{r}} . \quad (3.35)$$

The remaining lattice transformations do not give rise to further reduction of the symmetry group. We may now write down a Landau-Ginsburg effective field theory, symmetric under transformations (3.34) and (3.35):

$$\begin{aligned} S = & \int d\mathbf{k} \left[(r + \kappa k^2) \left(|\psi_{1,\mathbf{k}}|^2 + |\psi_{2,\mathbf{k}}|^2 \right) + (a + bk^2) \left(\psi_{1,\mathbf{k}}\psi_{2,-\mathbf{k}} + h.c. \right) \right] \\ & - \int d\mathbf{r} \left[\beta \left(\psi_{1,\mathbf{r}}^2\psi_{2,\mathbf{r}} + \psi_{2,\mathbf{r}}^2\psi_{1,\mathbf{r}} + h.c. \right) + \gamma \left(\psi_{1,\mathbf{r}}^3 + \psi_{2,\mathbf{r}}^3 + h.c. \right) \right] \\ & + \int d\mathbf{r} \left[u \left(|\psi_{1,\mathbf{r}}|^4 + |\psi_{2,\mathbf{r}}|^4 \right) + u' |\psi_{1,\mathbf{r}}|^2 |\psi_{2,\mathbf{r}}|^2 + \right. \\ & \left. u'' \left(\psi_{1,\mathbf{r}}\psi_{2,\mathbf{r}} + h.c. \right) \left(|\psi_{1,\mathbf{r}}|^2 + |\psi_{2,\mathbf{r}}|^2 \right) \right] + \dots . \end{aligned} \quad (3.36)$$

3.2.4 Phase Diagram

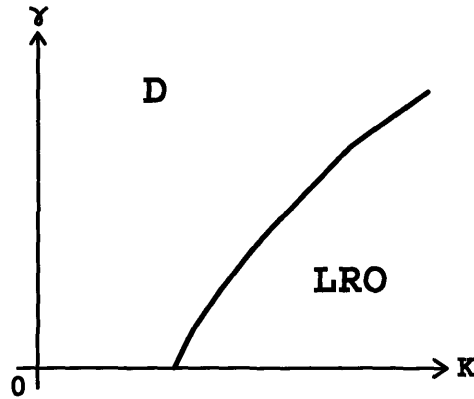
It is clear that at least for the coupling r sufficiently large and positive in (3.36) a stable disordered phase will exist where the \mathbb{Z}_3 symmetry is unbroken. This then corresponds to the translation symmetric phase of the original lattice model.

Ordered phases are also possible in this theory. In order to reveal their structure, we simply consider the static classical XY field configurations that minimize the action

of the effective XY model (3.25). Let us ignore the terms $\mathcal{O}(K^2, \gamma^2)$, and restrict our attention to configurations where the value $2\pi\chi_{\mathbf{r}}$ depends only on the sublattice to which the site \mathbf{r} belongs. The energy per unit-cell of such configurations is:

$$E = -3K \left[\cos 2\pi \left(\chi_1 - \chi_2 + \frac{1}{6} \right) + \cos 2\pi \left(\chi_2 - \chi_3 + \frac{1}{6} \right) + \cos 2\pi \left(\chi_3 - \chi_1 + \frac{1}{6} \right) \right] - \gamma \sum_{n=1}^3 \cos 2\pi (\chi_n - \chi_n^{(0)}) , \quad (3.37)$$

where we have labeled the sublattices by 1, 2, 3 in such a way that the background gauge field vector $A_{\mathbf{r}\mathbf{r}'}^{(0)}$ circulates in the direction $1 \rightarrow 2 \rightarrow 3 \rightarrow 1$. Two kinds of states can be found. For sufficiently large γ , the XY field simply follows the “external” XY field: $\chi_{\mathbf{r}} = \chi_{\mathbf{r}}^{(0)}$, and an XY “spin density wave” is established at the wavevector \mathbf{Q} . Naively, the XY rotation and lattice symmetries appear explicitly broken in this state. However, the angular order parameter $2\pi\chi_{\mathbf{r}} = 2\pi\chi_{\mathbf{r}}^{(0)}$ is invariant under the lattice translations (3.26) (and other lattice transformations), so that this state of the effective XY model corresponds to the disordered state of the original spin model. On the other hand, if $\gamma = 0$ the ordering will be determined by the nearest-neighbor interaction K . As we have argued before, there are two ordering wavevectors ($\mathbf{q} = 0$ and $\mathbf{q} = -\mathbf{Q}$) preferred by the K term, but neither of them coincides with the wavevector that describes spatial variations of the external XY field $\chi_{\mathbf{r}}^{(0)}$. Consequently, any small non-zero γ will introduce frustration, and deform the spontaneously ordered XY “spin density wave” preferred by the K term. Even though the precise description of the ordering pattern is complicated, it is at least apparent that the XY fields $\chi_{\mathbf{r}}$ align with the external field $\chi_{\mathbf{r}}^{(0)}$ on one sublattice of the triangular lattice, while on the other two sublattices they cant toward the external field, simultaneously trying to preserve the preferred ordering wavevector. Arbitrary choice of sublattice for the alignment gives rise to a three-fold degeneracy, so that the γ term breaks the continuous XY symmetry down to a \mathbb{Z}_3 subgroup, associated with lattice transformations (as evident in the Equation (3.34)). However, choice of the “parent” ordering wavevector ($\mathbf{q} = 0$ or $\mathbf{q} = -\mathbf{Q}$) for sufficiently small γ is also available, and we will briefly discuss its physical origin later.



D corresponds to the disordered phase of the original Kagome spin model. LRO is a spontaneously long-range ordered phase.

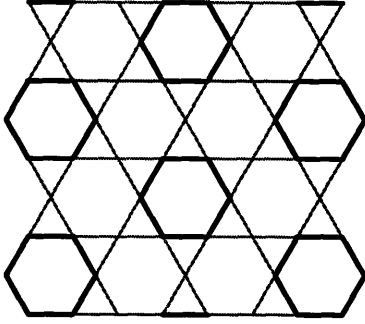
Figure 3-8: Schematic phase diagram of the effective XY model

We can finally sketch the phase diagram of the effective XY model (3.25), as shown in the Fig. 3-8. The phase D is invariant under lattice translations (3.26) and global spin-flip (3.38), so that it corresponds to the disordered phase of the original spin model (3.4), realized for $\Gamma \gg t$. The spontaneously long-range ordered phase LRO is obtained in the opposite limit of strong hexagon ring-exchange $\Gamma \ll t$. This phase is interesting in its own right, and we will discuss it more in the next section. After understanding it better, we will argue that the phase transition is probably of the second order.

3.2.5 Phase With Broken Translational Symmetry

We have seen that translational symmetry is broken in a three-fold degenerate manner in the LRO phase. However, the order parameter has an additional Ising-like degree of freedom. Formally, it is the freedom to choose the ordering wavevector $\mathbf{q} = 0$ or $\mathbf{q} = -\mathbf{Q}$ in the effective XY model, and we will now reveal its physical meaning.

One symmetry transformation that we have ignored so far is the global spin-flip in the original spin model on the Kagome lattice: $S_i^z \rightarrow -S_i^z$. It is straight forward to trace back how this transformation affects the quantities of the $U(1)$ gauge theory, and its dual theory on the triangular lattice. For example, at the level of Equation (3.18), which describes the dual theory on the triangular lattice with integer-valued



The most symmetric pattern of three-fold translational symmetry breaking on the Kagome lattice. Roughly speaking, the six spins on the emphasized hexagons are alternating, and coherently resonating as a singlet $\frac{|\uparrow\uparrow\uparrow\downarrow\downarrow\rangle + |\downarrow\downarrow\downarrow\uparrow\uparrow\rangle}{\sqrt{2}}$, while the remaining spins are ferromagnetically aligned with each other and break the global spin-flip symmetry. Note that in the Hamiltonian (3.4) the energy is reduced by $\mathcal{O}(t)$ on every resonating hexagon.

Figure 3-9: Long-range ordered phase

gauge field $A_{rr'}$, and integer-valued $\chi_r - \chi_r^{(0)}$, the global spin-flip corresponds to:

$$\begin{aligned} A_{rr'} &\longrightarrow (A_{rr'}^{(0)} + \chi_{r'}^{(0)} - \chi_r^{(0)}) - A_{rr'} \\ \chi_r &\longrightarrow -\chi_r - \chi_r^{(0)}. \end{aligned} \quad (3.38)$$

Note that the action (3.18) is invariant under this transformation, and that the integer constraints are not affected. Only the second part of this transformation (involving the χ_r field) survives in the effective XY theory (3.25). If we now turn to the continuum limit, we find from (3.31), (3.32) and (3.38) that the global spin-flip is represented by:

$$\psi_{1,\mathbf{r}} \longrightarrow \psi_{2,\mathbf{r}}^* \quad , \quad \psi_{2,\mathbf{r}} \longrightarrow \psi_{1,\mathbf{r}}^* . \quad (3.39)$$

Since the fields $\psi_{1,\mathbf{r}}$ and $\psi_{2,\mathbf{r}}$ describe the XY “spin density waves” at wavevectors $\mathbf{q} = 0$ and $\mathbf{q} = -\mathbf{Q}$ respectively, we see that the spin-flip formally exchanges these two kinds of order in the effective theory. Apparently, this transformation is completely independent from lattice translations. Therefore, the choice of the “parent” ordering wavevector ($\mathbf{q} = 0$ or $\mathbf{q} = -\mathbf{Q}$) in the spontaneously ordered phase must correspond to the choice of direction of the global magnetization.

In conclusion, the LRO phase is spontaneously magnetized. This provides important for understanding the order parameter more microscopically. Since the translation symmetry is broken in a three-fold degenerate manner, the spatial pattern of symmetry breaking is most naturally given by the Figure 3-9. From knowing that the LRO phase is shaped by dominant hexagon ring-exchange ($\Gamma \ll t$) we can expect

that every emphasized hexagon in this pattern represents a group of six anti-aligned spins that coherently fluctuate in a singlet fashion (this minimizes the ring-exchange energy). Then, the broken Ising symmetry requires that the remaining spins (which do not belong to the emphasized hexagons) carry net Ising magnetization. We would like to note that such a state fits description of a state with one-third of saturated magnetization on the Kagome lattice that was found responsible for plateaus in the magnetization curves of some Kagome-based systems [76]. Therefore, this phase should be smoothly connected to the regions with the magnetization plateau.

It is also worth noting that a small *longitudinal* field in the original Kagome lattice spin model would lift the two-fold Ising degeneracy, but not the three-fold lattice degeneracy of the LRO phase. This is another support of the Ising symmetry breaking. The three-fold anisotropic XY model in such circumstances would have symmetries of a 3-state clock model on the triangular lattice, which is known to experience a second-order phase transition into a disordered phase [77, 78, 79]. Therefore, the phase transition in the Figure 3-8 is most likely second-order.

3.3 Discussion

The theory of the Kagome lattice quantum Ising model that we have presented reveals that a disordered ground state is found for weak transverse fields. This disordered phase breaks no symmetries and is not topologically ordered either. It is therefore expected to be smoothly connected to the completely uncorrelated phase at large transverse fields. The same conclusion has been strongly suggested by Monte Carlo simulations [67, 68], where no phase transition was detected as the strength of transverse field was varied.

We have demonstrated how the Kagome lattice quantum Ising model can be described by a compact U(1) gauge theory with some fixed background charge at each lattice site. Such a gauge theoretic description has been useful in studies of similar Ising models on other frustrated lattices. The crucial distinction between the Kagome and other common systems is in the fact that the U(1) gauge theory of the

Kagome system contains a dynamical matter field. Without a matter field, these gauge theories of the frustrated magnets in two-dimensions always ultimately live in a confined phase that breaks translation symmetry. The latter is caused by the fixed background charge in the gauge theory. However, in the presence of dynamical matter fields a translation invariant (“Higgs”) phase is generally possible. In situations where the matter field has gauge charge 2 (as happens in the gauge theoretic description of quantum dimer models on non-bipartite lattices) such a Higgs phase also possesses topological order and associated “vison” excitations: for instance, there is a non-trivial ground state degeneracy on topologically non-trivial manifolds. In the problem discussed in this chapter the matter field had gauge charge 1. The resulting Higgs phase, while translation invariant, is topologically trivial. This then lends strong support to the conjecture in Ref.[68] that weak transverse fields on the Kagome Ising magnet lead to a phase that is smoothly connected to the trivial paramagnet that obtains at strong transverse fields.

In fact, topological triviality of the discovered disordered phase is a very interesting detail. From the beginning of the quest for interesting quantum spin liquids, the frustrated magnets had been looked upon with great hope. In particular, the systems with extremely large classical ground state degeneracy have attracted considerable attention. The pyrochlore and Kagome lattices are thought to be ideal candidates for the spin liquid, because their corner-sharing structure provides such extremely large degeneracy, which is then dramatically lifted even by weak quantum fluctuations. However, in the case of the Kagome lattice transverse-field quantum Ising model, the corner-sharing geometry seemingly makes the lattice virtually disconnected. Even though there is no long-range order in the ground state, the obtained disordered phase is not a topologically ordered spin liquid. One may then ask whether a frustrated, but somewhat more connected lattice is a better platform to seek topologically non-trivial spin liquids. Another question is if a more correlated spin dynamics, such as the one found in anisotropic easy-axis Heisenberg models, is more likely to yield such interesting spin liquids. In the next chapter we attempt to find some answers to these questions.

Chapter 4

Bridging Between Ising and Heisenberg Magnets on the Kagome Lattice

Discussion in the previous two chapters provided insight into two characteristic problems. The Kagome lattice Heisenberg model was studied using a \mathbb{Z}_2 gauge theory, which discovered likely phases of this system at expense of one not well controlled approximation. On the other hand, somewhat less natural Ising model in weak transverse field was understood with much more mathematical rigor, at least when it comes to which phases are possible. Our main goal in this chapter is to explore the XXZ model on the Kagome lattice. This model is dynamically very similar to the truly challenging Heisenberg model, yet it can be studied with tools appropriate for the quantum Ising models.

We will first develop a new U(1) gauge theory using a transverse field Ising model. It will give us more insight into the weak transverse field quantum dynamics, reproduce the disordered phase found in the previous chapter and even suggest that the Gutzwiller-like projection is a good route to constructing variational wavefunctions in this problem. Then, the U(1) gauge theory will be extended to the XXZ model. By maximizing entropy of quantum fluctuations (an extension of the mean-field theory to frustrated systems) we will find a disordered and a valence-bond crystal phase. It

will be argued that the former is a spin liquid (with topological order), and that the latter is probably the same ordered phase that was found in the isotropic Heisenberg model in chapter 2.

In this chapter we also attempt to learn general lessons on the role played by lattice structure, symmetries and type of dynamics in shaping phases of frustrated quantum magnets. The present analysis is focused on the prototype Kagome lattice Ising antiferromagnets, but the range of explored models admits all characteristic quantum paramagnetic phases: disordered, spin liquid, and valence-bond solid. Through connecting these outcomes with both the fundamental and microscopic properties of the models, and with information that emerges from calculations, we can suggest some conclusions of broader significance for the spin models on other lattices. The Kagome lattice is an excellent choice for this pursuit because it is one of the few simple spin systems (with only nearest-neighbor interactions) where disordered and spin liquid phases are believed to exist.

4.1 Models and Overview

In this chapter we analyze the nearest-neighbor spin $S = \frac{1}{2}$ quantum Ising antiferromagnets on the Kagome lattice (Fig. 2-2). Two kinds of spin dynamics will be explored, represented by the following simple models:

- transverse field Ising model (TFIM):

$$H = J_z \sum_{\langle ij \rangle} S_i^z S_j^z - \Gamma \sum_i S_i^x ; \quad (4.1)$$

- XXZ model:

$$H = J_z \sum_{\langle ij \rangle} S_i^z S_j^z \pm J_\perp \sum_{\langle ij \rangle} (S_i^x S_j^x + S_i^y S_j^y) . \quad (4.2)$$

In contrast to the transverse field case, the XXZ dynamics preserves total Ising magnetization, making the Hamiltonian (4.2) symmetric under global spin-flip. Furthermore, the transverse field gives rise to the most local kind of spin dynamics, while

the XXZ dynamics involves pairs of spins, and thus introduces some correlation. It will become apparent that these two fundamental differences yield very different low energy physics. The consequent analysis will also admit introduction of other dynamical processes, spatially extended to larger clusters of spins, but consistent with the symmetries of these two basic models.

The calculations will be restricted to weak dynamical perturbations of the pure Ising model: $\Gamma, J_{\perp} \ll J_z$. This limit is a combination of analytical convenience, and essential physical interest in the context of frustrated magnetism. The main question being asked is how the quantum fluctuations (created by weak dynamical perturbations) lift degeneracy of the pure Ising model. Is the ground state ordered like in most other two-dimensional Ising systems? Under what general circumstances a completely disordered ground state is possible, with or without non-trivial topology? In attempt to answer these questions, we will formulate a lattice field theory and apply to it a technique specialized for frustrated systems, but otherwise analogous to the usual mean-field approach in the unfrustrated problems. Namely, instead of finding the mean-field solutions that minimize energy in various parameter regimes, we will seek solutions that maximize “entropy” of quantum fluctuations [71]. When needed, those solutions will be subject to a verification of stability. This will provide a reliable picture of the phases that exist in these models. Some more introductory reading for methods that we will use can be found in the References [70, 72, 73].

Physics of the Kagome TFIM is trivial when the transverse field Γ is large, while in the limit $\Gamma \ll J_z$ the quantum dynamics, as a matter of principle, has a chance to yield interesting valence bond ordered or disordered ground-states. Even though the effect of small transverse fields has been already understood in Chapter 3, the following approach is going to bring some new insight. Of course, much closer to the true challenge of Kagome Heisenberg antiferromagnet is the XXZ model, which can be regarded as its anisotropic version when the proper sign for J_{\perp} is taken in (4.2). That choice of sign, unfortunately, leads to a well known “sign problem”. While calculations will be ultimately performed in the case when there is no “sign problem” (which is analogous to (4.1)), it will be argued that for questions of interest the

choice of sign for J_{\perp} does not matter. In fact, even though the easy-axis anisotropy is strong in the limit $J_{\perp} \ll J_z$, a sensible comparison with the isotropic Heisenberg model will become apparent.

The TFIM model is discussed in Section 4.2, while the XXZ model is studied in Section 4.3. Initial discussion of the XXZ model relies heavily on the definitions and ideas introduced in the TFIM Section (sections 4.2 through 4.2.3). Readers interested only in the physical nature of the valence-bond ordered and spin liquid phases of the XXZ models can skip all calculations and go directly to the sections 4.3.6 and 4.3.7. All conclusions are summarized and bigger perspective is taken in the Discussion.

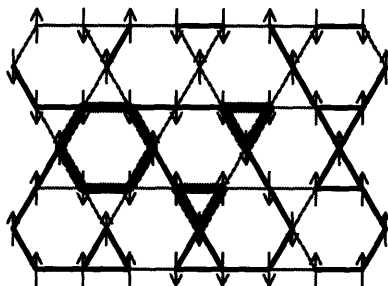
4.2 Transverse Field Ising Model

4.2.1 Compact U(1) Gauge Theory of the Frustrated Bonds

We start from the Kagome lattice Ising model in a weak transverse field $\Gamma \ll J_z$:

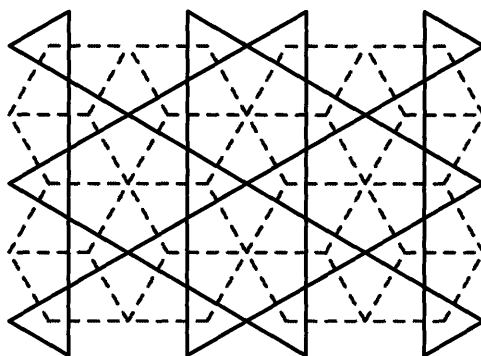
$$H = J_z \sum_{\langle ij \rangle} S_i^z S_j^z - \Gamma \sum_i S_i^x. \quad (4.3)$$

Let us first understand the ground states of the pure Ising Hamiltonian ($\Gamma = 0$). They are the *least frustrated* states in which the number of *frustrated* bonds (two aligned spins) is minimized. If every frustrated bond is visualized by a dimer, then every appropriate dimer covering determines a spin configuration up to a global spin flip. Consider a loop on the Kagome lattice (Fig. 4-1). The unfrustrated bonds on the loop mark locations where the two neighboring spins on the loop have different orientation. When going one full circle around the loop one ends at the same spin from which one started, so that the number of times the spin orientation is changed must be even. Therefore, every loop contains an even number of unfrustrated bonds, and the parity of the number of dimers on the loop is determined by the loop size. The number of dimers on the triangular (hexagonal) Kagome plaquettes must be



Every loop holds an even number of unfrustrated bonds. Dimers represent the frustrated bonds, or pairs of aligned spins.

Figure 4-1: Frustrated bonds on the Kagome lattice



Dice lattice is plotted dashed. Duality transforms a Kagome site into the dice plaquette inside which it sits, and vice versa. The 3-coordinated dice sites and Kagome triangles transform into each other, as well as the 6-coordinated dice sites and Kagome hexagons. Every Kagome bond intersects one dual dice bond.

Figure 4-2: Duality between the Kagome and dice lattices

odd (even). This is the only constraint for the Kagome lattice dimer coverings that correspond to arbitrary spin states.

It will be convenient to immediately switch to the dual picture. Duality between the Kagome and dice lattices is depicted in the Fig. 4-2. Since every Kagome bond corresponds to one dice lattice bond, the frustrated bonds can be represented by dimers on either lattice. An example is shown in the Fig. 4-3. There must be an odd (even) number of dimers emanating from every 3-coordinated (6-coordinated) dice lattice site. The number of dimers (and thus frustration) is minimized if there is exactly one dimer emanating from every 3-coordinated dice lattice site. This condition fixes the number of dimers in the least frustrated states, since the dice lattice is bipartite. Degeneracy of the least frustrated states is apparently huge.

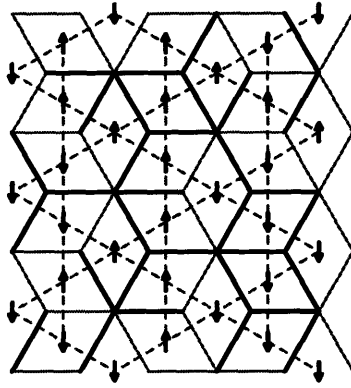


Figure 4-3: Frustrated bonds represented by dimers on the dice lattice

Small dynamical perturbations will mix the least frustrated states and lift their immense degeneracy. In principle, one can perturbatively derive an effective theory that describes dynamics at energy scales well below J_z . This effective theory lives in the Hilbert space spanned only by the least frustrated states. Therefore it takes form of a soft-core quantum dimer model on the dice lattice, where exactly one dimer emanates from every 3-coordinated dice site, while an arbitrary even number of dimers emanate from every 6-coordinated site. For our purposes it will be sufficient to concentrate just to the first order of degenerate perturbation theory:

$$H_{\text{eff}} = -\frac{\Gamma}{2} \sum_{\diamond} (|\diamond\rangle\langle\diamond| + h.c.) - \frac{\Gamma}{2} \sum_{\diamond} (|\diamond\rangle\langle\diamond| + h.c.) . \quad (4.4)$$

The dimer dynamics consists of two different flips on the dice plaquettes that are consistent with minimum frustration (see Fig. 4-5). Note that these two processes involve flipping of only one spin on the Kagome lattice. For the purposes of simplicity and staying close to the original spin dynamics, we will not consider a more general dimer model with different energy scales for the two types of flips. Since the dice lattice is bipartite, it is possible to apply standard techniques and cast this dimer model as a compact $U(1)$ gauge theory [70]. From that point on, duality transformations and lattice-field-theoretical methods are at disposal to study possible phases. After understanding phases that the lattice theory yields, it will be apparent that sufficiently small higher order perturbations cannot destabilize them.

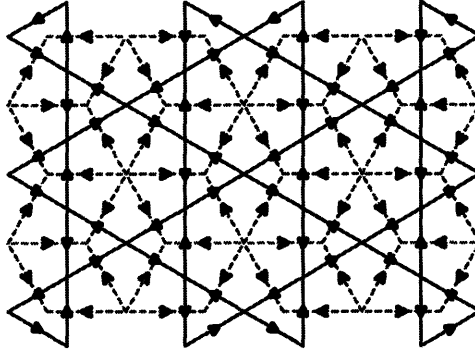
$i, j \dots$	Kagome lattice sites, or dual dice plaquettes
$p, q \dots$	dual dice lattice sites, or Kagome plaquettes
p_3	3-coordinated dice sites, or Kagome triangles
p_6	6-coordinated dice sites, or Kagome hexagons
$\langle ij \rangle$	Kagome lattice bonds
$\langle pq \rangle$	dual dice lattice bonds

Table 4.1: Notation for the Kagome and dual dice lattices

Some comments are in order before proceeding. First, the dimer representation is insensitive to global spin flip. This is of no concern for the models studied here, since magnetically ordered phases will not be found. Secondly, the dice lattice dimer model in its own right has non-trivial topology (topological order is possible), just like the other quantum dimer models. However, only one of its topological sectors corresponds to physical spin states on a torus. Therefore, the original spin model need not have any topological order.

Calculations in this thesis rely heavily on duality between the Kagome and dice lattices (see Fig. 4-2). In order to facilitate mathematical manipulations, we will treat both lattices on the same footing, and regard pairs of objects related by duality as identical. Notation that we will use from now on is summarized in the Table 4.1. Note that, according to this principle, any quantity that lives on a Kagome bond equivalently lives on the dual dice bond, and may be labeled by either Kagome, or dice bond labels. Also, we will apply the following convention: if an equation shows relationship between expressions defined on different lattices, the dual lattice objects are always implied (for example, Kagome site \Leftrightarrow dual dice plaquette, Kagome bond \Leftrightarrow dual dice bond. . .).

Let us also introduce a vector notation. We will distinguish vectors R_{pq} from the corresponding bond scalars $R_{\langle pq \rangle}$ in that the vectors will change sign if the bond orientation is reversed: $R_{pq} = -R_{qp}$, while the scalars will not: $R_{\langle pq \rangle} = R_{\langle qp \rangle}$. In order to establish a formal connection between the bond vectors and scalars, we assign orientation to the lattice bonds. Let the vector η_{pq} equal +1 if the bond $\langle pq \rangle$ is oriented from p to q , and -1 otherwise. Then, the vectors and corresponding bond scalars are related by $R_{pq} = \eta_{pq} R_{\langle pq \rangle}$. These relations are applicable to both



The bipartite dice lattice bonds are oriented from the 6-coordinated site to the 3-coordinated site. Every Kagome bond orientation is locked to the orientation of the dual dice bond by the “right hand rule”. Note that the Kagome orientations circulate around triangles and hexagons in the different directions.

Figure 4-4: Reference bond orientations of the Kagome and dice lattices

the dice and Kagome lattices. Bond orientation will transform by duality according to the “right hand rule”. Since the dice lattice is bipartite, we will orient its bonds in a natural way, and chose the orientation to be from the 6-coordinated to the 3-coordinated site on every bond. This fixes orientation of the Kagome bonds as well, and we show both in the Fig. 4-4.

Now we can define the electric field E_{pq} as a vector corresponding to the scalar bond energy $E_{\langle pq \rangle}$:

$$E_{\langle pq \rangle} = \begin{cases} 0 & , \text{ vacancy (unfrustrated bond } \langle pq \rangle) \\ 1 & , \text{ dimer (frustrated bond } \langle pq \rangle) \end{cases}$$

$$E_{pq} = \eta_{pq} E_{\langle pq \rangle} . \quad (4.5)$$

Hilbert space of the least frustrated states has restrictions that are easily expressed in the form of a Gauss’ Law. The number of dimers $E_{pq} = \eta_{pq}$ emanating from any 3-coordinated site is one, and from any 6-coordinated site an even number ($2n_{p_6}$). We use the convention that every dice bond is oriented from the 6-coordinated to the

3-coordinated site, and write:

$$\begin{aligned}
(\forall p_3) \quad \sum_{q \in p_3} E_{p_3 q} &= -1 , \\
(\forall p_6) \quad \sum_{q \in p_6} E_{p_6 q} &= 2n_{p_6} .
\end{aligned} \tag{4.6}$$

Interpretation of this Gauss' Law is that there is a fixed background charge -1 on every 3-coordinated dice site, and a number $0 \leq n_{p_6} \leq 3$ of charge 2 bosons on every 6-coordinated site. The charged bosons are independent degrees of freedom living on the 6-coordinated dice sites. Formally, they emerge because the dice lattice dimer model is not hard-core.

Dynamics of the fields and particles can be easily formulated if the Hilbert space is expanded to allow arbitrary integer strength of the electric field, and arbitrary particle occupation. Promoting E_{pq} and n_{p_6} into free integers between $-\infty$ and $+\infty$ makes it easy to write the creation and annihilation operators: $\exp(\pm i\mathcal{A}_{pq})$ for the field lines, and $\exp(\pm i\varphi_{p_6})$ for the particles. The vector potential \mathcal{A}_{pq} and the boson phase φ_{p_6} are conjugate angle operators to the electric field E_{pq} and particle number n_{p_6} respectively:

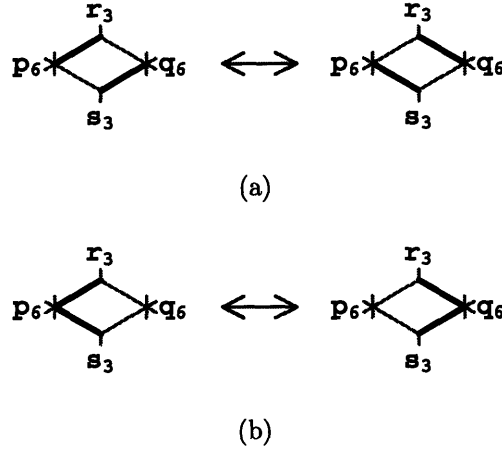
$$[\mathcal{A}_{pq}, E_{pq}] = [\varphi_{p_6}, n_{p_6}] = i . \tag{4.7}$$

After the Hilbert space has been expanded, we must at least introduce a large energy cost to all “unphysical” states, so that the low energy physics will still correspond to the dimer model (4.4). This is achieved in the large U limit through the following new term in the Hamiltonian:

$$H_u = U \sum_{\langle pq \rangle} \left(E_{\langle pq \rangle} - \frac{1}{2} \right)^2 = U \sum_{\langle pq \rangle} E_{pq}^2 + \text{const.} . \tag{4.8}$$

The term linear in electric field is a global constant, since it expresses the fixed total number of dimers on the dice lattice (in the least frustrated states).

Now we formulate dynamics of (4.4) in the U(1) language. The two processes of interest are shown in the Fig. 4-5. Recall that every dimer means $E_{\langle pq \rangle} = 1$, and



(a) Number of dimers emanating from every site is preserved; (b) a pair of dimers is exchanged between two 6-coordinated sites.

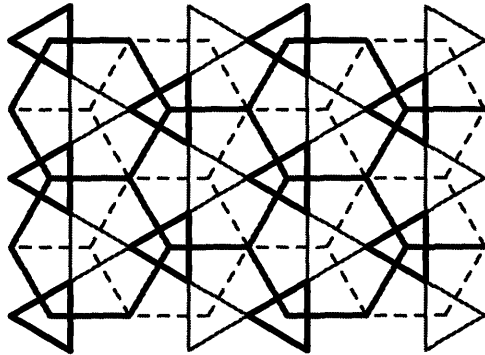
Figure 4-5: Elementary processes on a dice plaquette that preserve the minimum frustration

every vacancy $E_{\langle pq \rangle} = 0$, and that n_{p_6} is the number of dimer pairs emanating from a 6-coordinated site. Therefore, we can easily exploit the dice bond orientations, and arrange the creation and annihilation operators to describe the allowed dimer flip processes (a) and (b) shown in the Fig. 4-5:

$$\begin{aligned}
(a) &\sim \exp(i\mathcal{A}_{\langle p_6 s_3 \rangle}) \exp(-i\mathcal{A}_{\langle q_6 s_3 \rangle}) \exp(i\mathcal{A}_{\langle q_6 r_3 \rangle}) \exp(-i\mathcal{A}_{\langle p_6 r_3 \rangle}) + h.c. \\
&= 2 \cos(\mathcal{A}_{p_6 s_3} + \mathcal{A}_{s_3 q_6} + \mathcal{A}_{q_6 r_3} + \mathcal{A}_{r_3 p_6}) \\
&= 2 \cos\left(\sum_{pq}^{\circlearrowleft} \mathcal{A}_{pq}\right), \tag{4.9}
\end{aligned}$$

$$\begin{aligned}
(b) &\sim \exp(i\varphi_{q_6}) \exp(-i\varphi_{p_6}) \times \\
&\quad \times \exp(-i\mathcal{A}_{\langle p_6 s_3 \rangle}) \exp(i\mathcal{A}_{\langle q_6 s_3 \rangle}) \exp(i\mathcal{A}_{\langle q_6 r_3 \rangle}) \exp(-i\mathcal{A}_{\langle p_6 r_3 \rangle}) + h.c. \\
&= 2 \cos(\varphi_{q_6} - \varphi_{p_6} - \mathcal{A}_{p_6 s_3} - \mathcal{A}_{s_3 q_6} + \mathcal{A}_{q_6 r_3} + \mathcal{A}_{r_3 p_6}) \\
&= 2 \cos\left(\varphi_{q_6} - \varphi_{p_6} + \eta_{p_6 q_6} \sum_{pq}^{\circlearrowleft} \varepsilon_{\langle pq \rangle} \mathcal{A}_{pq}\right). \tag{4.10}
\end{aligned}$$

In the last lines of these expressions the sums are taken around a plaquette in the counter-clockwise sense; this is the lattice circulation, or the curl. Expression (4.9) is the usual “magnetic” energy, while expression (4.10) is boson hopping between



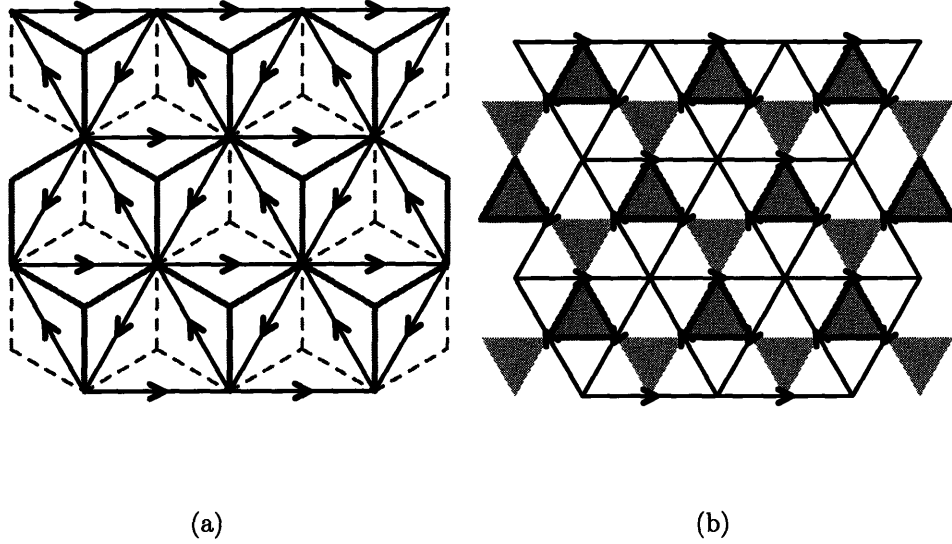
$\varepsilon_{\langle ij \rangle} \equiv \varepsilon_{\langle pq \rangle}$ take the value -1 on the emphasized bonds, and $+1$ on all other bonds.

Figure 4-6: Special bond signs on the Kagome and dice lattices

neighboring 6-coordinated sites. In this thesis we will not use a more conventional form of particle hopping that involves an “integral” of the vector potential along only one path between the two sites. In the equation (4.10) we have introduced two new symbols: $\varepsilon_{\langle pq \rangle}$ and $\eta_{p_6 q_6}$. The former is needed to correct the signs of \mathcal{A}_{pq} that appear in the circulation. Note that the signs have been altered with respect to the ordinary circulation in (4.9) only on one of the two paths that connect the two 6-coordinated sites. This allows us to choose $\varepsilon_{\langle pq \rangle}$ as shown in the Fig. 4-6. The other symbol, $\eta_{p_6 q_6}$ is needed to ensure that expression inside the cosine of (4.10) transforms properly when the sites p_6 and q_6 are exchanged. This is a new vector, defined on the triangular lattice formed by the 6-coordinated dice sites, or equivalently the centers of the Kagome hexagons. Since it takes values ± 1 , it defines bond orientations shown in the Fig. 4-7. Notice that $\eta_{p_6 q_6}$ must be related to $\varepsilon_{\langle pq \rangle}$: if one takes a closer look at the cosines in (4.10), one can see that when the boson hops from p_6 to q_6 , the circulation starting from p_6 must first go through the $\varepsilon_{\langle pq \rangle} = -1$ bonds. When this is satisfied for the counter-clockwise circulation, $\eta_{p_6 q_6}$ should be $+1$, otherwise it should be -1 . Exactly this is achieved by relating η and ε vectors as shown in the Fig. 4-7.

Finally, we can summarize the compact U(1) gauge theory on the dice lattice. The Hamiltonian is:

$$H = U \sum_{\langle pq \rangle} E_{pq}^2 - \Gamma \sum_{\diamond} \left[\cos \left(\sum_{pq} \mathcal{A}_{pq} \right) + \cos \left(\varphi_{q_6} - \varphi_{p_6} + \eta_{p_6 q_6} \sum_{pq} \varepsilon_{\langle pq \rangle} \mathcal{A}_{pq} \right) \right], \quad (4.11)$$



Bond orientations represent $\eta_{p_6q_6}$. Dice and Kagome bonds with $\varepsilon_{\langle pq \rangle} \equiv \varepsilon_{\langle ij \rangle} = -1$ are emphasized. Notice in (b) that every triangular lattice bond contains one Kagome site.

Figure 4-7: Bond orientations of the triangular lattice formed by the Kagome hexagon centers

and the Hilbert space is constrained by the Gauss' Law:

$$\begin{aligned}
 (\forall p_3) \quad \sum_{q \in p_3} E_{p_3q} &= -1, \\
 (\forall p_6) \quad \sum_{q \in p_6} E_{p_6q} &= 2n_{p_6} + 2.
 \end{aligned} \tag{4.12}$$

For convenience that will become apparent later, we have shifted n_{p_6} by one in the bottom expression (this sets to zero the total background charge on the lattice). In the limit of $U \rightarrow \infty$ this Hamiltonian is an exact rewriting of the effective theory (4.4). For finite and large U , one perturbatively obtains a theory as a Γ/U expansion that introduces dimer flip processes on larger loops. This physically corresponds to further-neighbor and multiple-spin exchange that would be also generated by not so small Γ in the original spin model (4.3). Owing to this approximate correspondence between finite U and larger Γ , we might have means to qualitatively see some trends beyond very small Γ/J_z .

4.2.2 Duality Transformation

The path-integral corresponding to (4.11) describes a (2+1)D electrodynamics. All fluctuations are constrained by (4.12). The action will contain a usual Berry's phase (we will omit the time index):

$$S_B = -i \sum_{\tau} \left(\sum_{\langle pq \rangle} \mathcal{A}_{pq} \Delta_{\tau} E_{pq} + \sum_{p_6} \varphi_{p_6} \Delta_{\tau} n_{p_6} \right), \quad (4.13)$$

and a potential energy part:

$$S_{\text{pot}} = U \delta\tau \sum_{\tau} \sum_{\langle pq \rangle} E_{pq}^2, \quad (4.14)$$

where $\delta\tau$ is imaginary time increment. The kinetic energy, which involves the cosines in (4.11), can be brought to a more tractable form by applying the Villain's approximation. Two new fields will appear and play a significant role: magnetic field scalar B_i that lives on the Kagome sites dual to the dice plaquettes, and particle current $j_{p_6 q_6}$ that lives as a vector on the triangular lattice bonds. Both will be integer valued, reflecting the compactness of the U(1) gauge theory, and fluctuations of both will be suppressed by the scale $g = |\log(\Gamma\delta\tau/2)|$. They take part in the action as follows:

$$S_{\text{kin}} = \sum_{\tau} \left[g \left(\sum_i B_i^2 + \sum_{\langle p_6 q_6 \rangle} j_{p_6 q_6}^2 \right) + i \sum_i B_i \sum_{pq} \overset{\curvearrowright}{\mathcal{A}}_{pq} + i \sum_{\langle p_6 q_6 \rangle} j_{p_6 q_6} \left(\varphi_{q_6} - \varphi_{p_6} + \eta_{p_6 q_6} \sum_{pq} \overset{\curvearrowright}{\varepsilon}_{\langle pq \rangle} \mathcal{A}_{pq} \right) \right]. \quad (4.15)$$

After writing this, the angles \mathcal{A}_{pq} and φ_{p_6} can be formally integrated out. Fluctuations of the boson phases φ_{p_6} will give rise to the particle current conservation law:

$$(\forall p_6) \quad \Delta_{\tau} n_{p_6} + \sum_{q_6 \in p_6} j_{p_6 q_6} = 0. \quad (4.16)$$

Fluctuations of the vector potential will give rise to the Maxwell's equation for the magnetic field curl: \mathcal{A}_{pq} is coupled to the magnetic field B_i , and current $j_{p_6 q_6}$ in

(4.15), as well as the time derivative of the electric field E_{pq} in (4.13), which is the “displacement” current. However, this equation will take an unusual form, because the particle and displacement currents formally live on different lattices. The easiest way to derive it is to rewrite the terms in which \mathcal{A}_{pq} appears using the Kagome lattice notation. For this purpose, let us note that the particle current $j_{p_6q_6}$ is related to the triangular lattice bond variable $j_{\langle p_6q_6 \rangle}$ by: $j_{p_6q_6} = \eta_{p_6q_6} j_{\langle p_6q_6 \rangle}$, which in turn can be regarded as actually living on the sites of the Kagome lattice (see Fig. 4-7). Therefore, we can label $j_{\langle p_6q_6 \rangle}$ as j_i , where i is the Kagome site that sits on the triangular bond $\langle p_6q_6 \rangle$. From (4.13) and (4.15) we have:

$$\begin{aligned}
\mathcal{A}_{pq} \Delta_\tau E_{pq} &\equiv \mathcal{A}_{ij} \Delta_\tau E_{ij} \\
B_i \sum_{pq} \mathcal{A}_{pq} &\equiv B_i \sum_{j \in i} \mathcal{A}_{ij} \\
j_{p_6q_6} \eta_{p_6q_6} \sum_{pq} \varepsilon_{\langle pq \rangle} \mathcal{A}_{pq} &\equiv j_i \sum_{j \in i} \varepsilon_{\langle ij \rangle} \mathcal{A}_{ij} .
\end{aligned} \tag{4.17}$$

The vector potential fluctuations set to zero the sum of everything coupled to \mathcal{A}_{ij} on every Kagome bond $\langle ij \rangle$. This is the Maxwell’s equation:

$$(\nabla \langle ij \rangle) \quad \Delta_\tau E_{ij} = B_i - B_j + \varepsilon_{\langle ij \rangle} (j_i - j_j) . \tag{4.18}$$

Once the phase and vector potential fluctuations have been integrated out, the remaining action contains only integer valued fields:

$$S = g \sum_\tau \left[\sum_i (B_i^2 + j_i^2) + \sum_{\langle ij \rangle} E_{ij}^2 \right] , \tag{4.19}$$

whose fluctuations are subject to the constraints (4.12), (4.16), and (4.18). For convenience, we have chosen the imaginary time increment $\delta\tau$ such that $g = U\delta\tau$; this will not affect the low energy physics, at least for large U .

Now we can proceed by solving the constraints. To this end, we want to completely switch back to the Kagome lattice. The duality transformation that follows had been

worked out in two typical cases. (a) If the compact U(1) gauge theory contains no charged particles, then the dual theory is an integer-valued height model. (b) If the particles and the electric field live on the same lattice, then the dual theory has a non-compact U(1) gauge structure, and a charged matter field [70]. The case (a) emerges from the hard-core dimer models on bipartite lattices, while the case (b) has been proposed as an approximate description of the hard-core dimer models on non-bipartite lattices. Our case is somewhat in between. It turns out that the dual theory for our case resembles the height model.

It is convenient to redefine the magnetic field and current as time derivatives of two integer-valued “height” fields, χ_i and λ_i :

$$B_i = \Delta_\tau \chi_i \quad , \quad j_i = \Delta_\tau \lambda_i . \quad (4.20)$$

Now, by introducing a $\lambda_{p_6 q_6}$ vector analogous to $j_{p_6 q_6}$, we can write solutions of the current conservation (4.16) and Maxwell’s equation (4.18):

$$n_{p_6} + \sum_{q_6 \in p_6} \lambda_{p_6 q_6} = 0 , \quad (4.21)$$

$$E_{ij} = \chi_i - \chi_j + \varepsilon_{\langle ij \rangle} (\lambda_i - \lambda_j) + \zeta_{ij} , \quad (4.22)$$

where ζ_{ij} is an integer that does not vary with time, and will be determined by substituting this expression into the Gauss’ Law (4.12). For consistency, let us first rewrite the Gauss’ Law using the Kagome lattice labels:

$$\begin{aligned} (\nabla \Delta_{p_3}) \quad \sum_{ij}^{\triangle_{p_3}} E_{ij} &= 1 , \\ (\nabla \circ_{p_6}) \quad \sum_{ij}^{\hexagon_{p_6}} E_{ij} &= -2n_{p_6} - 2 . \end{aligned} \quad (4.23)$$

The electric field divergence on the 3 and 6-coordinated dice sites in (4.12) transforms by duality into the lattice curl on the Kagome triangles and hexagons respectively.

Taking curls of (4.22) will annihilate χ_i on all Kagome plaquettes, as well as λ_i on the Kagome triangles, since $\varepsilon_{\langle ij \rangle}$ is fixed on every triangle (see Fig. 4-6). However, λ_i will not be annihilated by the curls on the Kagome hexagons. One can easily show that:

$$\sum_{ij}^{\circlearrowleft p_6} \varepsilon_{\langle ij \rangle} (\lambda_i - \lambda_j) = 2 \sum_{q_6 \in p_6} \lambda_{p_6 q_6} , \quad (4.24)$$

which in turn is equal to $-2n_{p_6}$ according to (4.21). Consequently, the equations that ζ_{ij} must satisfy are:

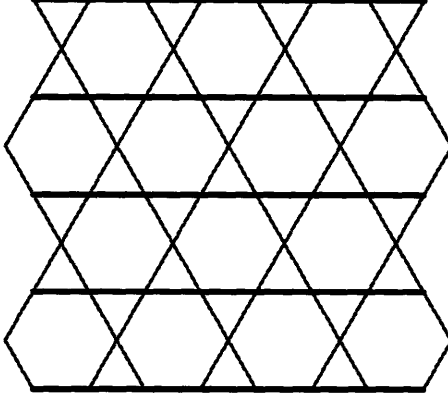
$$\begin{aligned} (\forall \Delta_{p_3}) \quad \sum_{ij}^{\triangleleft p_3} \zeta_{ij} &= 1 , \\ (\forall \square_{p_6}) \quad \sum_{ij}^{\circlearrowleft p_6} \zeta_{ij} &= -2 . \end{aligned} \quad (4.25)$$

There are many possible choices. In order to reveal them more tractably, let us use the Kagome bond orientations in Fig. 4-4, and switch to the appropriate bond scalars $\zeta_{\langle ij \rangle}$ (notice that the counter-clockwise circulations coincide with the bond orientations on the triangles, but not on the hexagons):

$$\begin{aligned} (\forall \Delta_{p_3}) \quad \sum_{\langle ij \rangle}^{\Delta_{p_3}} \zeta_{\langle ij \rangle} &= 1 , \\ (\forall \square_{p_6}) \quad \sum_{\langle ij \rangle}^{\square_{p_6}} \zeta_{\langle ij \rangle} &= 2 . \end{aligned} \quad (4.26)$$

If we decide to use only values 0 and 1 for $\zeta_{\langle ij \rangle}$, and visualize the value 1 as a dimer, we see that every triangular plaquette must hold one dimer, and every hexagonal plaquette two dimers. One such configuration is depicted in the Fig. 4-8. The other possible configurations need not be periodic on the lattice, but “breaking” of the translational symmetry is unavoidable as long as $\zeta_{\langle ij \rangle}$ are integers.

This concludes solution of all the constraints (4.12), (4.16), and (4.18). The final lattice field theory describes fluctuations of the two integer-valued height fields



Every dimer represents $\zeta_{\langle ij \rangle} = 1$, and vacancy $\zeta_{\langle ij \rangle} = 0$.

Figure 4-8: One characteristic and periodic configuration of background field

on the (2+1)D Kagome lattice. We obtain the action by substituting (4.20) and (4.22) into (4.19):

$$S = g \sum_{\tau} \left[\sum_i \left((\Delta_{\tau} \chi_i)^2 + (\Delta_{\tau} \lambda_i)^2 \right) + \sum_{\langle ij \rangle} \left(\chi_i - \chi_j + \varepsilon_{\langle ij \rangle} (\lambda_i - \lambda_j) + \zeta_{ij} \right)^2 \right]. \quad (4.27)$$

4.2.3 Degeneracy and Fluctuations

Before proceeding with analysis of fluctuations in the lattice theory (4.27), we have to reveal several of its important properties. We begin by finding all configurations of integer-valued $\chi_i = \chi_i^{(0)}$ and $\lambda_i = \lambda_i^{(0)}$ that minimize the action. Clearly, $\chi_i^{(0)}$ and $\lambda_i^{(0)}$ should have no time dependence. However, in terms of spatial variations, there will be a large degeneracy. Let us define:

$$\xi_{ij} = \chi_i^{(0)} - \chi_j^{(0)} + \varepsilon_{\langle ij \rangle} (\lambda_i^{(0)} - \lambda_j^{(0)}) + \zeta_{ij}. \quad (4.28)$$

At a saddle-point, the action reduces to the sum of ξ_{ij}^2 on all Kagome bonds. The constraints that ξ_{ij} must obey can be extracted by tracing back ξ_{ij} to E_{ij} . Recall that this lattice field theory describes a particular soft-core dimer model in which $E_{\langle ij \rangle} = 1$ represents a dimer. Therefore, the action will be minimized for all allowed dimer coverings of the Kagome lattice, by taking $\xi_{\langle ij \rangle} = 1$ for a dimer, and 0 for a vacancy. There will be one dimer on every Kagome triangle, and an arbitrary

even number of dimers on every Kagome hexagon. Note that every action minimum corresponds to two least frustrated spin configurations of the Kagome Ising model (4.3), which are related to each other by the global spin flip.

Shifting the height fields by $\chi_i^{(0)}$ and $\lambda_i^{(0)}$ allows us to study fluctuations about a particular saddle-point. The action takes a more general form:

$$S = g \sum_{\tau} \left[\sum_i \left((\Delta_{\tau} \chi_i)^2 + (\Delta_{\tau} \lambda_i)^2 \right) + \sum_{\langle ij \rangle} \left(\chi_i - \chi_j + \varepsilon_{\langle ij \rangle} (\lambda_i - \lambda_j) + \xi_{ij} \right)^2 \right]. \quad (4.29)$$

After ‘‘summation by parts’’, we can write it in a matrix form:

$$\begin{aligned} \frac{S}{g} &= \sum_{\tau} \sum_i \left[2\chi_i \sum_{j \in i} \xi_{ij} + 2\lambda_i \sum_{j \in i} \varepsilon_{\langle ij \rangle} \xi_{ij} \right. \\ &\quad \left. + \chi_i \left(6\chi_i - (\chi_{i,\tau+1} + \chi_{i,\tau-1}) - \sum_{j \in i} (\chi_j + \varepsilon_{\langle ij \rangle} \lambda_j) \right) \right. \\ &\quad \left. + \lambda_i \left(6\lambda_i - (\lambda_{i,\tau+1} + \lambda_{i,\tau-1}) - \sum_{j \in i} (\lambda_j + \varepsilon_{\langle ij \rangle} \chi_j) \right) \right] \\ &= \boldsymbol{\chi}^T \mathbf{C} \boldsymbol{\chi} + (\boldsymbol{\chi}^T \boldsymbol{\xi} + \boldsymbol{\xi}^T \boldsymbol{\chi}). \end{aligned} \quad (4.30)$$

We have dropped the term $\sum_{\langle ij \rangle} \xi_{ij}^2$ since it evaluates to a constant (total number of frustrated bonds) in all minimally frustrated states. Vectors $\boldsymbol{\chi}$ and $\boldsymbol{\xi}$ are defined on the entire lattice, and have two components per Kagome site (grouped within brackets in the following representation):

$$\begin{aligned} \boldsymbol{\chi} &= [\cdots ()_{i'} (\chi_i, \lambda_i)_i ()_{i''} \cdots]^T \\ \boldsymbol{\xi} &= \left[\cdots ()_{i'} \left(\sum_{j \in i} \xi_{ij}, \sum_{j \in i} \varepsilon_{\langle ij \rangle} \xi_{ij} \right)_i ()_{i''} \cdots \right]^T. \end{aligned} \quad (4.31)$$

It is crucially important to understand properties of the saddle-point vectors $\boldsymbol{\xi}$ and the coupling matrix \mathbf{C} . They follow in a straight-forward manner from (4.30) and (4.31), but due to tediousness of algebra, we defer derivation to the Appendix D. Here we will only summarize results:

- all saddle-point vectors ξ have the same norm:

$$\xi^T \xi = \text{const.} ; \quad (4.32)$$

- all saddle-point vectors ξ are degenerate eigenvectors of the coupling matrix C :

$$C\xi = 6\xi . \quad (4.33)$$

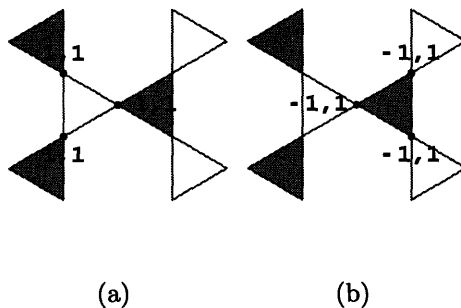
In fact, the coupling matrix C is completely dispersionless: its eigenvalues have only frequency dependence, and no dependence on spatial wavevectors. If the height fields were real instead of integer numbers, there would be six localized bare modes per Kagome lattice unit-cell. Two would be “gapless” (zero eigenvalue at zero frequency) and degenerate, while the other four would be “gapped” and degenerate. The “gapless” bare modes are actually unphysical, and merely a redundancy of the state representation in terms of the height fields. Exciting them at arbitrary places and frequencies does not affect at all the only physical quantity in the problem, the bond energy E_{ij} (see Fig. 4-9). Their existence can also be confirmed by counting arguments: there are six bond variables (E_{ij}), and two constraints on the Kagome triangles (Gauss’ Law) per unit-cell, leaving only four independent variables per unit-cell. Also note that because of (4.33) the gapless bare modes do not couple to the saddle-point vectors ξ in (4.30). In other words, they behave much like some “gauge” degrees of freedom.

The lattice theory (4.29) that we want to analyze is very similar to the simple and well understood integer-valued height model. In $2 + 1$ dimensions the height model is known to order and give a “smooth” phase. This means that fluctuations of the height field χ_i are such that the average $\langle (\chi_i - \chi_j)^2 \rangle$ does not diverge as the sites i and j go far apart. The question that we now ask is whether the Kagome double-height theory (4.29) also lives in a “smooth” phase, and what kind of lattice symmetry breaking (if any) is obtained. We will try to find answers in a fashion inspired by the Reference [71]. First we investigate which microstates (among those that mini-

mize action) are entropically selected by quantum fluctuations. Such microstates are most frequently visited by the system as it fluctuates. If we somehow found that the preferred microstates possessed long-range order, then we would have to verify whether that order is truly stable against fluctuations. Note that the formal lack of dispersion in the coupling matrix \mathbf{C} does not automatically signal localization, and hence the “rough” phase: the bare modes are strongly interacting in order to give only integer-valued height fields on all sites.

Finding the microstates that are most frequently visited by the system is an extension of the standard mean-field approach. If there were no frustration, the most frequently visited microstate would be the one that minimizes energy (action). However, in presence of frustration and classical ground-state degeneracy, entropical effects play a role, and the appropriate quantity to minimize is “free energy”. We are looking for a way to visualize the pattern of possible lattice symmetry breaking that is selected by fluctuations. Since a long-range order would unavoidably imply existence of a static order parameter, we can consider a quantity which reflects whether the system spends an extended amount of time in a neighborhood of some trial microstate ψ :

$$e^{-F(\psi)} \propto \sum_{\psi'} \theta(\psi, \psi') e^{-S(\psi')} . \quad (4.34)$$



The pairs of numbers in the figure indicate all non-zero values of (χ_i, λ_i) that constitute a redundant integer-valued field configuration (up to a multiplicative integer constant). One can easily see from (4.22) that arbitrary superposition of these configurations does not affect the bond energy E_{ij} on any bond. $\varepsilon_{\langle ij \rangle}$ is -1 on the bonds of the shaded triangles, and $+1$ on the other bonds.

Figure 4-9: Unphysical fluctuations in the lattice field theory

The neighborhood of the trial microstate ψ is specified by the positive function $\theta(\psi, \psi')$: it should be largest when $\psi' = \psi$, and monotonously decrease when the number of local differences between the microstates ψ and ψ' increases. Physically, $F(\psi)$ is the “free energy” associated with fluctuations from the vicinity of the microstate ψ , and we seek the “mean-field” state ψ that minimizes it. There is a variety of choices for the neighborhood function that would yield the same (and correct) microstates at the minimum of free energy, especially in the systems with discrete degrees of freedom (although at present there is no exact criterion for making a good selection).

There are two ways to relate the procedure outlined above to more conventional ways of thinking. First, the expression (4.34) is calculation of a complicated response function. The system is probed by non-local probes that couple to entire microstates and detect arbitrary-ranged spatial and temporal correlations. If lattice symmetries are spontaneously broken, the system will respond most noticeably to the probe that matches the symmetry breaking pattern. Alternatively, one can calculate some correlation function of local operators and detect long-range order, but in our Kagome problem such a standard approach turns out to be much more difficult when discreteness of fields has to be taken into account. Second relationship relates the “free energy” to probability amplitudes of quantum states. In frustrated systems we analyze how the degeneracy of minimally frustrated states is lifted by quantum fluctuations, that is by off-diagonal perturbations which mix such states. The resulting ground-state wavefunction may be a superposition of many minimally frustrated states. If some of these states were entropically selected by quantum fluctuations, their probability amplitudes in the ground-state superposition would be larger (by modulus). Their corresponding microstates (in the lattice field theory formulation) would also have smaller “free energy”. Therefore, the “free energy” is a rough indicator of probability amplitudes. This can be seen more formally if the probability amplitude a_ψ of a state ψ is calculated from the imaginary-time (or finite tempera-

ture) path-integral:

$$|a_\psi|^2 = \text{tr} \left(e^{-\int d\tau H} |\psi\rangle\langle\psi| \right) \propto \sum_{\{\psi'(\tau)\}} |\langle\psi|\psi'(\tau_0)\rangle|^2 e^{-S(\{\psi'(\tau)\})} . \quad (4.35)$$

The overlap $|\langle\psi|\psi'(\tau_0)\rangle|^2$ in the path-integral plays a role of a very sharp neighborhood function (and has its essential properties), so that this expression has a very similar structure to that of (4.34). The only crucial difference is that here the overlap is calculated for only one instant of time τ_0 (for which the operator $|\psi\rangle\langle\psi|$ is specified in the Heisenberg picture).

We now turn to our specific problem given by the action (4.29). Recall that the saddle-point vectors ξ correspond to static spin states. Since the action is expanded about the saddle-point ξ in the expression (4.29), any non-zero values of the height fields mean moving away from that saddle-point. This allows us to define the neighborhood function θ in a soft, but controlled way:

$$\theta(\psi, \psi') = \exp(-gm^2 \chi^T \chi) , \quad (4.36)$$

where m^2 is a tunable parameter that controls the neighborhood size. Then, the free energy of a state is:

$$e^{-F(\xi)} = \sum_{\chi} e^{-S'(\chi;\xi)} = \sum_{\chi} e^{-g[\chi^T C \chi + (\chi^T \xi + \xi^T \chi) + m^2 \chi^T \chi]} . \quad (4.37)$$

Without the “mass” term m^2 the free energy would not depend on the saddle-points, because mere shifts of variables in the path integral that leave the action invariant would switch between them. This addition to the theory does not alter its fundamental properties. The physical bare modes are “gapped” to begin with, and the mass only changes the gap in the coupling matrix. On the other hand, the “gapless” unphysical bare modes do not couple to the physical degrees of freedom, and giving them mass is only a convenient way to handle them (integrate them out). Also note that the neighborhood function does not alter symmetries and the nature of disper-

sion in the action, and thus cannot introduce unwanted effects at the neighborhood boundary.

We can make progress in two limits: very small and very large coupling constant g . For $g \ll 1$ the summation over integer fields χ in (4.37) can be approximated by an integration:

$$e^{-F(\xi)} \approx \int_{-\infty}^{\infty} \mathcal{D}\chi e^{-S'(\chi; \xi)} \propto \exp \left[g \xi^T (\mathbf{C} + m^2)^{-1} \xi \right]. \quad (4.38)$$

However, since all saddle-point vectors are degenerate eigenvectors of the coupling matrix (4.33) and have the same normalization (4.32), the free energy will have no dependence on the saddle-points.

It is instructive to compare this calculation with the appropriate sine-Gordon theory (which was used for a similar problem in Reference [71]). An alternative procedure to the one shown here is to soften the integer-valued height fields χ_i and λ_i by adding sine-Gordon terms $-\gamma \cos(2\pi\chi_i)$ and $-\gamma \cos(2\pi\lambda_i)$ to the action (4.29). This formulation is useful for renormalization group arguments that establish stability of ordered phases. However, the only tractable approach for finding entropically selected states is to Taylor-expand the sine-Gordon terms. If expansion is terminated at quadratic order (as was done in Reference [71]), one obtains precisely the free energy in the small- g limit (4.38), with $gm^2 = 2\pi^2\gamma$. Unfortunately, as we have seen, this does not yield any entropical selection of states in the Kagome problem. Therefore, one must explore what happens when quartic and higher order corrections are included in expansion of the sine-Gordon terms. In fact, we will be able to include all such corrections at once in the following calculation in a large- g limit.

For $gm^2 \gg 1$ it is convenient to perform the Poisson re-summation in (4.37). Let us introduce a vector μ with integer components $\mu_i^{(k)}$ ($k = 1, 2$), and write:

$$\begin{aligned} e^{-F(\xi)} &= \sum_{\mu} \int_{-\infty}^{\infty} \mathcal{D}\chi \exp \left[-S'(\chi; \xi) - i\pi(\mu^T \chi + \chi^T \mu) \right] \\ &\propto \sum_{\mu} \exp \left[g \left(\xi + \frac{i\pi}{g} \mu \right)^T (\mathbf{C} + m^2)^{-1} \left(\xi + \frac{i\pi}{g} \mu \right) \right]. \end{aligned}$$

This expression simplifies considerably due to (4.32) and (4.33):

$$e^{-F(\boldsymbol{\xi})} \propto \sum_{\boldsymbol{\mu}} \exp \left[-\frac{\pi^2}{g} \boldsymbol{\mu}^T (\mathbf{C} + m^2)^{-1} \boldsymbol{\mu} + \frac{i\pi}{6 + m^2} (\boldsymbol{\mu}^T \boldsymbol{\xi} + \boldsymbol{\xi}^T \boldsymbol{\mu}) \right]. \quad (4.39)$$

Note that we could also add an explicit “vortex core” term $u\boldsymbol{\mu}^T\boldsymbol{\mu}$ to the free energy. It would soften the integer-valued constraints for the height fields, and yield a sine-Gordon theory in the large u limit. Doing this would be useful if we needed to discuss stability of phases, but for the purposes of present problem this will prove to be unnecessary. The smallest eigenvalue of the matrix $\mathbf{C} + m^2$ in the last equation is m^2 . Therefore, in the limit of $gm^2 \gg 1$ (and $u \ll 1$), the only rapidly varying part of the exponent on the right-hand side is the purely imaginary part. We can easily understand the oscillatory effect that it induces as long as $m^2 \ll 1$. First, note that components of the saddle-point vectors $\boldsymbol{\xi}$ always have integer values: all possibilities are shown in the Table 4.2. Then, we can decompose the integer-valued components of the vector $\boldsymbol{\mu}$ into two parts:

$$\mu_i^{(k)} = 6\mathcal{M}_i^{(k)} + \delta\mu_i^{(k)} \quad , \quad \delta\mu_i^{(k)} \in \{0 \dots 5\}. \quad (4.40)$$

Since the quadratic part of the exponent in (4.39) varies only very slowly, we can neglect fluctuations of $\delta\boldsymbol{\mu}$ in it. Similarly, since $m^2 \ll 1$, we can neglect fluctuations of \mathcal{M} in the oscillatory part (they approximately contribute a $2\pi \times$ integer phase). We approximately have:

$$e^{-F(\boldsymbol{\xi})} \propto \sum_{\boldsymbol{\mu}} \exp \left[-\frac{(6\pi)^2}{g} \mathcal{M}^T (\mathbf{C} + m^2)^{-1} \mathcal{M} + \frac{i\pi}{6 + m^2} (\delta\boldsymbol{\mu}^T \boldsymbol{\xi} + \boldsymbol{\xi}^T \delta\boldsymbol{\mu}) \right]. \quad (4.41)$$

Clearly, the oscillatory part will give rise to a destructive interference for every non-zero component of the saddle-point vector $\boldsymbol{\xi}$ (yielding factors of the order of m^2 , or $(gm^2)^{-1}$ in the path-integral weight). In order to minimize the free energy $F(\boldsymbol{\xi})$, the saddle-point vector $\boldsymbol{\xi}$ should have as many zero components as possible. The

appropriate quantity to consider is:

$$n_p = 2n_c + n_a , \quad (4.42)$$

where n_a , n_b and n_c are respectively the total numbers of the A, B, and C type sites from the Table 4.2 in a saddle-point vector. Configurations that maximize n_p are preferred, and entropically selected by fluctuations.

Simple algebra can be worked out to find n_p . The total number of Kagome lattice sites is:

$$n_a + n_b + n_c = N , \quad (4.43)$$

while the total number of dimers in a least frustrated state is:

$$\frac{1}{2}(2n_a + n_b) = \frac{2N}{3} , \quad (4.44)$$

since one dimer sits on every Kagome triangle, and the triangles share corners instead of bonds. Combining these two equations we find:

$$n_a = \frac{N}{3} + n_c , \quad n_b = \frac{2N}{3} - 2n_c . \quad (4.45)$$

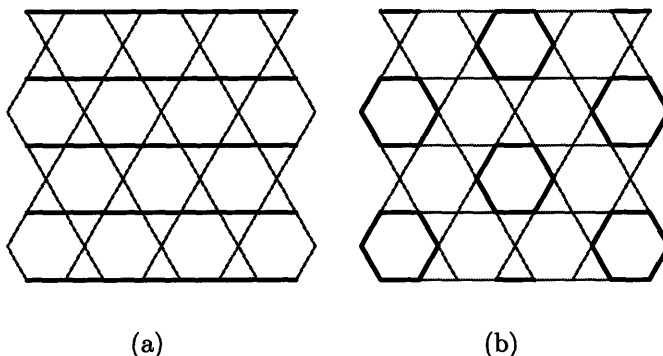
In order for all n_a , n_b , and n_c to be positive and smaller than N , n_c must be bounded between 0 and $N/3$. We see that n_p is maximized simply when the number of C-sites is maximized, which means: $n_a = 2N/3$, $n_b = 0$, $n_c = N/3$. Note that the preferred configurations also have the maximum number of *flippable* spins, whose flipping costs no energy. Every A-site is a flippable spin, because the numbers of frustrated and unfrustrated bonds emanating from it are equal (flipping a spin toggles bond energy on every emanating bond). Some untypical preferred configurations are shown in the Fig. 4-10.

The total number of preferred configurations is macroscopically large. This can be demonstrated by observing that they map to the hard-core dimer coverings of the *honeycomb* lattice. The preferred configurations have only A and C type sites. Two

	A ₁ ⌘	A ₂ ⌘	B ⌘	C ⌘
$\sum_{j \in i} \xi_{ij}$	± 2	0	± 1	0
$\sum_{j \in i} \varepsilon_{(ij)} \xi_{ij}$	0	± 2	± 1	0

All possible local configurations of dimers (frustrated bonds) at the saddle-points, and the corresponding values of the saddle-point vector components. The site i sits at the center of the bowtie, and may be of type A (two varieties), B, or C. Description of the saddle-points in terms of dimers is given in Section 4.2.3.

Table 4.2: Site classification



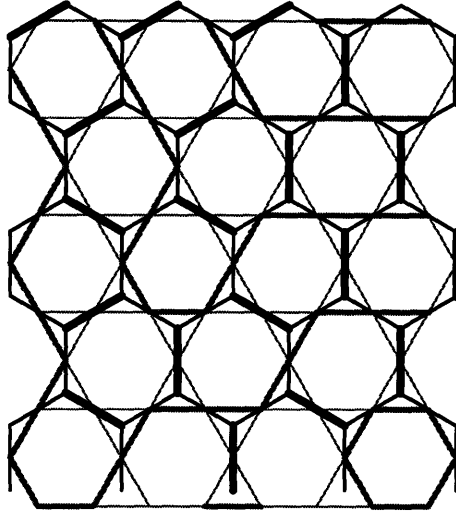
Two periodic (not typical) preferred dimer configurations (with maximum flippability). Every site with two dimers emanating from it holds a flippable spin, and only every third site holds an unflippable spin.

Figure 4-10: Examples of preferred states

C-sites cannot be neighbors, but their number should be maximized, so that every C-site can be represented by a dimer on the corresponding *honeycomb* lattice bond, as depicted in the Fig. 4-11. A transition graph can be found by overlapping any two *honeycomb* lattice dimer coverings, and it consists of isolated loops, the smallest having six *honeycomb* bonds. Therefore, the preferred configurations on the Kagome lattice are only locally different from one another, and may be transformed into one another by flipping six or more flippable spins (one at a time).

4.2.4 Disorder-by-Disorder

The conclusion so far is that the maximally flippable states may be entropically selected by fluctuations, to smaller or greater extent depending on the value of g . If we naively traced back connections between g and the parameters of the original spin



Maximally flippable states map to the honeycomb lattice hard-core dimer coverings. The Kagome triangle centers form a honeycomb lattice whose bonds go through the Kagome sites. For every Kagome bowtie with a C element from the Table 4.2 put a dimer on the honeycomb lattice.

Figure 4-11: Maximally flippable states

model, we would find that, generally speaking, smaller g describes stronger further-neighbor and multiple-spin exchange processes.

In principle, the maximally flippable states will be mixed together in the ground state, since it takes only local fluctuations to change between them. Our findings so far have included only effects of “small” fluctuations about various saddle-points. Even though a smaller value of m^2 can always be chosen to expand the scope of included fluctuations, too small m^2 may invalidate the approximations that made the calculations possible. Hence, certain “large” fluctuations are beyond reach of this formalism. Precisely these fluctuations decide whether the maximally flippable states are evenly mixed with all other states or not. If they are, the ground state is chaotic and disordered. The only chance for a valence bond order is if something suppressed the fluctuations into all but the maximally flippable states. Then, the effective degrees of freedom would be only the honeycomb lattice dimer coverings, and their local dynamics would yield a plaquette dimer long-range order typical of dimer models on bipartite lattices. It is our goal here to determine whether such long-range order might be stable.

There are several arguments that can be made in favor of the disordered phase. The first thing to observe is that the minimum of the free energy is extremely widely and evenly distributed over a large number of disordered states (mappable to the honeycomb lattice dimer coverings). This means that the system does not spend much time fluctuating near any particular one of them, likely ruling out a static order parameter, and thus lattice symmetry breaking. Secondly, due to the degeneracy in the action, it is possible to make local field changes that correspond to flipping a single spin without paying energy on the spatial links. Since such small fluctuations of the flippable spins are energetically controlled only along one dimension (imaginary time), there is nothing to stop them from proliferating. This would be true even if the “smooth” phase were obtained in the “height” action: the macroscopic degeneracy due to geometric frustration allows many spatially different patterns that break the “height” symmetry. In fact, every least frustrated state has a macroscopic number of flippable spins (see from (4.45) that $n_a \geq \frac{N}{3}$). Therefore, there is no mechanism to suppress fluctuations into any possible least frustrated state. Note that for all but the maximally flippable states to be suppressed, the only favorable flipping processes would have to simultaneously involve at least six spins (dimer flip on a *honeycomb* lattice hexagon).

Another consequence of abundant single-spin fluctuations is absence of magnetic order in the ground state. In our problem this also contradicts possibility of the valence bond order, since it would be accompanied by a net Ising moment. All maximally flippable states have macroscopic magnetization $M = \pm \frac{N}{3}$. To see this, note in the Fig. 4-10 that all flippable spins (A-type sites) must be aligned, since they are connected to each other either through one frustrated bond (dimer), or through two unfrustrated bonds.

It is apparent by now that all minimally frustrated spin configurations are mixed into the disordered and featureless ground state. The correlations are short-ranged since there is a macroscopic number of flippable spins in every least frustrated state, making the spins virtually independent. A property that distinguishes the Kagome from the other lattices is the formal lack of dispersion in the lattice field theory. We

interpret this as a signal that excitations are very heavy or perhaps even localized (exactly true in the small- g limit). Indeed, strictly short-ranged spin-spin correlations, consistent with very undispersive modes, have been observed in the Monte Carlo simulations [67, 68].

4.2.5 Variational Wavefunctions for the Ground and Excited States

The analysis of the lattice field theory has yielded two essential results that can help us sketch the ground and excited states of the Hamiltonian (4.4). They are: a) no symmetry is spontaneously broken, b) excitations have localized character (very large effective mass). We use the free energy $F(\xi)$ from the previous section as a rough indication of the probability amplitudes that different dimer configurations have in the ground state. The ground state is a smooth superposition of all possible configurations $|\psi\rangle$ of frustrated bonds:

$$|0\rangle = \sum_{\psi} a_{\psi} |\psi\rangle . \quad (4.46)$$

The amplitudes of the similar states are roughly equal in magnitude. This is required in order for two states different by a single spin flip to give a large matrix element $\langle\psi_1|(-\Gamma S^x)|\psi_2\rangle$ and yield a significant energy gain. However, the amplitudes depend on flippability of the states $|\psi\rangle$. The state with a larger number of flippable spins will have a larger probability $|a_{\psi}|^2$.

Due to a very localized nature of excitations, we can say that the physics of this model is very similar to the physics of completely disconnected quantum spins in transverse field, for which all eigenstates are known. Although the actual flippable spins interact, their interaction seems to be largely inconsequential. This suggests that many good variational wavefunctions (for ground and excited states at $\Gamma \ll J_z$) can be obtained by a simple Gutzwiller's projection: take the states of the non-interacting Kagome spins in a transverse field and project them to the manifold of

least frustrated states. All excitations are gapped, and the gap is $\sim \Gamma$.

Finally, we recall that this disordered quantum phase does not have topological order in the original spin model. Clearly, it is stable against small higher order perturbations in Γ/J_z . In fact, it obtains for all values of the transverse field Γ , without any intermediate phase transitions [26, 67, 68].

4.3 XXZ Model and Heisenberg Model With Easy-Axis Anisotropy

In this section we analyze the XXZ model on the Kagome lattice, and its extensions:

$$H = J_z \sum_{\langle ij \rangle} S_i^z S_j^z + J_\perp \sum_{\langle ij \rangle} (S_i^x S_j^x + S_i^y S_j^y) , \quad (4.47)$$

with $J_z > 0$, and $|J_\perp| \ll J_z$. The analysis will closely follow that of the transverse field Ising model in Section 4.2, and rely on the notation and conventions defined there. Many similarities will be encountered, except that the formalism will be of greater complexity. One apparent difference, however, is that the total magnetization in z direction is a good quantum number in this model.

In order to make connection to the isotropic Heisenberg model, which is our primary motivation, we will attempt to calculate with $J_\perp > 0$. This will give rise to a Berry's phase in the path-integral formulation, which in turn creates a well known "sign problem". Our calculations ultimately rely on absence of the "sign problem", so that they can be rigorously performed only for $J_\perp < 0$ (which is an interesting problem in its own right, describing repulsive hard-core bosons). However, we will provide strong arguments that the actual sign of J_\perp does not matter when it comes to how the lattice symmetries are spontaneously broken. The argument will be partially based on the form that the Berry's phase takes in the path-integral.

As before, we begin by considering an effective theory that describes the physics

at the energy scales well below J_z :

$$H_{\text{eff}} = \frac{J_{\perp}}{2} \sum_{\langle ij \rangle} \mathcal{P}_0 (S_i^+ S_j^- + S_i^- S_j^+) \mathcal{P}_0 + \mathcal{O}\left(\frac{J_{\perp}^2}{J_z}\right). \quad (4.48)$$

This theory lives in the Hilbert space spanned by the least frustrated states of the pure Ising model, and \mathcal{P}_0 is the projection operator to this space. It describes dynamics of the flippable spin-pairs on the Kagome lattice bonds. In order for a pair of spins to be flippable, the spin configuration must be minimally frustrated before and after the pair is flipped. Note that this automatically requires that the two spins be antialigned (Fig. 4-12). The effective theory can again be expressed as a soft-core dimer model in the same Hilbert space as the one that described the TFIM model, but with more complicated dynamics. We will reformulate it as a $U(1)$ gauge theory, derive a dual lattice field theory for it, and explore the possible phases. This time we will find a valence bond crystal and a spin liquid.

4.3.1 $U(1)$ Gauge Theory and Duality Transformation

The only difference between the XXZ effective dimer model and that of the TFIM model (4.4) is that now the elementary loops on which the dimers can be flipped enclose two dice lattice plaquettes, instead of one (since two spins are flipped at a time). There are four such processes, and they are shown in the Fig. 4-13.

The $U(1)$ gauge theory is built the same way as in Section 4.2.1. The electric field and the charge-2 bosons, whose fluctuations are controlled by the Gauss' Law (4.12) and the potential energy (4.8), represent low energy degrees of freedom. The new form of the kinetic energy can be easily obtained by comparing the two-plaquette processes in the Fig. 4-13 with the single-plaquette processes in the Fig. 4-5. The two

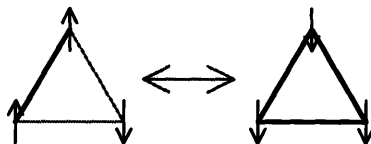
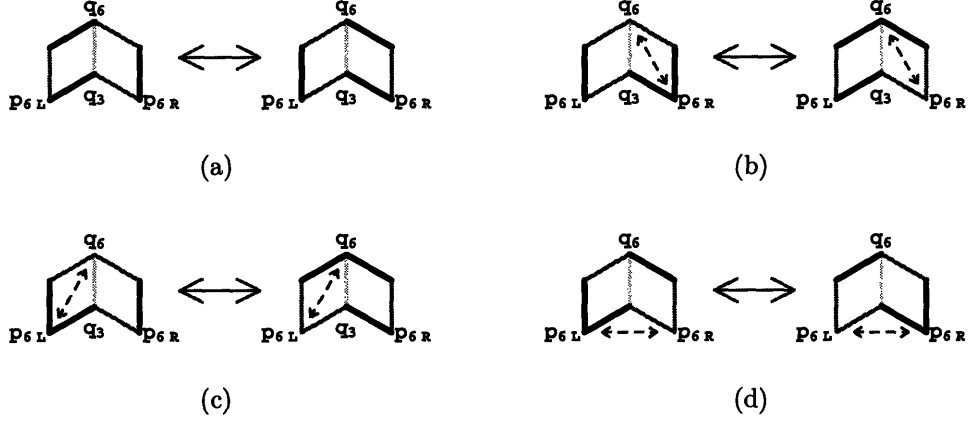


Figure 4-12: Flipping a pair of aligned spins creates extra frustration



Minimum of frustration is achieved if there is one dimer emanating from every 3-coordinated dice site, and an even number of dimers emanating from every 6-coordinated site. Dashed arrows show between which two 6-coordinated sites a pair of dimers is exchanged (charge-2 boson hopping in the U(1) gauge theory). These processes preserve global Ising magnetization: the bond between the two plaquettes is always unfrustrated.

Figure 4-13: Four possible processes that keep frustration at the minimum

$$H_{\text{kin}}^{(\alpha)} = J_{\perp} \sum_{\langle q_6 q_3 \rangle} \cos(h_{\langle q_6 q_3 \rangle}^{(\alpha)}) \quad , \quad \alpha \in \{a, b, c, d\}$$

$$\begin{aligned}
h_{\langle q_6 q_3 \rangle}^{(a)} &= \varepsilon_{\langle q_6 q_3 \rangle} \sum_{pq} \mathcal{A}_{pq} + \varepsilon_{\langle q_6 q_3 \rangle} \sum_{pq} \mathcal{A}_{pq} \\
h_{\langle q_6 q_3 \rangle}^{(b)} &= \varepsilon_{\langle q_6 q_3 \rangle} \sum_{pq} \mathcal{A}_{pq} + \left((\varphi_{q_6} - \varphi_{p_{6R}}) \eta_{p_{6R} q_6} + \sum_{pq} \varepsilon_{\langle pq \rangle} \mathcal{A}_{pq} \right) \\
h_{\langle q_6 q_3 \rangle}^{(c)} &= \left((\varphi_{p_{6L}} - \varphi_{q_6}) \eta_{q_6 p_{6L}} + \sum_{pq} \varepsilon_{\langle pq \rangle} \mathcal{A}_{pq} \right) + \varepsilon_{\langle q_6 q_3 \rangle} \sum_{pq} \mathcal{A}_{pq} \\
h_{\langle q_6 q_3 \rangle}^{(d)} &= \left((\varphi_{p_{6L}} - \varphi_{q_6}) \eta_{q_6 p_{6L}} + \sum_{pq} \varepsilon_{\langle pq \rangle} \mathcal{A}_{pq} \right) + \left((\varphi_{q_6} - \varphi_{p_{6R}}) \eta_{p_{6R} q_6} + \sum_{pq} \varepsilon_{\langle pq \rangle} \mathcal{A}_{pq} \right)
\end{aligned}$$

Kinetic energy operators corresponding to the processes in the Fig. 4-13. Notation for the sites is defined in the figure: $\langle q_6 q_3 \rangle$ is the bond shared between the two dice plaquettes, while p_{6L} and p_{6R} are the bottom 6-coordinated sites on the left and right plaquette respectively. Only the bonds with arrows are included in the sums.

Table 4.3: Kinetic energy operators in the XXZ U(1) gauge theory

single-plaquette processes consistent with the low energy physics can be combined in four different ways to give the allowed two-plaquette processes. In combining them, the middle bond $\langle q_6 q_3 \rangle$ is flipped twice, so that there is no net change on it. This gives us operators in the Table 4.3. Argument of each cosine is the sum of two corresponding single-plaquette circulations and boson hopping(s) from the expressions (4.9) and (4.10), but multiplied by the factors of $\eta_{\langle pq \rangle}$ and $\varepsilon_{\langle pq \rangle}$ in such a way that contribution of the central bond $\langle q_6 q_3 \rangle$ is properly canceled out. Then, if we label the four processes by $\alpha = a, b, c, d$, the U(1) effective Hamiltonian is:

$$H = U \sum_{\langle pq \rangle} E_{pq}^2 + \sum_{\alpha} H_{\text{kin}}^{(\alpha)}. \quad (4.49)$$

The $U \rightarrow \infty$ limit is an exact rewriting of the effective dimer model, while a finite U introduces various new dynamical processes, defined on larger dimer loops (spin clusters), but consistent with the global spin-flip symmetry of the XXZ model.

We proceed by writing the path-integral for the U(1) Hamiltonian, respecting the constraints given by the Gauss' Law (4.12). The action will contain the Berry's phase (4.13) and the potential energy term (4.14) as before. However, this time the Villain's approximation will give rise to four integer-valued massive fields $K_{\langle pq \rangle}^{(\alpha)}$ ($\alpha = a, b, c, d$) that live on the dice lattice bonds, and couple to the arguments of cosines $h_{\langle pq \rangle}^{(\alpha)}$ from the Table 4.3:

$$S_{\text{kin}} = \sum_{\tau} \sum_{\langle pq \rangle} \sum_{\alpha} \left[g \left(K_{\langle pq \rangle}^{(\alpha)} \right)^2 + i K_{\langle pq \rangle}^{(\alpha)} \left(h_{\langle pq \rangle}^{(\alpha)} + \pi \right) \right].$$

An additional Berry's phase $\sim i\pi K_{\langle pq \rangle}^{(\alpha)}$ appears because the coupling J_{\perp} is positive. It is again possible to define the magnetic field B_i and the particle current $j_{p_6 q_6}$. The magnetic field couples to the plain plaquette curl of the vector potential, while the

current couples to the boson hopping:

$$\begin{aligned}
S_{\text{kin}} = & \sum_{\tau} \sum_{\langle pq \rangle} \sum_{\alpha} \left[g \left(K_{\langle pq \rangle}^{(\alpha)} \right)^2 + i\pi K_{\langle pq \rangle}^{(\alpha)} \right] \\
& + \sum_{\tau} \left[i \sum_i B_i \sum_{pq}^{\circlearrowleft_i} \mathcal{A}_{pq} + i \sum_{\langle p_6 q_6 \rangle} j_{p_6 q_6} \left(\varphi_{q_6} - \varphi_{p_6} + \eta_{p_6 q_6} \sum_{pq}^{\circlearrowleft_i} \varepsilon_{\langle pq \rangle} \mathcal{A}_{pq} \right) \right].
\end{aligned} \tag{4.50}$$

In terms of the fields $K_{\langle pq \rangle}^{(\alpha)}$, magnetic field and particle current (labeled by the Kagome sites) are:

$$\begin{aligned}
B_i = & \sum_{pq}^{\circlearrowleft_i} \varepsilon_{\langle pq \rangle} \left(K_{\langle pq \rangle}^{(a)} + \frac{1 - \eta_{pq}}{2} K_{\langle pq \rangle}^{(b)} + \frac{1 + \eta_{pq}}{2} K_{\langle pq \rangle}^{(c)} \right), \\
j_i = & \sum_{pq}^{\circlearrowleft_i} \left(K_{\langle pq \rangle}^{(d)} + \frac{1 - \eta_{pq}}{2} K_{\langle pq \rangle}^{(c)} + \frac{1 + \eta_{pq}}{2} K_{\langle pq \rangle}^{(b)} \right).
\end{aligned} \tag{4.51}$$

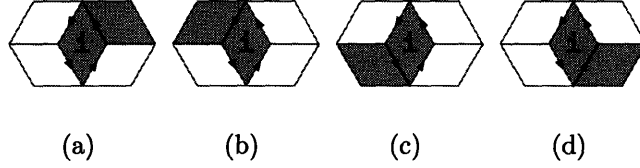
We sketch the derivation of these equations in the Fig. 4-14 and its caption. Magnetic field and the particle current are integer-valued fields, and the action is seemingly reduced to the form that pertains to the TFIM model. When the vector potential \mathcal{A}_{pq} and the particle phase φ_{p_6} are integrated-out, the same current conservation (4.16) and Maxwell's (4.18) equations are recovered.

4.3.2 “Sign-Problem” Can Be Avoided

We can again introduce the height fields χ_i and λ_i as in (4.20). For this purpose, it would be convenient to express the $K_{\langle pq \rangle}^{(\alpha)}$ fields as time derivatives. Since the path-integral has a closed boundary condition in imaginary time, and $\sum_{\tau} K_{\langle pq \rangle, \tau}^{(\alpha)}$ need not be zero, we can generally write:

$$K_{\langle pq \rangle, \tau}^{(\alpha)} = \Delta_{\tau} \kappa_{\langle pq \rangle, \tau}^{(\alpha)} + \delta_{\tau, \beta} \tilde{K}_{\langle pq \rangle}^{(\alpha)}, \tag{4.52}$$

where the time dependencies have been explicitly shown ($\beta \rightarrow \infty$ is the “last” moment of time). Ignoring for a moment the magnetic field and current terms from (4.50),



The goal is to associate B_i to the curl of \mathcal{A}_{pq} , and j_i to the curl of $\varepsilon_{\langle pq \rangle} \mathcal{A}_{pq}$. For each of the four plaquette pairs in the figures (a) through (d), a counter-clockwise circulation (of \mathcal{A}_{pq} or $\varepsilon_{\langle pq \rangle} \mathcal{A}_{pq}$) is taken on the central plaquette, labeled by its dual Kagome site i . The fields $K_{\langle pq \rangle}^{(\alpha)}$ on the emphasized bonds will be coupled to this circulation, and we simply collect those coupled to the curl of \mathcal{A}_{pq} into B_i , and those coupled to the curl of $\varepsilon_{\langle pq \rangle} \mathcal{A}_{pq}$ into j_i . However, there is a small complication. Let us call a plaquette “left” or “right” according to its position when the plaquette pair is rotated to point “upward” like in the Fig. 4-13. Then, for the pairs (a) and (c), the plaquette i is “left”, while for the pairs (b) and (d), i is the “right” plaquette. The fields $K_{\langle pq \rangle}^{(b)}$ and $K_{\langle pq \rangle}^{(c)}$ couple to circulations of the different quantities on the “left” and “right” plaquettes (see Table 4.3). Therefore, the “left” and “right” must be distinguished. Notice that the oriented emphasized bond in the figures (a) and (c) points from the 3-coordinated site toward the 6-coordinated site ($\eta_{pq} = -1$), and the opposite in the figures (b) and (d) ($\eta_{pq} = +1$). This can be used to determine when the circulation is made on the “left” or on the “right” plaquette, and this is the origin of the η_{pq} terms in (4.51).

Figure 4-14: Explanation for the derivation of equations (4.51)

the kinetic part of the action becomes:

$$\begin{aligned}
S_{\text{kin}} &\sim \sum_{\langle pq \rangle, \alpha} \left[\sum_{\tau=0}^{\beta-1} g \left(\Delta_{\tau} \kappa_{\langle pq \rangle}^{(\alpha)} \right)^2 + g \left(\kappa_{\langle pq \rangle, 0}^{(\alpha)} - \kappa_{\langle pq \rangle, \beta}^{(\alpha)} + \tilde{K}_{\langle pq \rangle}^{(\alpha)} \right)^2 + i\pi \tilde{K}_{\langle pq \rangle}^{(\alpha)} \right] \\
&\rightarrow \sum_{\langle pq \rangle, \alpha} \left[\sum_{\tau=0}^{\beta-1} g \left(\Delta_{\tau} \kappa_{\langle pq \rangle}^{(\alpha)} \right)^2 - i\pi \left(\kappa_{\langle pq \rangle, 0}^{(\alpha)} - \kappa_{\langle pq \rangle, \beta}^{(\alpha)} \right) \right] \quad (4.53)
\end{aligned}$$

The field $\tilde{K}_{\langle pq \rangle}^{(\alpha)}$ was integrated out in the last line, and an emerging additive constant was discarded. The boundary conditions in imaginary time now appear open, and the extra Berry’s phase, due to the positive J_{\perp} , appears only at the boundary. In fact, the Berry’s phase is sensitive only to the parity of the integer-valued fields at the boundary. Whenever fluctuations render this parity short-range correlated along time, one may expect that the Berry’s phase will not affect macroscopic properties of the theory. This will certainly happen in any disordered phase. However, it can also happen in a “smooth” phase that describes a plaquette valence-bond order:

macroscopic degeneracy created by geometric frustration allows many locally different “smooth” states, and small fluctuations between them are extremely abundant, especially on the corner-sharing lattices such as the Kagome.

Therefore, we will assume in the following that the Berry’s phase shapes only certain local properties of fluctuations, and neglect it for the purposes of discussing the possible phases of the theory. The affected local properties can be revealed from a microscopic point of view. Positive value of the coupling J_{\perp} in the XXZ model (4.47) prefers the spin singlet formation on the Kagome bonds: $|\uparrow\downarrow\rangle - |\downarrow\uparrow\rangle$. If J_{\perp} were negative, the antiferromagnetic triplets would be favored instead: $|\uparrow\downarrow\rangle + |\downarrow\uparrow\rangle$. Note that at least due to the strong Ising antiferromagnetic interaction, the “true ferromagnetic” nature of the negative J_{\perp} would be suppressed. Macroscopic physics of such triplet bonds must be very similar to that of the singlet bonds, because in both cases every spin can be paired with only one of its neighbors. Even the same higher order processes, such as the valence-bond movements on the closed loops, would be preferred by either sign of J_{\perp} .

Essentially, for certain purposes, “sign problem” that would be created by the Berry’s phase in a Monte Carlo calculation can be simply avoided by changing the sign of J_{\perp} .

Passing completely to the Kagome lattice notation, and neglecting the Berry’s phase, the action of the final field theory becomes:

$$S = g \sum_{\tau} \sum_{\langle ij \rangle} \left[\sum_{\alpha} \left(\Delta_{\tau} \kappa_{\langle ij \rangle}^{(\alpha)} \right)^2 + \left(\chi_i - \chi_j + \varepsilon_{\langle ij \rangle} (\lambda_i - \lambda_j) + \zeta_{ij} \right)^2 \right], \quad (4.54)$$

where the fluctuations of the height fields are constrained by the equations (4.51) in the dual form:

$$\begin{aligned} \chi_i &= \sum_{j \in i} \varepsilon_{\langle ij \rangle} \left(\kappa_{\langle ij \rangle}^{(a)} + \frac{1 - \eta_{ij}}{2} \kappa_{\langle ij \rangle}^{(b)} + \frac{1 + \eta_{ij}}{2} \kappa_{\langle ij \rangle}^{(c)} \right), \\ \lambda_i &= \sum_{j \in i} \left(\kappa_{\langle ij \rangle}^{(d)} + \frac{1 - \eta_{ij}}{2} \kappa_{\langle ij \rangle}^{(c)} + \frac{1 + \eta_{ij}}{2} \kappa_{\langle ij \rangle}^{(b)} \right). \end{aligned} \quad (4.55)$$

$$\begin{aligned}
(\mathbf{C}_{\text{pot}\boldsymbol{\kappa}})_{\langle ij \rangle}^{(a)} &= \varepsilon_{\langle ij \rangle} \left(4\chi_i - \sum_{k \in i} (\chi_k + \varepsilon_{\langle ik \rangle} \lambda_k) \right) + \varepsilon_{\langle ij \rangle} \left(4\chi_j - \sum_{k \in j} (\chi_k + \varepsilon_{\langle jk \rangle} \lambda_k) \right) \\
(\mathbf{C}_{\text{pot}\boldsymbol{\kappa}})_{\langle ij \rangle}^{(b)} &= \left[\left(4\lambda_i - \sum_{k \in i} (\lambda_k + \varepsilon_{\langle ik \rangle} \chi_k) \right) + \varepsilon_{\langle ij \rangle} \left(4\chi_j - \sum_{k \in j} (\chi_k + \varepsilon_{\langle jk \rangle} \lambda_k) \right) \right]_{i \rightarrow j} \\
(\mathbf{C}_{\text{pot}\boldsymbol{\kappa}})_{\langle ij \rangle}^{(c)} &= \left[\varepsilon_{\langle ij \rangle} \left(4\chi_i - \sum_{k \in i} (\chi_k + \varepsilon_{\langle ik \rangle} \lambda_k) \right) + \left(4\lambda_j - \sum_{k \in j} (\lambda_k + \varepsilon_{\langle jk \rangle} \chi_k) \right) \right]_{i \rightarrow j} \\
(\mathbf{C}_{\text{pot}\boldsymbol{\kappa}})_{\langle ij \rangle}^{(d)} &= \left(4\lambda_i - \sum_{k \in i} (\lambda_k + \varepsilon_{\langle ik \rangle} \chi_k) \right) + \left(4\lambda_j - \sum_{k \in j} (\lambda_k + \varepsilon_{\langle jk \rangle} \chi_k) \right)
\end{aligned}$$

For the components of type (b) and (c), the sites i and j must be chosen in such a way that the bond orientation is from i toward j .

Table 4.4: Action of the spatial (potential) part of the coupling matrix on the field vectors

$$\begin{aligned}
\boldsymbol{\xi}_{\langle ij \rangle}^{(a)} &= \varepsilon_{\langle ij \rangle} \sum_{k \in i} \xi_{ik} + \varepsilon_{\langle ij \rangle} \sum_{k \in j} \xi_{jk} \\
\boldsymbol{\xi}_{\langle ij \rangle}^{(b)} &= \left[\sum_{k \in i} \varepsilon_{\langle ik \rangle} \xi_{ik} + \varepsilon_{\langle ij \rangle} \sum_{k \in j} \xi_{jk} \right]_{i \rightarrow j} \\
\boldsymbol{\xi}_{\langle ij \rangle}^{(c)} &= \left[\varepsilon_{\langle ij \rangle} \sum_{k \in i} \xi_{ik} + \sum_{k \in j} \varepsilon_{\langle jk \rangle} \xi_{jk} \right]_{i \rightarrow j} \\
\boldsymbol{\xi}_{\langle ij \rangle}^{(d)} &= \sum_{k \in i} \varepsilon_{\langle ik \rangle} \xi_{ik} + \sum_{k \in j} \varepsilon_{\langle jk \rangle} \xi_{jk}
\end{aligned}$$

For the components of type (b) and (c), the sites i and j must be chosen in such a way that the bond orientation is from i toward j .

Table 4.5: Components of the XXZ saddle-point vectors

4.3.3 Degeneracy and Fluctuations

The action (4.54) resembles very much that of the TFIM model (4.27). However, it could give rise to a very different physics. Certain kind of fluctuations are forbidden by the action (4.54), and the remaining ones might be able to entropically select some ordered state. The forbidden fluctuations are those that change the total magnetization of the Kagome Ising antiferromagnet. Mechanism for this is provided by the constraints on the spatial configurations of χ_i and λ_i , which emerge from (4.55). Natural degrees of freedom in this field theory are $\kappa_{\langle ij \rangle}^{(\alpha)}$, and they live on the Kagome bonds, reflecting the nature of XXZ perturbation.

Therefore, we will adapt the analysis of the TFIM model to these new degrees of freedom, and write the action (4.54) in the matrix form. First, we note that the action is minimized by the same height field configurations χ_i and λ_i as before. By

shifting variables and expanding about a particular saddle-point, the potential part of the action becomes:

$$S_{\text{pot}} = g \sum_{\tau} \sum_{\langle ij \rangle} \left(\chi_i - \chi_j + \varepsilon_{\langle ij \rangle} (\lambda_i - \lambda_j) + \xi_{ij} \right)^2, \quad (4.56)$$

where ξ_{ij} has been defined in Section 4.2.3. Then, we apply the re-summation formula:

$$\sum_i a_i \sum_{j \in i} b_{\langle ij \rangle} = \sum_{\langle ij \rangle} (b_{\langle ij \rangle} a_i + b_{\langle ji \rangle} a_j) \quad (4.57)$$

to the expressions (4.55), and substitute result in (4.30). This gives us a matrix form of the action (4.54):

$$\frac{S}{g} = \boldsymbol{\kappa}^T \mathbf{C} \boldsymbol{\kappa} + (\boldsymbol{\kappa}^T \boldsymbol{\xi} + \boldsymbol{\xi}^T \boldsymbol{\kappa}). \quad (4.58)$$

Components of the vector $\boldsymbol{\kappa}$ are the $\kappa_{\langle ij \rangle}^{(\alpha)}$ fields. Structure of the coupling matrix in terms of the natural degrees of freedom, and the saddle-point vectors are given in the Tables 4.4 and 4.5 respectively.

Now, we repeat the analysis from the sections 4.2.3 and 4.2.3 in order to find the effect of fluctuations. Crucial pieces of information are how the saddle-point vectors are normalized, and how the coupling matrix acts on them:

- all saddle-point vectors $\boldsymbol{\xi}$ have the same norm:

$$\boldsymbol{\xi}^T \boldsymbol{\xi} = \text{const.}; \quad (4.59)$$

- all saddle-point vectors $\boldsymbol{\xi}$ are degenerate eigenvectors of the coupling matrix \mathbf{C} :

$$\mathbf{C} \boldsymbol{\xi} = 36 \boldsymbol{\xi}. \quad (4.60)$$

In full analogy to the TFIM case, the coupling matrix \mathbf{C} is completely dispersionless. There are 24 bare modes per unit-cell of the Kagome lattice (unit-cell has six bonds), and all of them are localized. Only four of them have a non-zero eigenvalue at zero

frequency (equal to 36), while the other 20 are “gapless” and unphysical fluctuations (due to redundancy of representation).

4.3.4 Revealing the Long-Range Order

In the quest for potential order-by-disorder, we proceed in exactly the same fashion as before. The XXZ model only brings a new complication: total Ising magnetization is conserved. Every value of total magnetization defines a separate sector of states, and fluctuations in the lattice field theory (4.54) cannot mix states from different sectors. In principle, entropical effects of fluctuations should be investigated for every sector separately. However, we only need to focus to the sector of zero Ising magnetization, since the XXZ coupling clearly favors it.

We introduce the free energy $F(\boldsymbol{\xi})$ of fluctuations about a saddle-point $\boldsymbol{\xi}$, and search for the saddle-points that minimize it. For small g the same situation occurs as in the TFIM case (see equation (4.38)): there is no entropical selection of the saddle-points. Thus, a disordered ground state is obtained, which in the XXZ case in fact has topological order, as will be argued at the end of Section 4.3.6. New interesting things happen for large g . The free energy $F(\boldsymbol{\xi})$ in the large g limit, after the Poisson re-summation, is given by the approximate expression analogous to (4.41):

$$e^{-F(\boldsymbol{\xi})} \propto \sum_{\boldsymbol{\mu}} \exp \left[-\frac{(36\pi)^2}{g} \boldsymbol{\mathcal{M}}^T (\boldsymbol{C} + m^2)^{-1} \boldsymbol{\mathcal{M}} + \frac{i\pi}{36 + m^2} (\boldsymbol{\delta}\boldsymbol{\mu}^T \boldsymbol{\xi} + \boldsymbol{\xi}^T \boldsymbol{\delta}\boldsymbol{\mu}) \right], \quad (4.61)$$

where the integer Poisson fields $\mu_{\langle ij \rangle}^{(\alpha)}$ ($\alpha = a \dots d$), forming the vector $\boldsymbol{\mu}$, have been decomposed as:

$$\mu_{\langle ij \rangle}^{(\alpha)} = 36 \mathcal{M}_{\langle ij \rangle}^{(\alpha)} + \delta\mu_{\langle ij \rangle}^{(\alpha)}, \quad \delta\mu_{\langle ij \rangle}^{(\alpha)} \in \{0 \dots 35\}. \quad (4.62)$$

The free energy is minimized when the saddle-point vector $\boldsymbol{\xi}$, given in the Table 4.5, has the maximum number of zero components. All other possible values of the components $\boldsymbol{\xi}$ are integers and factors of 36, so that only the zero components avoid

destructive interference in (4.61).

In order to discover which saddle-point dimer coverings are preferred and minimize the free energy, we need to characterize them in terms of the local dimer configurations at the Kagome sites, bonds and triangles. The Kagome sites have already been characterized by the number of dimers emanating from them, in the Table 4.2. All non-equivalent dimer arrangements in the neighborhood of a Kagome bond are systematically shown in the Table 4.6, together with the corresponding numbers of the zero components of the saddle-point vector. Finally, triangles can be characterized by types of sites at their corners, and all possibilities are given in the Table 4.7. For every allowed type of triangle one can find three situations in the Table 4.6, corresponding to three bonds on the triangle (one of which is frustrated), and collect the total number of the saddle-point zero components that such a triangle would contribute. By adding contributions of all triangles, that is all bonds, we obtain the following “scoring” number that should be maximized:








$$n'_p = 8n_{bbb} + 2n_{abb} + 2n_{aab} + 6n_{aac} + 2n_{abc} + 4n_{bbc} . \quad (4.63)$$

The quantities $n_{bbb} \dots n_{bbc}$ denote total numbers of various kinds of triangles in a given saddle-point dimer configuration. At this stage, we have to investigate possible relationships between these numbers. The first thing to note is that the total number of Kagome triangles is:

$$n_{bbb} + n_{abb} + n_{aab} + n_{aac} + n_{abc} + n_{bbc} = \frac{2N}{3} . \quad (4.64)$$

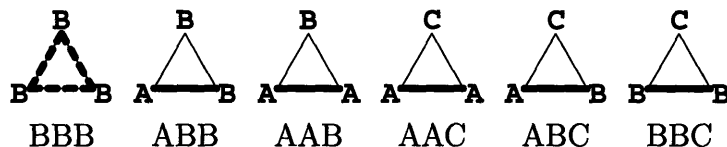
Then, using the Table 4.7, we can count the total numbers of A, B, and C sites:

$$\begin{aligned} n_a &= \frac{1}{2}(2n_{aab} + 2n_{aac} + n_{abb} + n_{abc}) , \\ n_b &= \frac{1}{2}(3n_{bbb} + 2n_{abb} + 2n_{bbc} + n_{aab} + n_{abc}) , \\ n_c &= \frac{1}{2}(n_{aac} + n_{abc} + n_{bbc}) . \end{aligned} \quad (4.65)$$

						
B,C	B,C	B,C	A,B	A,B	A,B	A,B
4	0	2	0	2	0	2

All possible non-equivalent configurations of frustrated bonds in the neighborhood of a Kagome bond. The types of sites are labeled according to the scheme from the Table 4.2 (for the bottom site on the central triangle there are always two options). This table shows the number of zero-valued components $\xi_{\langle ij \rangle}^{(\alpha)}$, $\alpha = a \dots d$ of the saddle-point vector, for the horizontal bond $\langle ij \rangle$ on the central triangle.

Table 4.6: Bond characterization



All possible kinds of Kagome triangles are shown. The site types A,B, and C are defined in the Table 4.2. Note that two C-sites can never be neighbors, and that three A-sites cannot sit on the same triangle. The dimers emphasize which bond must be frustrated in a given situation (there are multiple choices only for the case BBB).

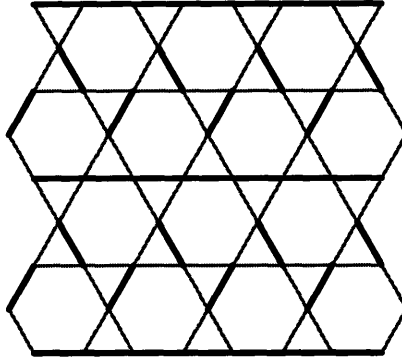
Table 4.7: Triangle characterization

By combining these equations with (4.45), one finds that n_a , n_b , n_c , n_{abb} , and n_{abc} can be expressed in terms of independent variables n_{bbb} , n_{aac} , n_{bbc} , and n_{aab} . The “scoring” number n'_p can now be simplified using the identity (4.64). The quantity that has to be maximized is:

$$n_p = 3n_{bbb} + 2n_{aac} + n_{bbc} , \quad (4.66)$$

and the variables appearing in it are independent, although subject to inequalities $0 \leq n_a \leq N$, \dots , $0 \leq n_{bbc} \leq 2N/3$.

Finding the absolute maximum of n_p is a well posed problem of linear programming. It can be shown that it is obtained when the number of C-type sites is maximized, which gives rise to the very same states preferred by the fluctuations of the TFIM model (see Fig. 4-10). However, these are not the saddle-points that we are looking for: they have a macroscopic Ising magnetization. Besides, instead of being maximally flippable, as in the case of the TFIM model, they are now minimally flippable; in fact, they have no flippable spin-pairs at all. If we want to find the config-



The lattice symmetries are “broken” in the stripe-like fashion. There are only type A and B sites in this state, and the number of BBB triangles is large (they sit between the straight chains of dimers). The total magnetization is zero: every two spins connected by a vacant bond are antialigned, so that the straight chains alternate in magnetization, as well as the dimers in the middle along the chains.

Figure 4-15: Preferred saddle-point configuration with zero magnetization, entropically selected by the XXZ fluctuations

urations with zero magnetization that maximize n_p , we must explore a path different from having a large number of C sites. This is, in principle, a difficult problem, and an exact analytical solution is not available at this time. Instead, we guess that n_{bbb} should be made as large as possible. This yields the configurations without any C sites, and with a large number of B sites (see (4.45)). The best choice is: $n_a = N/3$, $n_b = 2N/3$, $n_{bbb} = n_{aab} = N/3$. It is possible, though relatively complicated, to demonstrate that configurations with these parameters break lattice symmetries in a unique stripe-like fashion shown in the Fig. 4-15. It turns out that such states are not magnetized at all, and that they have a large number of flippable spin-pairs. Their scoring number ($n_p = N$) is significantly larger than that of a typical unmagnetized state (a fraction of N). Therefore, they are excellent candidates for the preferred configurations. No better configurations were found when every least frustrated state with zero magnetization was explicitly examined using the computer (the sample had 24 sites and closed boundary conditions).

In conclusion, for large g the preferred configurations of frustrated bonds that minimize the free energy break the lattice symmetries in the stripe-like way, as shown in the Fig. 4-15. This indicates that a valence-bond ordered phase could be realized in the XXZ model when dynamics is dominated by the short-ranged spin-pair flips

(the larger g , the weaker further-neighbor and multiple-spin exchange). It is now necessary to verify stability of such an ordered phase.

4.3.5 Stability of the Ordered Phase

A usual way to determine whether fluctuations ultimately destroy long-range order involves renormalization group (RG). The lattice field theory (4.54) of the XXZ model resembles an integer-valued height model, and one might naively hope that the RG arguments could be applicable to it. In a standard and simple integer-valued height model (on the square lattice, for example) one first softens the integer constraints for the height fields by writing a sine-Gordon theory. Then, one checks how the sine-Gordon coupling flows under RG, starting from various parameter values in the theory. If it flows toward zero, then the integer constraints are irrelevant at the macroscopic scales, and the height model may be found in the “rough” disordered phase. Alternatively, the flow can be toward infinity, in which case the “smooth” long-range ordered phase is realized. In the context of frustrated magnetism, the appropriate height model typically comes with a static background field (ξ in our case), so that the “smooth” phase also breaks lattice symmetries [71].

Therefore, let us write a sine-Gordon theory for the XXZ model, based on the action (4.58):

$$S_{\text{sg}} = g\boldsymbol{\kappa}^T \mathbf{C}\boldsymbol{\kappa} + g(\boldsymbol{\kappa}^T \boldsymbol{\xi} + \boldsymbol{\xi}^T \boldsymbol{\kappa}) - \gamma \sum_{\tau, \langle ij \rangle, \alpha} \cos(2\pi \kappa_{\langle ij \rangle}^{(\alpha)}) .$$

The $\kappa_{\langle ij \rangle}^{(\alpha)}$ fields are now real-valued, and their deviation from integers is penalized by the sine-Gordon term, especially in the large γ limit. It is convenient to shift the variables $\boldsymbol{\kappa}$ by $\mathbf{C}^{-1}\boldsymbol{\xi} = \boldsymbol{\xi}/36$, and remove the linear terms:

$$S_{\text{sg}} = g\boldsymbol{\kappa}^T \mathbf{C}\boldsymbol{\kappa} - \gamma \sum_{\tau, \langle ij \rangle, \alpha} \cos\left(2\pi\left(\kappa_{\langle ij \rangle}^{(\alpha)} - \frac{1}{36}\xi_{\langle ij \rangle}^{(\alpha)}\right)\right) .$$

Unfortunately, it is not possible to directly apply the RG treatment to this theory.

The bare modes (modes of the coupling matrix \mathbf{C}) are not only dispersionless, but some of them appear gapless as well. The “gapless” bare modes are redundancy of representation, but they still pose a technical difficulty. It is through the sine-Gordon coupling that they at least acquire dispersion. The sine-Gordon term mixes the bare modes when they describe non-integer fluctuations of the height fields. Let us relabel the fields $\kappa_{\langle ij \rangle}^{(\alpha)}$ as $\kappa_{n,\mathbf{r}}$, where \mathbf{r} is a vector specifying a Kagome lattice unit-cell, and $n \in \{1, 2 \dots 24\}$ is an index specifying the bond $\langle ij \rangle$ (one of six) and the flavor α (one of four) within the unit-cell. Then, we can express the fields as linear combinations of the 24 local bare modes $\Phi_{n,\mathbf{r}}$:

$$\kappa_{n,\mathbf{r}} = \sum_{m=1}^{24} \sum_{\Delta\mathbf{r}} W_{nm,\Delta\mathbf{r}} \Phi_{m,\mathbf{r}+\Delta\mathbf{r}} . \quad (4.67)$$

One can formally integrate out the four physical (massive) modes: $\Phi_{21,\mathbf{r}}, \Phi_{22,\mathbf{r}}, \Phi_{23,\mathbf{r}}, \Phi_{24,\mathbf{r}}$, and obtain an effective theory as perturbative expansion in γ . The effective theory is a complicated expression involving cosine terms whose arguments are linear combinations of the remaining twenty modes:

$$S_{\text{eff}} = g \sum_{n=1}^{20} \sum_{\mathbf{r}} (\Delta_{\mathbf{r}} \Phi_{n,\mathbf{r}})^2 \quad (4.68)$$

$$- \gamma \sum_{n,\mathbf{r}} C_n \cos \left(2\pi \sum_{m=1}^{20} \sum_{\Delta\mathbf{r}} W_{nm,\Delta\mathbf{r}} \Phi_{m,\mathbf{r}+\Delta\mathbf{r}} - 2\pi \frac{1}{36} \xi_{n,\mathbf{r}} \right) + \mathcal{O}(\gamma^2) .$$

The redundancy of representation survives in the effective theory through periodicity of the cosines. However, the redundancy is easily removed by treating the mode amplitudes in the effective theory as angles: the physical degrees of freedom (which have been integrated-out) enter the effective theory precisely through the residual $[0, 2\pi)$ amplitudes of the remaining modes.

Let us for a moment expand the cosine terms to the quadratic order, and obtain a Gaussian theory for the twenty modes. In absence of the saddle-point background

$\xi = 0$, such a theory would be trivial:

$$\xi_{n,\mathbf{r}} = 0 \quad \Rightarrow \quad S_{\text{gauss}} = \sum_{n,\mathbf{r}} \left[(\Delta_{\mathbf{r}} \Phi_{n,\mathbf{r}})^2 + m^2 \Phi_{n,\mathbf{r}}^2 \right].$$

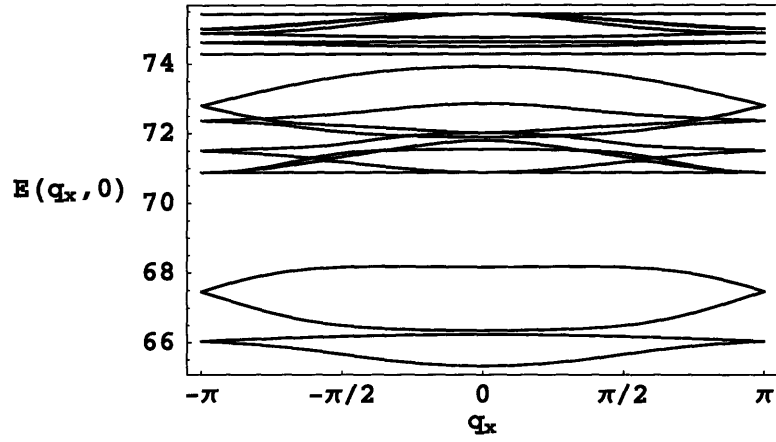
This means that the effective theory (4.68) retains the nature of the original sine-Gordon model: small fluctuations of the bare modes are gapped. However, we are concerned only with the vicinity of the candidate valence-bond ordered state (Fig. 4-15). For the saddle-point vector ξ that describes this stripe pattern the effective band structure in the Gaussian approximation is shown in the Fig. 4-16. Apart from having frequency dependence, the lowest lying mode is dispersive in the direction along the stripes, but not in the perpendicular direction. Nevertheless, full spatial dispersion can be expected if one goes beyond the Gaussian approximation, because the lowest lying mode is actually coupled to some higher modes that are dispersive in the perpendicular direction. The results of this approximation are only good for arguing that dispersion emerges. There is no simple way of telling what changes beyond the quadratic approximation. Therefore, the correct way in which lattice symmetries are eventually broken may not be possible to guess from this information.

We can now write the effective theory in a form that manifestly separates the dispersive and sine-Gordon parts. If we partially expand the cosines from (4.68) in the following way (suppressing the n and \mathbf{r} indices of $\xi_{n,\mathbf{r}}$ and $x_{n,\mathbf{r}} = \sum_{m,\Delta\mathbf{r}} W_{nm,\Delta\mathbf{r}} \Phi_{m,\mathbf{r}+\Delta\mathbf{r}}$):

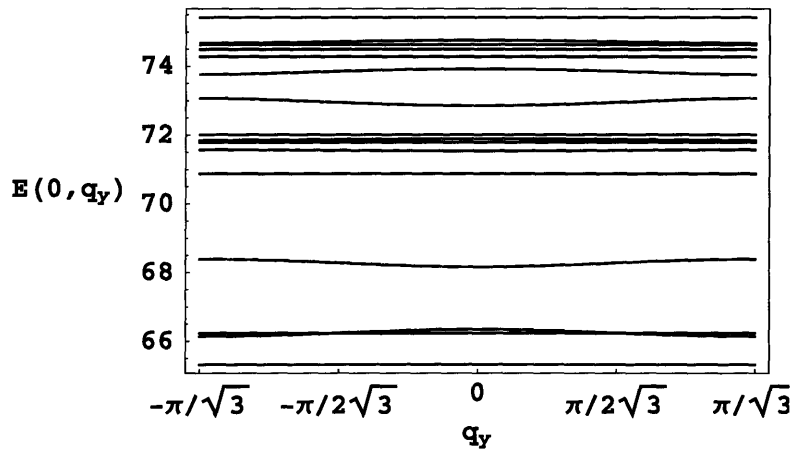
$$\begin{aligned} \sum_{n,\mathbf{r}} C_n \cos\left(2\pi x - \frac{2\pi\xi}{36}\right) &= \sum_{n,\mathbf{r}} C_n \left\{ 2\pi x \sin\left(\frac{2\pi\xi}{36}\right) \right. \\ &\quad \left. + a \cos(2\pi x) + \left[\cos\left(\frac{2\pi\xi}{36}\right) - a \right] \left(1 - \frac{(2\pi x)^2}{2}\right) \right\} + \mathcal{O}(x^3), \end{aligned}$$

then for a proper choice of the constant a the effective theory becomes:

$$\begin{aligned} S_{\text{eff}} &\approx g \Phi^T C_{\text{eff}}(\xi) \Phi - \gamma \left(\mathbf{h}^T(\xi) \Phi + \Phi^T \mathbf{h}(\xi) \right) \\ &\quad - a\gamma \sum_{n,\mathbf{r}} C_n \cos\left(2\pi \sum_{m=1}^{20} \sum_{\Delta\mathbf{r}} W_{nm,\Delta\mathbf{r}} \Phi_{m,\mathbf{r}+\Delta\mathbf{r}}\right), \end{aligned} \quad (4.69)$$



(a)



(b)

Calculations were performed at zero frequency in quadratic approximation, for the pattern of frustrated bonds in the Figure refEAHMstripeSP. The wavevector \mathbf{q} is taken (a) along the stripes, (b) perpendicular to the stripes. The vertical scale is given in arbitrary units, but proportional to γ . The Kagome lattice unit-cell had to be doubled, so that 40 modes are shown; only the dispersionless branches are degenerate. Note that the lowest lying mode is dispersive in only one spatial direction, but also that some higher modes have dispersion in the other direction.

Figure 4-16: Effective band structure of the sine-Gordon theory for the entropically selected state

where the coupling matrix $C_{\text{eff}}(\boldsymbol{\xi})$ collects all space-time dispersion (brought up by the non-trivial $\boldsymbol{\xi} \neq 0$), and has no gap at $\mathbf{q} = 0$. The remaining cosines open up a gap for small fluctuations, thereby justifying the quadratic expansion that took place. This is an effective sine-Gordon theory. As a matter of principle, the RG treatment is now applicable. Even if the dispersion were ultimately created only in one spatial dimension (along the stripes), combined with the dispersion in time it would give a “smooth” phase for sufficiently large g and γ . If the full $(2 + 1)$ D dispersion were obtained, then only the “smooth” phase would exist, since the sine-Gordon coupling would always flow toward infinity. In any event, existence of the “smooth” phase means that the valence-bond long-range order for large g is stable. For small g , however, the “smooth” phase is disordered since the fluctuations cannot select an ordered state from the degenerate manifold.

This concludes our discussion of the lattice field theory. In the following, we take a completely different point of view, and provide a more physical picture of the discovered XXZ phases.

4.3.6 Valence-Bond Picture of the Ordered Phase

In this section we use some simple physical arguments and show that the short-range valence-bond picture applies extremely naturally to the XXZ model on the Kagome lattice. This will allow us to identify a physical “order parameter” for the valence-bond ordered phase of the Kagome XXZ model, and construct qualitatively good variational wavefunctions.

Let us seek variational ground states of the Hamiltonian (4.47) with $J_{\perp} > 0$ that are described in terms of the *singlet bonds* (symmetric triplet bonds for $J_{\perp} < 0$). Energy minimum requirements shaped by the J_z and J_{\perp} terms can be met by following these criteria:

- number of frustrated bonds is minimized,
- total Ising magnetization is zero,
- number of flippable spin-pairs is maximized.

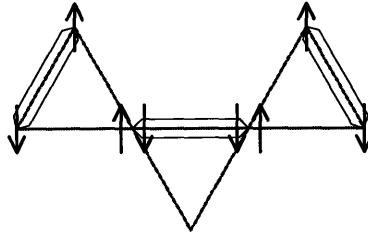


Figure 4-17: Covering the lattice with flippable pairs of spins

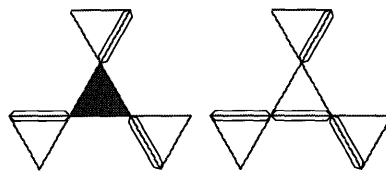
First, we explore circumstances in which a pair of spins on a Kagome bond is *flippable*. The XXZ perturbation J_{\perp} in (4.2) can flip a pair of antialigned spins, but one must make sure that both initial and final states are minimally frustrated. Figure 4-17 shows a flippable pair of spins on the central horizontal bond. Regardless of whether the two antialigned spins on the central horizontal bond are in the state $|\uparrow\downarrow\rangle$ or $|\downarrow\uparrow\rangle$, every triangle has exactly one frustrated bond, which is a condition for minimum frustration. This requires that the two opposite bonds on the neighboring triangles hold a pair of antialigned spins each. Clearly, energy will be gained by allowing the flippable pair of spins to resonate between the two possible states and form a singlet bond. If the other two pairs of antialigned spins were also flippable, more energy could be gained by turning them into singlet bonds as well. Attempt to create as many flippable pairs as possible leads to the hard-core dimer coverings of the Kagome lattice, where every dimer represents a *singlet bond* (in contrast to the earlier representation, when dimer was a *frustrated* bond). Corner-sharing structure of the Kagome lattice and easy-axis anisotropy make this short-range valence-bond picture extremely natural: singlet pairs can be close-packed without (almost) any extra frustration.

However, the hard-core dimer coverings of the Kagome lattice are not quite acceptable. It is known that they unavoidably have a fixed number of so called *defect* triangles that hold no dimers on their bonds (see Section 2.2.4). This means that there would be macroscopically many triangles with all three bonds occasionally frustrated, and the first criterion would be violated. An example of a defect triangle is shown shaded in the Figure 4-18(a). In order to make sure that two of its bonds are always unfrustrated, two of its spins must be always anticorrelated. One variational

mechanism that achieves this is the following. Let us choose two spins on the defect triangle and force them to be always antialigned. Then, we can denote those two spins by a dimer, like in the Figure 4-18(b). This allows at least the dimer on the top triangle to resonate as a singlet bond, but there are now four spins connected by the dimers, thus antiferromagnetically correlated. Certainly, those four spins could also resonate together while keeping their correlations, but the energy gain would be much smaller than that brought by a singlet bond (this is a higher order process). Generally, two singlet bonds are lost for every defect triangle. The dimers no longer represent only the singlet bonds, but any pair of anticorrelated spins.

This situation can be improved. It is possible to arrange the defect triangles close to each other in such a way that they share the singlet bonds that are going to be lost. Consider a *perfect* hexagon in the Figure 4-19(a). It holds three dimers on its bonds, and therefore has three defect triangles around it in a hard-core dimer covering. By putting three extra dimers on the hexagon, the defect triangles are removed, and the six spins on the hexagon are forced to be antiferromagnetically correlated. Only three singlet bonds are lost per three defect triangles. This is clearly energetically favorable, and consequently the singlet bonds will arrange in a way that maximizes the number of perfect hexagons. Every perfect hexagon can then gain additional energy by correlated fluctuations of its six spins. Furthermore, the groups of singlet bonds may be able to collectively resonate on the closed resonant loops. Variational states that maximize the number of perfect hexagons have been discussed in Section 2.2.4 (see Figure 4-20).

This variational picture seems to apply very well whenever physics of the Kagome spin models is describable by the short-range valence bonds. We now apply it to the ordered phase of the XXZ model. The lattice field theory in the preceding sections was able to establish stability of a valence-bond order without full precision in determining how the lattice symmetries should be ultimately broken. It only produced information on which particular microstate is most frequently visited by the system (pattern of frustrated bonds in Fig. 4-15); the other nearby microstates are not energetically suppressed, so that they are visited extremely often as well. We can

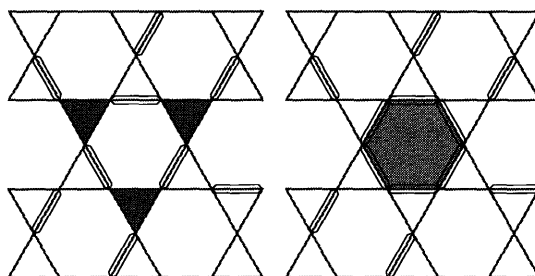


(a)

(b)

(a) A defect triangle (shaded) holds no dimers on its bonds. As the neighboring singlet bonds fluctuate independently, all three spins on it are occasionally aligned, making all three bonds frustrated. (b) A dimer is placed on the defect triangle, relaxing its frustration at all times, but simultaneously correlating antiferromagnetically a group of four spins.

Figure 4-18: Unfrustrating the defect triangles

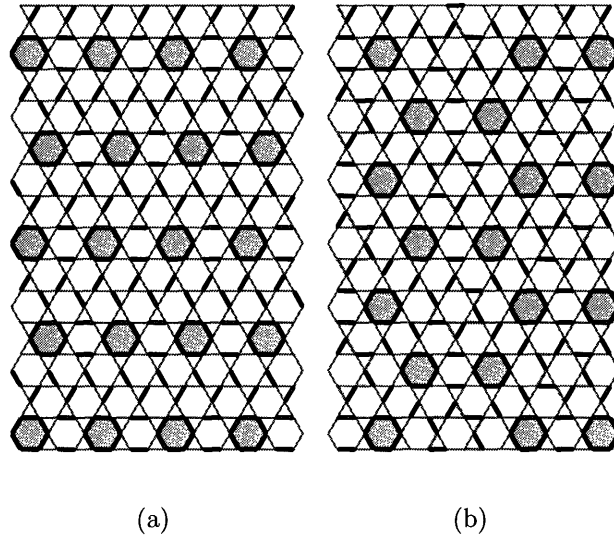


(a)

(b)

(a) A perfect hexagon holds three dimers, and has three defect triangles (shaded) around it in a hard-core dimer covering. (b) Covering all bonds of the perfect hexagon by dimers removes the defect triangles, and correlates antiferromagnetically all spins on the hexagon. Only three singlet bonds are lost per three defect triangles.

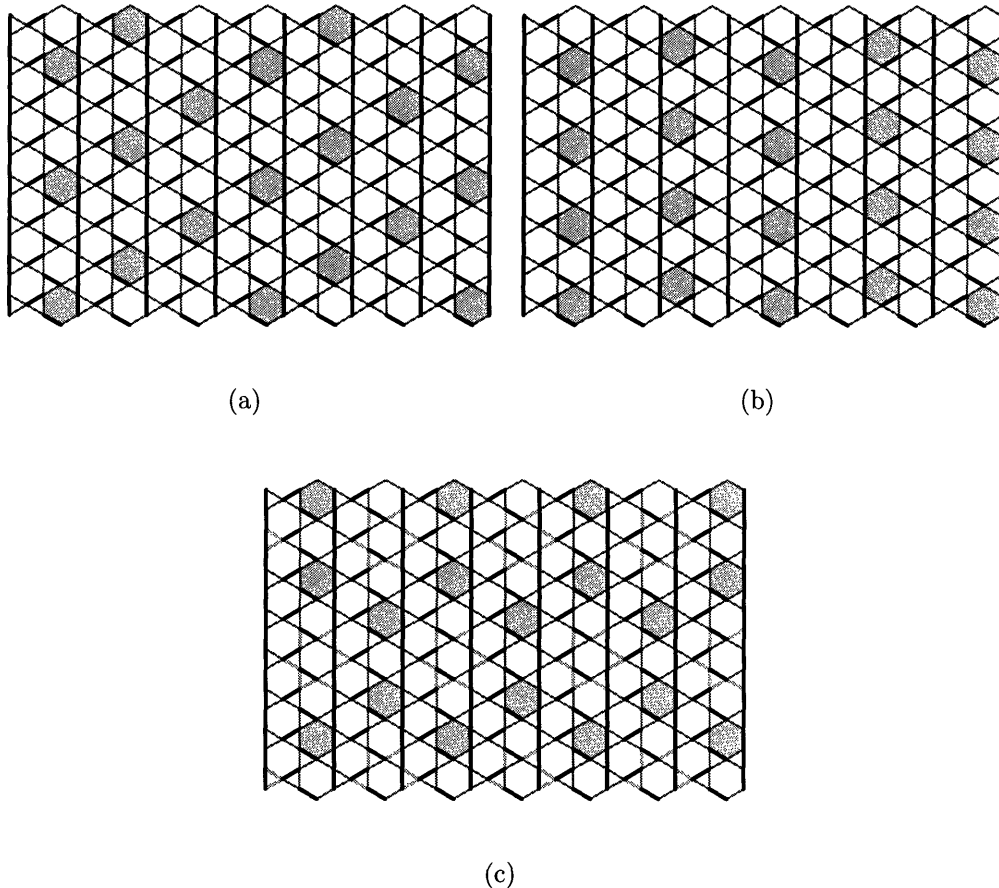
Figure 4-19: Perfect hexagons minimize XXZ exchange energy



(a) stripe pattern, (b) honeycomb pattern. The number of emphasized perfect hexagons is maximized (1/6 of all hexagons). In the *honeycomb* pattern there are star-shaped resonant loops of singlet bonds, one sitting inside every honeycomb super-cell. There are two possible singlet bond arrangements on every loop, and more energy can be gained by resonant fluctuations between them.

Figure 4-20: Characteristic variational ground-states

now combine this information with the variational states and try to find out how the frustrated-bond and singlet-bond pictures can be compatible. Our assumption is that the correct ordering pattern must be “synchronized” with the state most frequently visited by the system. The Figure 4-21 compares the entropically preferred stripe-like configuration of frustrated bonds with the only two compatible variational states. The scenarios (a) and (b) involve the stripe pattern of perfect hexagons. Intuitively, the case (a) does not seem likely, because the two stripe orientations of the compared states are different. In the case (b), the stripe orientations of the two compared states are the same, but the overlap period in the direction perpendicular to the stripes is relatively large. Perhaps the best match is accomplished in the scenario (c). The honeycomb pattern of perfect hexagons is also the most symmetric among all variational states, and the set of its symmetries is the closest to that of the Kagome lattice. Unfortunately, at this stage there is no unambiguous way of telling which match is truly the best, but we recall that exactly this honeycomb pattern emerged from the analysis of the isotropic Heisenberg model (Chapter 2) as a likely ground-state. Based



Dimers represent the frustrated bonds, and the emphasized hexagons are perfect. (a) and (b) demonstrate two possible ways of overlapping the stripe variational states, and (c) demonstrates the overlap with the honeycomb variational state. The repeating unit-cell of the overlap has 18 sites in (a), and 36 sites in (b) and (c).

Figure 4-21: Overlap between the preferred configuration of frustrated bonds and the variational states

on all these arguments, we can propose the honeycomb variational state as the most likely qualitative description of the ordered ground state of the XXZ model.

4.3.7 Spin Liquid Phase

Let us now turn to the disordered phase. Our goal is to show that conservation of total Ising spin has profound consequences for the topological properties of disordered phases. Consider an arbitrary Hamiltonian that is invariant under the global spin-flip. It can be always expressed as a sum of local Hermitian operators that flip an equal number of “up” and “down” pointing spins. Eigenstates of all such operators either

have any particular spin on the lattice fixed, or involved in a group of an even number of coherently fluctuating spins (for example, such group of two neighboring spins is a singlet or an antiferromagnetic triplet valence-bond, appropriate for the pure XXZ dynamics). These eigenstates are somehow eventually superposed to give the ground state of the Hamiltonian. If all the spins fluctuate in the ground state so that there is no average magnetization on any site, then the ground state is a superposition of only the “valence-group” states in which *every* spin belongs to a finite even-sized group of coherently fluctuating spins. This is a generalization of the valence-bond states (whose superpositions would yield the singlet ground states).

It is now possible to define topological sectors of these “valence-group” states. Choose an arbitrary pairing of spins within every group: every spin must be paired with one other spin (need not be a neighbor). Visualize the pairings by strings on the lattice that connect the paired spins (overlaps and shapes of the strings do not matter). A transition graph between any two string configurations can be constructed by overlapping them, in analogy to the hard-core dimer coverings. Then, any two “valence group” states from the superposition that forms the ground state will have the transition graph composed of finite closed loops (as long as the Hamiltonian has only local dynamics). If now the lattice is placed on a torus, there will be two topologically non-equivalent closed paths that go around the torus and intersect the bonds of the lattice. The topological sector of a string configuration is determined by the parities of the number of strings that each of these paths intersect. Two string configurations will belong to different topological sectors only if any of the paths intersects their transition graph an odd number times. Clearly, this can never happen if the transition graphs always consist of finite closed loops: the ground state has a topological order.

Therefore, any disordered state of the XXZ model is automatically a spin liquid, with four degenerate ground states on a torus. A characteristic feature of the Kagome lattice (and other corner-sharing lattices) is a manifestly weak dispersion in the far limit for which the spin liquid obtains. This indicates that correlations in the spin liquid (away from the critical point) must be strictly short-ranged, virtually vanishing

beyond a few lattice constants.

4.4 A Big Picture

4.4.1 Phase Diagram of the Kagome Quantum Ising Models

We have explored two kinds of the Kagome lattice quantum Ising antiferromagnets. The first kind was endowed by spin dynamics that did not conserve total Ising spin, and was represented by the transverse field Ising model (TFIM). The second kind conserved total spin, and its simplest form was given by the XXZ model. Both TFIM and XXZ models contain only the shortest-range dynamical processes consistent with the required symmetries, acting as small perturbations to the pure Ising model. The considered extensions include further-neighbor and multiple-spin exchange dynamics, and thus they may reflect physics of the TFIM and XXZ models with stronger dynamical energy scale (closer to the Ising interaction J_z). The quantum phases found in these models are summarized in the Table 4.8.

The disordered phase of the TFIM and related models was found to have no topological order. Consistently, the table indirectly suggests that the same phase should be realized for all values of transverse field. Our approach allowed us to gain some information about probability amplitudes that various spin configurations have in the ground state superposition. Together with this information, the finding that excitations appear heavy or localized even for weak transverse fields suggested the following variational wavefunctions for many states: eigenstates of decoupled spins in transverse field should be projected to the manifold of minimized Ising frustration. It

dominant dynamical processes:	simple short-ranged	multiple-spin and ring exchange...
do not conserve $\sum_i S_i^z$	disordered	disordered
conserve $\sum_i S_i^z$	valence-bond crystal	spin liquid

Table 4.8: Quantum phases of the Kagome lattice Ising antiferromagnets with different kinds of spin dynamics

is evident that the corner-sharing structure of the Kagome lattice is responsible for the very weak dispersion or perhaps even localized nature of fluctuations.

Much richer physics is found when total Ising spin is conserved. The XXZ and related models give rise to at least two non-trivial phases. The calculations indicated that the valence-bond order was most likely to be found for short-ranged and small dynamical perturbations, such as the one in the Heisenberg model with strong easy-axis anisotropy (simple XXZ model). Furthermore, a combination of arguments led to essentially two most probable ordered states, the stripe and honeycomb shaped patterns (Fig. 4-20). While no good arguments to rule one of them were provided, we suspect that the more symmetric honeycomb pattern is realized in most typical situations (no specially favored dynamical processes). This result is of potentially great importance, because the same type of lattice symmetry breaking has been proposed to occur in the ideal isotropic Heisenberg model (Chapter 2), and accounted for the seemingly gapless band of singlet excitations observed in numerics. Physics of the ideal Heisenberg model is still largely mysterious: its ground state could be a spin liquid. Indeed, these calculations indicate that as complexity of dynamical processes increases, which is similar to what happens when the amount of easy-axis anisotropy is reduced in the XXZ model, a phase transition into the spin liquid must occur. If our calculations could indeed qualitatively describe the anisotropy reduction, a question would arise whether the phase transition happens before or after the full isotropy is reached. In any case, both the valence-bond crystal and spin liquid phases found here are gapped (gap energy scale may be very small), and the same is expected to be true for the isotropic Heisenberg model, regardless of what phase it actually lives in (unless it sits at the critical point).

4.4.2 Roles of Geometry and Quantum Dynamics

One important question, driven by efforts to discover unconventional Mott insulators, is under what circumstances can disordered and spin liquid phases be found in frustrated spin models. One mechanism that clearly emerges is adding sufficiently strong further-neighbor and multiple-spin exchange processes. This has been already

indicated in various other cases [14, 47, 48, 65]. However, corner-sharing lattices have been in focus due to a belief that even with the shortest-range dynamical processes one can still obtain spin liquid physics. At least for the transverse field Ising model a disordered ground state is found in the Kagome system, making a sharp contrast to other usually studied systems [26]. This disordered phase is conventional (not topologically ordered). Also, the system behaves almost as completely decoupled. Apparently, completely local transverse field dynamics is unable to bring up correlations in a poorly connected lattice. However, as soon as the transverse field is replaced by the next least correlated kind of dynamics (XXZ), a valence-bond ordered phase seems to emerge instead of a spin liquid. Since this happens in one of the most prominent systems for the short-range spin liquid, it is reasonable to speculate that the spin liquid in similar weakly perturbed quantum antiferromagnets quite generally requires further-neighbor, multiple-spin and ring exchange dynamics. Having a less connected lattice makes it easier for a trivial disordered phase to appear as a result of short-range dynamics, but perhaps not so much easier for the spin liquid phase.

Also, the arguments from the end of Section 4.3.7 indicate that conservation of total Ising spin is a sufficient condition for topological order of translationally symmetric phases that have no net magnetic moment on any site. The $SU(2)$ symmetric models, such as the Heisenberg model, are included as a special case, in agreement with an extension of the Lieb-Schultz-Mattis theorem to higher dimensions [80]. Clearly, the spin liquid can exist beyond this condition: as a stable phase, it can resist sufficiently weak spin non-conserving perturbations.

Chapter 5

Quantum Ising Models on Other Frustrated Lattices

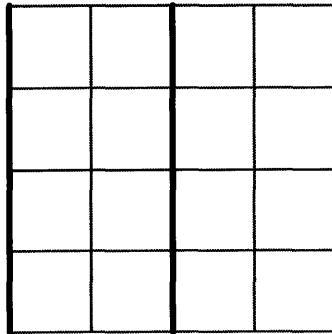
Methods that were applied to Kagome models in the previous chapter are suitable for exploring order-by-disorder in frustrated quantum Ising systems on various other lattices. In this chapter we will demonstrate those approaches using two examples: transverse field Ising model on the square lattice, and XXZ model on the triangular lattice. The first example is easy to handle, and final results have been obtained in literature by various means, including analytical [71] and numerical [6], thus providing a testing ground for the methods. The second example has a historical value as being similar to the first system in which a Resonant Valence Bond state was proposed by Anderson [8]. The calculations will begin by deriving appropriate lattice field theories for these two problems. Then, stability of their ordered phases will be established. Emphasis will be placed on revealing how lattice symmetries are broken in these ordered phases. Since foundation for the following calculations is laid down in the previous chapter, discussion will be concise. These problems will also provide a sharp contrast to the equivalent problems on the Kagome lattice, and serve as an illustration of how special the Kagome lattice is.

5.1 Fully Frustrated Square Lattice

In this section we explore the quantum Ising model in weak transverse field on the fully frustrated square lattice:

$$H = J_z \sum_{\langle ij \rangle} \varepsilon_{\langle ij \rangle} S_i^z S_j^z - \Gamma \sum_i S_i^x . \quad (5.1)$$

Factors $\varepsilon_{\langle ij \rangle}$ take values ± 1 on the square lattice bonds in such a way that product of $\varepsilon_{\langle ij \rangle}$ on the four bonds of every plaquette is -1 ; one possible choice is given in Figure 5-1. The role of $\varepsilon_{\langle ij \rangle}$ is to introduce frustration (otherwise, spins order antiferromagnetically), which results in requirement that there be an odd number of frustrated bonds (with $\varepsilon_{\langle ij \rangle} S_i^z S_j^z > 0$) on every square plaquette. Frustrated bonds can be visualized by dimers on a dual square lattice: we place a dimer on every dual lattice bond that intersects a frustrated bond of the original lattice (see Figure 4-3 for analogous visualization on a different lattice). Since dimers cost energy we minimize their number in the least frustrated states, and arrive at hard-core dimer coverings of the dual square lattice where only one dimer emanates from every dual square lattice site. Transverse field then gives dynamics to those dimers, which is captured by a quantum dimer model. At the first order of perturbation theory in small $\Gamma \ll J_z$ we



Ising couplings on emphasized bonds have opposite sign ($\varepsilon_{\langle ij \rangle} = -1$) from the couplings on other bonds ($\varepsilon_{\langle ij \rangle} = +1$).

Figure 5-1: Fully frustrated square lattice

have:

$$H = -\frac{\Gamma}{2} \sum_{\square} \left(|\square\rangle \langle \square| + h.c. \right) . \quad (5.2)$$

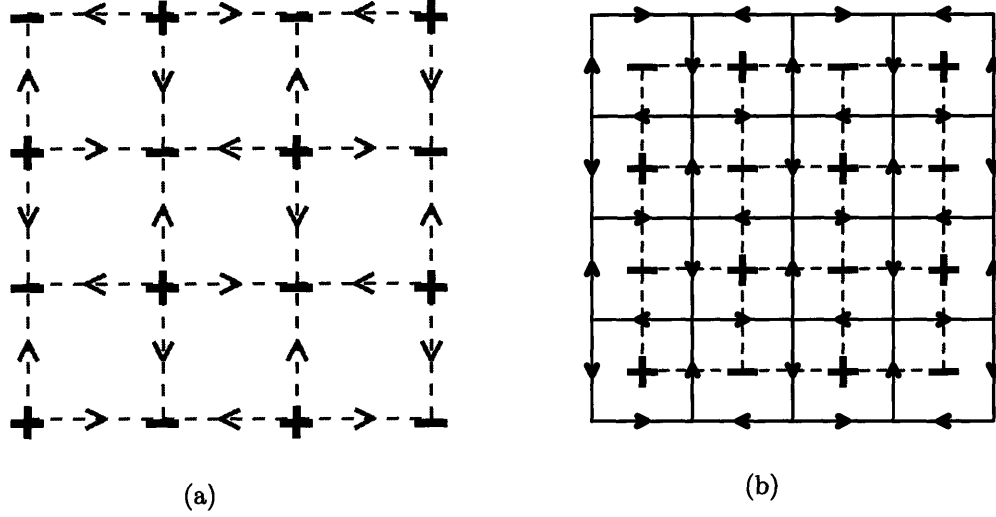
Following Chapter 4 we switch to appropriate gauge-theoretical description. We will label the original lattice sites by $i, j \dots$, and the dual lattice sites by $p, q \dots$. The dual square lattice is bipartite: there are two kinds of sites, denoted by $+$ and $-$ in Figure 5-2(a), and the sites of one kind are connected only to the sites of the other kind. If the dual bonds are oriented from $+$ to $-$ as in Figure 5-2(a), then we can introduce an electric field vector $E_{pq} = -E_{qp}$. Electric field lines *along the bond orientation* will represent dimers: one dimer is $E_{pq} = 1$ if the bond is oriented as $p \rightarrow q$. For mathematical convenience, we expand our model and allow more than one dimer on a bond so that E_{pq} may take arbitrary integer values. This only introduces benign changes at high energies, since the dimers are costly and at low energies we still have the physical states with zero or one dimers on every dual lattice bond. The dimer hard-core condition is expressed in form of a Gauss' Law:

$$(\forall p) \quad \sum_{q \in p} E_{pq} = \epsilon_p , \quad (5.3)$$

where due to alternating dual bond orientations a fixed background charge ϵ_p had to be introduced. This background charge takes values ± 1 on the dual lattice sites precisely as indicated in 5-2(a), so that the dual bond orientations reflect orientation of electric field lines. Quantum dynamics from (5.2) is then expressed using a vector potential operator \mathcal{A} , which is an angle conjugate to the integer-valued electric field:

$$H = U \sum_{\langle pq \rangle} E_{pq}^2 - \Gamma \sum_{\square} \cos \left(\sum_{pq} \overset{\square}{\mathcal{A}}_{pq} \right) . \quad (5.4)$$

This is a pure compact U(1) gauge theory with a staggered background fixed charge $\epsilon_p = \pm 1$ shown in Figure 5-2(a). In the large- U limit the low-energy field configurations correspond to the physical minimally frustrated states of Ising spins on the original lattice. Note that there are no fluctuating charge degrees of freedom (in



(a) Fixed background charge distribution $\epsilon_p = \pm 1$ on the dual lattice, and orientation of the dual lattice bonds. Bond orientation corresponds to natural electric field lines created by the background charge. (b) Orientation η_{ij} of the original lattice bonds. Dual lattice is plotted dashed for comparison. Note the “right-hand-rule” relationship between bond orientations on the original and dual lattices. Dual background charge ϵ_p transforms by duality into a “staggered flux” on the original lattice.

Figure 5-2: Square lattice staggered flux and dual background charge

contrast to the Kagome models).

Following the Chapter 4 further, we write the appropriate path-integral with aim to perform duality transformation and eventually obtain a lattice field theory:

$$\int_{-\pi}^{\pi} \mathcal{D}\mathcal{A}_{pq} \sum_{\{E_{pq}\}} \exp \left\{ - \sum_{\tau} \left[U \delta\tau \sum_{\langle pq \rangle} E_{pq}^2 - \Gamma \delta\tau \sum_{\square} \cos \left(\sum_{pq} \mathcal{A}_{pq} \right) - i \sum_{\langle pq \rangle} \mathcal{A}_{pq} \Delta_{\tau} E_{pq} \right] \right\} .$$

The cosine terms with vector potential curls can be expanded using the Villain’s approximation. This introduces an integer-valued magnetic field scalar B_i that lives

on sites of the original square lattice:

$$\int_{-\pi}^{\pi} \mathcal{D}\mathcal{A}_{pq} \sum_{\{E_{pq}\}} \sum_{\{B_i\}} \exp \left\{ - \sum_{\tau} \left[U \delta\tau \sum_{\langle pq \rangle} E_{pq}^2 + g \sum_i B_i^2 + i \sum_i B_i \sum_{pq} \mathcal{A}_{pq} - i \sum_{\langle pq \rangle} \mathcal{A}_{pq} \Delta_{\tau} E_{pq} \right] \right\} .$$

Here, $g = |\log(\Gamma\delta\tau/2)|$ and $\delta\tau$ is an imaginary time increment. Without going into technical details, which are a simpler version of those from Chapter 4, we integrate out the vector potential \mathcal{A}_{pq} and write a simple action (in the same universality class as the original problem) with one coupling constant:

$$S = g \sum_{\tau} \left[\sum_{\square_i} B_i^2 + \sum_{\langle pq \rangle} E_{pq}^2 \right] . \quad (5.5)$$

This is accompanied by a new constraint (Maxwell's equation) in addition to the Gauss' Law:

$$(\forall \langle ij \rangle) \quad \Delta_{\tau} E_{ij} = B_i - B_j . \quad (5.6)$$

In the last formula the dual lattice electric field E_{pq} is represented as a vector on the original square lattice E_{ij} . The dual bond $\langle pq \rangle$ and the original lattice bond $\langle ij \rangle$ intersect each other, and their orientations are related by the "right-hand rule": $\hat{z} \times \vec{E}_{ij} = \vec{E}_{pq}$ (see Figure 5-2(b)).

Duality transformation is applied to solve the constraints (5.6) and (5.3):

$$\begin{aligned} E_{ij} &= \chi_i - \chi_j + \zeta_{ij} \\ B_i &= \Delta_{\tau} \chi_i . \end{aligned} \quad (5.7)$$

The integer-valued fields χ_i live on the imaginary time-stacked original square lattice, and ζ_{ij} is a background integer vector field that creates a "staggered flux" through

the original lattice plaquettes:

$$(\forall \square_p) \quad \sum_{ij} \zeta_{ij} = -\epsilon_p . \quad (5.8)$$

Such background is needed in order to satisfy (5.3) on the dual lattice. One possible choice for ζ_{ij} is to set it to 1 on all emphasized bonds in Figure 5-1 (zero on other bonds), and make its vector orientation follow the arrows from Figure 5-2(b). Switching to the three-dimensional labeling of the original lattice sites $\mathbf{r} \equiv (i, \tau) \equiv (x, y, \tau)$, and introducing $\zeta_{\mathbf{r}, \mathbf{r}+\hat{\tau}} = 0$, we write the final lattice theory (height model):

$$S = g \sum_{\langle \mathbf{r}\mathbf{r}' \rangle} \left(\chi_{\mathbf{r}} - \chi_{\mathbf{r}'} + \zeta_{\mathbf{r}\mathbf{r}'} \right)^2 . \quad (5.9)$$

It is known that the three-dimensional integer-valued height models always live in the “smooth” phase. The height symmetry is broken ($\chi_{\mathbf{r}}$ is long-range correlated), so that it only remains to find whether (and how) the lattice symmetries are broken due to the non-trivial background $\zeta_{\mathbf{r}\mathbf{r}'}$. We proceed by using the same strategy as in the Chapter 4. The action (5.9) has many degenerate minimums that correspond to the hard-core dimer coverings of the dual lattice, that is to the minimally frustrated spin states on the original lattice. Quantum fluctuations can entropically select few of them, which is reflected in the minimum of “free energy”. We compute the “free energy” F of a saddle-point configuration $\chi_i^{(0)}$ by expanding the action about that saddle-point and introducing by hand a small “mass” to all deviations from it:

$$e^{-F(\xi)} = \sum_{\{\chi_{\mathbf{r}}\}} \exp \left\{ -g \left[\sum_{\langle \mathbf{r}\mathbf{r}' \rangle} \left((\chi_{\mathbf{r}} - \chi_{\mathbf{r}}^{(0)}) - (\chi_{\mathbf{r}'} - \chi_{\mathbf{r}'}^{(0)}) + \xi_{\mathbf{r}\mathbf{r}'} \right)^2 + m^2 \sum_{\mathbf{r}} \left(\chi_{\mathbf{r}} - \chi_{\mathbf{r}}^{(0)} \right)^2 \right] \right\} . \quad (5.10)$$

The generalized background field $\xi_{\mathbf{r}\mathbf{r}'} = \chi_{\mathbf{r}}^{(0)} - \chi_{\mathbf{r}'}^{(0)} + \zeta_{\mathbf{r}\mathbf{r}'}$ satisfies the same constraints as $\zeta_{\mathbf{r}\mathbf{r}'}$, and directly represents different minimally frustrated spin states. The goal is now to find which configuration of frustrated bonds in the original spin model yields minimum of the free energy. For this purpose we can introduce background field

scalars $\xi_{\langle ij \rangle} = \eta_{ij} \xi_{ij}$, where the ‘‘bond orientation’’ vectors η_{ij} take value 1 on every bond in directions specified by Figure 5-2(b). The constraint (5.8) that ξ_{ij} must also obey now reads:

$$(\forall \square) \quad \sum_{\langle ij \rangle}^{\square} \xi_{\langle ij \rangle} = 1 , \quad (5.11)$$

so that $\xi_{\langle ij \rangle} = 1$ means that the bond $\langle ij \rangle$ is frustrated (zero means unfrustrated bond). This expression directly illustrates that the minimally frustrated states have one frustrated bond on every plaquette. In the three-dimensional notation we write $\xi_{\langle ij \rangle}$ as $\xi_{\mathbf{r}, \mathbf{r}+\hat{x}} \equiv \xi_{\mathbf{r}}^x$ on horizontal, and $\xi_{\mathbf{r}, \mathbf{r}+\hat{y}} \equiv \xi_{\mathbf{r}}^y$ on vertical bonds (zero on temporal bonds). The constraint (5.11) is then:

$$(\forall \mathbf{r}) \quad \xi_{\mathbf{r}}^x + \xi_{\mathbf{r}+\hat{x}}^y + \xi_{\mathbf{r}+\hat{y}}^x + \xi_{\mathbf{r}}^y = 1 . \quad (5.12)$$

When evaluating (5.10) we are faced with two difficulties: it is hard to integrate out integer-valued height fields, and the action has three-dimensional dispersion which makes it diagonalizable only in momentum space. The first difficulty can be avoided in the small g limit, where the summation can be approximated by an integration. In the following we focus on that limit. Treating the height fields $\chi_{\mathbf{r}}$ as real variables, it is straight-forward to evaluate the Gaussian integral obtained from (5.10):

$$F(\xi) = -g \int \frac{d^2 \mathbf{k}}{(2\pi)^3} \frac{|(\text{div} \xi)_{\mathbf{k}}|^2}{C_{\mathbf{k}} + m^2} + g \sum_{\langle ij \rangle} \xi_{\langle ij \rangle}^2 . \quad (5.13)$$

Note that we are not interested in time variations of the background ξ . Presence of such variations would only move us away from the action minimums, and yield larger values for the free energy than the ones we will find. Therefore, we assume that $\xi_{\langle ij \rangle}$ and $\xi_{\mathbf{r}}$ do not depend on imaginary time, and restrict ourselves to two-dimensional integration over momenta. Here $C_{\mathbf{k}}$ is diagonalized coupling matrix from the action (5.9) at zero frequency:

$$C_{\mathbf{k}} = 4 - 2(\cos k_x + \cos k_y) . \quad (5.14)$$

The new quantity $(\text{div} \xi)_{\mathbf{k}}$ is Fourier transform of the background field divergence

$(\text{div}\xi)_{\mathbf{r}} = \xi_{\mathbf{r},\mathbf{r}+\hat{x}} + \xi_{\mathbf{r},\mathbf{r}+\hat{y}} + \xi_{\mathbf{r},\mathbf{r}-\hat{x}} + \xi_{\mathbf{r},\mathbf{r}-\hat{y}}$. We can express it using the background field scalars introduced earlier:

$$(\text{div}\xi)_{\mathbf{k}} = \xi_{\mathbf{k}-\mathbf{Q}}^x - \xi_{\mathbf{k}-\mathbf{Q}}^y + e^{-i(\mathbf{k}-\mathbf{Q})\hat{x}} \xi_{\mathbf{k}-\mathbf{Q}}^x - e^{-i(\mathbf{k}-\mathbf{Q})\hat{y}} \xi_{\mathbf{k}-\mathbf{Q}}^y, \quad (5.15)$$

where $\mathbf{Q} = \pi(\hat{x} + \hat{y})$. Due to the constraints (5.12) there is only one independent background field $\rho_{\mathbf{r}}$ per square lattice unit-cell, which determines both $\xi_{\mathbf{r}}^x$ and $\xi_{\mathbf{r}}^y$. Fourier transform of (5.12) gives us for $\mathbf{k} \neq 0$:

$$\begin{aligned} \xi_{\mathbf{k}}^x &= -(1 + e^{ik_x})\rho_{\mathbf{k}} \\ \xi_{\mathbf{k}}^y &= (1 + e^{ik_y})\rho_{\mathbf{k}}. \end{aligned} \quad (5.16)$$

We want to express the free energy in terms of the independent background fields $\rho_{\mathbf{k}}$. First, for $\mathbf{k} \neq 0$ the background field divergence becomes:

$$(\text{div}\xi)_{\mathbf{k}} = C_{\mathbf{k}}\rho_{\mathbf{k}}, \quad (5.17)$$

with $C_{\mathbf{k}}$ given by (5.14). Next, we note that the second term in (5.13) is not necessary to keep. We want to compare through free energy only the integer configurations of $\xi_{\langle ij \rangle}$ that correspond to minimally frustrated states. For such configurations this term evaluates to a constant (total number of dimers), and thus we will drop it from now on. This will yield an incomplete expression for the free energy that is not independent of real-valued $\xi_{\mathbf{r}}$ when $m^2 = 0$.¹ This artifact is of no concern for us, since we are

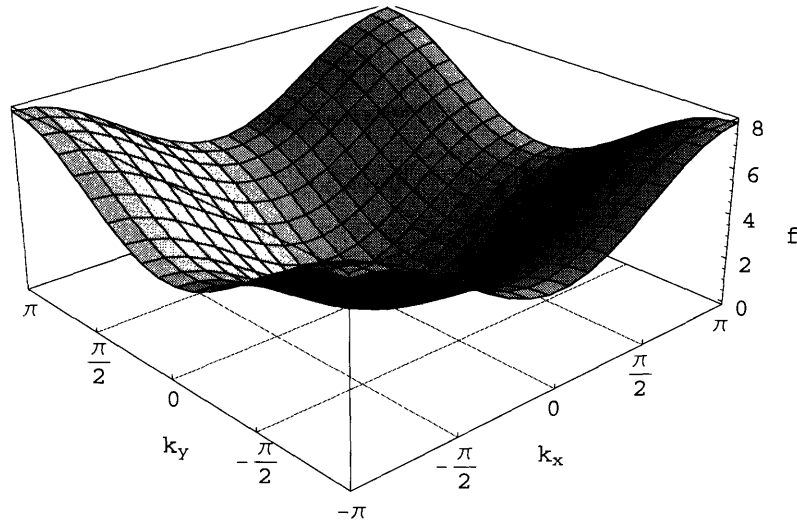
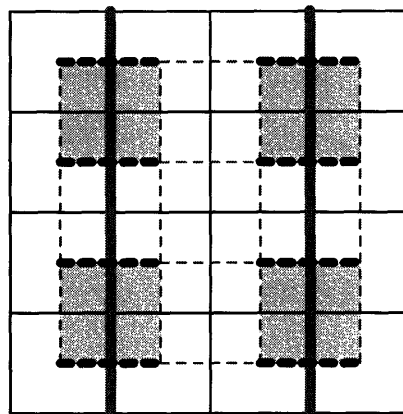


Figure 5-3: Free energy spectral weight of the square lattice transverse field Ising model



Entropically selected arrangement of frustrated bonds is shown on the original lattice (full lines) and the dual lattice (dashed lines). Picture on the dual lattice corresponds to the columnar dimer long-range order. This is the closest static configuration of frustrated bonds to the preferred ordering wavevector $Q = \pi\hat{x} + \pi\hat{y}$. However, the lattice rotation symmetry can be restored in the “plaquette phase” where the pairs of parallel dimers resonate between two possible states on every emphasized dual square plaquette. Such state is characterized precisely by the ordering wavevector Q .

Figure 5-4: Valence-bond crystal in the square lattice transverse field Ising model

$-g \int d^2\mathbf{k} f_{\mathbf{k}} |\rho_{\mathbf{k}}|^2$. The “spectral weight” $f_{\mathbf{k}}$ in the first Brillouin zone is plotted in Figure 5-3. Clearly, the free energy is minimized best by increasing the amplitude $\rho_{\mathbf{k}}$ at wavevector $\mathbf{k} = \mathbf{Q} = \pi\hat{x} + \pi\hat{y}$. This indicates how the lattice symmetries are broken. Actual values that the independent background amplitudes $\rho_{\mathbf{k}}$ may take at various momenta are limited by the requirement that $\xi_{\mathbf{r}}^x$ and $\xi_{\mathbf{r}}^y$ take values 0 or 1 when calculated from inverse Fourier transform of (5.16). Such configurations correspond to the minimally frustrated spin states. The best choice is an arrangement of frustrated bonds with periodicity as close to $\mathbf{k} = \mathbf{Q}$ as possible. When frustrated bonds are visualized as dimers on the dual square lattice, this arrangement is the columnar-ordered dimer covering, displayed in Figure 5-4. Therefore, in the limit $g \ll 1$ a valence-bond crystal is established entropically by quantum fluctuations. Note that this conclusion remains valid for all values of m^2 .

The most interesting question is what happens in the large- g limit, where we must handle the height fields χ_i in (5.10) as integers. This limit describes best the pure quantum Ising model in weak transverse field, with only the lowest order (most local) resonances. In other words, this is when neglecting dimer flips on large loops in (5.2) is most justified. In Chapter 4 we were able to perform calculations on the Kagome lattice in this limit because the action was diagonalizable in real space where all integer constraints hold. On the square lattice, the action must be diagonalized in momentum space, and this makes the problem very hard. We will not attempt to solve it here. Instead, we can argue on physical grounds that translational symmetry will still be broken.

In the small- g limit fluctuations entropically select certain long-range ordered states from the degenerate classical manifold. These states are selected because the number of ways in which the small fluctuations can transform them into other low-energy states is the largest among all states. Thus, the system simply spends most of time fluctuating in their vicinity. Structure of the degenerate classical manifold and nature of local fluctuations do not depend on g (this is set by the form of action (5.9)). Therefore, at large g the same entropical selection mechanism will be in place. The only thing that changes by increasing g is amount of fluctuations. When fluctuations

are reduced at larger g , the entropically selected long-range order can be only more stable. Therefore, we conclude that translational symmetry is broken in the large- g limit the same way as for small g .

At the end, let us note that these calculations are performed essentially identically on the triangular lattice transverse field Ising model, where analogous order-by-disorder is found.

5.2 Triangular Lattice XXZ Model

This section will present preliminary calculations that discover order-by-disorder in the XXZ model on triangular lattice. We will analyze the following Hamiltonian:

$$H = J_z \sum_{\langle ij \rangle} S_j^z S_j^z - J_\perp \sum_{\langle ij \rangle} (S_j^x S_j^x + S_j^y S_j^y) . \quad (5.19)$$

This is a frustrated model: for $J_\perp = 0$ there are many classical degenerate ground states. While our calculations can be “rigorous” only for small $J_\perp > 0$, chances are that the valence-bond crystal that we will find obtains also for $J_\perp < 0$, only with singlet instead of triplet valence-bonds. The XXZ model with $J_\perp < 0$ is a more standard spin Hamiltonian, and was originally proposed by Anderson to give rise to a spin liquid [8].

The mapping used in Chapter 4 and in the previous section leads us to a representation of the classical ground-states as hard-core dimer coverings of the dual honeycomb lattice. In the limit $J_z \gg J_\perp > 0$ we apply perturbation theory to the first order and obtain an effective dimer model. Every plaquette of the honeycomb lattice corresponds to a triangular lattice spin, and since dimers visualize frustrated bonds, flipping a spin toggles dimer occupancy on the dual hexagon’s bonds. The XXZ exchange J_\perp flips two spins at a time, hence the dimer model has dimer-flip terms on pairs of hexagons. We immediately write such effective theory in the form

of compact U(1) gauge theory on the honeycomb lattice:

$$H = U \sum_{\langle pq \rangle} E_{pq}^2 - J_{\perp} \sum_{\text{hex}} \cos \left(\sum_{pq} \mathcal{A}_{pq} \right). \quad (5.20)$$

As usual, this is accompanied by the Gauss' Law:

$$(\forall p) \quad \sum_{q \in p} E_{pq} = \epsilon_p, \quad (5.21)$$

where ϵ_p is staggered background charge on the honeycomb lattice sites (see Figure 5-6(a)). Just like in the previous section, there is no fluctuating charged matter field. Next, we formulate a path-integral and expand the cosines in (5.20) using Villain's approximation. The action is:

$$S = \sum_{\tau} \left[g \sum_{\langle pq \rangle} E_{pq}^2 + g \sum_{\langle ij \rangle} B_{\langle ij \rangle}^2 + i \sum_{\langle ij \rangle} B_{\langle ij \rangle} \sum_{pq} \mathcal{A}_{\langle pq \rangle} - i \sum_{\langle pq \rangle} \mathcal{A}_{pq} \Delta_{\tau} E_{pq} \right], \quad (5.22)$$

where the Villain's "magnetic field" scalar $B_{\langle ij \rangle}$ lives on the triangular lattice bonds. We again label by $i, j \dots$ the original (triangular) lattice sites, and by $p, q \dots$ the dual (honeycomb) lattice sites. Note that every triangular lattice bond $\langle ij \rangle$ specifies a pair of honeycomb lattice plaquettes, and that bond labels in brackets $\langle ij \rangle$ indicate scalar quantities ($B_{\langle ij \rangle} = B_{\langle ji \rangle}$), while without brackets pq they indicate vector quantities ($E_{pq} = -E_{qp}$). It is convenient to rewrite terms with vector potential \mathcal{A}_{pq} in dual form on the triangular lattice:

$$\begin{aligned} \sum_{\langle pq \rangle} \mathcal{A}_{pq} \Delta_{\tau} E_{pq} &= \sum_{\langle ij \rangle} \mathcal{A}_{ij} \Delta_{\tau} E_{ij} \\ \sum_{\langle ij \rangle} B_{\langle ij \rangle} \sum_{pq} \mathcal{A}_{pq} &= \sum_{\langle ij \rangle} \mathcal{A}_{ij} \left(\sum_{k \in i} B_{\langle ik \rangle} - \sum_{k \in j} B_{\langle jk \rangle} \right). \end{aligned} \quad (5.23)$$

As usual, duality transforms oriented bonds according to the "right-hand rule", and

thus exchanges curls for divergencies between the two dual lattices. After integrating out the vector potential we have:

$$S = g \sum_{\tau} \sum_{\langle ij \rangle} \left(E_{ij}^2 + B_{\langle ij \rangle}^2 \right), \quad (5.24)$$

and a new constraint (Maxwell's equation):

$$(\nabla \langle ij \rangle) \Delta_{\tau} E_{ij} = \sum_{k \in i} B_{\langle ik \rangle} - \sum_{k \in j} B_{\langle jk \rangle}. \quad (5.25)$$

The constraints (5.21) and (5.25) can be solved just like in Chapter 4:

$$\begin{aligned} E_{ij} &= \chi_i - \chi_j + \zeta_{ij} \\ B_{\langle ij \rangle} &= \Delta_{\tau} \kappa_{\langle ij \rangle}, \end{aligned} \quad (5.26)$$

where χ_i and $\kappa_{\langle ij \rangle}$ are integer-valued fields. The Gauss' Law (5.21) turns by duality into a curl on the triangular lattice, and determines the integer-valued background vector field ζ_{ij} :

$$(\nabla \Delta_p) \sum_{ij} \zeta_{ij} = -\epsilon_p. \quad (5.27)$$

The simplest acceptable configuration is shown in Figure 5-5 (vector ζ_{ij} is 1 on all emphasized bonds in the same lattice direction, while it is 0 on all other bonds). Relationship between χ_i and $\kappa_{\langle ij \rangle}$ follows by substituting (5.26) into (5.25):

$$\chi_i = \sum_{j \in i} \kappa_{\langle ij \rangle}. \quad (5.28)$$

We can now write the final lattice field theory on the triangular lattice:

$$S = g \sum_{\tau} \sum_{\langle ij \rangle} \left[\left(\Delta_{\tau} \kappa_{\langle ij \rangle} \right)^2 + \left(\sum_{k \in i} \kappa_{\langle ik \rangle} - \sum_{k \in j} \kappa_{\langle jk \rangle} + \zeta_{ij} \right)^2 \right]. \quad (5.29)$$

If we were to consider the XXZ model (5.19) with $J_{\perp} < 0$, we would have obtained an

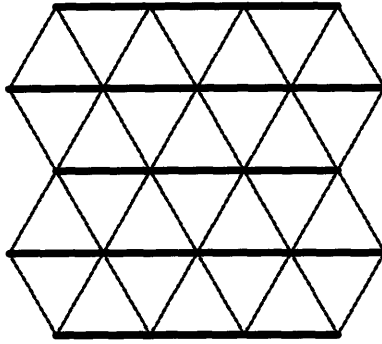


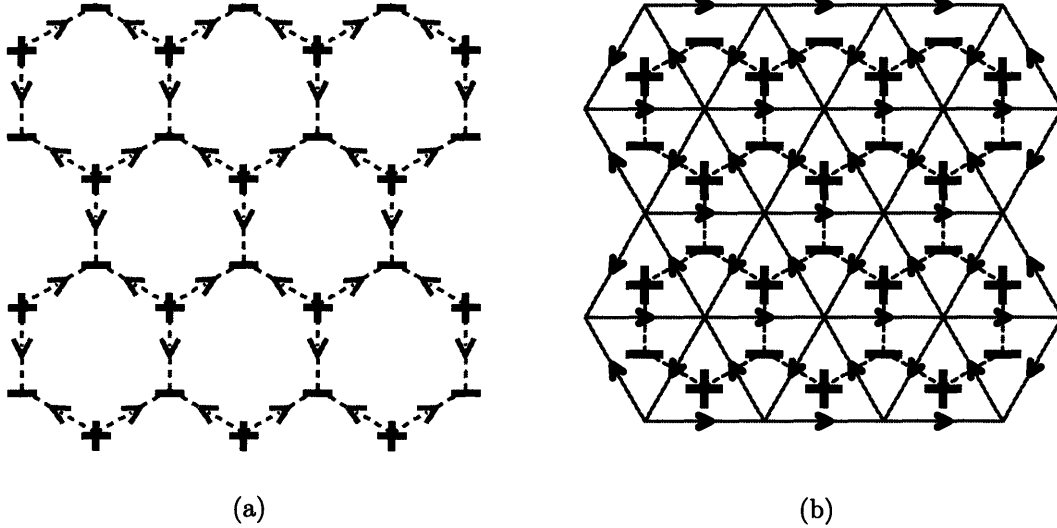
Figure 5-5: A background field configuration on the triangular lattice

additional Berry's phase in this action. As demonstrated in Chapter 4, the Berry's phase would couple to the fields only on the imaginary time boundaries. In spin liquid and even plaquette phases (where the valence-bonds resonate) this is unlikely to affect pattern of lattice symmetry breaking. Hence, we expect that the same order-by-disorder that we are going to find for small $J_{\perp} > 0$ exists in more standard spin models with $J_{\perp} < 0$.

We again note that every minimally frustrated state of the original spin model is represented by a $\kappa_{\langle ij \rangle}$ field configuration that minimizes action. We expand the action (5.29) about any such configuration $\kappa_{\langle ij \rangle}^{(0)}$, and absorb the shift of variables that took place into $\zeta_{ij} \rightarrow \xi_{ij} = \chi_i^{(0)} - \chi_j^{(0)} + \zeta_{ij}$, where $\chi_i^{(0)}$ is obtained from $\kappa_{\langle ij \rangle}^{(0)}$ according to (5.28). The generalized background bond-vector field ξ_{ij} satisfies the same constraints as ζ_{ij} , and directly represents different minimally frustrated states of the original spin model. Relationship between ξ_{ij} and spin states is expressed using the bond-scalar notation: $\xi_{\langle ij \rangle} = \eta_{ij} \xi_{ij}$, where η_{ij} are triangular lattice bond-orientation vectors that take value +1 on every bond in directions depicted in Figure 5-6(b). Then, $\xi_{\langle ij \rangle} = 1$ stands for a frustrated bond $\langle ij \rangle$, while $\xi_{\langle ij \rangle} = 0$ is an unfrustrated bond.

In order to facilitate calculations we express the lattice field theory (5.29) in matrix form. Let us introduce a lattice-vector $\boldsymbol{\kappa}$ whose components are the fields $\kappa_{\langle ij \rangle}$ on all triangular lattice bonds, and rewrite (5.29) as:

$$\frac{S}{g} = \boldsymbol{\kappa}^T \mathbf{C} \boldsymbol{\kappa} + (\text{div} \boldsymbol{\xi}^T \boldsymbol{\kappa} + \boldsymbol{\kappa}^T \text{div} \boldsymbol{\xi}) + \sum_{\langle ij \rangle} \xi_{ij}^2. \quad (5.30)$$



(a) Fixed background charge distribution $\epsilon_p = \pm 1$ on the dual lattice, and orientation of the dual lattice bonds. Bond orientation corresponds to natural electric field lines created by the background charge. (b) Orientation η_{ij} of the original lattice bonds. Dual lattice is plotted dashed for comparison. Note the “right-hand-rule” relationship between bond orientations on the original and dual lattices. Dual background charge ϵ_p transforms by duality into a “staggered flux” on the original lattice.

Figure 5-6: Triangular lattice staggered flux and dual background charge

Components of the lattice-vector $\mathbf{div}\boldsymbol{\xi}$ are divergencies of bond-vectors ξ_{ij} on all lattice bonds. In order to see this and reveal structure of the coupling matrix \mathbf{C} , we note that the action (5.29) has form:

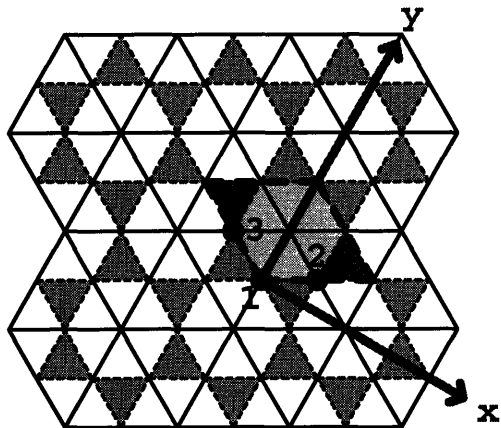
$$S = g \sum_{\langle ij \rangle} \left(\chi_i - \chi_j + \xi_{ij} \right)^2. \quad (5.31)$$

Then, we expand the square, substitute (5.28) and obtain:

$$(\mathbf{div}\boldsymbol{\xi})_{\langle ij \rangle} = \sum_{k \in i} \xi_{ik} + \sum_{k \in j} \xi_{jk} \quad (5.32)$$

$$(\mathbf{C}\boldsymbol{\kappa})_{\langle ij \rangle} = 6 \left(\sum_{k \in i} \kappa_{\langle ik \rangle} + \sum_{k \in j} \kappa_{\langle jk \rangle} \right) - \left(\sum_{k \in i} \sum_{l \in k} \kappa_{\langle kl \rangle} + \sum_{k \in j} \sum_{l \in k} \kappa_{\langle kl \rangle} \right), \quad (5.33)$$

where we did not take into account parts of the coupling matrix \mathbf{C} that are defined on temporal bonds. Time derivatives will not play any role in the following calcula-



Every triangular lattice bond (solid line) can be viewed as a site of a Kagome lattice (dashed line). The unit-cell used in this section is emphasized, and it has three depicted and labeled Kagome sites. A choice of coordinate system is also shown; edge of a unit-cell has unit length.

Figure 5-7: Kagome lattice representation of triangular lattice bonds

tions, which aim to reveal the pattern of lattice symmetry breaking. The role of time derivative terms is only to stabilize a long-range order. Note that our representation has more degrees of freedom than the original spin model. This can be easily understood by recalling that the starting $U(1)$ gauge-theoretical formulation (5.20) had three electric field quantities E_{pq} and two Gauss' Law constraints (5.21) per unit-cell, while the present theory has just three independent bond-scalars $\kappa_{\langle ij \rangle}$ per unit-cell. This redundancy of representation was introduced by the Villain's approximation, and as a consequence the coupling matrix \mathbf{C} has degenerate non-physical modes with zero eigenvalue (at zero frequency). However, our approach will naturally project the action (5.30) to the sector of physical modes, and reveal a $(2 + 1)D$ dispersion of the projected coupling matrix \mathbf{C} . The physical degrees of freedom essentially make a discrete $(2 + 1)D$ height model, so that this theory lives in the "smooth" phase where a long-range order is stable. This conclusion is reached along the same lines as in the case of the Kagome XXZ model in Chapter 4.

We now embark on finding how the lattice symmetries are broken in the stable ordered phase. From this point on we will simplify calculations by dropping the last term of (5.30). It evaluates to a constant (total number of frustrated bonds) for

every integer-valued configuration of $\xi_{\langle ij \rangle}$ that corresponds to a minimally frustrated state. It will be also convenient to change lattice labeling to that of a Kagome lattice. All degrees of freedom live on the triangular lattice bonds $\langle ij \rangle$, which are equivalently sites \mathbf{r} of a Kagome lattice (see Figure 5-7). Let us represent (5.32) in matrix form:

$$\text{div}\boldsymbol{\xi} = \mathbf{W}\boldsymbol{\xi} , \quad (5.34)$$

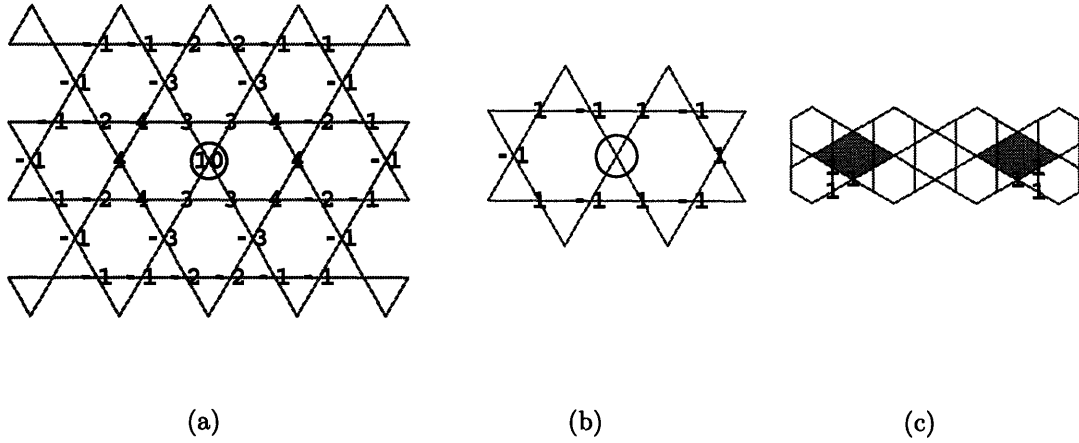
where components of the lattice-vector $\boldsymbol{\xi}$ are the background fields $\xi_{\langle ij \rangle} \equiv \xi_{\mathbf{r}}$ on triangular lattice bonds, or equivalently Kagome lattice sites. In Figures 5-8 (a) and (b) we show structure of the matrices \mathbf{C} and \mathbf{W} respectively by evaluating how they act on a unit site-localized lattice-vector. These matrices can be diagonalized in momentum space by working with 3×3 blocks that correspond to Kagome lattice unit-cells in Figure 5-7. It turns out that the matrix \mathbf{W} projects-out the non-physical modes (due to redundancy of representation). When projected to the space of physical degrees of freedom, the 3×3 blocks obtained after diagonalization reduce to scalars in momentum space (one for every Kagome unit-cell):

$$\begin{aligned} C_{\mathbf{k}} &= 36 - 4 \left[\cos\left(\frac{\sqrt{3}}{2}k_x + \frac{1}{2}k_y\right) + \cos\left(-\frac{\sqrt{3}}{2}k_x + \frac{1}{2}k_y\right) + \cos(-k_y) \right]^2 \\ W_{\mathbf{k}} &= 2i \left[\sin\left(\frac{\sqrt{3}}{2}k_x + \frac{1}{2}k_y\right) + \sin\left(-\frac{\sqrt{3}}{2}k_x + \frac{1}{2}k_y\right) + \sin(-k_y) \right] . \end{aligned} \quad (5.35)$$

Constraints that the background fields $\xi_{\mathbf{r}}$ must satisfy (the same as 5.27) can also be expressed in matrix form. There are two of them per Kagome unit-cell, one for every Kagome triangle. In the Kagome momentum space representation on 3×3 blocks these constraints read:

$$\begin{aligned} \frac{1}{2}(\mathbf{h}_{1,\mathbf{k}}^\dagger \boldsymbol{\xi}_{\mathbf{k}} + h.c.) &= (2\pi)^2 \delta(\mathbf{k}) \\ \frac{1}{2}(\mathbf{h}_{2,\mathbf{k}}^\dagger \boldsymbol{\xi}_{\mathbf{k}} + h.c.) &= (2\pi)^2 \delta(\mathbf{k}) , \end{aligned} \quad (5.36)$$

where the correspondint unit-cell-vectors $\mathbf{h}_{1,\mathbf{k}}$ and $\mathbf{h}_{2,\mathbf{k}}$ are depicted in real-space in Figure 5-8(c). In this notation, bold symbols with a position or momentum index



(a) Action of the coupling matrix C in the lattice field theory. Non-zero values of $(C\kappa)_r$ are shown at all sites r for $\kappa_r = \delta_{r,0}$, where the site at the origin is circled. (b) Action of the matrix W on $\kappa_r = \delta_{r,0}$. (c) Unit-cell vectors $h_{1,r}$ and $h_{2,r}$, which implement background field constraints. A constraint is imposed on every triangular lattice plaquette, that is on every Kagome lattice triangle, so that there are two of them in every unit-cell.

Figure 5-8: Triangular lattice XXZ model represented on the Kagome lattice

denote unit-cell-vectors with three components.

We are finally ready to explore possible order-by-disorder. As argued before, the lattice field theory (5.29) is essentially a $(2+1)$ D height model (after the redundancy of representation is removed), so that the height symmetry is always broken. Possible breaking of translational symmetry is achieved entropically by quantum fluctuations, and this is reflected in the “free energy” F :

$$e^{-F(\xi)} = \sum_{\kappa} e^{-S(\kappa;\xi) - gm^2 \kappa^T \kappa}. \quad (5.37)$$

The action S (Equation (5.30)) is expanded about one of its degenerate ground-states, which is specified by ξ , and a “mass” tunable parameter gm^2 is included to penalize fluctuations away from the chosen ground-state configuration ξ . The free energy is minimized at the most favorable states by entropy. We proceed by calculating F in the only presently tractable limit. If g is small enough, we can approximate summation over integer-valued height fields κ_r by a Gaussian integration. Ignoring the last term

of (5.30), which is a constant for valid backgrounds ξ , we find:

$$F(\xi) = -g \int \frac{d^2\mathbf{k}}{(2\pi)^3} \frac{|W_{\mathbf{k}}|^2}{C_{\mathbf{k}} + m^2} |\xi_{\mathbf{k}}|_{\text{phys.}}^2, \quad (5.38)$$

where $|\xi_{\mathbf{k}}|_{\text{phys.}}^2$ is modulus squared of the Kagome unit-cell-vector $\xi_{\mathbf{k}}$ projected to the space of physical degrees of freedom. We want to minimize this free energy subject to constraints (5.36). The vectors $\xi_{\mathbf{k}}$ that satisfy (5.36) have the following form for $\mathbf{k} \neq 0$:

$$\xi_{\mathbf{k}} = \left[1 - e^{ik_y}, \quad e^{i\left(-\frac{\sqrt{3}}{2}k_x + \frac{1}{2}k_y\right)} - 1, \quad e^{i\left(\frac{\sqrt{3}}{2}k_x + \frac{1}{2}k_y\right)} - 1 \right]^T \rho_{\mathbf{k}}. \quad (5.39)$$

Projecting them to the space of physical degrees of freedom, and taking modulus squared gives:

$$|\xi_{\mathbf{k}}|_{\text{phys.}}^2 = \frac{8 \sin^2\left(\frac{\sqrt{3}}{2}k_x + \frac{1}{2}k_y\right) \sin^2\left(-\frac{\sqrt{3}}{2}k_x + \frac{1}{2}k_y\right)}{3 + \cos\left(\frac{\sqrt{3}}{2}k_x + \frac{1}{2}k_y\right) + \cos\left(-\frac{\sqrt{3}}{2}k_x + \frac{1}{2}k_y\right) + \cos k_y} |\rho_{\mathbf{k}}|^2, \quad (5.40)$$

where $\rho_{\mathbf{k}}$ is scalar amplitude of the physical background mode at wave-vector \mathbf{k} (one per Kagome unit-cell). This expression needs to be substituted into (5.38) in order to obtain the final formula for free energy.

The final free energy is a weighted sum of the physical background $\rho_{\mathbf{k}}$ at all wavevectors:

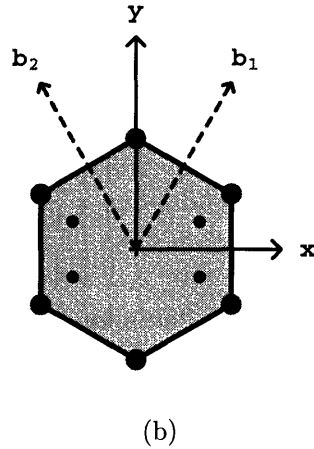
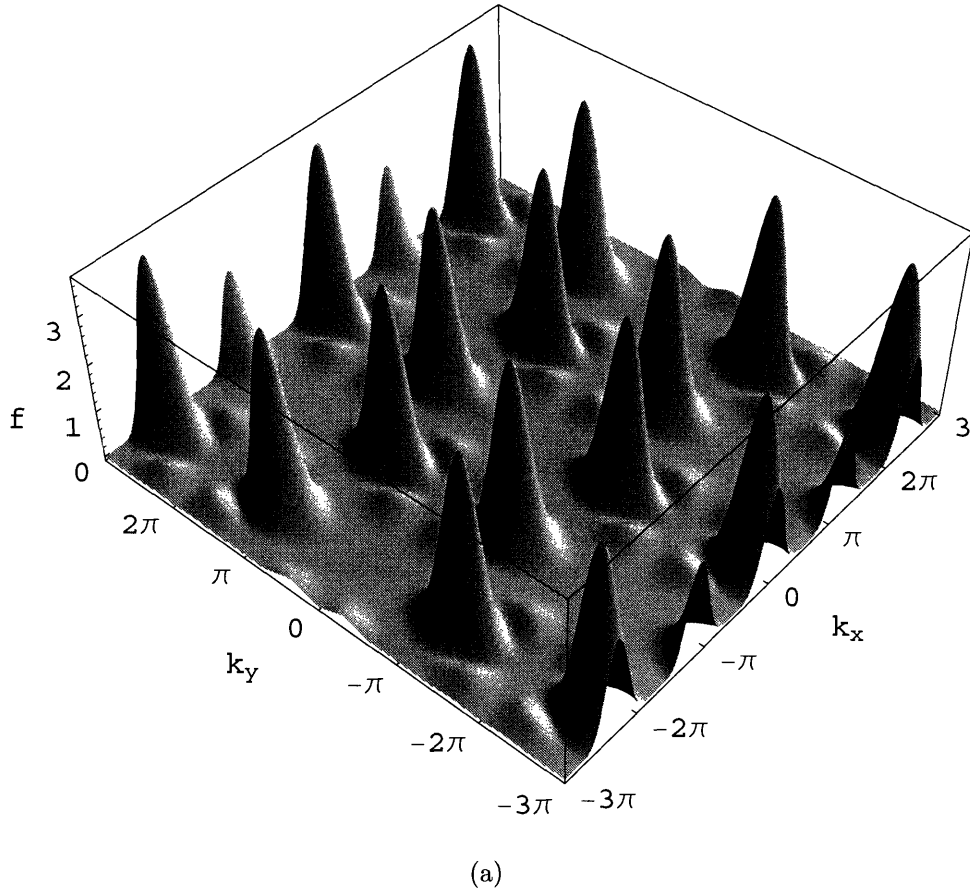
$$F(\rho) = -g \int d^2\mathbf{k} f_{\mathbf{k}} |\rho_{\mathbf{k}}|^2. \quad (5.41)$$

Figure 5-9(a) shows a plot of the weight-factors $f_{\mathbf{k}}$ as a function of wavevector. For reference, the first Brillouin zone and peak positions of the weight are shown in Figure 5-9(b). Peaks reveal wavevectors that are entropically favored by quantum fluctuations. There are two sets of peaks: primary at $\mathbf{q}' = \pm \frac{4\pi}{3} \hat{\mathbf{y}}$ (and equivalent wavevectors), and secondary at $\mathbf{q}'' = \pm \left(\frac{4\pi}{3\sqrt{3}} \hat{\mathbf{x}} \pm \frac{\pi}{3} \hat{\mathbf{y}} \right)$ (and equivalent wavevectors). Lattice symmetries are broken with two characteristic periods $\Delta\mathbf{r}$ obtained from $\Delta\mathbf{r}\mathbf{q} = 2\pi$. The primary period exactly corresponds to the columnar dimer order when frustrated bonds are visualized as dimers on the honeycomb lattice (see Figure

5-10). The secondary period breaks lattice rotation symmetry, and is characteristic of the XXZ model. In contrast, transverse field Ising model on triangular lattice produces only the primary period, in analogy to the square lattice model considered in the previous section.

Interestingly, the lattice rotation symmetry breaking is also evident if we try to guess the arrangement of frustrated bonds that is entropically selected by quantum fluctuations. Such configurations should conform to the discovered periodicities, but include only values 0 and 1 for the background fields $\xi_{\langle ij \rangle}$ on every triangular lattice bond (1 means that the bond is frustrated). In addition, the entropically selected states should have zero Ising magnetization (which is a good quantum number), since this minimizes the XXZ exchange energy. Precisely the requirement of zero magnetization is responsible for lattice rotation symmetry breaking. This can be easily understood by observing that the unit-cell of the primary ordering pattern (dimer-columnar order in Figure 5-10) has an odd number of spins (nine). The unit-cell must be doubled so that it could carry a zero total spin, and this requires picking a direction on the lattice. A guess for an acceptable entropically selected arrangement of frustrated bonds is shown in Figure 5-11.

As we have seen, in the small- g limit a valence-bond crystal is obtained in the triangular lattice XXZ model. It is similar to the order-by-disorder on triangular lattice caused by weak transverse field dynamics, but it breaks lattice rotation symmetry. However, only in the large- g limit one truly captures dynamics of small XXZ exchange, without proliferation of multiple spin-exchange and other higher-order (more non-local) processes. While presently we cannot perform calculations in this limit, we can argue that the same long-range valence-bond order persists. The argument is the same as given at the end of the previous section.



(a) Free energy spectral weight (plotted beyond the first Brillouin zone). (b) The first Brillouin zone and peak positions of the spectral weight. Primary peaks (large dots) lie at the Brillouin zone edges ($\mathbf{q}' = \frac{4\pi}{3}\hat{\mathbf{y}}$ and rotations by 60°), while the secondary peaks (smaller dots) lie within the zone ($\mathbf{q}'' = \pm(\frac{4\pi}{3\sqrt{3}}\hat{\mathbf{x}} \pm \frac{\pi}{3}\hat{\mathbf{y}})$). Reciprocal lattice vectors are \mathbf{b}_1 and \mathbf{b}_2 . Recall that the unit-length in real space corresponds to the Kagome unit-cell size.

Figure 5-9: Free energy spectral weight of the triangular lattice XXZ model

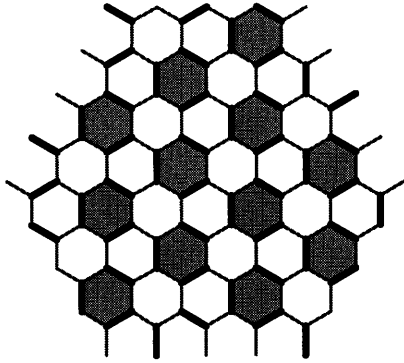


Figure 5-10: Columnar order of dimers on the honeycomb lattice

If frustrated bonds of the original spin model are visualized as dimers on the intersecting bonds of the dual honeycomb lattice, then the best match to the dominant period at q' is achieved by the columnar state. This is precisely the state that would have been entropically selected by the transverse field Ising model on triangular lattice. Another possibility is the plaquette phase in which every shaded Benzene-like hexagon resonates.

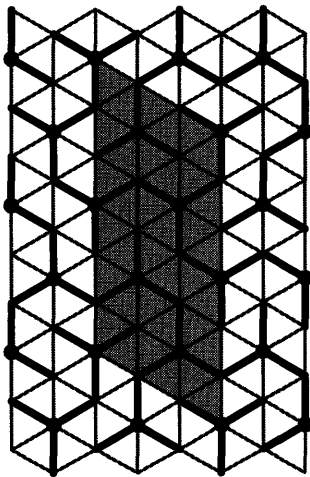


Figure 5-11: An entropically favored state in the triangular lattice XXZ model

A guessed arrangement of frustrated bonds on the triangular lattice that is entropically selected by quantum XXZ dynamics. The unit-cell of this structure is shaded and contains 18 sites. This is the smallest size that allows total Ising magnetization to be zero within the unit-cell, while it captures the underlying order at the primary ordering wavevector q' . This unit-cell is doubled with respect to that of the dual honeycomb dimer picture in Figure 5-10. Periodic rings emphasize corresponding positions of the shaded Benzene-like hexagons in the Figure 5-10, whose periodicity is characterized by q' (note that these are triplets of frustrated bonds that emanate from the same site). In addition, the structure of frustrated bonds has been modified to form a large number of flippable spin-pairs.

Chapter 6

Conclusions

This thesis includes several ideas and projects on frustrated quantum magnets from its author's last three years of graduate studies at MIT. Since the contents of this work could never match ambitious and general scope of its title (which sounds like a title of a review book written by a well known expert), the author hopes that it at least brings some fresh insight into the field of frustrated quantum magnetism, and opens some doors for future research on various related topics. Sadly, the subject is so complex and undeveloped that it took an entire Ph. D. to learn available and discover new theoretical tools on just one frustrated system, the Kagome lattice antiferromagnet.

Luckily, however, this particular two-dimensional lattice, with very peculiar and almost unnatural crystal structure, turned out to be much less frightening than it might seem at first glance. Typically, after certain barriers of initial creativity and mathematical complexity are crossed, problems on the Kagome lattice are solvable to a large extent. In Chapter 2 we have explicitly revealed ground-state and excitations of a complicated ordered paramagnetic phase in the Kagome quantum Heisenberg model; in Chapters 3 and 4 we have found field-theoretical descriptions of the Kagome lattice quantum Ising models with transverse field and XXZ dynamics, and explored their phase diagrams. These kinds of results are typically obtained on other lattices either numerically (Monte Carlo or exact diagonalization), or in semiclassical limits (large- N). From this experience, it seems that the friendliness of the Kagome lattice comes from its poorly connected crystal structure, which sometimes makes

it dangerously close to a collection of disconnected sites and hinders conventional approaches.

Therefore, in retrospect, the Kagome antiferromagnets may be a small subset of interesting problems, but they are tractable, and they apparently host certain important examples of unconventional quantum paramagnetic phases. The combination of these two advantages makes the Kagome systems very valuable in learning about new exotic states of strongly correlated electrons, and in some instances even provides pointers to understanding microscopic roots of such exotic behavior. Besides, with current trends in numerical and experimental research, chances are that the Kagome antiferromagnets will be among the first systems whose theoretically predicted exotic properties will be independently verified.

In the following concluding sections we will briefly review the phases found in the Kagome antiferromagnets, and the new methods used to find them. Then, we will finish by discussing further directions in which this research could continue, and some open problems.

6.1 Phases of the Kagome Lattice Antiferromagnets

In this thesis we have studied quantum Ising and Heisenberg antiferromagnets on the Kagome lattice. Even though the quantum Ising models may perhaps be less natural than the Heisenberg model, they admitted reliable field-theoretical treatment and possessed great flexibility in terms of perturbations whose effects could be analyzed. We can now systematically review the discovered Ising phases on the Kagome lattice and perturbations that create them.

When the Kagome lattice Ising antiferromagnet acquires quantum dynamics from a weak transverse field, the ground-state is a conventional disordered paramagnet. No symmetries are broken at zero temperature, and there is no topological order. This phase is expected to be smoothly connected to regions with large transverse

fields or high temperatures, where the spins become decoupled. In fact, the lack of spatial dispersion in the field-theoretical description indicates that the spins are almost decoupled even at zero temperature and small transverse fields. Apparently, the poorly connected Kagome net is responsible for such localized nature of quantum fluctuations. All excitations are gapped at an energy scale set by the transverse field. Simplicity of this model allowed us even to construct decent variational wavefunctions for the ground and excited states, and reach all these conclusions with two independent approaches in Chapters 3 and 4. It is important to realize that in spite of all triviality, the Kagome lattice is already very special. Even trivial disordered phases are not found in any other explored two-dimensional quantum Ising model in weak transverse field. Instead, if the Neel phase is unstable, quantum fluctuations seem to always entropically select some valence-bond ordered phase.

The transverse field gives dynamics to isolated spins and hence gives rise to the least interesting phases. More exotic paramagnetic phases occur when the quantum dynamics is more correlated. In the XXZ model, and some generalizations to models with conserved total Ising magnetization, we found two phases. One of them is a complicated valence-bond crystal, with a large unit-cell. The order is stabilized by non-trivial interactions between the valence bonds (at higher orders of perturbation theory in small XXZ exchange coupling). Particular pattern of lattice symmetry breaking is not completely clear from the approach that led to these conclusions in Chapter 4, but two candidate order parameters have been proposed. Size of the unit-cell hints a possibility that the gap to excited states may be significantly smaller than the energy scale given by the XXZ exchange, which would make this ordered phase unconventional. The other phase found to be possible in generalized XXZ models is a spin liquid. It naturally occurs in presence of further-neighbor and multiple-spin exchange. Coherent nature of quantum fluctuations that preserve total Ising magnetization was found to yield topological order in otherwise disordered phases. In the Kagome system, excitations in this topological phase appear to be very heavy or localized, making individual spins virtually independent, as well as any finite clusters of spins, but keeping some coherence at macroscopic scales. It is interesting to note,

however, that without help from further-neighbor and multiple-spin exchange perturbations, pure and weak XXZ dynamics prefers the valence-bond order, even on the very frustrated Kagome lattice.

Yet another peculiar phase was found in Chapter 3 when the Kagome lattice Ising model is given quantum dynamics in form of a ring-exchange on hexagonal plaquettes. For weak ring-exchange, but strong enough in comparison to transverse field and XXZ exchange, an ordered phase with spontaneously acquired ferromagnetic Ising magnetization seems to occur. One third of all spins participate in creating non-zero total magnetization, while the other spins fluctuate on periodically distributed hexagonal plaquettes (being set in motion by the ring-exchange). Translational symmetry is broken with a nine-site unit-cell. The features of this phase make it strikingly similar to the phase with one-third of saturated Ising magnetization that is induced by large external longitudinal magnetic fields in the XXZ models. Such a phase was found responsible for a plateau in the magnetization curve.

Clearly, the Kagome Ising antiferromagnet is a factory of exotic quantum phases. Due to a large variety of different phases, we can consider it a prime specimen among two-dimensional frustrated magnets suitable for learning more general lessons. If any lesson is to be learned, it is that a long-range order in two-dimensional systems with discrete degrees of freedom and local dynamics is extremely robust, even in very poorly connected lattices. Only two ways to restore all symmetries were found. One is a poorly connected lattice combined with the most local dynamics (transverse field); this gives rise to a trivial paramagnetic phase with no topological order. The other is proliferation of less local perturbations, such as further-neighbor and multiple-spin exchange; this mechanism should work on every lattice. Another lesson is that topological order generally obtains when perturbations that *conserve total Ising magnetization* are dominant and restore all symmetries.

The XXZ model on the Kagome lattice has an added importance: it is an anisotropic Heisenberg model. In Chapter 2 we studied the isotropic Heisenberg model on the Kagome lattice using completely different methods than those applied to the Ising models. The Heisenberg model attracts considerable attention in the condensed mat-

ter community, mainly because of its puzzling spectrum, claimed to contain gapless singlet modes in absence of any symmetry breaking and in presence of a finite spin-gap. Our approach to this problem started from a qualitatively constructed effective theory, which supported two quantum phases. One of them is an exotic valence-bond crystal. Its unit-cell is large (36 sites), and translational symmetry is broken in a 12-fold degenerate way. Elementary singlet excitations appear at an extremely small energy scale, much lower than the exchange coupling, but they are gapped. They also seem to be very heavy (large effective mass). The other phase is a spin liquid characterized by a clear and large gap to all excitations, and again by an extremely large effective mass. From comparison with available numerical studies of the Kagome Heisenberg model, and from some analytical considerations, we concluded that the valence-bond ordered phase is the best candidate to explain the mysterious spectrum. Unusually small gap is thus a consequence of frustration, which yields emergent physics at low energies, and not necessarily a consequence of proximity to a quantum critical point. These conclusions are further backed up by comparison with our results on the XXZ model: one of the candidate ordered phases found in the XXZ model is exactly the same as the valence-bond crystal of the Heisenberg model. A possible scenario is that the XXZ and Heisenberg models on the Kagome lattice are smoothly connected.

6.2 New Methods for Frustrated Quantum Magnets

All methods used in this thesis are centered about quantum models with discrete degrees of freedom. They are either a starting point (Ising models), or low energy effective theories of models with continuous degrees of freedom (a \mathbb{Z}_2 gauge theory obtained from the Heisenberg model). Discreteness is clearly the heart of success in this work.

The Heisenberg model on the Kagome lattice was treated by a slave-fermion formu-

lation in Chapter 2, where interactions between the slave particles were implemented through a \mathbb{Z}_2 gauge field. Certainly, other types of gauge fields could have been used in this kind of formulation, but a choice of discrete fields yields added simplicity at later stages of analysis. The Kagome problem involves gapped spinful excitations, and abundant spinless excitations below the spin-gap. Therefore, an effective theory for the spinless states is naturally obtained by integrating out the spinful slave particles. This effective theory is a pure \mathbb{Z}_2 gauge theory on the Kagome lattice, or equivalently a fully frustrated quantum Ising model on the dual dice lattice. A qualitative Hamiltonian for the spinless singlet excitations was constructed by symmetry arguments. In the Kagome case it was possible to find the ground and excited states of the effective theory within a second order degenerate perturbation theory. This is perhaps a unique example of a complicated problem which can be handled by elementary perturbative techniques.

A more controlled kind of calculations is possible when the starting point is a frustrated quantum Ising model on a lattice whose dual lattice is bipartite. Then, there are standard techniques based on quantum dimer representations, compact $U(1)$ gauge theory, duality transformations and field theory, which are very powerful for exploring phase diagrams. Due to mathematical complexity such approaches have not been applied to the Kagome systems until now. In the Chapters 3 and 4 we demonstrated two ways to apply these techniques on the Kagome lattice. The first directly exploits corner-sharing structure of the lattice, and its microscopic degrees of freedom are fluctuating spins. Its advantage is ultimate simplicity, which allows a neat demonstration of an elusive disordered phase created by transverse field dynamics. The second approach is applicable to a larger variety of lattices, and its microscopic degrees of freedom are fluctuating frustrated bonds. Though more complicated, it proved to be more suitable for revealing patterns of lattice symmetry breaking in the Kagome quantum Ising models.

An extension of a mean-field method to frustrated systems was also introduced in this thesis (Chapter 4). If there are numerous degenerate states that minimize action of a particular frustration problem, it is possible to partially integrate out

quantum fluctuations and calculate which degenerate states are favored by entropy. Such states are represented by larger probability amplitudes in the ground-state wavefunction, and if they possess long-range order an ordered quantum phase may result. Our method should also work generally, when ordered states are shaped both by minimizing energy and maximizing entropy. In fact, one can say that we find states with minimized quantum free energy. This method was first applied to the Kagome Ising models with transverse field and XXZ dynamics in Chapter 4, and then to models on the square and triangular lattices in the Chapter 5. In all cases it revealed valence-bond ordered phases, except in the transverse field Ising model on the Kagome lattice, where no long-range order was entropically selected.

6.3 Open Problems

There are several directions in which the research presented in this theses could immediately continue. The methods developed here are applicable to various frustrated magnets, and can be used for more systematic study of the physics of frustration.

The \mathbb{Z}_2 gauge theoretical approach from Chapter 2 could be applicable to all frustrated quantum magnets that have abundant singlet states deep below a finite spin-gap. Apart from the Kagome system, examples include the checkerboard Heisenberg antiferromagnet, and perhaps the pyrochlore antiferromagnet. A naive expectation is that a valence-bond crystal (plaquette phase) generally settles down in this approach, with highest possible density of smallest resonating valence-bond loops that the given lattice can support. This precisely describes the ordered phase found numerically in the checkerboard system [62]. In the pyrochlore system, this picture would predict two possibilities, one with clear gap to all excitations, and one with extremely small gap (similar to the Kagome case), but both ordered in a staggered fashion (every other tetrahedron carries a resonant loop). These conclusions are very preliminary and intuitive, so that more research is needed in order to verify them.

The $U(1)$ gauge theoretical approach from Chapter 4 is applicable to a wide range of frustrated quantum Ising systems in two dimensions. As long as Ising interactions

are nearest-neighbor and frustrated on a lattice whose dual lattice is bipartite, virtually any kind of spin dynamics can be studied. This provides an opportunity to systematically explore many cases (different lattice geometries, further-neighbor and multiple-spin exchange, etc.), and seek correspondence between microscopic details of the frustrated models and macroscopic properties of the realized phases. An interesting question is what a weak ring-exchange can do to the Ising model on triangular lattice. This problem is related to at least two important physical systems. One is an $SU(2)$ symmetric spin model with ring-exchange on the triangular lattice, which was studied numerically and showed in certain regimes a very similar spectrum to that of the Kagome Heisenberg antiferromagnet (seemingly gapless singlet states below a finite spin-gap [47, 48]). The other is given by the BEDT-TTF organic superconductors, which are potential hosts of spin liquid phases.

Clearly, much work is yet to be done on three-dimensional frustrated quantum magnets. Approaches from this thesis are applicable in three dimensions as well, where only the duality transformations proceed differently than in two dimensions. Specifically, in this thesis we have exploited simplicity of the Ising-like models that are dual to gauge theories in two dimensions. In three dimensions, appropriate dual models are again gauge theories, and may lead to reduced stability of entropically selected ordered phases (when there is too much entropy). This has been already demonstrated in a pyrochlore XXZ-like model, where a spin liquid was found as a stable phase [81].

Finally, several big questions remain. Fundamental importance of frustrated systems lies in their ability to produce emergent physics at low energies that has very little or no resemblance to the physics at high energy scales. In that sense these systems can be viewed as condensed matter analogues of phenomena observed in the standard model of elementary particle physics. Just like strong nuclear interactions balance each other out at very high energy scales and leave much weaker electromagnetic and ultimately gravitational forces to rule in our world, violently competing forces in frustrated magnets reach some sort of equilibrium at energy scales set by the exchange and let much weaker perturbations decide about particular macroscopic

features. The research presented in this thesis has already encountered some complex phenomena familiar from our world. For example, exchange interactions on the Kagome lattice led to a complicated honeycomb crystal arrangement of valence bonds with a unit-cell large enough to shield independent degrees of freedom inside the honeycomb cells (Chapter 2). Similar situation occurs in every crystal of atoms, where atoms lend some of their electrons to stabilize the crystal, but keep some other electrons shielded in core orbitals as local independent degrees of freedom. Another phase that could be stabilized in the Kagome antiferromagnets has a stripe-like long-range order with a large unit-cell, so that electron fractionalization happens in one dimension, between the stripes (Chapter 2). Such unusual spin liquid behavior (co-existing with crystalline order), in which one direction is spontaneously selected for a translationally invariant order parameter, somewhat resembles situations found in liquid crystals. Possibilities seem endless. From a theoretical point of view, frustrated magnets may be a great laboratory for learning about new phases of matter and ways in which laws of nature emerge from collective behavior. Some ideas even consider possibility that the laws of nature in our universe are shaped by collective behavior at some high energy scales. From an experimental point of view, there is an exciting hope that in condensed matter systems one could probe physics both at high energy scales and emergent low energy scales, in contrast to the particle physics where some high energy scales are just too high. However, at present it seems that in condensed matter systems the low energy scales may be just too low. We are only yet to observe complicated valence-bond crystals and spin liquids in clean materials at extremely low temperatures.

Another big question is how applicable the points of view presented in this theses are to the other strongly correlated systems that share certain things is common with frustrated magnets. Cuprates may belong to this class of systems, since physics of their pseudo-gap phase seems to be that of magnetism frustrated by charge fluctuations. It is the author's hope that the extended mean-field approach explained in Chapter 4 can be improved and applied to fermionic systems as well. This approach can handle both energetic and entropical effects of quantum fluctuations, and could

be appropriate to shed more light on the order parameter in the pseudo-gap phase (which might be entropically determined by quantum fluctuations). At present, it is only possible to illustrate this approach on a bosonic caricature of the cuprates. Suppose that a $t - J$ model of the cuprates is tweaked so that electron creation and annihilation operators become bosonic. Then the model describes three kinds of particles: spin-up electron, spin-down electron, and hole. When the J interaction is decomposed into Ising and XXZ parts, the XXZ exchange describes hopping of spin-up and spin-down electrons, while the Ising part corresponds to a short-range repulsion between same-spin electrons. Similarly, holes can hop on the lattice, and one can include into the model their short-range repulsion as well (this is very realistic). All three kinds of particles could be controlled by “chemical potentials”: doping for holes, and magnetic field for spin-up and down electrons. All particles are hard-core in this toy model. One way to study such a model is by Monte Carlo - this is how the whole phase diagram of the model could be explored. For more physical insight, an effective low energy theory can be derived in certain limits, and set up as a lattice field-theoretical problem. Then, order-by-disorder could be studied using the extended mean-field technique, and stability of ordered phases could be addressed using field-theoretical methods. Hopefully, there are many ways in which ideas from this thesis can be extended.

Appendix A

Ground-State Average of the Gauge Field

Here we derive the ground-state average $\langle \sigma_{ij}^x \rangle$ in the \mathbb{Z}_2 gauge theory (2.4). We are interested in the limit of $h_0 \gg t_{ij}, \Delta_{ij}$ where we can apply perturbation theory. Ground-states $|\alpha\rangle$ of the unperturbed part $H_0 = -h_0 \sum_{\langle ij \rangle} \sigma_{ij}^x$ are degenerate: they have $\sigma_{ij}^x = 1$ on every bond, while the spinon degrees of freedom are arbitrary (subject to the gauge constraint (2.5)). The perturbation H' can be written as:

$$H' = - \sum_{\langle ij \rangle} \sigma_{ij}^z \left[t_{ij} \sum_{\alpha=\uparrow\downarrow} (f_{\alpha i}^\dagger f_{\alpha j} + h.c.) + \Delta_{ij} (f_{\uparrow i}^\dagger f_{\downarrow j}^\dagger - f_{\downarrow i}^\dagger f_{\uparrow j}^\dagger + h.c.) \right] = \sum_{\langle ij \rangle} \sigma_{ij}^z \mathcal{F}_{ij}. \quad (\text{A.1})$$

Let us express the true ground-state $|0\rangle$ of the total Hamiltonian H as a superposition of unperturbed ground-states $|\alpha\rangle$ and first excited states $\sigma_{ij}^z |\beta_{ij}\rangle$. Note that both $|\alpha\rangle$ and $|\beta_{ij}\rangle$ have $\sigma_{ij}^x = 1$ on every bond. In order to satisfy the gauge constraint (2.5), all states $|\alpha\rangle$ must have exactly one spinon on each site, while all states $|\beta_{ij}\rangle$ must have zero or two spinons on the sites i and j and one spinon on every other site.

Ignoring everything beyond the second order of perturbation theory we have:

$$\begin{aligned}
|0\rangle &= |A\rangle + |B\rangle & (\text{A.2}) \\
|A\rangle &= \sum_{\alpha} a_{\alpha} |\alpha\rangle \\
|B\rangle &= \sum_{\langle ij \rangle} \sum_{\beta_{ij}} b_{\beta_{ij}} \sigma_{ij}^z |\beta_{ij}\rangle .
\end{aligned}$$

Note that the states $|A\rangle$ and $|B\rangle$ are not normalized in this notation. Amplitudes a_{α} and $b_{\beta_{ij}}$ can be obtained by calculating the matrix elements $\langle \alpha | H | 0 \rangle$ and $\langle \beta_{ij} | \sigma_{ij}^z H | 0 \rangle$ respectively. Taking into account that H' has non-zero matrix elements only between two unperturbed states whose σ_{ij}^z configurations differ only at one bond, we derive:

$$\begin{aligned}
a_{\alpha} &= \frac{1}{E - E_0} \sum_{\langle ij \rangle} \sum_{\beta_{ij}} b_{\beta_{ij}} \langle \alpha | H' \sigma_{ij}^z | \beta_{ij} \rangle = \frac{1}{E - E_0} \langle \alpha | H' | B \rangle & (\text{A.3}) \\
b_{\beta_{ij}} &= \frac{1}{E - E_1} \sum_{\alpha} a_{\alpha} \langle \beta_{ij} | \sigma_{ij}^z H' | \alpha \rangle = \frac{1}{E - E_1} \langle \beta_{ij} | \sigma_{ij}^z H' | A \rangle ,
\end{aligned}$$

where E is the true ground-state energy, and $E_n = -(N - n)h_0$ are energies of the unperturbed ground and excited states. Substituting this into (A.2) yields:

$$\begin{aligned}
|A\rangle &= \frac{1}{E - E_0} \sum_{\alpha} |\alpha\rangle \langle \alpha | H' | B \rangle & (\text{A.4}) \\
|B\rangle &= \frac{1}{E - E_1} \sum_{\langle ij \rangle} \sum_{\beta_{ij}} \sigma_{ij}^z |\beta_{ij}\rangle \langle \beta_{ij} | \sigma_{ij}^z H' | A \rangle .
\end{aligned}$$

We are now ready to calculate the ground-state average $\langle 0|\sigma_{ij}^x|0\rangle$ at the second order of perturbation theory. Noting that $\langle \beta_{ij}|\sigma_{ij}^z H'|A\rangle = \langle \beta_{ij}|\mathcal{F}_{ij}|A\rangle$ we have:

$$\begin{aligned}
\langle 0|\sigma_{ij}^x|0\rangle &= \langle A|\sigma_{ij}^x|A\rangle + \langle B|\sigma_{ij}^x|B\rangle & (A.5) \\
&= \langle A|A\rangle + \frac{1}{(E - E_1)^2} \times \\
&\times \sum_{\langle p_1 q_1 \rangle} \sum_{\beta_{p_1 q_1}} \sum_{\langle p_2 q_2 \rangle} \sum_{\beta_{p_2 q_2}} \langle A|\mathcal{F}_{p_1 q_1}|\beta_{p_1 q_1}\rangle \langle \beta_{p_1 q_1}|\sigma_{p_1 q_1}^z \sigma_{ij}^x \sigma_{p_2 q_2}^z|\beta_{p_2 q_2}\rangle \langle \beta_{p_2 q_2}|\mathcal{F}_{p_2 q_2}|A\rangle \\
&= \langle A|A\rangle + \frac{1}{(E - E_1)^2} \sum_{\langle pq \rangle} \sum_{\beta_{pq}} \left(1 - 2\delta_{\langle pq \rangle, \langle ij \rangle}\right) \langle A|\mathcal{F}_{pq}|\beta_{pq}\rangle \langle \beta_{pq}|\mathcal{F}_{pq}|A\rangle \\
&= \langle A|A\rangle + \frac{1}{(E - E_1)^2} \sum_{\langle pq \rangle} \left(1 - 2\delta_{\langle pq \rangle, \langle ij \rangle}\right) \langle A|\mathcal{F}_{pq}^2|A\rangle .
\end{aligned}$$

Finally, we note that $-\mathcal{F}_{ij}^2$ is proportional to $\mathbf{S}_i \mathbf{S}_j$ when one spinon occupies every site (the proportionality constant is positive); this fact leads to the antiferromagnetic Heisenberg model at the second-order perturbation theory. The state $|A\rangle$ has normalization close to unity, while the correction to the zeroth-order $\langle 0|\sigma_{ij}^x|0\rangle$ is small:

$$\langle 0|\sigma_{ij}^x|0\rangle = C_1 + C_2 \langle \mathbf{S}_i \mathbf{S}_j \rangle \quad , \quad 1 \approx C_1 \gg C_2 > 0 , \quad (A.6)$$

where the average on the right-hand side is calculated only in the spinon sector.

Appendix B

Estimates of the Couplings in the \mathbb{Z}_2 Gauge Theory

Let us express the Hamiltonian (2.4) in the slave-particle path-integral, as it was done in the Reference [16]. The action involves the spinon Grassmann field $f_{\alpha i}$ living on the sites i of the (2+1)D lattice, and the gauge Ising-like field σ_{ij} living on the lattice bonds:

$$S = - \sum_{\langle ij \rangle} \sigma_{ij} \left[\tilde{t}_{ij} (\bar{f}_{\alpha i} f_{\alpha j} + c.c.) + \tilde{\Delta}_{ij} (\bar{f}_{\uparrow i} \bar{f}_{\downarrow j} - \bar{f}_{\downarrow i} \bar{f}_{\uparrow j} + c.c.) \right] - \sum_i \bar{f}_{\alpha i} f_{\alpha i} + S_B, \quad (\text{B.1})$$

where the Berry's phase S_B that realizes projection to the physical Hilbert space is given by:

$$e^{-S_B} = \prod_{i,j=i-\hat{\tau}} \sigma_{ij}. \quad (\text{B.2})$$

The action (B.1) is an exact rewriting of the Heisenberg model in the limit $\tilde{t}_{ij}, \tilde{\Delta}_{ij} \ll 1$ [16]. We obtain it upon integrating out σ_{ij} , and $J\Delta\tau \sim (\tilde{t}_{ij}^2, \tilde{\Delta}_{ij}^2)$, where $\Delta\tau \rightarrow 0$ is the imaginary-time lattice spacing used in the path-integral (of the Heisenberg model). We can relate the action coupling constants \tilde{t}_{ij} and $\tilde{\Delta}_{ij}$ to the Hamiltonian (2.4) coupling constants, t_{ij} and Δ_{ij} . In order to simplify notation, from now on we will use one symbol \tilde{t} to represent all the couplings in the action, and t for all the

couplings in the Hamiltonian. The connection is:

$$\tilde{t}_{ij} \sim \begin{cases} 1 & , \text{ on the temporal links } \langle ij \rangle \\ t\delta & , \text{ on the spatial links } \langle ij \rangle \end{cases} ,$$

where $\delta = \sqrt{\Delta\tau/h_0} \rightarrow 0$. Now we integrate out the spinon field, and obtain a pure \mathbb{Z}_2 gauge theory with the action:

$$S = -\log \det A(\sigma_{ij}; \tilde{t}_{ij}) + S_B = -\sum_{\square} \tilde{K}_{\square} \prod_{\square} \sigma_{ij} + S_B . \quad (\text{B.3})$$

The matrix A above is the matrix that couples the spinons in (B.1). In the expanded form, this action must contain various gauge-invariant products of σ_{ij} on the closed loops, with the loop-dependent coupling constants \tilde{K}_{\square} . The very assumption that this expansion is possible and convergent is an essential one, and it requires a large spin-gap (of the order of J), determined at a microscopic scale. A large spin-gap guaranties that the effective theory will have only local terms, and significance of various closed loops in (B.3) will rapidly decrease with increasing loop size, making the expansion convergent. At this point we are not providing any formal estimate of the spin-gap. We simply use some external sources to obtain information about it, for example the numerics.

Using the fact that a σ_{ij} factor always comes together with a \tilde{t}_{ij} factor in (B.1), we can estimate the coupling constants \tilde{K}_{\square} (to the lowest order):

$$\tilde{K}_{\square} \sim \prod_{\square} \tilde{t}_{ij} , \quad (\text{B.4})$$

and this implies that \tilde{K}_{\square} can be treated as small numbers, scaling as δ^n with n being the number of spatial links in the loop. In order to formally derive the connection between this action and the Hamiltonians (2.8) and (2.13), we consider only the simple lattices with two spatial dimensions, and neglect all higher order loop terms (enclosing more than one elementary plaquette). If the action contains only the elementary plaquettes, we can readily construct the *dual* theory, as outlined in [16].

It takes the form of the Ising model on the fully frustrated dual lattice:

$$S = - \sum_{\langle lm \rangle} \tilde{K}_{lm} \epsilon_{lm} v_l v_m . \quad (\text{B.5})$$

The Berry's phase S_B in (B.3) is responsible for appearance of the frozen field ϵ_{lm} that lives on the links of the dual lattice; products of ϵ_{lm} on all dual lattice plaquettes must be -1 . The only fluctuating field is the vison Ising field v_l . This duality transformation establishes connection between the coupling constants \tilde{K}_\square defined for a plaquette and \tilde{K}_{lm} defined for the dual bond piercing that plaquette:

$$\tanh \tilde{K}_\square = e^{-2\tilde{K}_{lm}} \quad , \quad \tanh \tilde{K}_{lm} = e^{-2\tilde{K}_\square} . \quad (\text{B.6})$$

For simplicity, assume that there is only one kind of elementary plaquettes. Then, the Hamiltonian that describes the dual theory has the form:

$$H = -h \sum_{\langle lm \rangle} \epsilon_{lm} v_l^z v_m^z - K \sum_l v_l^x . \quad (\text{B.7})$$

The connection between the action (B.5) and Hamiltonian above is:

$$\begin{aligned} K \Delta\tau &= e^{-2\tilde{K}_{lm}} \quad , \quad \text{on the temporal dual links } \langle lm \rangle ; \\ h \Delta\tau &= \tilde{K}_{lm} \quad , \quad \text{on the spatial dual links } \langle lm \rangle . \end{aligned}$$

Now we can estimate the values of the Hamiltonian coupling constants. The temporal elementary plaquettes always have 4 bonds (two spatial and two temporal), while we assume that the spatial elementary plaquettes have n bonds. It follows that:

$$\begin{aligned} K \Delta\tau &= e^{-2\tilde{K}_{lm}(\text{dual temporal link})} = \tanh \tilde{K}_\square(\text{spatial plaq.}) \quad (\text{B.8}) \\ &\xrightarrow{\Delta\tau \rightarrow 0} t^n \left(\frac{\Delta\tau}{h_0} \right)^{n/2} , \end{aligned}$$

$$\begin{aligned} h \Delta\tau &= \tilde{K}_{lm}(\text{dual spatial link}) = -\frac{1}{2} \log \tanh \tilde{K}_\square(\text{temporal plaq.}) \quad (\text{B.9}) \\ &\xrightarrow{\Delta\tau \rightarrow 0} -\log [t \sqrt{\Delta\tau/h_0}] . \end{aligned}$$

Taking the ratio of (B.8) and (B.9), and noting that the Heisenberg model exchange coupling is $J \sim t^2/h_0$, we obtain:

$$\frac{K}{h} = \frac{2(J\Delta\tau)^{n/2}}{|\log(J\Delta\tau)|}. \quad (\text{B.10})$$

The energy scale of J is also a measure of the spin-gap. Since the spinons have to be integrated out, the starting path-integral must accurately represent the energy scales above the spin-gap. The energy cut-off must be much larger than the spin-gap, and hence $J\Delta\tau \ll 1$. This is also compatible with request $\tilde{t}_{ij}, \tilde{\Delta}_{ij} \ll 1$, needed for the path-integral with action (B.1) to reduce to the Heisenberg model. Consequently, $h \gg K$ (for arbitrary $n \geq 0$).

This simple analysis suggests that the large- h limit of (2.13) is a good effective theory for the singlet physics below the spin-gap. It also seems natural to expect from (B.10) that the higher-order loop terms, present in the more accurate effective Hamiltonian, have the coupling constants K_n which decay with the loop length n as $K_n \propto x^n$, where $x = \sqrt{J\Delta\tau} \ll 1$.

As a matter of principle, this approach can be useful even for extensions of the Heisenberg model. The next-nearest and further neighbor exchange interactions are reflected in the action (B.1) as additional spinon hopping and pairing terms mediated by the \mathbb{Z}_2 gauge field. The spinons can still be integrated out (provided that there is a large spin-gap), and the pure \mathbb{Z}_2 gauge theory (B.3) would effectively live on the more complicated lattice which has bonds between all pairs of sites that host an exchange coupling. The dual theory would, in general, be more complicated than the frustrated Ising model (the effective lattice may not even be planar), but we could still write an effective Hamiltonian like (2.8) together with the gauge condition (2.9), and expect a large- h limit to be realized. Similarly, the ring exchange interactions can be implemented in the action (B.1) by explicitly adding the loop products of the gauge field to it. This would yield larger values for the loop couplings K_n in the pure \mathbb{Z}_2 gauge theory, possibly making them comparable with h in magnitude.

Appendix C

Degenerate Perturbation Theory

Let the Hamiltonian H be sum of two components, H_0 and H' . Let the unperturbed part H_0 have a degenerate manifold of ground-states $|\alpha\rangle$ with energy E_0 , and gapped excited states $|\beta\rangle$ with energies E_β . Assume that the perturbation H' is small compared to $E_\beta - E_0$ (typical values used here). We first express a true ground-state $|\psi\rangle$ of H with energy E as a superposition of all H_0 eigenstates, which will be generically labeled $|\gamma\rangle$. The set of equations for the amplitudes in this superposition $a_\gamma = \langle\gamma|\psi\rangle$ is:

$$(E - E_\gamma)a_\gamma = \sum_{\gamma_1} \langle\gamma|H'|\gamma_1\rangle a_{\gamma_1} . \quad (\text{C.1})$$

Amplitudes a_β of the high-energy states can be eliminated iteratively from this system of equations:

$$\begin{aligned} (E - E_0)a_{\alpha_0} &= \sum_{\alpha_1} \langle\alpha_0|H'|\alpha_1\rangle a_{\alpha_1} + \sum_{\beta_1} \sum_{\gamma_2} \langle\alpha_0|H'|\beta_1\rangle \frac{1}{E - E_{\beta_1}} \langle\beta_1|H'|\gamma_2\rangle a_{\gamma_2} \quad (\text{C.2}) \\ &= \sum_{\alpha_1} \langle\alpha_0|H'|\alpha_1\rangle a_{\alpha_1} + \sum_{\beta_1} \sum_{\alpha_2} \langle\alpha_0|H'|\beta_1\rangle \frac{1}{E - E_{\beta_1}} \langle\beta_1|H'|\alpha_2\rangle a_{\alpha_2} + \dots \\ &= \sum_{n, \{\beta_i\}}^{i=1\dots n-1} \sum_{\alpha_n} \left[w_{0,1} \frac{1}{\Delta E - u_1} w_{1,2} \frac{1}{\Delta E - u_2} w_{2,3} \dots w_{n-1,n} \right] a_{\alpha_n} , \end{aligned}$$

where $w_{i,j} = \langle\beta_i|H'|\beta_j\rangle$, for $1 \leq i, j \leq n-1$, $w_{0,1} = \langle\alpha_0|H'|\beta_1\rangle$, and $w_{n-1,n} = \langle\beta_{n-1}|H'|\alpha_n\rangle$, while $\Delta E = E - E_0$ and $u_i = E_{\beta_i} - E_0$. This is now a system of

equations that resembles an eigen-problem: non-trivial solutions for a_α exist only for certain values of ΔE . However, the dependence on ΔE is non-linear, and the “eigen-vectors” will not be orthogonal beyond the second order of perturbation theory. Ideally, we want to construct an effective Hamiltonian, defined in the Hilbert subspace spanned by the low-energy states $|\alpha\rangle$, whose energy spectrum coincides with the actual low-energy spectrum of the full Hamiltonian, and whose eigenstates are as close as possible to the true physical low-energy states $|\psi\rangle$. If we represent (C.2) in matrix form $A(\Delta E)a = 0$, where a is an “eigen-vector”, then we can define a unitary matrix $U(\Delta E)$ that diagonalizes $A(\Delta E)$. Since ΔE is a small number, all dependences on it can be expanded, and the matrices U could be obtained perturbatively, in principle. This would also allow solving perturbatively for the “eigen-values” ΔE . Finally, knowing the ground-state energy ΔE_0 , and the excited state energies ΔE_i , the ideal effective Hamiltonian would be

$$H_{\text{eff}} = E_0 + U^\dagger(\Delta E_0) \text{diag}(\Delta E_0, \Delta E_1, \Delta E_2 \dots) U(\Delta E_0) . \quad (\text{C.3})$$

Situation is much simpler up to the second order of perturbation theory: ΔE does not appear at all on the right-hand-side of (C.2), so that we have a proper eigen-problem. The remaining E on the left-hand-side can be directly turned into the effective Hamiltonian:

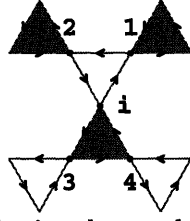
$$H_{\text{eff}}^{(2)} = E_0 + \sum_{\alpha_0, \alpha_1} |\alpha_0\rangle w_{0,1} \langle \alpha_1| - \sum_{\alpha_0, \alpha_2} \sum_{\beta_1} |\alpha_0\rangle \frac{w_{0,1} w_{1,2}}{u_1} \langle \alpha_2| . \quad (\text{C.4})$$

Appendix D

Properties of the TFIM Lattice Theory

Here we derive two important properties of the lattice field theory (4.27) with regard to its saddle-points. The saddle-point vectors ξ are given by (4.31), where the bond variables $\xi_{\langle ij \rangle}$ describe the dimer coverings of the Kagome lattice with one dimer on every triangle, and an arbitrary even number of dimers on every hexagon. The value $\xi_{\langle ij \rangle} = 1$ represents a dimer, while $\xi_{\langle ij \rangle} = 0$ represents a vacancy. First, let us calculate the normalization of the saddle-point vectors ξ (the $\xi_{\langle ij \rangle}$ variables have no time dependence, and we will drop the summation over time):

$$\begin{aligned} \xi^T \xi &\propto \sum_i \left[\left(\sum_{j \in i} \xi_{ij} \right)^2 + \left(\sum_{j \in i} \varepsilon_{\langle ij \rangle} \xi_{ij} \right)^2 \right] \\ &= \sum_i \left[2 \sum_{j \in i} \xi_{ij}^2 + \sum_{\substack{j_1 \neq j_2 \\ j_1, j_2 \in i}} \left(1 + \varepsilon_{\langle ij_1 \rangle} \varepsilon_{\langle ij_2 \rangle} \right) \xi_{ij_1} \xi_{ij_2} \right] \\ &= \text{const.} + 4 \sum_i \left(\xi_{i1} \xi_{i2} + \xi_{i3} \xi_{i4} \right). \end{aligned} \tag{D.1}$$



$\varepsilon_{\langle ij \rangle}$ is -1 on the bonds of the shaded triangles, and $+1$ on the other bonds. Kagome bond orientations are also shown.

Figure D-1: Local neighborhood of a Kagome site

In the last line we have used the notation from the Fig. D-1. Switching to the bond variables, we have:

$$\begin{aligned}
 \boldsymbol{\xi}^T \boldsymbol{\xi} &\propto \text{const.} - 4 \sum_i \left(\xi_{\langle i1 \rangle} \xi_{\langle i2 \rangle} + \xi_{\langle i3 \rangle} \xi_{\langle i4 \rangle} \right) & (D.2) \\
 &= \text{const.} - 2 \sum_{\Delta} \left(\sum_{\langle ij \rangle \in \Delta} \xi_{\langle ij \rangle} \right)^2 + 2 \sum_{\langle ij \rangle} \xi_{\langle ij \rangle}^2 \\
 &= \text{const.} .
 \end{aligned}$$

We have used the facts that the sum of $\xi_{\langle ij \rangle}$ on every triangle is 1, since every triangle holds one dimer (N is the number of Kagome sites), and that the total number of dimers on the lattice is fixed (equal to the number of triangles). We see that all saddle-point vectors $\boldsymbol{\xi}$ have the same normalization.

Now let us calculate how the coupling matrix \mathbf{C} from the action acts on the saddle-point vectors $\boldsymbol{\xi}$. The quadratic parts of the expression (4.30) reveal how the matrix \mathbf{C} acts on the height field vectors $\boldsymbol{\chi}$ whose components are χ_i and λ_i . Substituting there $\sum_{j \in i} \xi_{ij}$ for every χ_i , and $\sum_{j \in i} \varepsilon_{\langle ij \rangle} \xi_{ij}$ for every λ_i reveals the action of \mathbf{C} on the saddle-point vectors $\boldsymbol{\xi}$:

$$\begin{aligned}
 (\mathbf{C}\boldsymbol{\xi})_{\chi_i} &= \sum_{j \in i} \omega_{\langle ij \rangle} ; & (D.3) \\
 (\mathbf{C}\boldsymbol{\xi})_{\lambda_i} &= \sum_{j \in i} \varepsilon_{\langle ij \rangle} \omega_{\langle ij \rangle} ,
 \end{aligned}$$

where $\omega_{(ij)}$ is neither a vector, nor a bond scalar:

$$\omega_{(ij)} = 4\xi_{ij} - \left(\sum_{k \in j} \xi_{jk} + \varepsilon_{(ij)} \sum_{k \in j} \varepsilon_{(jk)} \xi_{jk} \right). \quad (\text{D.4})$$

Since we need to find the sums of $\omega_{(ij)}$ around a particular site, let us take a closer look at the neighborhood of a site i , and refer to the Fig. D-1:

$$\begin{aligned} \omega_{(ij)} &= 4\xi_{ij} - \sum_{k \in j} \xi_{jk} \left(1 + \varepsilon_{(ij)} \sum_{k \in j} \varepsilon_{(jk)} \right) \\ &= 4\xi_{ij} - 2\delta_{j,1}(\xi_{ji} + \xi_{12}) - 2\delta_{j,2}(\xi_{ji} + \xi_{21}) - 2\delta_{j,3}(\xi_{ji} + \xi_{34}) - 2\delta_{j,4}(\xi_{ji} + \xi_{43}) \\ &= 6\xi_{ij} - 2\left(\delta_{j,1}\xi_{12} + \delta_{j,2}\xi_{21} + \delta_{j,3}\xi_{34} + \delta_{j,4}\xi_{43} \right). \end{aligned} \quad (\text{D.5})$$

Then:

$$\begin{aligned} \sum_{j \in i} \omega_{(ij)} &= 6 \sum_{j \in i} \xi_{ij} - 2\left(\xi_{12} + \xi_{21} + \xi_{34} + \xi_{43} \right) \\ &= 6 \sum_{j \in i} \xi_{ij}; \\ \sum_{j \in i} \varepsilon_{(ij)} \omega_{(ij)} &= 6 \sum_{j \in i} \varepsilon_{(ij)} \xi_{ij} - 2\left(\varepsilon_{(i1)}\xi_{12} + \varepsilon_{(i2)}\xi_{21} + \varepsilon_{(i3)}\xi_{34} + \varepsilon_{(i4)}\xi_{43} \right) \\ &= 6 \sum_{j \in i} \varepsilon_{(ij)} \xi_{ij}. \end{aligned} \quad (\text{D.6})$$

We see that the action of \mathbf{C} on a vector whose components are $\sum_{j \in i} \xi_{ij}$ and $\sum_{j \in i} \varepsilon_{(ij)} \xi_{ij}$ simply reproduces those components, with an additional factor of 6. Therefore, all saddle-point vectors ξ are degenerate eigenvectors of the coupling matrix \mathbf{C} , with an eigenvalue 6.

Bibliography

- [1] J. G. Bednorz, K. A. Muller; Z. Phys. B **64** 188 (1986)
- [2] S. Kivelson, D. S. Rokhsar, J. Sethna; Phys. Rev. B **35**, 8865 (1987)
- [3] R. Moessner, S. L. Sondhi, P. Chandra; Phys. Rev. B **64**, 144416 (2001)
- [4] R. Moessner, S. L. Sondhi; Phys. Rev. Lett. **86**, 1881 (2001)
- [5] R. Moessner, S. L. Sondhi; cond-mat/0205029 (2002)
- [6] P. W. Leung, K. C. Chiu, K. J. Runge; Phys. Rev. B **54**, 12938 (1996)
- [7] S. Sachdev, R. N. Bhatt; Phys. Rev. B. **41**, 9323 (1990)
- [8] P. W. Anderson; Mat. Res. Bull **8**, 153 (1973)
- [9] P. W. Anderson; Science **235**, 1196 (1987)
- [10] X. G. Wen, Q. Niu; Phys. Rev. B **41**, 9377 (1990)
- [11] P. A. Lee, N. Nagaosa; Phys. Rev. B **45**, 966 (1992)
- [12] X. G. Wen; Phys. Rev. B **44**, 2664 (1991)
- [13] N. Read, S. Sachdev; Phys. Rev. Lett. **66**, 1773 (1991)
- [14] S. Sachdev, N. Read; Int. J. Mod. Phys. B **5**, 219 (1991)
- [15] C. Mudry, E. Fradkin; Phys. Rev. B **49**, 5200 (1994)
- [16] T. Senthil, M. P. A. Fisher; Phys. Rev. B **62**, 7850 (2000)

- [17] T. Senthil; cond-mat/0105104 (2001)
- [18] T. Senthil, M. P. A. Fisher; Phys. Rev. B **63**, 134521 (2001)
- [19] D. A. Bonn, J. C. Wynn, B. W. Gardner, Y.J. Lin, R. Liang, W. N. Hardy, J. R. Kirtley, K. A. Moler; Nature 414, 887 (2001)
- [20] R. Coldea, D. A. Tennant, Z. Tylczynski; Phys. Rev. B **68**, 134424 (2003)
- [21] R. H. McKenzie; Comments Cond. Mat. Phys. **18** 309 (1998)
- [22] Y. Shimizu, K. Miyagawa, K. Kanoda, M. Maesato, G. Saito; cond-mat/0307483
- [23] A. Yu. Kitaev; Ann. Phys. **303**, 2 (Jan. 2003)
- [24] L. B. Ioffe *et al.*; Nature **415**, 503 (2002)
- [25] P. Nikolic, T. Senthil; Phys. Rev. B **68**, 214415 (2003)
- [26] P. Nikolic, T. Senthil; cond-mat/0402262 (2004)
- [27] P. Nikolic; cond-mat/0403332
- [28] H. Franco, R. E. Rapp, H. Godfrin; Phys. Rev. Lett. **57**, 1161 (1986)
- [29] D. S. Greywall, P. A. Busch; Phys. Rev. Lett. **62**, 1868 (1989)
- [30] V. Elser; Phys. Rev. Lett. **62**, 2405 (1989)
- [31] C. Broholm, G. Aeppli, G. P. Espinosa, A. S. Cooper; Phys. Rev. Lett. **65**, 3173 (1990)
- [32] B. Martinez *et al.*; Phys. Rev. B **46** 10786 (1992)
- [33] Y. J. Uemura *et al.*; Phys. Rev. Lett. **73**, 3306 (1994)
- [34] A. P. Ramirez, G. P. Espinosa, A. S. Cooper; Phys. Rev. Lett. **64**, 2070 (1990)
- [35] A. P. Ramirez, B. Hessen, M. Winklemann; Phys. Rev. Lett. **84**, 2957 (2000)
- [36] A. S. Wills, *et al.*; Phys. Rev. B **62**, R9264 (2000)

- [37] A. S. Wills, A. Harrison, C. Ritter, R. I. Smith; *Phys. Rev. B* **61**, 6156 (2000)
- [38] M. Nishiyama, S. Maegawa, T. Inami, Y. Oka; *Phys. Rev. B* **67**, 224435 (2003)
- [39] I. S. Hagemann, Q. Huang, X. P. A. Gao, A. P. Ramirez, R. J. Cava; *Phys. Rev. Lett.* **86** 894 (2001)
- [40] Z. Hiroi, M. Hanawa, N. Kobayashi, M. Nohara, H. Takagi, Y. Kato, M. Takigawa; *J. Phys. Soc. Jpn.* **70**, 3377 (2001)
- [41] C. Zeng, V. Elser; *Phys. Rev. B* **51**, 8318 (1995)
- [42] Ch. Waldtmann *et al.*; *Eur. Phys. J. B* **2**, 501 (1998)
- [43] C. Lhuillier, G. Misguich; in *High Magnetic Fields* edited by C. Berthier, L. Levy, G. Martinez (Springer, Berlin 2002), 161-190; cond-mat/0109146 (2001)
- [44] P. Sindzingre, C. Lhuillier, J. B. Fouet; Proceedings of the 11th International Conference on Recent Progress in Many-Body Theories, 90-98 (Manchester, 2001); cond-mat/0110283 (2001)
- [45] G. Misguich, D. Serban, V. Pasquier; cond-mat/0310661 (2003)
- [46] P. Sindzingre *et al.*; *Phys. Rev. Lett.* **84**, 2953 (2000)
- [47] G. Misguich, C. Lhuillier, B. Bernu, C. Waldtmann; *Phys. Rev. B* **60**, 1064 (1999)
- [48] W. LiMing, G. Misguich, P. Sindzingre, C. Lhuillier; *Phys. Rev. B* **62**, 6372 (2000)
- [49] M. Mambrini, F. Mila; *Eur. Phys. J. B* **17**, 651 (2000)
- [50] S. Sachdev; *Phys. Rev. B* **45**, 12377 (1992)
- [51] J. B. Marston, C. Zeng; *J. Appl. Phys.* **69**, 5962 (1991)
- [52] G. Misguich, D. Serban, V. Pasquier; *Phys. Rev. Lett.* **89**, 137202 (2002)
- [53] G. Misguich, D. Serban, V. Pasquier; cond-mat/0302152 (2003)

- [54] M. B. Hastings; Phys. Rev. B **63**, 014413 (2001)
- [55] K. Yang, L. K. Warman, S. M. Girvin; Phys. Rev. Lett. **70**, 2641 (1993)
- [56] R. Shankar, D. Shubashree; Phys. Rev. B **61**, 12126 (2000)
- [57] A. V. Syromyatnikov, S. V. Maleyev; Phys. Rev. B **66**, 132408 (2002); cond-mat/0304570 (2003)
- [58] A. V. Syromyatnikov, S. V. Maleyev; J. Exp. Th. Phys. **98**, 538 (2003)
- [59] R. Moessner, S. L. Sondhi; Phys. Rev. B **65**, 024504 (2001)
- [60] R. A. Jalabert, S. Sachdev; Phys. Rev. B **44**, 686 (1991)
- [61] J. Vidal, R. Mosseri, B. Doucot; Phys. Rev. Lett. **81**, 5888 (1998)
- [62] J. B. Fouet, M. Mambrini, P. Sindzingre, C. Lhuillier; Phys. Rev. B **67**, 054411 (2003)
- [63] S. R. White, R. R. P. Singh; Phys. Rev. Lett. **85**, 3330 (2000)
- [64] J. N. Reimers, A. J. Berlinsky, A. C. Shi; Phys. Rev. B **43**, 865 (1991)
- [65] L. Balents, M. P. Fisher, S. M. Girvin; Phys. Rev. B **65**, 224412 (2002)
- [66] D. Blankschtein, M. Ma, A. N. Berker; Phys. Rev. B **30**, 1362 (1984)
- [67] R. Moessner, S. L. Sondhi; Phys. Rev. B **63**, 224401 (2001)
- [68] R. Moessner, S. L. Sondhi, P. Chandra; Phys. Rev. Lett. **84**, 4457 (2000)
- [69] S. Sachdev and R. Jalabert; Mod. Phys. Lett. **B4**, 1043 (1990)
- [70] S. Sachdev, M. Vojta; J. Phys. Soc. Jpn. **69** Suppl. B, 1 (2000);
- [71] W. Zheng, S. Sachdev; Phys. Rev. B **40**, 2704 (1989)
- [72] A. M. Polyakov; Gauge Fields and Strings, Harwood academic, New York (1987)

- [73] E. Fradkin; Field theories of condensed matter systems, Addison-Wesley, Redwood City, Calif. (1991)
- [74] N. Read, S. Sachdev; Phys. Rev. B **42**, 4568 (1990)
- [75] N. Read, S. Sachdev; Phys. Rev. Lett. **62**, 1694 (1989)
- [76] A. Honecker, J. Schulenburg, J. Richter; cond-mat/0309425 (2003)
- [77] F. Y. Wu; Rev. Mod. Phys. **54**, 235 (1982)
- [78] J. Jose, L. Kadanoff, S. Kirkpatrick, D. R. Nelson; Phys. Rev. B **16**, 1217 (1977)
- [79] S. Elitzur, R. Pearson, J. Shigemitsu; Phys. Rev. D **19**, 3698 (1979)
- [80] M. B. Hastings; cond-mat/0305505
- [81] M. Hermele, M. P. A. Fisher, L. Balents; cond-mat/0305401 (2003)